THE ROLES OF DOPAMINE AND THE SODIUM PUMP IN THE SPINAL CONTROL OF LOCOMOTION

Laurence Picton

A Thesis Submitted for the Degree of PhD
at the
University of St Andrews

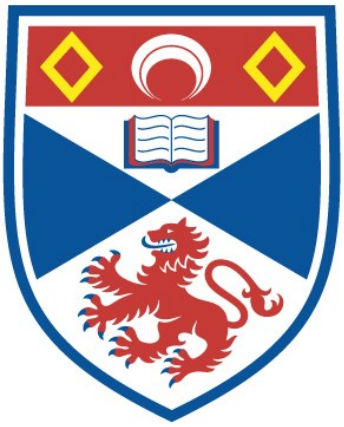

2017

The roles of dopamine and the sodium pump in the spinal control of locomotion

Laurence Picton

This thesis is submitted in partial fulfilment for the degree of Doctor of Philosophy at the University of St Andrews

September 2016

DECLARATION

1. Candidate's declarations:

I, Laurence Picton, hereby certify that this thesis, which is approximately 55,000 words in length (excluding references), has been written by me, and that it is the record of work carried out by me, or principally by myself in collaboration with others as acknowledged, and that it has not been submitted in any previous application for a higher degree.

I was admitted as a research student in September 2012 and as a candidate for the degree of PhD in September 2012; the higher study for which this is a record was carried out in the University of St Andrews between 2012 and 2016.

Date: Signature of candidate:

2. Supervisor's declaration:

I hereby certify that the candidate has fulfilled the conditions of the Resolution and Regulations appropriate for the degree of PhD in the University of St Andrews and that the candidate is qualified to submit this thesis in application for that degree.

Date: Signature of supervisor:

3. Permission for publication:

In submitting this thesis to the University of St Andrews I understand that I am giving permission for it to be made available for use in accordance with the regulations of the University Library for the time being in force, subject to any copyright vested in the work not being affected thereby. I also understand that the title and the abstract will be published, and that a copy of the work may be made and supplied to any bona fide library or research worker, that my thesis will be electronically accessible for personal or research use unless exempt by award of an embargo as requested below, and that the library has the right to migrate my thesis into new electronic forms as required to ensure continued access to the thesis. I have obtained any third-party copyright permissions that may be required in order to allow such access and migration, or have requested the appropriate embargo below.

The following is an agreed request by candidate and supervisor regarding the publication of this thesis:

a) No embargo on print or electronic copy

Date: Signature of candidate:

Signature of supervisor:

Were an old student given an hour in which to revisit the St. Andrews of his day, would he spend more than half of it at lectures? He is more likely to be heard clattering up bare stairs in search of old companions.

J.M. Barrie, Rector's speech (1922)

Acknowledgements

First and foremost, I want to thank Prof Keith Sillar for being a mentor to me during my time in St Andrews. It has been a genuine privilege to be a member of the Sillar lab, and Keith's influence on myself, in the lab, and as head of department has fostered an environment not only of world-class research, but also of community, friendship and laughter. It is people like Keith who make this university such a unique and special place to study and I have an enormous amount to thank him for.

My sincerest thanks also go to Dr Gareth Miles for all his invaluable advice, support and guidance throughout my PhD, but also for making academic life in the Bute building so enjoyable.

I thank the SCAM community for their help, support and encouragement. Special thanks go to HongYan and Stephen for being so welcoming when I first joined them in the lab, and for patiently teaching me the skills of electrophysiology. Thanks also to Filipe ("nappy"), David ("the hair"), Emily, Anna-Claire, Monica, Julius, Amit and many others for all the great craic over the years.

I am grateful to Isobel Maynard, John Macintyre, Jill Wightman and others for lab and animal support, with special thanks to Isobel for all our daily chats, which never failed to make me laugh and were always a welcome distraction from thesis writing. I also thank Dr Bill Heitler for advice and discussion that always helped ideas flourish, and for kindly allowing the free use of Dataview software that made all my analysis possible.

I thank my thesis examiners, Dr Stefan Pulver and Dr Joe McDearmid, for valuable discussion and feedback that made me think more deeply about my data. I am also grateful for the financial support of the BBSRC EastBio programme.

Above all I want to thank my family - most of all my amazing parents - for their endless, loving support in life and throughout my studies. This thesis is dedicated to you.

Finally, I thank Jo for all her love and support, and for the sacrifices she made for me; I couldn't have done it without you.

Thank you.

Contents

Abbreviations

5-HT: 5-hydroxytryptamine (serotonin)
8-bromo-cGMP: 8-bromoguanosine cyclic monophosphate
AADC: aromatic amino acid decarboxylase
aCSF: artificial cerebrospinal fluid
ADHD: attention deficit/hyperactivity disorder
AHP: afterhyperpolarisation
aIN: ascending interneuron
ALS: amyotrophic lateral sclerosis
AMPA: α-amino-3-hydroxy-5-methyl-4-isoxazolepropionic acid
ANOVA: analysis of variance
ATP: adenosine triphosphate
ATPase: adenosine triphosphate enzyme
BaCl: barium chloride
BMP: bone morphogenetic protein
Ca^{2+}: calcium ion
cAMP: cyclic adenosine monophosphate
cGMP: cyclic guanosine monophosphate
CAPOS syndrome: cerebellar ataxi, areflexia, pes cavus, optic atrophy and sensorineural hearing loss syndrome
CPG: central pattern generator
Cs^{+}: cesium
cIA: circumferential ascending interneuron
cIN: commissural interneuron
DA: dopamine
DAB: diaminobenzidine
DC: direct current
DDT: descending dopaminergic tract
DDN: dopaminergic diencephalospinal neurons
DEA-NO: diethylammonium (Z)-1-(N,N-diethylamino)diazen-1-ium-1,2-diolate
DHO: dihydro-ouabain
dIN: descending interneuron
dla: dorsolateral ascending interneuron
dlc: dorsolateral commissural interneuron
dpf: days post-fertilisation
DLSC: dorsolateral suprachiasmatic nuclei
DR: dorsal root
EN1: engrailed-1
EPSP: excitatory postsynaptic potential
FB: forebrain
F-I relationship: frequency-current relationship
GABA: gamma-aminobutyric acid
GIRK: G-protein coupled inwardly-rectifying potassium channel
GPCR: G-protein coupled receptor
GTP: guanosine-5'-triphosphate
HCG: human chorionic gonadotrophin
HCN channel: hyperpolarisation-activated cyclic nucleotide-modulated channel
HN: heart interneuron
I_A: A-type potassium current
I_{CaV}: voltage-dependent calcium current
I_{can}: calcium-dependent cation current
I_h: hyperpolarisation-activated cation current
I_{KV}: voltage-dependent potassium current
I_{KNa}: sodium-dependent potassium current
I_{Nap}: persistent sodium current
IPSP: inhibitory postsynaptic potential
iPSC: induced pluripotent stem cell

IR: input resistance
I-V relationship: current-voltage relationship
K^+: potassium ion
K_i: inhibition constant
K_{ir}: inwardly-rectifying potassium channel
K_m: apparent affinity constant
L-DOPA: levodopa
L-NAME: L-NG-nitroarginine methyl ester
LVA calcium channel: low voltage-activated calcium channel
mAHP: medium afterhyperpolarisation
MB: midbrain
MEA: multi-electrode array
MHR neuron: mid-hindbrain reticulospinal neuron
MN: motoneuron
MNTB: medial nucleus of the trapezoid body
mRNA: messenger ribonucleic acid
mV: millivolt
mS: millisecond
MYA: million years ago
NA: noradrenaline
Na^+: sodium ion
NMDA: N-methyl-D-aspartic acid
NO: nitric oxide
NOS: nitric oxide synthase
OC: otic capsule
PBS: phosphate-buffered saline
PE: pineal eye
PIR: post-inhibitory rebound
PKA: protein kinase A
PKC: protein kinase C
PreBötC: preBötzinger complex
PY neuron: pyloric constrictor neuron
PT: posterior tuberculum
PTH: post-tetanic hyperpolarisation
RB: Rohon-Beard sensory neuron
RDP: rapid-onset dystonia parkinsonism
RLS: restless leg syndrome
RMP: resting membrane potential
sAHP: slow afterhyperpolarisation
SC: spinal cord
SCN: suprachiasmatic nucleus
SEM: standard error of the mean
SERCA: sarcoendoplasmic reticulum Ca^{2+}-ATPase
Shh: sonic hedgehog
SNAP: S-nitroso-N-acetyl-DL-penicillamine
SOD1: superoxide dismutase 1
STG: stomatogastric ganglion
TEA: tetraethylammonium
TH: thyroid hormone
TH: tyrosine hydroxylase
TRP channel: transient receptor potential channel
TTX: tetrodotoxin
usAHP: ultra-slow afterhyperpolarisation
VD interneuron: ventricular dilator interneuron
VNO: vomeronasal organ
VTA: ventral tegmental area

Abstract

Rhythmically active, locomotor networks of the spinal cord are subject to both neuromodulation and activity-dependent homeostatic regulation. I first show that the neuromodulator dopamine exerts potent inhibitory effects on the central pattern generator (CPG) circuit controlling locomotory swimming in post-embryonic *Xenopus* tadpoles. Dopamine, acting endogenously on spinal D2-like receptors, reduces spontaneous fictive swimming occurrence and shortens, slows and weakens swimming. The mechanism involves a TTX-resistant hyperpolarisation of rhythmically active CPG neurons, mediated by the direct opening of a K^+ channel with GIRK-like pharmacology. This increases rheobase and reduces spike probability.

I next explore how sodium pumps contribute to the activity-dependent regulation of the *Xenopus* swim circuit, and possible interactions of the pumps with modulators, temperature and ionic conductances. I characterise the pump-mediated ultra-slow afterhyperpolarisation (usAHP), and show that monensin, a sodium ionophore, enhances pump activity, converting the usAHP into a tonic hyperpolarisation; this decreases swim episode duration and cycle frequency. I also characterise a ZD7288-sensitive Ih current, which is active in excitatory dIN interneurons and contributes to spiking. Blocking Ih with ZD7288 decreases swim episode duration and destabilises swim bursts. Both Ih and the usAHP increase with temperature, which depolarises CPG neurons, decreases input resistance, and increases spike probability; this increases cycle frequency, but the enhanced usAHP shortens swimming. I also show that the usAHP is diminished by nitric oxide, but enhanced by dopaminergic signalling.

Finally, I explore sodium pumps in the neonatal mouse. The sodium pump blocker ouabain increases the duration and frequency of drug- and sensory-induced locomotion, whilst monensin has opposite effects. Decreasing inter-episode interval also shortens and slows activity, a relationship abolished by ouabain, implicating sodium pumps in a feedforward motor memory mechanism. Finally, I show that the effects of ouabain on locomotion are dependent on dopamine, which enhances a TTX- and ouabain-sensitive usAHP in spinal neurons.

Collaboration statement

Parts of this work were performed in collaboration with HongYang Zhang and Filipe Nascimento. All collaborations and publication adaptations (published and submitted) are detailed at the beginning of each data chapter, with details of author contributions.

Introduction

Motor control

To move things is all that mankind can do … whether in whispering a syllable or felling a forest.

Charles Sherrington (Linacre lecture, Cambridge, 1924)

The study of motor control aims to understand how animals, including ourselves, generate purposeful movement. Even the simplest of our actions - such as reaching out to grasp an object – involves a complex series of brain computations that coordinate the precise sequence of flexor and extensor muscle contractions at multiple joints that direct our arms through the air, manipulate our fingers, and adjust our movement in light of sensory feedback. How we coordinate the full ensemble of our muscles to generate whole-body movements, such as dancing, or playing badminton, remains only partially understood, not least because it involves complex cross-talk between so many areas of the nervous system - the motor cortex, cerebellum, somatosensory cortex, basal ganglia, and networks in the spinal cord.

One way to simplify the study of movement is to focus on behaviours which are rhythmic, such as breathing, chewing, or locomoting. This approach provides neurobiologists with a repeatable and comparatively simple behaviour to study, and because these behaviours do not rely on the brain it allows us to isolate the networks physically. A second way to simplify the problem is to study less evolutionarily complex organisms than ourselves, whilst, wherever possible, identifying conserved principles of rhythm generation. At one end of the scale, the control of movement may involve very few neurons. The nematode *C. elegens* has only around 300 neurons in its entire nervous system, of which approximately 75 are devoted to mediating the body wall contractions that thrust the animal forwards. Horses, at the other end of the scale, have around 1.2 billion neurons, many millions of which are involved in coordinating the movement of their four limbs to switch between multiple gaits: *walk*, *trot*, *canter* and *gallop*. The most favoured models in the vertebrate motor control field, such as lamprey, zebrafish, tadpoles, and mice, usually fall somewhere in between: complex enough that the principles

are never too far removed from understanding something about ourselves, yet simple enough that important discoveries are always within reach.

This thesis focuses on two animal models: *Xenopus* tadpoles and neonatal mice. More specifically, this thesis aims to explore the role of the neuromodulator dopamine, the role of the ubiquitously expressed sodium pump, and the interactions between dopamine and the pump in the context of the rhythm-generating networks in the spinal cord of tadpoles and mice. This thesis has also uncovered topics relevant to the sodium pump and dopamine, such as the Ih current and temperature.

The Central Pattern Generator

One of the most important discoveries in the field of motor control was the finding that the neural architecture controlling rhythmic motor behaviours is located in the brainstem and spinal cord, and not the brain, and that its intrinsic activity does not depend on sensory input (for a historical review of the literature see (Stuart & Hultborn, 2008)). Some of the earliest work on mammalian locomotion was conducted by Sir Charles Sherrington, who studied spinal reflexes in cats and dogs. He postulated that rhythmic locomotion in mammals involved a chain of reflexes, whereby muscle contraction and joint movement resulted in the activation of proprioceptors, which in turn provided feedback excitation to the spinal cord to trigger the next phase in a cycle of activity; a process known as “reflex stepping” (Sherrington, 1906, 1910). However, in a seminal paper entitled “The intrinsic Factors in the Act of Progression in the Mammal (1911)”, the Scottish physiologist, and student of Sherrington, Thomas Graham Brown presented data demonstrating that rhythmic locomotor output persists in the cat even when all sensory pathways are removed (Figure 1), thereby contradicting the standing hypothesis. Brown concludes: “*The rhythmic sequence of the act of progression is consequently determined by phasic changes innate in local centers …*“. In other words, all the neural circuitry needed for rhythmic locomotion is present within the spinal cord, and the network can function independently of peripheral inputs. Brown proposed a new theory, known as the “*half-center model*”, which states that there is intrinsic rhythmicity within the spinal

network itself as a result of its configuration into two mutually inhibitory flexor and extensor "half-centers" ((Brown, 1911, 1914), Figure 1). Thus, when the flexor unit is active, the extensor unit is inhibited, and eventual "fatigue" of the flexor module disinhibits the extensor module, which itself now inhibits the flexor module, and so on, in alternation, to produce rhythmic output.

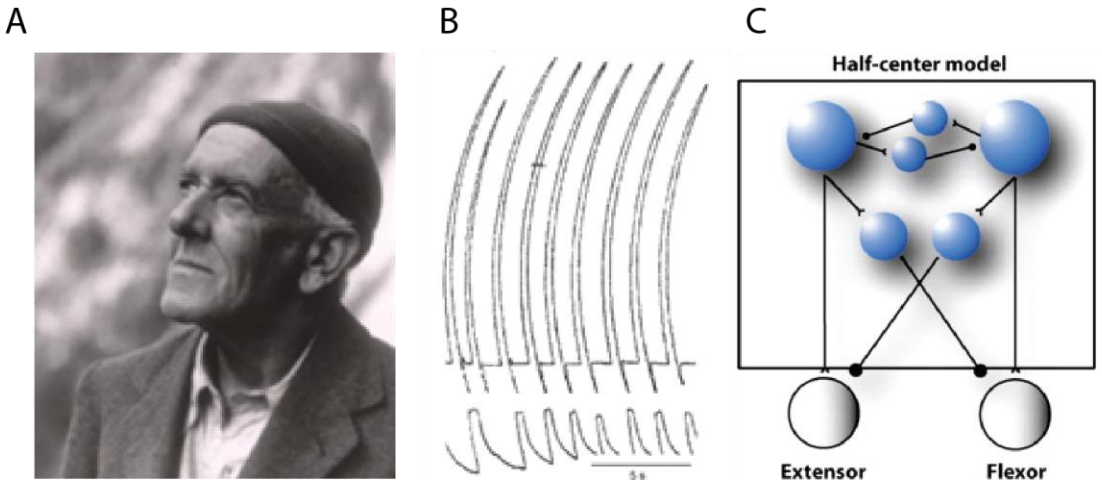

Figure 1. The half center model. **A.** The neurophysiologist Thomas Graham Brown. **B.** A recording from muscle in a de-afferented cat that was the first demonstration that the central pattern generator for mammalian locomotion is located entirely in the spinal cord and can function independently of peripheral input. The recordings were made from completely de-afferented muscles in a decerebrate cat. The upper trace is a recording from tibialis anterior, and the lower trace from gastrocnemis muscle. Rises in the traces show contraction, the falls denote relaxation. Taken from (Stuart & Hultborn, 2008), originally from (Brown, 1911). **C.** A simplified schematic of the half-center model. Blue circles represent interneurons and black/white circles represent motoneurons. Taken from (Guertin, 2009).

Brown's model was generally overlooked for approximately half a century in favour of reflex theories of locomotion, until it was revived in the 1960's and 1970's through extensive work in invertebrates (reviewed in (Mulloney & Smarandache, 2010)). Using the abdominal nerve cord of the crayfish, it was shown that bursts of rhythmic activity driving swimmeret movement continued even when sensory connections were ablated (Hughes & Wiersma, 1960). Around the same time, it was shown that the rhythmic output driving wing movements in locusts also continued when peripheral inputs were completely removed (Wilson, 1961). These two landmark papers sparked an explosion of invertebrate research in a range of rhythmic networks, including those controlling the leech heartbeat, the stomatogastric system of

crustaceans, feeding in *Aplysia*, and swimming in the leech, *Tritonia* and *Clione*[1] *(*reviewed in (Marder *et al.*, 2005)). Using L-DOPA to stimulate activity, Anders Lundber & Elzbieta Jankowska also eventually provided evidence of reciprocal inhibition between interneuron populations in the lumbar region of the cat spinal cord, thus providing the neural substrate for Brown's mammalian half-centers (Jankowska *et al.*, 1965, 1967). It has since been consistently demonstrated, across species that swim, fly, crawl or run, that the rhythmic patterns of neural activity that control locomotion are generated centrally and without the need for sensory feedback, and these networks have been grouped under the umbrella term Central Pattern Generators (CPGs)[2]. Interestingly, there is also recent, compelling evidence that spinal CPGs also underlie locomotion in humans (Dimitrijevic *et al.*, 1998; Danner *et al.*, 2015). Whilst these CPG networks reside in the spinal cord, the brain is obviously important for locomotor rhythms, and plays at least two major roles: the *planning and initiation* of movement and the *neuromodulation* of locomotor patterns (see later section on neuromodulation).

Most CPG networks appear to have some element of reciprocal inhibition between groups of neurons that can be described as having a half-center configuration. However, as more research was devoted to the study of CPGs, especially in mammals, it was quickly realised that there was no "catch-all" half-center model sufficient to explain all locomotor rhythm generation, especially the more complex motor rhythms involved in quadruped stepping. Indeed, the half-center model has been revised and refined a number of times. Perhaps the most influential of these revisions was the "Unit Burst Generator" model, based initially on studies in the cat, which suggests that instead of a single half-center oscillator there are multiple units of half-centers which are linked together in a chain (Grillner, 1981). This refined model was later used to explain the CPG controlling swimming in the aquatic vertebrate, the

[1] *Aplysia* = Spotted sea hare*; Tritonia* = Sea slug; *Clione* = Sea angel
[2] The term Central (nervous) Pattern Generator was first used in an article in published 1965 (Wilson & Wyman, 1965).

lamprey, which became one of the main model systems in the study of locomotor CPGs (Grillner, 2003).

With this general introduction to the CPG completed, let's next examine in detail the CPGs involved in controlling swimming in *Xenopus* tadpoles, and walking in mice.

The swimming network in Xenopus tadpoles

The African clawed frog (*Xenopus laevis)* is an aquatic amphibian native to sub-saharan Africa. The species was originally bred in Britain in large numbers for use as a pregnancy test[3], although since the invention of home pregnancy test kits in the 1960's, they are now mostly used for biological research. Since then, *Xenopus* oocytes and young *Xenopus* tadpoles have been used extensively in the study of the nervous system, and the spinal network underlying swimming in *Xenopus* tadpoles is one of the best understood CPGs of all vertebrates.

Different stages of *Xenopus* development are characterised based upon anatomical and behavioural characteristics (Nieuwkoop & Faber, 1956). During the first few days of post-hatching development (stage 37-45), tadpoles primarily lie dormant and rely on their yolk sac for nutrients, usually only swimming when stimulated. By stage 45, approximately 4 days old, *Xenopus* tadpoles have consumed their yolk sac and switch to a free-swimming and filter-feeding lifestyle, which is accompanied by major anatomical changes (gut, anus and mouth formation) as well as major changes to the nervous system (Currie *et al.*, 2016). Under the control of thyroid hormones (THs), tadpoles enter metamorphosis after around 24 days (approximately stage 53). This involves the development of fore- and hind-limbs, a concurrent loss of the tail, and a switch from a tail-based mode of locomotion to an axial-based mode (Combes *et al.*, 2004; Rauscent *et al.*, 2006; Sillar *et al.*, 2008). However, the most studied stages of development, from a motor control perspective, are newly hatched stage 37/8

[3] The urine of pregnant women contains the hormone human chorionic gonadotrophin (hCG), which when injected into a female *Xenopus* frog it induces egg production (Olszynko-gryn, 2013).

tadpoles (around 2 days old) and stage 42 larval tadpoles (around 3 days old), and the network controlling swimming at these stages is incredibly well defined (reviewed in (Roberts *et al.*, 2008, 2010, 2012; Zhang *et al.*, 2011))

Tail-based swimming in stage 37/8 - 42 *Xenopus* tadpoles is mediated by 10 - 30 Hz left-right rhythmic contractions of segmental myotomal muscles that run along the length of the animal. This left-right alternation, in combination with a rostro-caudal delay of contractions along the body, generates undulating movements that propagate backwards along the animal. These undulations accelerate water backwards, in turn providing the forward thrust that propels the tadpole forwards through water.

These rhythmic contractions of the myotomes are coordinated by iterated subpopulations of spinal neurons (~20 - 150 per segment (Roberts *et al.*, 2010)) that form the CPG, which is organised into half-centres in the spinal cord and hindbrain. The activity of this CPG network mediates the timing, intensity and phasing of locomotor output. At the embryonic stage of development, the swimming CPG contains around 10 types of neuron involved in swimming (Figure 2, (Roberts *et al.*, 2012)). However, evidence suggests that the network can produce the autonomous rhythmic output required for swimming with only four main types of neuron following stimulation from the Rohon-Beard sensory neurons which run along the dorsal midline of the spinal cord(Roberts *et al.*, 2010). I will next describe each of these main neuron types in turn.

The main neuron type providing the excitatory drive to the swim network are the excitatory descending interneurons (dIN's), and these are the first neuron type to fire in each swim cycle (Dale & Roberts, 1985; Li *et al.*, 2006). The dINs co-release glutamate and acetylcholine (Li *et al.*, 2004*b*) and fire a single, comparatively long (1.9 ms) action potential per swim cycle. This action potential is sustained by a prolonged depolarisation as a result of ascending axons that provide feedback onto themselves through glutamatergic excitation via NMDA receptors.

The dINs mostly provide rhythmic excitation to a number of other swim CPG interneurons (cINs, MNs and aINs; see below).

Commissural interneurons (cIN's) provide glycine-mediated, reciprocal mid-cycle inhibition to multiple neuron types of the contralateral 'half-centre', thereby contributing to the left-right alternation during swimming. During each swim cycle, the spiking of a cIN generates a large IPSP in the contralateral dIN. This midcycle inhibition generates post-inhibitory rebound in the dIN, leading to the next cycle of dIN excitation, which in turn excites the cINs, and so on. The frequency of swimming is therefore dependent on the strength of this phasic inhibition from the cINs, and therefore changes in cIN excitability can alter the swim frequency (Li & Moult, 2012). However, rhythm generation can also be generated in the absence of mid-cycle inhibition from cINs, because dINs also display NMDA receptor mediated pacemaker firing properties when depolarised (Li *et al.*, 2010). Thus, there seems to be an interplay between phasic inhibition (cIN) and background excitation (dIN pacemaker properties) that maintains rhythm generation in *Xenopus* tadpoles (Li & Moult, 2012). In relation to Brown's original half-center model (see earlier), it appears that in *Xenopus* tadpoles at least, rhythm generation in the spinal cord is mediated by a combination of the traditional half-center network configuration as well as pacemaker properties in the main excitatory interneuron population; although an additional component thought to be required is tonic excitation, which is embedded into the spinal circuit through NMDA receptor activation in the dIN population.

Ascending interneurons (aINs) are ipsilateral inhibitory interneurons, with ascending and descending axon branches, which limit the firing of various CPG neurons. The aINs play two main roles in the swim network. Firstly, aINs provide phasic, glycinergic inhibition to dorsolateral ascending (dla) and commissural (dlc) cells, which are both sensory interneurons activated by Rohon-Beard neurons innervating the trunk. This phasic inhibition prevents these sensory interneurons from firing from tail stimulation if such stimulation happens to coincide with flexion on the same side, thus providing a form of sensory gating that prevents the interruption of ongoing swimming (Sillar & Roberts, 1988; Li *et al.*, 2002). Secondly, aINs also

provide phasic inhibition to MNs, cINs and dINs, which is thought to help synchronise the firing of these CPG neurons (Li *et al.*, 2004*a*). The aIN neurons are homologous to CiA interneurons in zebrafish (Drapeau *et al.*, 2002), and V1 interneurons in mammals (Gosgnach *et al.*, 2006), which all share the expression of the transcription factor grailed-1 (En1).

Finally, motoneurons (MNs) themselves release acetylcholine onto their target muscle, stimulating their contraction, as well as onto one another (Reith, 1998; Roberts *et al.*, 2010). In the hatchling tadpole, MNs can only fire a single action potential per cycle. However, by stage 42, motoneurons are able to discharge multiple spikes per cycle, enabling more flexibility in the frequency and intensity of the swimming pattern through the recruitment and de-recruitment of motoneurons with different firing thresholds and firing probabilities (Sillar *et al.*, 1991; Zhang *et al.*, 2011).

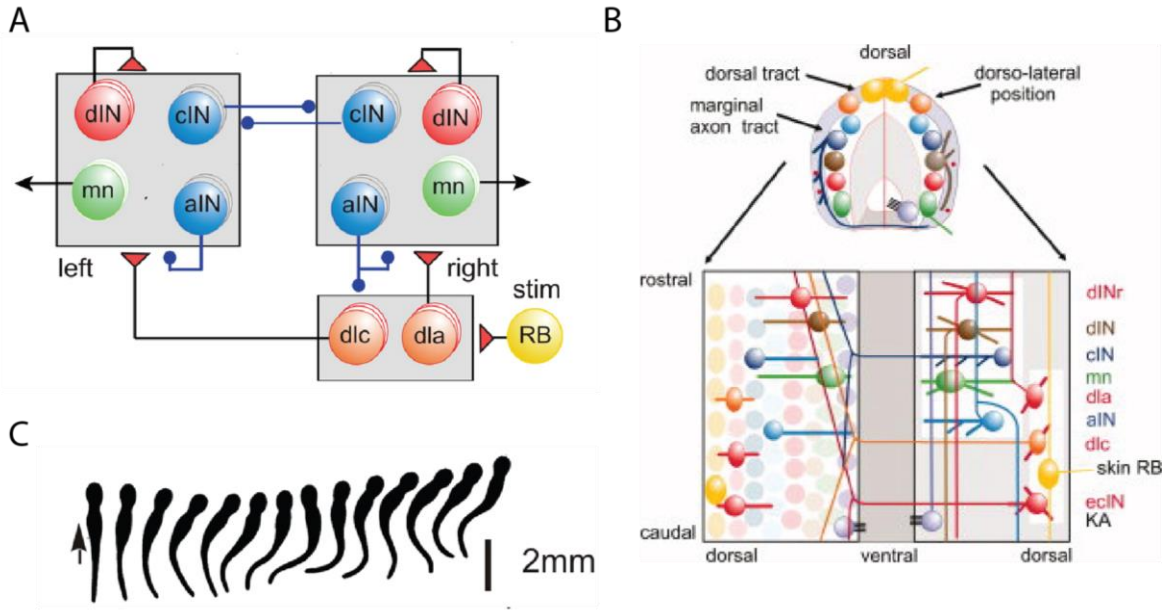

Figure 2. The swim CPG of Xenopus tadpoles. A. Schematic representation of the Xenopus tadpole CPG network showing the main neuron types. Taken from (Roberts *et al.*, 2010). **B.** Semi-realistic representation of the main CPG neuron types in the spinal cord to illustrate their dorsoventral position and interconnectivity. Taken from (Roberts *et al.*, 2012). **C.** Tadpole swimming as viewed from above. Taken from a high speed video taken at 200 fps. Taken from (Roberts *et al.*, 2010).

In addition to the spinal neurons described above, there are a number of important neuron types which aren't part of the core CPG in *Xenopus,* but which play an important role in shaping the output of the swim network. One example are the mid-hindbrain reticulospinal

(MHR) neurons (Perrins *et al.*, 2002). MHR neurons provide GABAergic input to the spinal cord and inhibit swim neurons by acting on $GABA_A$ receptors, with their firing resulting in a barrage of IPSPs. Thus, pathways that activate the MHR population results in strong inhibition of swimming. Once such pathway involves the cement gland, the mucous-producing organ on the front of the head which allows the tadpole to hang from the surface of the water (Boothby & Roberts, 1992; Lambert *et al.*, 2004). The cement gland activates trigeminal sensory neurons which in turn activate the MHR neurons, causing GABAergic inhibition of spinal neurons. Early in development, this pathway provides tonic inhibition to help to keep the tadpole sessile - the tadpole spends most of its time hanging from the surface of the water, which tonically stimulates the cement gland. As the tadpole develops into a free-feeding, more active lifestyle, the cement gland pathway degenerates; MHR input to the spinal cord is maintained, however, and becomes a target for neuromodulation, for example by nitric oxide (Reith, 1996; McLean & Sillar, 2004).

The walking CPG network in mice

Compared to the networks controlling swimming in aquatic vertebrates (*Xenopus*, zebrafish, lamprey), the locomotor network controlling walking in mice is much less well understood, mainly because of the comparatively large number of neurons and neuronal subtypes in the mammalian spinal locomotor network. However, advances in molecular tools have allowed neuronal subtypes of the CPG to be defined based on specific genetic markers. Different neuron subtypes are found at different layers along the dorsoventral axis of the spinal cord, and this layering is determined by gradients of signalling molecules (morphogens) early in development (Jessell, 2000; Goulding, 2009).

During embryonic stages of development, the morphogen sonic hedgehog (Shh) is secreted from the ventrally located floor plate and notochord, whilst bone morphogenetic proteins (BMP's) are secreted dorsally from the roof plate and epidermis. The release of these molecules from opposite surfaces of the spinal cord generates a dorsoventral concentration gradient of signalling molecules along the axis of the neural tube. Subsequently, progenitor

cells at different levels of the cord are exposed to different combinations of these developmental cues. Differences in the expression of homeodomain transcription factors, which are activated at different levels in the Shh-BMP gradient, results in the formation of progenitor domains, where the neurons contained in each progenitor domain are locked into a particular cell fate. In the dorsal half of the spinal cord, commissural and association neurons develop. However, the core CPG neurons reside in the ventral half of the spinal cord, where five main progenitor domains are formed (pV3, pMN, pV2, pV1, pV0; Figure 3). In turn, these progenitor domains generate five layers in the developed spinal cord containing the main neuronal subtypes involved in locomotion: motoneurons (MNs), and four classes of interneuron: V3, V2, V1, V0. In addition, neurons developing in the more dorsally-located pd6 progenitor domain (which become dI6 interneurons), are also known to contribute to core CPG output in neonatal mice (Dyck *et al.*, 2012). The specific roles of these individual cell types are beginning to be defined (Kiehn, 2016).

V0 interneurons are known to express the transcription factor Dbx1 (Pierani *et al.*, 2001) and are subdivided into two subpopulations. The ventral $V0_V$ population, which also express Evx1 (Moran-Rivard *et al.*, 2001), are glutamatergic neurons; whilst the inhibitory dorsal $V0_D$ population, which don't express Evx1, are GABAergic or glycinergic neurons. The V0 interneurons are thought to play a critical role in the control of left-right alternation, as ablation of the V0 population abolishes this property altogether (Lanuza *et al.*, 2004; Talpalar *et al.*, 2013). V1 interneurons express the transcription factor En1 (Moran-Rivard *et al.*, 2001), are generally inhibitory, and include the Renshaw and Ia interneuron populations. The role of the V1 population includes setting the speed of locomotion (Gosgnach *et al.*, 2006), but they also appear to play a role in flexor-extensor alternation (Zhang *et al.*, 2014). The V2 interneuron population is split into excitatory V2a interneurons, which express Chx10; and inhibitory V2b interneurons, which express Gata2/3 (Goulding, 2009). The V2a interneurons contribute to left-right alternation (Crone *et al.*, 2008; Zhong *et al.*, 2010), whilst the V2b population (along with V1) contributes to flexor-extensor alternation (Zhang *et al.*, 2014). The V3 neuron

population are excitatory, Sim-1 expressing neurons, which play a role in promoting robust rhythmic output with strict left-right alternation (Zhang *et al.*, 2008). The dorsally-located dI6 interneurons express Ibx1, are rhythmically active during fictive locomotion, and can be divided into two subpopulations (Dyck *et al.*, 2012). One population is thought to help coordinate motoneuron output, and the other displays oscillatory properties that suggest a contributing role to rhythm generation. Finally, motoneurons, which arise from the pMN progenitor domain, express the transcription factor Hb9, and innervate muscle (Jessell, 2000).

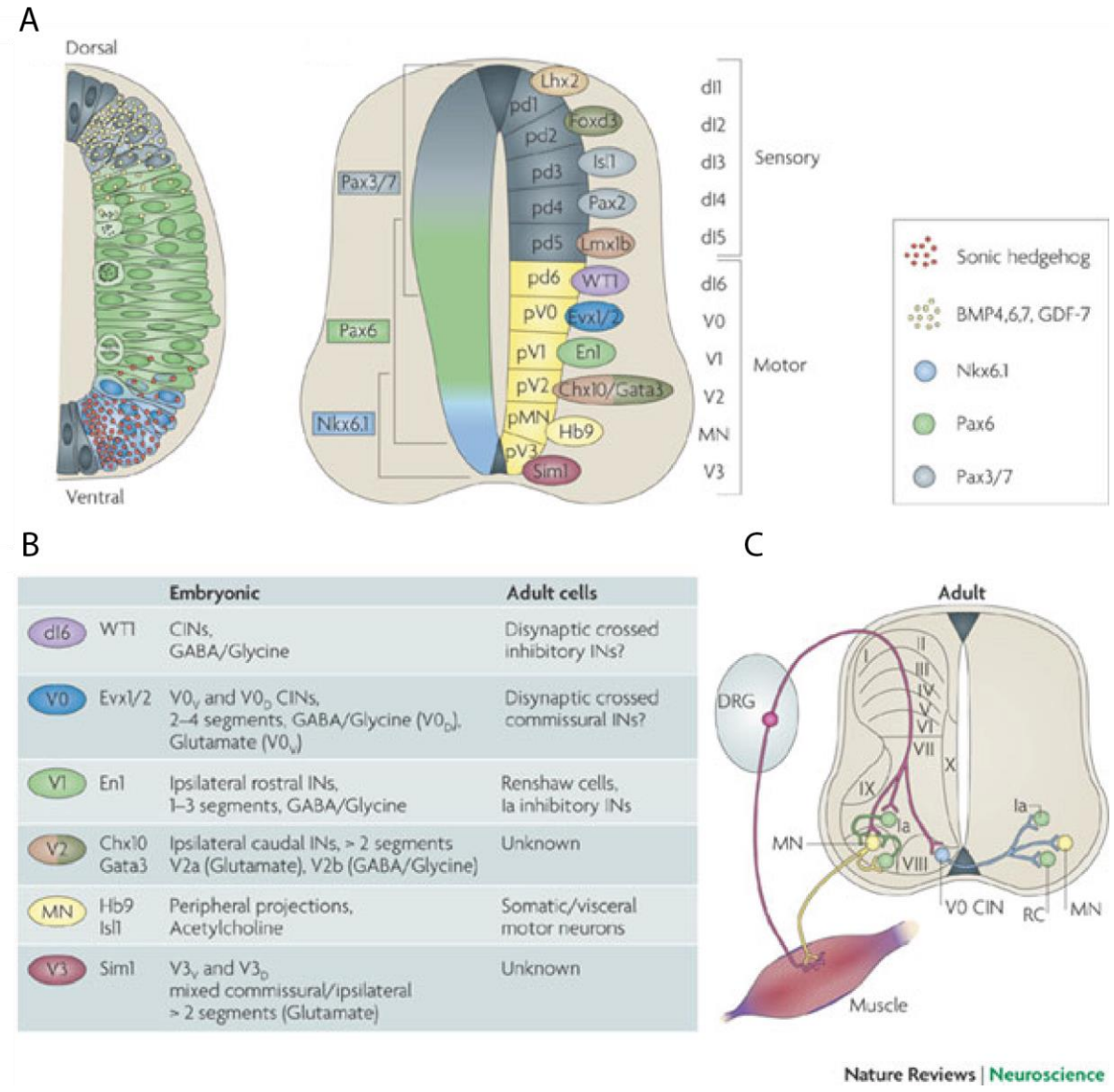

		Embryonic	Adult cells
dI6	WT1	CINs, GABA/Glycine	Disynaptic crossed inhibitory INs?
V0	Evx1/2	$V0_V$ and $V0_D$ CINs, 2–4 segments, GABA/Glycine ($V0_D$), Glutamate ($V0_V$)	Disynaptic crossed commissural INs?
V1	En1	Ipsilateral rostral INs, 1–3 segments, GABA/Glycine	Renshaw cells, Ia inhibitory INs
V2	Chx10 Gata3	Ipsilateral caudal INs, > 2 segments V2a (Glutamate), V2b (GABA/Glycine)	Unknown
MN	Hb9 Isl1	Peripheral projections, Acetylcholine	Somatic/visceral motor neurons
V3	Sim1	$V3_V$ and $V3_D$ mixed commissural/ipsilateral > 2 segments (Glutamate)	Unknown

Figure 3. The spinal network involved in the control of walking in mice. A. Semi-realistic diagram showing the dorsoventral distribution of progenitor domains in the mammalian spinal cord. The transcription factors and cell fates of each domain are indicated. **B.** Summary table showing the

properties of the six main neuron subtypes in the mammalian spinal CPG. **C.** Summary of the connectivity of the neuron types in the adult spinal cord. A, B and C taken from (Goulding, 2009).

Neuromodulation

An important principle of motor control is that the CPG networks of the spinal cord that generate repetitive, rhythmic movements, are not immutable, but are intrinsically flexible to be able to respond to changes in the environment such as obstacles, or threats from predators (Harris-Warrick, 2011; Miles & Sillar, 2011). Indeed, CPG networks are subject to profound modulatory influences, which alter neuronal properties and synaptic strengths to confer flexibility on locomotor output and behaviour. Sources of neuromodulators are present both intrinsically within the spinal cord and extrinsically in higher centres of the brainstem and many via changes in intracellular 2nd messenger concentrations following activation of G protein coupled receptors (GPCRs) (for a recent review see (Miles & Sillar, 2011)). The range of neuromodulators involved comprises a heterogeneous list of signalling molecules including classical neurotransmitters, peptides, biogenic amines and the gaseous free radical nitric oxide. The biogenic amines serotonin, noradrenaline and dopamine, emanating primarily from brainstem nuclei, form diffuse modulatory systems that project to spinal sensory and motor circuits and are known to modulate CPG output. Dopamine plays an especially important role and is a widely distributed and phylogenetically conserved modulator of central neural circuits.

A: CPG neuromodulation by dopamine

Dopamine is a catecholamine which is synthesised in neurons via a stepwise biochemical process involving the conversion of tyrosine to L-DOPA (by the enzyme tyrosine hydroxylase, TH), which is in turn converted to dopamine (by the enzyme aromatic amino acid decarboxylase, AADC). In vertebrates, the dopamine system has long been associated with motor control largely due to the Parkinsonian symptoms related to the loss of dopaminergic neurons in the substantia nigra (Dauer & Przedborski, 2003). Other disorders that may involve changes in the dopaminergic system include restless leg syndrome (RLS) (Clemens *et al.*, 2006) and attention deficit/hyperactivity disorder (ADHD) (Swanson *et al.*, 2007). There is also growing evidence that descending pathways to the spinal cord release dopamine to modify

ongoing rhythmic output produced by spinal CPGs (see (Sharples *et al.*, 2014) for a recent review).

Dopaminergic fibres forming descending tracts from the brainstem offer a rich source of neuromodulatory input to the axial spinal circuits of fish (lamprey (McPherson & Kemnitz, 1994) and zebrafish (Thirumalai & Cline, 2008)); amphibian tadpoles (Clemens *et al.*, 2012), and the appendicular spinal circuits of mammals (Han *et al.*, 2007). The diencephalic dopaminergic tract (DDT) forms a phylogenetically conserved descending projection which is present in all vertebrates studied to date and provides the earliest aminergic projection to the developing spinal cord. Dopamine acts upon two principal classes of receptor which generally exert inhibitory (D2-like: D2,D3,D4) or excitatory (D1-like: D1,D5) influences on neural circuits (Beaulieu & Gainetdinov, 2011).

Invertebrates

The complex role of dopamine as a neuromodulator of rhythmic circuits is arguably best understood in invertebrate systems. The effects of dopamine can have different consequences for the network depending on the cell type affected, and this is best illustrated by dopaminergic effects at the pyloric network of the crustacean stomatogastric ganglion (STG), where dopamine modulates a range of different ionic conductances (Harris-Warrick & Johnson, 2010). The STG generates rhythmic movements of the gut during feeding, and the network itself contains 14 individually identifiable neurons whose nuanced responses to dopamine have been extensively studied. For example, dopamine applied to spontaneously active ventricular dilator (VD) interneurons causes them to hyperpolarise and become silent (Flamm & Harris-Warrick, 1986). This is mediated by a combination of a reduction in a voltage-dependent calcium current ($I_{ca(v)}$) as well as an enhancement of an A-type potassium current (I_A) (Harris-Warrick *et al.*, 1998; Johnson *et al.*, 2003). In addition, an opposing excitatory effect involving the enhancement of an Ih current is also observed in this cell type, and short dopamine applications produce brief inhibition followed by excitation. Thus, within just one of

the STG neurons, three conductances are affected, two of which are inhibitory and one of which is excitatory.

Other cell types, such the pyloric constrictor (PY) neurons, have a different complement of dopamine targets, and in this case spike frequency is increased through a dopaminergic *reduction* in I_A current. Indeed, I_A currents appear to be modulated by dopamine in almost every cell type in the network, but in different directions and via different mechanisms (Harris-Warrick *et al.*, 1998). Overall, dopamine has shown to have complex, and sometimes opposing effects on individual neurons of the STG network and many currents have been implicated including I_A, I_h, $I_{K(v)}$, and $I_{ca(v)}$. In addition to affecting individual cellular properties, dopamine also has multiple effects on the synaptic interconnectivity between neurons in the network (Johnson & Harris-Warrick, 1990; Harris-Warrick & Johnson, 2010).

The role of dopamine in the modulation of CPG output has also been studied in the leech. For drug-evoked and electrically-evoked swimming behaviour, dopamine (50 µM) potently inhibits CPG output and terminates ongoing swimming (Crisp & Mesce, 2004). On the other hand, dopamine has the opposite effect on crawling, and when bath-applied, activates the entire motor pattern required for vermiform crawling locomotor behaviour (Puhl & Mesce, 2008). The application of 75-100 µM dopamine to the isolated leech CNS generates coordinated burst firing in motoneurons and generates fictive crawling activity at the level of the whole network output. Furthermore, the pattern-generating kernel has been determined to be the segmental ganglion, which is capable of generating this motor output following dopamine application, even when completely isolated from the rest of the CNS. Overall, the opposing roles of dopamine on fictive swimming and crawling behaviour suggest that it plays a role in biasing the CPG network towards crawling. A similar role for dopamine has also been shown to be involved in dopaminergic modulation of nematode (*Caenorhabditis elegans*) locomotion (Vidal-Gadea *et al.*, 2011).

The mechanisms of dopaminergic modulation in the leech at the cellular level have also been studied and, as in the STG, complex and somewhat contradictory mechanisms appear to be at play (Crisp *et al.*, 2012). Dopamine appears to act partly via a D1-like, cAMP/PKA-dependent signalling pathway. This pathway activates burst firing in motoneurons that matches fictive crawling, by enhancing plateau potentials through a persistent sodium current. However, dopamine also appears to act via a separate pathway that is likely non-D1 receptor-mediated and independent of cAMP/PKA signalling. This pathway modifies the intrinsic properties of motoneurons, such as enhancing motoneuron AHPs, and raising their firing frequency following post-inhibitory rebound (PIR). Dopamine has also been shown to enhance the amplitude of post-inhibitory rebound (PIR) itself, but only in one specific motoneuron subtype (Vallecorsa *et al.*, 2007).

Aquatic vertebrates

The role of dopamine has also been explored extensively in aquatic vertebrates, especially in the lamprey and the zebrafish. The main source of dopamine in the lamprey spinal cord is a ventromedial plexus that spans the spinal cord, where dopamine is co-localised with serotonin (Schotland *et al.*, 1995). Using NMDA-induced fictive swimming, dopamine has been shown to have opposing effects on swim frequency depending on the concentration. Low dopamine concentrations (0.1-1 µM) cause an increase in swimming frequency, whilst high dopamine concentrations (>10 µM) have the opposite effect of decreasing swim frequency (McPherson & Kemnitz, 1994; Svensson *et al.*, 2003). In addition, high dopamine concentrations increase burst durations (Schotland *et al.*, 1995). At the cellular level, dopamine acts specifically on D2 receptors in motoneurons to decrease calcium entry, which in turn decreases Ca^{2+}-activated K^+ channels. As a result, the amplitude of the slow after-hyperpolarisation (sAHP) is diminished (Schotland *et al.*, 1995). Calcium entry into motoneurons is specifically through N- and L-type calcium channels via a G-protein dependent, voltage-independent pathway (Wikstrom *et al.*, 1999). Overall, the diminished sAHP is thought to slow swim frequency by delaying burst termination.

More recently, an alternative hypothesis has also been proposed to explain the slowing effect of dopamine on swim frequency, which involves the dopaminergic modulation of post-inhibitory rebound in a specific type of inhibitory interneuron (Wang *et al.*, 2011). In this study it was shown that the activation of D2 receptors mediates the depression of low-voltage activated (LVA; specifically L-type channels) calcium channels on spinal commissural interneurons (cINs). These LVA channels contribute to the post-inhibitory rebound (PIR) property of cINs, which normally hastens the onset swim cycles, so their inhibition by dopamine is thought to contribute to the slowing of swimming.

There is also evidence that synaptic modulation contributes to the control of swim frequency. For example, dopamine decreases polysynaptic IPSPs, suggesting a negative effect on inhibitory synaptic transmission, which has been proposed to explain the effect of low concentrations of dopamine on speeding up rhythm frequency (Kemnitz, 1997). Thus, the effects of dopamine on lamprey swim frequency appear to be mediated by a combination of a D2 receptor-mediated decrease in the sAHP in motoneurons (Schotland *et al.*, 1995); a decrease in post-inhibitory rebound in cINs (Wang *et al.*, 2011), as well as synaptic modulation (Kemnitz, 1997).

In another aquatic vertebrate, the zebrafish, dopaminergic input to the spinal cord comes exclusively from the descending dopaminergic diencephalic tract (DDT) and is fully established by 4 days post-fertilisation (4 dpf) (McLean & Fetcho, 2004*a*; Tay *et al.*, 2011), where endogenous dopamine plays a number of important roles in motor control. Early in development, dopaminergic input contributes to establishing the complement of spinal CPG cell types (Reimer *et al.*, 2013). In terms of neuromodulation of ongoing swimming, dopamine appears to have complex effects that are dependent on the developmental stage under investigation (Thirumalai & Cline, 2008; Lambert *et al.*, 2012; Jay *et al.*, 2015).

Between 3 and 5 dpf, larval zebrafish undergo a developmental transition from long, infrequent swim episodes to short, frequent episodes of swimming, and it has been suggested that this

transition to increased spontaneous swimming involves the temporal loss of D2-like receptor inhibition of the swim network (Thirumalai & Cline, 2008). In 3 day old zebrafish, dopamine acts on supraspinal D2-like receptors, via adenylate cyclase, to inhibit the occurrence of spontaneous swimming, although in this study no effects were observed on spinal neurons, and swim parameters were unaffected (Thirumalai & Cline, 2008). Blocking D2-like receptors, or ablating the descending dopaminergic neurons using the toxin MPTP, had the opposite effect at 3 dpf and increased spontaneous swim episodes. However, by 5 days old, blocking the D2-like receptors, or blocking dopamine reuptake, no longer had an excitatory effect on spontaneous swimming. Thus, this study concluded that dopamine acts, at least early in development, via D2-like receptors in the brain to suppress the occurrence of spontaneous locomotion, and there is a developmental loss of D2-like receptor mediated inhibition as development proceeds, to mediate the progression to a more active lifestyle.

A more recent study using a behavioural assay revealed a more nuanced role for dopamine, with multiple dopamine receptors contributing to swim modulation during development (Lambert et al., 2012). The authors identified that the developmental switch to short infrequent episodes occurred somewhere in the short time window between the evening of 3 dpf and the early morning of 4 dpf. If zebrafish were incubated with antagonists of the D1 or D4 receptor between 3dpf and 4dpf, the transition to the mature locomotor pattern did not occur, and fish continued to swim infrequently. Additionally, in the D4 antagonist group (but not the D1 group), swim episodes at 4 dpf were significantly longer, demonstrating that D4 receptors also act to shorten swim episode durations. The same effects occurred when the DDT input to the spinal cord was removed either through spinalisation, through removal of the entire caudal diencephalon, or through ablation of the dopaminergic *otpb* neurons that contribute to the DDT. Moreover, when an antagonist of the D1 or D4 receptor was transiently applied at 5 dpf, the animal reverted back to the younger swimming phenotype; from regular, short episodes to fewer, longer episodes. They also found that in spinalised animals, activation of the D4 receptor significantly shortened episode durations, demonstrating a spinal locus of

the D4 receptors that are targetted by descending DDT input. Overall, therefore, these results demonstrate that between 3 and 4 dpf, descending dopamine from the brain innervates the spinal cord and acts as an excitatory modulator of swimming through actions on D1 and D4 spinal receptors to increase the amount of spontaneous swimming, and acts as an inhibitory modulator *specifically* on spinal D4 receptors to shorten the duration of swim episodes. As a result, swimming switches from occasional long episodes to short, frequent episodes.

A more minor role of the D2/ D3 receptors was also identified (Lambert et al., 2012). Although there was no effect of incubating animals in the D2/D3 antagonists between 3 and 4 dpf, suggesting that they are not endogenously activated, they did however have an effect when applied transiently at 5 dpf, which increased spontaneous swimming, but with no effect on swim episode duration. Thus, although not endogenously active to mediate a change in behaviour during development, D2/D3 receptors are also present and mediate an inhibitory effect on the initiation of spontaneous swimming. Thus, whilst D1 and D4 receptors increase spontaneous swimming, D2/D3 receptors decrease spontaneous swimming. Overall, D4 receptors appear to play the most important role at early stages of zebrafish development. Activation of the D4 receptors in the spinal cord alone decreases episode duration, whilst incubation in a D4 antagonist prevents the switch from long, infrequent swimming to regular short swimming. Other receptors play various, more minor roles. As yet, the cellular mechanisms through which dopamine exerts its effects remain unexplored.

It is interesting that the locus of dopamine's actions (at least via the D4 receptor) in one study was thought to be in the spinal cord itself (Lambert et al., 2012), yet in the earlier study it was found that dopamine had no net effects on spinalised animals, or on any of the properties of spinal neurons (Thirumalai & Cline, 2008). One possibility is that the dopamine used in the earlier study may have been acting on multiple receptors with opposing actions on cell properties that were cancelling each other out; in support of this hypothesis is the fact that the earlier study used broad-spectrum agonists, whereas the latter study used drugs that were more specific to individual receptor subtypes. This hypothesis could also explain the fact that

the earlier study found no effects on the *pattern* of swimming, whereas clear effects on episode duration were found in the latter study. Interestingly, a recent study reporting the effects of genetic ablation of descending dopaminergic neurons also found an effect on overall swimming activity, but only transient effects on episode durations, which they suggested was due to regeneration of dopaminergic neurons between 5 and 7 dpf (Godoy *et al.*, 2015). Together, the results suggest that there may be a subset of dopamine receptors in the brain (probably D2/3) that inhibit spontaneous swim initiation when activated. In the spinal cord, there are probably multiple subtypes, but the D4 seems to dominate and when activated mediates shorter spontaneous swimming that is more frequent, with D1 also contributing to the increased frequency of episodes.

In a more recent study, the activity patterns of the neurons that comprise the DDT have also been characterised, as well as their influence on swimming (Jay *et al.*, 2015). In zebrafish, the population of dopamine neurons that project to the spinal cord are known as dopaminergic diencephalospinal neurons (DDNs), which are a population of around 5-7 large diameter neurons in the posterior tuberculum, homologous to the A11 dopaminergic neurons in the mammal (see later section on dopamine modulation in mammals). Jay et al. recorded from the DDNs at 4 dpf and found that the activity pattern of the population as a whole exhibited two main modes: *tonic* firing (~2 Hz spiking), interspersed with occasional *burst* firing (~0.6s long bursts ~18Hz spiking). In the presence of TTX, the DDNs were shown to receive a combination of glutamatergic and GABAergic mPSCs, with volleys of glutamatergic input mediating the bursting firing mode and irregular glutamate and GABA release underlying tonic firing. However, tonic bursting can also be sustained, albeit at a slower frequency, in the absence of synaptic signalling due to intrinsic membrane oscillations in the DDNs.

What is the relationship between the activity modes of the DDN population and swimming? Jay et al. found that tonic spiking was associated with periods of silence in the swim network, whilst bursting was associated with swimming activity. However, swimming occasionally occurred in the absence of burst firing in the DDNs, and bursting was occasionally observed

in the absence of swimming. Thus, bursting in the DDN population is not necessary or sufficient to initiate locomotion, but tonic and bursting modes of firing are strongly correlated with activity and quiescence of the swim network, respectively. The nature of the swimming pattern itself, however, was not related to the firing of the DDN population. Finally, to further establish the role of the DDNs in the swim network, the authors laser ablated the DDN population. Although both control and ablated animals exhibited the normal beat-glide swimming pattern interspersed with quiescence, with no differences in the parameters of swimming (episode duration, velocity), ablated animals swam significantly less distance in a given time period. In other words, the DDN population appears to have a net facilitatory effect on the occurrence, but not the patterning, of zebrafish swimming. At the level of the spinal cord itself, it has been suggested that tonic, low level DDN firing will largely activate D2-like receptors whilst the bursting mode will result in more dopamine in the spinal cord and activate D1-like receptors.

Xenopus laevis swim CPG

Although dopamine has not previously been studied in young *Xenopus* tadpoles, dopaminergic modulation has been explored in older, free-swimming larval *Xenopus laevis* tadpoles (Clemens *et al.*, 2012). At these stages of development, dopamine has opposing, concentration-dependent effects on swimming. At low dopamine concentrations (2 µM), high affinity D2-like receptors are activated which inhibits the occurrence of spontaneous swim episodes, with similar effects found for agonists at the D2-like receptor. Antagonists at the D2-like receptor had the opposite effects. High concentrations of dopamine, on the other hand, recruit the lower-affinity D1-like receptors and this results in an increase in the occurrence of the swim episodes, again with D1 receptor agonists mimicking this effect, and antagonists having the opposite effect (Clemens *et al.*, 2012). However, no significant effects were found on any of the other swim parameters such as episode duration, burst duration, swim frequency of burst amplitude.

It is known that TH-positive neurons are expressed in a range of areas of the central nervous system of *Xenopus* tadpoles at stage 37-42 including the olfactory bulb, the dorsolateral suprachiasmatic nuclei (DLSC), the posterior tuberculum (PT) and the ventral tegmental area (VTA) (Velázquez-Ulloa *et al.*, 2011). In particular, the latter two areas are involved in the control of movement yet little is known about the role of dopamine in the context of motor control at these stages of development. The earlier study on older, pre-metamorphic free swimming stages of tadpole development, obtained using extracellular ventral root recordings, did not address the cellular mechanisms responsible for dopamine's actions in the spinal cord or the developmental onset of the dopaminergic system, and these are the topics addressed in chapter 1.

Mammalian walking CPG

In the mammalian brain, aminergic neurons (A-cells) are grouped into discrete nuclei known as areas A1-A17 (Carlsson *et al.*, 1962; Dahlstroem & Fuxe, 1964). Dopaminergic input to the mammalian spinal cord derives mainly from the population of around 150-300 dopaminergic neurons in the diencephalic A11 area, specifically in the posterior hypothalamus, whose axons project caudally into predominantly the dorsal horn of the spinal cord, but also into the ventral horn and central canal (Bjorklund & Skagerberg, 1979; Sharples *et al.*, 2014). The precise effects of descending dopaminergic input to the mammalian locomotor network are complex, partly due to the heterogenous patchwork of receptor subtypes (including all of D1-D5) expressed in the ventral horn of the spinal cord, with motoneurons for example expressing all five dopamine receptors (Figure 4, (Zhu *et al.*, 2007; Sharples *et al.*, 2014). Moreover, it seems that the effects of dopamine on locomotor output also depend on the method used to evoke fictive walking (Humphreys & Whelan, 2012).

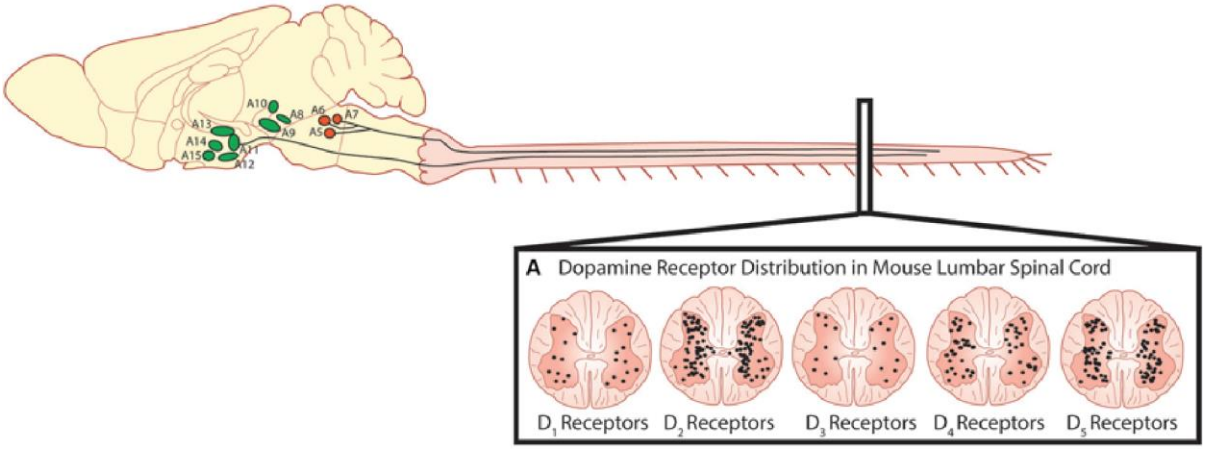

Figure 4. The distribution of dopamine receptor subtypes in the mouse lumbar spinal cord. Taken from (Sharples *et al.*, 2014).

For drug-induced locomotor activity in neonatal mice, however, it has been shown that exogenously applied dopamine slows the bursting rhythm through actions on D2-like receptors, and also stabilises the rhythm and increases the burst amplitude by acting through D1-like receptors (Whelan *et al.*, 2000; Sharples *et al.*, 2015). Similar effects have also been shown in rats (Barrière *et al.*, 2004). The mechanisms are not fully understood but in mice, at least, dopamine increases the excitability of motoneurons. For example, bath-applied dopamine increase spike frequency of motoneurons via a D1 receptor mediated depolarisation and a decrease in at least two potassium conductances: I_A, which regulates first spike latency; and SK_{CA}, which affects the mAHP (Han *et al.*, 2007). In addition to affecting motoneurons, dopamine has also been shown to have effects on the rhythm-generating Hb9 interneurons (Han *et al.*, 2007). Dopamine was found to be necessary (with NMDA and 5-HT), but not sufficient alone, to produce rhythmic burst firing in Hb9 interneurons and thus through an unknown mechanism appears to be responsible for facilitating oscillatory behaviour in spinal interneurons. These oscillations persisted in the presence of TTX, but at a much higher oscillation frequency, suggesting that there are spike-dependent mechanisms mediating the dopaminergic slowing of rhythm frequency. Beyond cellular properties, D1 receptor activation also facilitates glutamatergic synaptic transmission through an increase in AMPA-mediated currents (Han & Whelan, 2009).

B: Network roles for the sodium pump

A considerable amount of research into CPG network function has focused on how neuromodulators, such as dopamine (summarised above), target ion channels in neuronal networks to modulate rhythmic activity. Alternatively, network regulation may involve activity-dependent changes in the spinal network itself. For example, activity-dependent rises in intracellular ions, such as Na^+ and Ca^{2+}, may be detected by specific proteins embedded in the membranes of CPG neurons, triggering changes in neuronal excitability. One such protein which has consistently been found to sense activity-dependent changes in intracellular ions and mediate changes in cellular excitability is the Na^+/K^+-ATPase enzyme.

Rhythmic output from neural networks can be generated as a result of either i) the specific connectivity between the neurons in the network; ii) intrinsic rhythmic properties of the neurons themselves; or iii) a combination of both these elements (Grillner, 2006). Intrinsic rhythmic properties of neurons often depend on the voltage-dependent opening and closing of ion channels with specific temporal properties. However, there is an increasing realisation that in both vertebrates and invertebrates, dynamic, Na^+-dependent changes in sodium pump activity can play a role in rhythmic network activity.

Adenosine triphosphatase enzymes (ATPases) are integral membrane proteins that use the free energy (ΔG_{ATP}) released from the hydrolysis of ATP to transport ions across the cell membrane against their concentration gradient (Glitsch, 2001). There are multiple ATPase families: *F-type* ATPases are found in prokaryotes, mitochondria and chloroplasts; *V-type* ATPases are found in vacuolar membranes; and *P-type* ATPases[4], found in eukaryotes and bacteria and so-called because their action is mediated by a phosphorylation (P) mechanism (Aydemir-Koksoy, 2002). The Na^+/K^+-ATPase (also known the sodium pump) is a highly conserved member of the P-ATPases, which is found in all eukaryotic animal cell membranes,

[4] Other examples of P-ATPases include the calcium pump (Ca^{2+}-ATPase), the proton pump (H^+-ATPase) and the proton-potassium pump (H^+/K^+-ATPase) (Bublitz *et al.*, 2011).

and whose activity is thought to account for at least 50% of total energy consumption in the human brain (Engl & Attwell, 2015).

The sodium pump was first discovered by Jens Christian Skou[5] in 1957, and since then a considerable amount of research has focused on the structure-function relationships of the enzyme[6] (Xie & Askari, 2002). The sodium pump consists of two subunits, known as α and β, which occur with 1:1 stoichiometry (Glitsch, 2001; Aydemir-Koksoy, 2002). The α-subunit exists in 4 isoforms ($\alpha1$ – $\alpha4$), as does the smaller β-subunit ($\beta1$ - $\beta4$), which is a glycoprotein consisting of a single transmembrane domain (Kaplan, 2002). The larger α subunit is the main functional subunit responsible for transporting ions across the membrane, and also contains the binding site for inhibitors such as cardiac glycosides; whilst the β subunit is involved primarily in protein folding and trafficking the $\alpha\beta$ complex to the cell membrane (Morth *et al.*, 2011). The functional cycle of the sodium pump requires ATP, whose terminal phosphate interacts with a specific aspartate residue in a motif found exclusively on P-type ATPases (Kaplan, 2002). The ATP-bound sodium pump conformation is known as E1-ATP, and following the binding of intracellular sodium the ATP becomes phosphorylated, leading to a stepwise process of conformational change (from E1 to E2[7]) along with the successive binding and release of cations, phosphate and ATP which leads ultimately to the release of 3 Na^+ ions to the extracellular space and uptake of 2 K^+ ions ((Morth *et al.*, 2011), summarised in figure 5). Importantly, the mechanism of action of the Na^+/K^+-ATPase is dependent on intracellular sodium, with 3 Na^+ molecules required for the initial phosphorylation of ATP (Glitsch, 2001).

[5] Jens Christian Skou was jointly awarded the 1997 Nobel Prize in Chemistry for his role in the discovery of the sodium pump.

[6] A high resolution (2.6Å) crystal structure of the structurally-related sarcoendoplasmic reticulum Ca^{2+}-ATPase (SERCA) has enabled the identification of a nucleotide-binding domain (N-domain), an actuator-domain (A-domain) and a phosphorylation-domain (P-domain) in the structure of the P-ATPases (Kaplan, 2002).

[7] Note that it is the E2 conformation that cardiac glycosides such as ouabain bind, locking it in this conformation and preventing the continuation of the functional cycle.

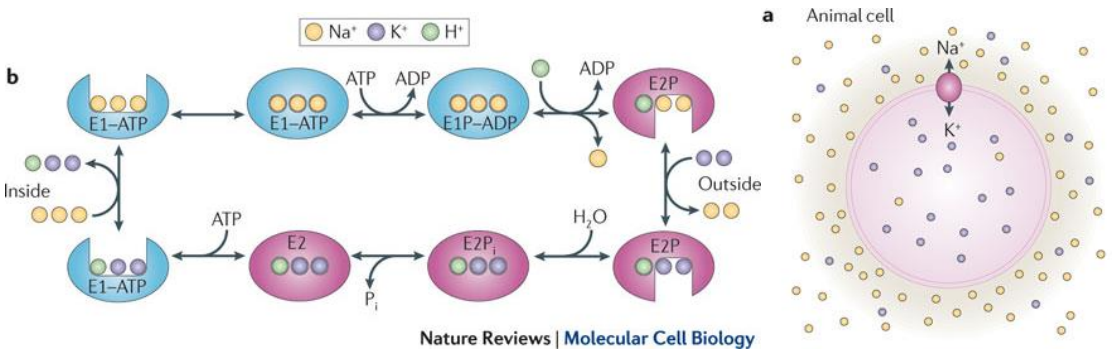

Figure 5. Summary of the reaction mechanism of the Na^+/K^+-ATPase that leads to the release of 3 Na^+ ions to the extracellular space and uptake of 2 K^+ ions into the cell. In the dephosphorylated E1 configuration (blue), the enzyme has a high affinity for ATP and Na^+ ions. The bound ATP becomes phosphorylated, which leads to a conformational change from E1 to E2 (pink). Because E2 has a high affinity for extracellular K+, Na+ ions get released to the extracellular space, and 3 K+ ions bind. The E2 becomes dephosphorylated, transferring these K+ ions into the cell, where the enzyme becomes the ATP- and Na+- binding E1 conformation again. Taken from Morth et al. (2011).

This functional cycle ultimately results in the transport of three Na^+ ions out and two K^+ ions into the cell, which maintains appropriate ionic gradients across the cellular membrane: high extracellular Na^+ and high intracellular potassium K^+ (Aydemir-Koksoy, 2002). Importantly though, this unequal exchange of positive charge (3:2 ratio) also means that the pump is *electrogenic* and therefore establishes and contributes a key hyperpolarising component to establish and maintain the resting membrane potential. Moreover, activity- and state-dependent changes in sodium pump activity can increase the contribution of the outward, hyperpolarising pump current and modify neuronal properties. Some of the earliest evidence for this existence of an electrogenic sodium pump contribution derives from experiments in cat motoneurons (Coombs *et al.*, 1955), and the squid giant axon (Hodgkin & Keynes, 1956), which responded to the injection of Na^+ ions with prolonged periods of membrane hyperpolarisation. However, it wasn't until a similar hyperpolarisation in mammalian nerve fibres was shown to be abolished by ouabain that these Na^+-dependent currents were attributed to changes in sodium pump activity (Ritchie & Straub, 1957; Connelly, 1959; Rang & Ritchie, 1968).

Different functional α subunit isoforms are expressed in different tissues. In the nervous system, the α1 and α3 isoforms are the most prevalent, with the α3 isoform found exclusively

in neurons (the α2 isoform is also present in the nervous system, but mostly in glia, whilst the α4 isoform is only found in the testes (Kim *et al.*, 2007)). Importantly, the α1 and α3 isoforms have distinct affinities for Na^+, resulting in different cellular roles (Aydemir-Koksoy, 2002; Bøttger *et al.*, 2011). The apparent affinities (K_m) for Na^+ are 8 - 17mM and 30 - 68mM for α1 and α3, respectively; whilst the inhibition constants (K_i) for ouabain are 40 - 140 μM and 0.03 - 0.2 μM for α1 and α3, respectively (Blanco & Mercer, 1998; Hamada *et al.*, 2003; Dobretsov & Stimers, 2005; Kim *et al.*, 2007). Thus, the α3 isoform has a lower sodium affinity and higher ouabain affinity, and this has important consequences for the activity of the sodium pump in the neuron. The general hypothesis is that α1 acts as the "housekeeper" subtype for the neuron: the basal intracellular Na^+ concentration in neurons is often around 10 mM (Dobretsov & Stimers, 2005), and therefore the α1 isoform is fully active at rest, thus contributing a *tonic* hyperpolarisation. The α3 isoform, on the other hand, is not maximally active at rest. Therefore any increases in intracellular Na^+ ions, which can range from 5-10mM following just a short burst of action potentials, can be sensed by the α3 sodium pumps, which subsequently increase their ion exchange activity (Figure 6; (Blanco & Mercer, 1998; Dobretsov & Stimers, 2005; Kim *et al.*, 2007; Azarias *et al.*, 2013)). Thus, depending on whether α3 or α1 subunits are involved, there is either a *tonic* contribution to the resting membrane potential (via α1) or a *dynamic* electrogenic contribution (via α3), and these contributions can usually be differentiated using different concentrations of ouabain to target different pump isoforms.

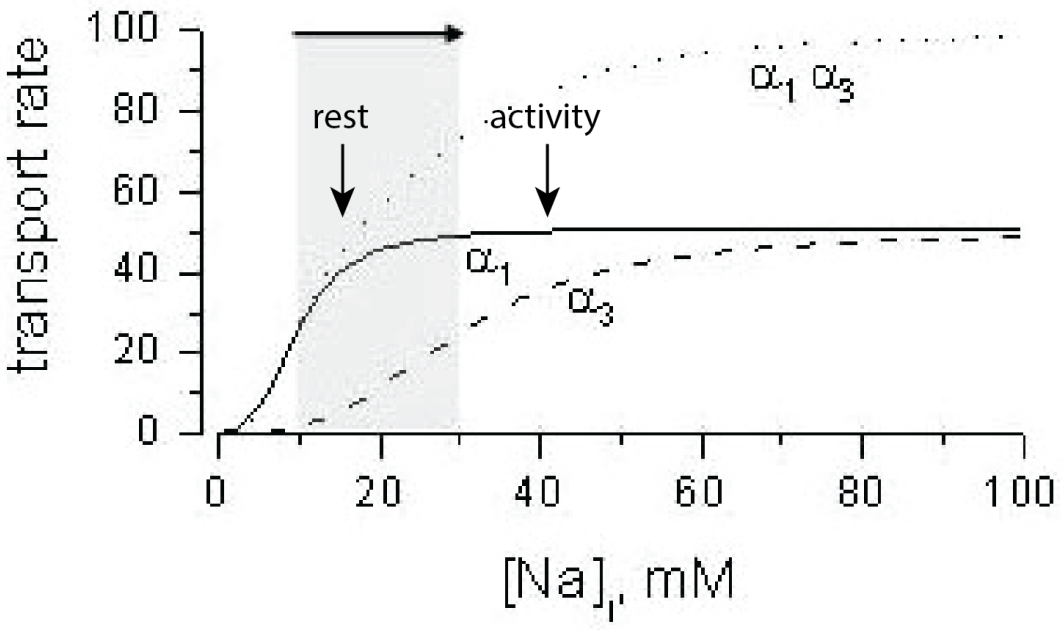

Figure 6. The effects of changing intracellular sodium concentration on the transport rate of α1 (solid line) and α3 (dashed line) sodium pump isoforms. Note that at resting intracellular sodium levels ("rest") the α1 subtype is maximally active, whereas the α3 subtype is only around 10% active. As intracellular sodium levels rise, for example due to intense spiking ("activity"), the transport rate of α1 remains roughly the same but increases for α3. Modified from (Dobretsov & Stimers, 2005).

The α3 sodium pump subtype is highly expressed in neurons in the human brain and spinal cord (Peng *et al.*, 1992). The importance of these α3 sodium pumps is reflected in the range of neurological disorders associated with its dysfunction (Arnaiz & Ordieres, 2014; Holm & Lykke-hartmann, 2016). There are currently three rare disorders known to be caused by mutations in the *ATP1A3* gene that encodes the α3 subunit, including Alternating Hemiplegia of Childhood (AHC, (Heinzen *et al.*, 2012)); Rapid-onset Dystonia Parkinsonism (RDP, (De Carvalho Aguiar *et al.*, 2004)); and Cerebellar ataxia, Areflexia, Pes cavus, Optic atrophy and Sensorineural hearing loss (CAPOS) syndrome (Demos *et al.*, 2014). Furthermore, dysfunction of the α3 sodium pump subtype is known to contribute to a whole range of other disorders including Amyotrophic Lateral Sclerosis (Ellis *et al.*, 2003; Ruegsegger *et al.*, 2015); epilepsy (Krishnan *et al.*, 2015); and bipolar disorder (Kirshenbaum *et al.*, 2012*a*). Thus, it is important that we understand the role of the sodium pumps, especially the α3 subtype, in all areas of the nervous system including the spinal cord.

1. Tonic pump currents

The RMP of neurons is usually mostly determined by the passive diffusion of K^+ ions through leak channels, but there is increasing evidence that tonic sodium pump currents, mediated by the $\alpha 1$ subtype (see above), also contribute to RMP. This is especially true for neurons with low membrane resistances, where the pump can play an important role in setting the resting potential (Trotier & Døving, 1996; Dobretsov & Stimers, 2005). This pump contribution varies across species and cell type (summarised in (Dobretsov & Stimers, 2005)). In extreme cases, the tonic outward sodium pump current may be the main contributor to the resting membrane potential, with little or no role for ionic conductances. For example, receptor neurons of the frog vomeronasal organ (VNO) are hyperpolarised to a RMP of -80 mV entirely through a tonic pump current (Trotier & Døving, 1996). The authors found that the effects on the RMP of manipulating extracellular K^+ concentration were the opposite to what would be predicted if the RMP was determined by K^+ currents; decreasing extracellular K^+ caused the membrane to depolarise, whilst increasing extracellular K^+ caused the membrane to hyperpolarise. These effects are in accordance with the hypothesis that the sodium pump is setting the resting potential; a prediction that was proven by blocking the pump using dihydro-ouabain (DHO), which caused a large depolarisation. It was shown that the resting potential of these cells was set by the tonic hyperpolarising pump current along with hyperpolarisation-activated current (I_h), which is tonically active at membrane potentials more negative than -80 mV (Trotier & Døving, 1996). A similar interaction between the sodium pump and I_h channels has also been shown to set the resting membrane potential in mesenphalic trigeminal neurons (Kang *et al.*, 2004).

A smaller, but still substantial contribution of the pump to the resting membrane potential has been documented for Purkinje cells of the rat cerebellum, where it was shown that the polarisation of the membrane was a product of a tonic hyperpolarising current caused by the sodium pump (Genet & Kado, 1997). The authors found that when they blocked the sodium pump using DHO, the Purkinje cells depolarised and fired continuously. The sodium pump

was found to be responsible at rest for a constant hyperpolarisation of around 25-27 mV, which acted to compensate inward-directed Na^+ fluxes likely mediated by the Na^+/Ca^{2+} exchanger and other channels (Genet & Kado, 1997; Dobretsov & Stimers, 2005). Moreover, it was hypothesised that the specific isoform distribution in the Purkinje cells was shaping these tonic pump currents. Significantly, the Purkinje cells of the cerebellar cortex are particularly rich in both the α1 and the α3 isoform. The authors suggest that the data supports the hypothesis outlined above; the continuous sodium influx saturates the α1 isoforms contributing to the tonic pump activity, whilst the presence of α3 isoforms enables the Purkinje cells to adapt to periods of high activity (Genet & Kado, 1997). This hypothesis was supported by the fact that the effects out DHO on RMP only occurred at the higher (>20 µM) concentrations, but not at low concentrations (1 µM), which would presumably only block the α3 subtypes.

2. Dynamic pump currents

Whilst tonic pump currents clearly play an important role some cell types, changes in substrate concentrations (Na^+, K^+, ATP) represent the most prevalent way that sodium pump activity is dynamically altered in the nervous system. Under normal conditions, ATP concentrations are generally at saturating levels in most cells and therefore ATP fluctuations generally do not to alter pump activity (Therien & Blostein, 2000). Similarly, extracellular K^+ binds at a high affinity to the sodium pump such that most of the time extracellular K^+ concentration also isn't a relevant factor. Changes in intracellular sodium, however, as a result of trains of action potentials, can have a potent influence on the activity of the sodium pump, as resting intracellular sodium concentrations are usually below the level required to saturate the α3 sodium pump isoform (Therien & Blostein, 2000). The most common context in which the activity of the sodium pump contributes to the output of a neural network is during particularly long and intense activity. The cells of some neuronal networks show a sodium pump-dependent, voltage-independent hyperpolarisation following frequent or intense firing, leading to a period of reduced excitability with suppressed neuronal firing. This pump-mediated

reduction in excitability tends to act on a longer timescale than other after-hyperpolarisation (AHP) mechanisms (i.e. fast, medium and slow AHPs), which are typically mediated by potassium or calcium conductances such as Ca^{2+}-activated K^+ currents (Parker *et al.*, 1996). The pump-mediated period of hyperpolarisation following sodium accumulation has been variously termed the "*post-tetanic hyperpolarisation* (PTH)" (Nakajima & Takahashi, 1966; Morita *et al.*, 1993; Parker *et al.*, 1996; Kim *et al.*, 2007; Kim & von Gersdorff, 2012); "*postactivation inhibition*" (Gocht & Heinrich, 2007); or the "*slow-*, or *ultra-slow afteryperpolarisation* (sAHP or usAHP: (Pulver & Griffith, 2010; Zhang & Sillar, 2012; Gulledge *et al.*, 2013))''. Although there are a number of names for this autoinhibition mechanism, these periods of reduced excitability share a number of common features, and it generally acts to integrate spike number over time. For example, the duration of the hyperpolarised period is usually proportional to the duration and intensity of the preceding period of spiking activity - as a function of the number of action potentials - and this relationship tends to be under the modulatory control of various pathways. Next, let's look at these pump currents in specific systems, and how they play a role in the networks in which they are found, starting with invertebrate model systems.

Invertebrate dynamic pump currents

Leech neurosecretory and sensory T-cells

Activity-dependent sodium pump currents have been documented in a whole range of invertebrate species, but are especially well-described in the leech (*Hirudo Medicinalis*) nervous system. Serotonergic Retzius neurons, for example, which are neurosecretory cells that receive input from chemo-, thermo- and mechano-receptors, show a distinct hyperpolarised period of quiescence following high intensity spiking, that is around 5 mV in amplitude, and lasts up to 30 seconds (Gocht & Heinrich, 2007). This has been described as the "*post-activation inhibition*", as spontaneous spiking was suppressed during the prolonged hyperpolarisation. The current is mediated by the sodium pump as it was reduced in both amplitude and duration by the application of the pump-blocker ouabain (10 µM). One of the

most interesting findings from this study was that the period of reduced excitability was shared by cells that were electrically coupled to the neuron being stimulated.

A similar activity-induced hyperpolarisation has been studied in leech tactile neurons (T sensory neurons) (Baylor & Nicholls, 1969; Catarsi *et al.*, 1993; Scuri *et al.*, 2002, 2007). Here, the activity-dependent hyperpolarisation is ~75% mediated by activation of the sodium pump, with the remaining contribution deriving from Ca^{2+}-dependent K^+ currents (Scuri *et al.*, 2002). Moreover, Scuri et al. (2007) explored the effect of this pump-mediated AHP on synaptic transmission in T-neurons. The authors injected presynaptic T-neurons with 3-second trains of high frequency, depolarising pulses to induce an AHP. Then, during the hyperpolarised period, they injected a single depolarising pulse into the fatigued T-cell and measured the synaptic potential of a post-synaptic neuron (a "follower" cell). The size of the post-synaptic response was significantly smaller during the AHP, indicating that synaptic strength was reduced by the AHP. Moreover, ouabain blocked the AHP and rescued the size of the postsynaptic response, essentially leading to synaptic facilitation (Scuri *et al.*, 2007). Thus, the activation of a pump-mediated AHP in T-sensory neurons of the leech leads to a decrease in synaptic strength during periods of high activity. The exact mechanism linking the pump-AHP to synaptic plasticity is unclear.

Given the importance of the sodium pump in the leech nervous system, it is hardly surprising that a number of modulatory pathways converging on the sodium pump have been defined in the leech. For example, it has been shown that the AHP in T-sensory cells is modulated by serotonin (Catarsi *et al.*, 1993; Scuri *et al.*, 2002, 2007). Catarsi, Scuri & Brunelli (1993) showed that the application of 5-HT caused a significant reduction (up to 77%) in the amplitude of the AHP. There was a delay to the effect, which also continued to occur around 20-30 minutes after washout, implying a 2^{nd} messenger signalling pathway. Indeed, the authors found that 5-HT was acting via the cAMP pathway to inhibit sodium pump function (Catarsi *et al.*, 1993). It was later shown in a paper by the same authors that cAMP, acting via the pump inhibition pathway, acts as a mechanism for synaptic facilitation by inhibiting the pump-

mediated AHP which, as described above, inhibits synaptic transmission (Scuri *et al.*, 2007). By injecting cAMP directly into presynaptic T-neurons, the AHP amplitude was smaller and the post-synaptic potentials increased in amplitude. Thus, in this context, 5-HT and/or cAMP acts to release the inhibitory influence of the pump on synapses to boost synaptic strength.

Aside from the leech, similar activity-dependent pump currents have been documented in a range of other invertebrate sensory neurons, such as crayfish stretch receptors (Nakajima & Takahashi, 1966; Sokolove & Cooke, 1971) and insect mechanoreceptors (French, 1989). Sodium pump currents have also been explored in neurosecretory neurons of the snail (*Helix pomatia*), where remarkably, neuronal sodium pump activity is modulated by weak static magnetic fields (Nikolić *et al.*, 2008, 2012).

Invertebrate CPG networks: leech and drosophila

In addition to sensory and neurosecretory systems, there is evidence that pump currents play an important role in controlling the rhythmic output of invertebrate CPG networks. One rhythmic network which is particularly well-studied is the network controlling the leech heartbeat, which is controlled by a relatively small network of 14 interneurons (per segment) which form a CPG (Tobin & Calabrese, 2005; Calabrese *et al.*, 2016). The two half-centres are coupled by two pairs of “oscillator interneurons”, which pace the rhythm of the heartbeat through endogenous bursting activity and reciprocal inhibitory synapses. A hypothetical model has been proposed to explain the bursting activity of heartbeat pacemaker neurons - non-inactivating sodium currents contribute to the depolarising phase of oscillations resulting in neuronal firing; as a result, there is a build-up of intracellular sodium, which activates the sodium pump, hyperpolarising the neurons and terminating the plateau phase of the cycle (Angstadt & Friesen, 1991). In support of this model, Tobin & Calabrese have shown that that blockade of the pump using ouabain (100 μM) increases burst frequency, presumably by abolishing the inter-burst hyperpolarisation (Tobin & Calabrese, 2005). Similarly, the endogenous neuropeptide myomodulin also increases rhythm frequency and is thought to act via a cAMP-dependent pathway to inhibit sodium pump activity (Tobin & Calabrese, 2005). A

recent paper, however, reveals a more dynamic role for the sodium pump, which involves complex interactions with an Ih current (Kueh *et al.*, 2016). The authors activated the sodium pump using the sodium ionophore monensin, which paradoxically had the same effect as blocking the pump – an increase in rhythm frequency. This apparent contradiction was resolved when they showed that blockade of Ih channels (using Cs^+) prevented the monensin acceleration of rhythm frequency, suggesting that the increased frequency was in fact an indirect activation of Ih. This was confirmed using single cell recordings, which revealed that monensin did indeed hyperpolarise heart interneurons[8], but this effect was more pronounced when Ih was blocked; thus demonstrating that pump activation does indeed activate Ih, leading to a faster rhythm. These findings were confirmed using computational modelling of the network, with the additional finding that the bursting rhythm itself depends on the presence of a dynamic pump current in interneurons, with a tonic pump current being insufficient to generate bursting (Kueh *et al.*, 2016).

Sodium pumps also play a particularly important role in the crawling locomotor behaviour of third instar *Drosophila* larvae (Pulver & Griffith, 2010). Crawling in *Drosophila* larvae is controlled by peristaltic waves of muscular contractions which generate forwards or backwards movement, and is under the control of high-frequency, endogenous bursting of ventral motoneurons. Following volleys of action potentials in each burst, these ventral motoneurons show a distinct hyperpolarisation, around 25 mV in amplitude, that lasts up to 20 s. These slow AHP's are mediated by the sodium pump as they are spike-dependent (abolished by TTX), occur with no change in input resistance, and are blocked by ouabain (Pulver & Griffith, 2010). Using the GAL4-UAS system, the authors also induced a dominant-negative form of the sodium pump (D369N) specifically in motoneurons, the genetic equivalent of selectively applying ouabain to this cell type. This abolished the motoneuron slow AHP's,

[8] Interestingly, the authors also found that monensin abolished the ability to generate a dynamic pump current in interneurons, thus essentially turning a *dynamic* pump current into a *tonic* pump current by maximising sodium pump activity. This effect of monensin is also observed in CPG neurons of both *Xenopus* tadpoles (chapter 2), and mice (chapter 3).

without affecting their input resistance, and resulted in a slower crawling behaviour in mutant animals. To explain this effect on frequency they explored a functional role of the pumps at the cellular level. The AHP was found to introduce a consistent delay to the first spike during bursts; the size of this delay was a function of the number of recent action potentials, which in turn determines the size of the subsequent hyperpolarisation. This delay was found to be mediated by I_A currents encoded by the Drosophila *Shal* gene (I_{shal}), which are inactivated at rest, but become de-inactivated by the pump-mediated hyperpolarisation. Thus, previous activity is encoded into the network as a form of spike-dependent cellular memory, whereby activity causes intracellular Na^+ accumulation, increases activation of the pump, hyperpolarises neurons to deinactivate I_{shal} currents, and this modifies the output of the network in a manner proportional to previous activity (Glanzman, 2010; Pulver & Griffith, 2010). In ouabain, or in the mutant ATPase animals, the loss of the AHP removed a core motor memory mechanism involved in the coordination and regulation of CPG firing, leading to a loss of segment-to-segment coordination and a slowing of the crawling frequency (Pulver & Griffith, 2010). This study provided electrophysiological, pharmacological, genetic and behavioural evidence for both the cellular and behavioural role of the sodium pump in *Drosophila* larvae locomotion (Pulver & Griffith, 2010). It is not yet known whether this mechanism is subject to modulation, but future studies will likely explore this possibility.

Vertebrate dynamic pump currents

In evolutionary terms, the α and β sodium pump subunits are believed to have diverged into different isoforms only after the invertebrate and vertebrate lineages split (Okamura *et al.*, 2003). Nevertheless, invertebrate AHPs generated by the more primitive sodium pump bear a great deal of similarity in property and function to those described in vertebrate systems. Moreover, across vertebrates species there is in fact a large degree of homology, especially for the neuronal α3 sodium pump subtype which has around 96% cross-species similarity (Takeyasu *et al.*, 1990; Dobretsov & Stimers, 2005). This conservation suggests that sodium pumps not only play an important role throughout vertebrate evolution, but it means that

comparisons can be made between highly divergent species, such as *Xenopus* tadpoles (chapter 2) and mice (chapter 3). In the next section, I will outline some of the best studied sodium pump currents in various vertebrate species.

Among non-mammalian vertebrates, a dynamic sodium pump current has been identified in sensory neurons of the lamprey (Parker *et al.*, 1996), motoneurons in the lizard and guinea pig (Morita *et al.*, 1993; del Negro *et al.*, 1999), and in C-fibres of bullfrogs (Kobayashi *et al.*, 1997). There is also some evidence that pump currents are generated in human motor axons following repetitive stimulation (Kiernan *et al.*, 2004). However, the vast majority of studies on the sodium pump have been on various tissues in the mammalian nervous system, mostly focusing on rodent models.

Sodium pumps and calcium at the Calyx of Held

Sodium pumps play an especially important role in the auditory system of mammals, where neurons regularly fire at high frequency and require a high fidelity of transmission. The Calyx of Held is an especially large synapse in the medial nucleus of the trapezoid body (MNTB) involved in auditory neurotransmission. Following a burst of action potentials evoked by a pure tone sound (or 100 Hz afferent fibre stimulation) there is a hyperpolarised period pre-synaptically at the rat Calyx of Held synapse, which has been termed the "*pre-synaptic post-tetanic hyperpolarisation*" (*pre*-PTH) (Kim *et al.*, 2007). The pre-PTH is large (~25 mV), and is mediated by the sodium pump as it is blocked by ouabain. The PTH shows two distinct decay phases: an initial rapid recovery, mediated by a depolarising K^+ current[9], followed by a slower recovery period mediated by Ih current. The authors showed that the pre-PTH is mediated by the $\alpha 3$ isoform and, interestingly, immature nerve terminals in younger rats which lack the $\alpha 3$ subunit showed much smaller and shorter PTH. Another interesting finding in this study was that intracellular Ca^{2+} selectively inhibited the pre-synaptic $\alpha 3$[10] sodium pumps, and reduced

[9] The K^+ current is depolarising as the PTH brings the membrane potential to ~-115 mV; below the reversal potential for K^+.
[10] The $\alpha 3$ subtype has a higher affinity for Ca^{2+} than other pump subtypes (Kim *et al.*, 2007).

the PTH amplitude. A fascinating mechanism was proposed whereby during periods of high activity, the increase in presynaptic Ca^{2+} inhibits the α3 sodium pump during activity to prevent premature AHP induction, which could cause action potential failure. Once activity stops, $[Ca^{2+}]_i$ falls dramatically, disinhibiting the α3 pumps and allowing the induction of the PTH and the important extrusion of accumulated intracellular sodium (Kim *et al.*, 2007). In a more recent paper it was also shown that there is a similar PTH post-synaptically at the Calyx of Held (*post*-PTH), but which is much smaller in amplitude (5-10 mV) (Kim & von Gersdorff, 2012).

Hippocampal pyramidal cells

Decades of research has focused on Ca^{2+}- and K^+-dependent AHP mechanisms in neocortex and hippocampus, yet there is recent evidence that the sodium pump also plays an extremely important role in AHP generation in hippocampal pyramidal cells (Gulledge *et al.*, 2013). Gulledge et al. identified a 20s hyperpolarisation, around 5-10 mV in amplitude, in response to high frequency firing (10–50 Hz, 1 or 3 s stimulation). Again, this is mediated by the sodium pump as it was abolished by TTX, ouabain, or the removal of extracellular K^+. The amplitude and duration of this long AHP was a function of the number of action potentials, but importantly, the pump current could be induced using physiologically relevant spike rates, which involved only a brief train of only ~15 action potentials. Moreover, action potential generation was inhibited during the the initial seconds of the hyperpolarisation. This is important from a motor control perspective, as each rhythmic burst in locomotor circuits may also only involve a few action potentials, which has often been viewed as too few spikes to contribute a dynamic pump current to an ongoing rhythm.

In terms of the characteristics of the pump AHP in hippocampal cells, there was an initial peak component (~1 s), which was actually found to be mediated by the inactivation of HCN (Ih) channels, along with a calcium-dependent K^+ channel. The longer duration hyperpolarisation (>20 s), however, was entirely pump-mediated. Unusually, the authors also observed a large conductance increase for the duration of the long hyperpolarisation, leading to initial speculation that Na^+-dependent K^+ channels may be involved. However, this was found to be

an Ih conductance that instead contributes to the recovery from the pump current. When Ih channels were blocked with Cs^+, the conductance change disappeared and the AHP doubled in duration. This is a particularly good example of the role Ih can play in setting the duration of a pump current. The differentiation between pump and K^+ current components was elegantly illustrated by the effects of removing extracellular K^+, which caused the peak component to increase in amplitude, but abolished the slow component. Interestingly, unlike a number of other studies, ouabain blocked the activity-dependent, dynamic pump current but had no effect on the RMP of pyramidal cells. This is likely to be due to the low (20 µM) concentration of ouabain used compared to other studies (typically 100 µM), but is an important illustration of the difference in the roles of the sodium pump isoforms and how they can be distinguished using different ouabain concentrations. Overall, this study was an interesting demonstration of how activity-dependent hyperpolarisations can involve, at least for the initial (~1s) component, Ih channels as well as Na^+- and Ca^{2+}-dependent K^+ currents. Finally, the authors also manipulated temperature. At room temperature, the calcium-dependent mechanisms dominated, but when raised to physiological temperature (35 °C), the calcium mechanisms were absent and the pump component dominated, which the authors suggest may be one of the reasons why decades of research on pyramidal cells have failed to identify the importance of the sodium pump in these neurons.

So far, all of the vertebrate studies outlined above have focused on sodium pump currents that are generated in response to particularly long or intense firing. For the final section of this introduction I will outline the role of similar pump currents in directly contributing to rhythmically active networks in the brain, brainstem and spinal cord of mammals. Because of the relatively slow timescale over which pump currents are generated, there is no evidence for a role of the sodium pump in controlling fast rhythms (i.e. > 10Hz). However, a number of studies have shown that sodium pumps can contribute to rhythms on a slower timescale. For example, there is evidence that pump activity contributes to 24 hour circadian rhythms (Wang & Huang, 2006; Wang *et al.*, 2012). However, most studies have explored roles for the sodium pump in

contributing to rhythms with timescales between these extremes, such as slow oscillations in the 0.1-1Hz range. Most of these networks are associated with motor control, such as the cerebellum (Forrest *et al.*, 2012), dopamine midbrain neurons (Johnson *et al.*, 1992), and spinal CPG networks (Ballerini *et al.*, 1997; Darbon *et al.*, 2003).

Rhythmic firing in dopaminergic midbrain neurons

The sodium pump has been shown to play a fundamental role in the NMDA-induced rhythmic firing pattern of dopaminergic neurons of the substantia nigra in the ventral midbrain (Johnson *et al.*, 1992; Shen & Johnson, 1998). These neurons, which are involved in the control of movement, typically show a regularly spaced firing pattern of single action potentials. In the presence of NMDA, however, the firing pattern changes to regularly spaced bursts of 2-10 action potentials separated by large hyperpolarised periods, lasting around 1-5s, that are up to 40 mV in amplitude. Johnson et al. (1992) showed that these hyperpolarised periods are a result of transient increases in the activation of the sodium pump. Unusually, although the hyperpolarisations were blocked by Na^+-free solution, ouabain (1-3 µM), strophanthidin (2-10 µM) and zero K^+, they were not blocked by TTX. The authors argue that rather than spike-dependent Na^+ entry, sodium instead enters the cell via NMDA channels during each oscillation. As sodium builds, the sodium pump increases its activity and hyperpolarises the cell, which in turn leads to the Mg^{2+}-dependent block of the NMDA receptor. As intracellular sodium gradually gets restored, and pump activity subsides, the cells start to depolarise, which unblocks the NMDA receptors and the leads to the initiation of the next rhythmic cycle. A theoretical model for this novel mechanism of neuronal bursting has also been generated (Figure 7, (Li *et al.*, 1996). This model incorporated the regenerative, inward NMDA current along with the outward pump current and concluded that this was sufficient to produce the 0.5Hz slow oscillation that is observed experimentally. Thus, this was one of the first studies which demonstrated that rhythmic firing within a network of neurons could be mediated by oscillations in sodium pump activity.

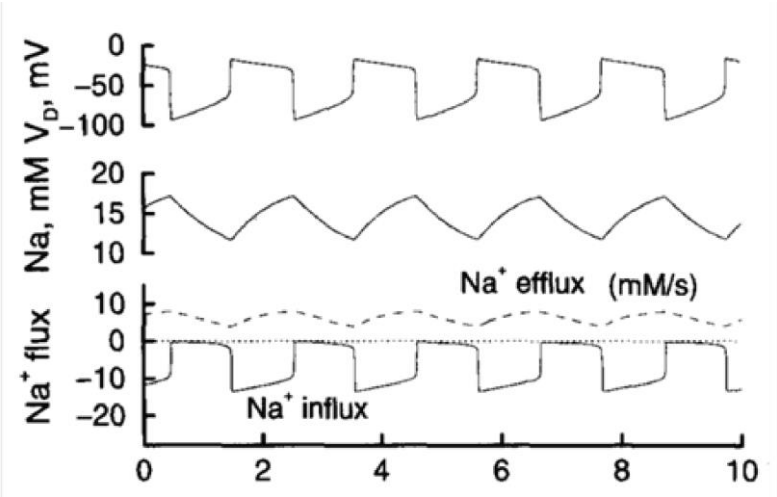

Figure 7. Burst firing in dopaminergic midbrain neurons. NMDA-induced oscillations in membrane potential (V_D, mV), intracellular Na^+ ion concentration (Na, mM) and Na^+ flux (Na^+ flux). During burst periods (negative V_D periods), intracellular Na+ flux is high (negative Na^+ flux values), causing intracellular Na^+ to build up (increase in Na), which increases sodium pump activity which in turn terminates the burst and causes and increase in Na^+ efflux. Taken from (Li *et al.*, 1996).

The NMDA-induced rhythm in the dopaminergic neurons of the ventral midbrain has also been shown to be modulated by nitric oxide (NO) (Cox & Johnson, 1998). L-arginine, the precursor substrate for NO synthesis, increased the size of the hyperpolarised period in-between bursts. On the other hand, the NOS inhibitor L-NAME decreased the bursting rhythm and often disrupted the rhythm altogether. The authors suggest that these effects are mediated by a modulatory increase in the activity of the sodium pump by NO. However, other possible explanations for the effects are that NO could have been acting directly on the NMDA receptor, or other channels, and these possibilities have not been pursued further.

Rhythmic firing in Cerebellar Purkinje cells

In addition to setting the RMP (see earlier), the sodium pump has also been shown to play a fundamental role in the rhythmic firing pattern displayed by Purkinje cells of the cerebellum, which is involved in the coordination of motor behaviour. Purkinje neurons display an intrinsic, repetitive trimodal firing pattern (repeat length 20s) that consists of 3 distinct phases: tonic spiking, followed by bursting, followed by a period of quiescence. Forrest et al. (2012) have provided a detailed computational model to explain this firing pattern, and suggest that "…*at*

the foundation of the purkinje cell's intrinsic multimodality, there is the working of just a single molecular species – the Na^+/K^+ pump".

Initially, there is a tonic firing period at the soma, during which time extracellular K^+ concentration gradually accumulates. The Purkinje dendrites have an intrinsic capacity to fire Ca^{2+} spikes, but this is "gated" during the tonic firing phase due to the presence of Kv1.2 channels, which hyperpolarise the dendrites and "clamp" their excitability to prevent Ca^{2+} spike generation. However, as tonic firing progresses, the build-up of extracellular K^+ diminishes the Kv1.2 current and eventually allows high-threshold Ca^{2+} spiking, causing the switch from tonic to bursting activity. During the burst period, intracellular sodium accumulates, which in turn increases sodium pump activity and the activation of a hyperpolarising pump current which switches the cell from bursting to quiescence. As the cell remains silent, high pump activity increases extracellular potassium and decreases intracellular sodium, the membrane potential recovers, and the trimodal pattern is reset and tonic firing at the soma can begin again, with Kv2.1 channels able to clamp the excitability of dendrites again (Forrest *et al.*, 2012). Although initially a controversial model[11], this is a fascinating example of how a relatively simple sodium pump current is incorporated into a complex, three-phase intrinsic rhythm involving Ca^{2+}-spiking and Kv2.1 channels.

Purkinje cells show heterogeneity in the repeat duration of this firing pattern - from 20 seconds to 20 minutes - and it is thought that this variation is due to differences in affinity of the sodium pump for Na^+ and K^+ that sets the duration of each phase. If the pump has a higher affinity for intracellular sodium (K_{Na}), the pumps become activated by accumulating sodium more rapidly, leading to a smaller burst period and a longer silent period. The higher the affinity for extracellular K^+, the longer the tonic period, as the pump acts to prevent K^+ accumulation during the tonic phase, thereby maintaining the driving force for Kv2.1 channels. These

[11] There was a delay of many years in publishing these results, as reviewers and journals were apparently doubtful about the re-appraisal of the role of the sodium pump in these neurons and routinely rejected the findings (Forrest, 2014).

variations in Na^+ and K^+ affinities could occur due to different isoform expression (see above), and indeed the Purkinje fibres are especially rich in the α3 pump isoform (Forrest, 2015). Alternatively, the variations in phase may be due to neuromodulation of the pumps. Indeed, ethanol is known to inhibit Purkinje sodium pumps and causes a loss of quiescent periods and induces continuous firing, similar to the effects of low concentrations of ouabain (Botta *et al.*, 2010; Forrest, 2015). These results have important implications for how alcohol disrupts motor control, and is the first time the sodium pump has been implicated in the effects of ethanol on the cerebellum. Moreover, it is an interesting example of how extrinsic modulation of the sodium pump can set the rhythm of an entire network of neurons.

Vertebrate CPG networks

The final section of this introduction on the sodium pump will outline the limited number of studies which have explored the role of the sodium pump in the rhythmic networks of the spinal cord and hindbrain, which includes the respiratory network and the locomotor network.

Respiratory CPG

A series of recent studies has identified a role for the sodium pump in rhythmic burst termination in the respiratory brainstem network (Del Negro *et al.*, 2009; Rubin *et al.*, 2009; Krey *et al.*, 2010; Tsuzawa *et al.*, 2015). Resting respiration relies on rhythmic, active muscle contractions that mediate inspiration, with passive expiration during the inter-burst interval. This inspiratory rhythm is controlled by the preBötzinger Complex (preBötC) in the medulla, which generates rhythmic output with a frequency of about 0.2 Hz, *in vitro*, in the absence of sensory or descending inputs (Del Negro *et al.*, 2009). Each inspiratory burst relies on a Ca^{2+}-dependent cation current (I_{can}), and a persistent sodium current (I_{NaP}), which both lead to a massive influx of sodium. During each inspiratory burst, the build-up of sodium activates the sodium pump, which subsequently generates a pump current of around 3-8 mV at each burst that contributes to the termination of each burst (Del Negro *et al.*, 2009; Krey *et al.*, 2010). Blockade of the pump using strophanthidin (10 µM) leads to a depolarisation of preBötC neurons of between around 1-20 mV, as well as an increase in the frequency of the rhythm,

until the rhythm eventually stops due to a depolarisation block of spiking (Del Negro *et al.*, 2009; Krey *et al.*, 2010); thus, there is both a *tonic* pump contribution to these neurons, as well as a dynamic, phasic hyperpolarisation with each inspiratory burst. The authors found that after the termination of a burst, the contribution of the dynamic pump current was very brief (50-200 ms) (Del Negro *et al.*, 2009), although in another study this was slightly longer and lasted up to 1.6 s (Krey *et al.*, 2010). However, it is worth considering the fact that these experiments were conducted in the absence of descending input, and therefore any modulators which may enhance the pump contribution are absent under these conditions. Computational models incorporating the rhythmic firing of pre-Botx neurons have supported a role for the sodium pump, along with other Na^+-dependent outward currents such as Na^+-dependent K^+ currents (IK–Na), in terminating rhythmic bursts (Rubin *et al.*, 2009).

The above experiments were conducted on rhythmically active slice preparations, but a recent study extended the findings to a whole brainstem-spinal cord preparation (Tsuzawa *et al.*, 2015). Recording from the fourth cervical ventral root (C4), the authors found that the application of ouabain (0.1-20 µM) caused a dose-dependent increase in inspiratory burst rate, in accordance with the studies in slice.

Locomotor CPG

Moving more caudal in the mammalian nervous system, there is strong evidence that the sodium pump also plays a role in rhythmic bursting in the mammalian spinal locomotor CPG, although so far studies have focused on disinhibited rhythms in rat whole-cord and slice preparations (Ballerini *et al.*, 1997; Rozzo *et al.*, 2002; Darbon *et al.*, 2003).

Synchronous (left-right synchrony), rhythmic bursting can be generated in mammalian spinal neurons by blocking fast inhibitory synaptic inputs (mediated by $GABA_A$ and glycine receptors with bicuculline and strychnine, respectively); this “disinhibited bursting” is thought to be generated by the same CPG that underlies locomotion, although the bursting rhythm differs from the faster left-right locomotor bursting pattern evoked by NMDA or serotonin in terms of both frequency and duration of bursts (Ballerini *et al.*, 1997). The origin of the excitatory drive

behind the disinhibited bursting rhythm has been shown to result from a wave of excitation as a result of spontaneous firing of neurons in the ventral horn, which spreads through the network via glutamatergic recurrent excitation (Darbon *et al.*, 2002; Rozzo *et al.*, 2002).

In rat whole spinal cord preparations displaying disinhibited bursting, application of the sodium pump blockers ouabain (10 μM), strophanthidin (4 μM), or zero K^+ solution, caused motoneurons to depolarise by around 5 mV, and rhythmic bursting became irregular as well as variable in duration and inter-burst interval, although left-right and flexor-extensor synchrony was retained (Ballerini *et al.*, 1997). Over longer periods, activity eventually fell silent, although activity could still be evoked using dorsal root stimulation (long continuous bursts of activity lasting ~ 1 min), indicating that the network was still functional. These results were repeated and expanded upon in a subsequent study (Rozzo *et al.*, 2002). However, in addition to replicating these findings they also observed the emergence of a new rhythm around an hour after blockade of the sodium pump (by ouabain or strophanthidin), which they termed “strophanthidin bursting” (Rozzo *et al.*, 2002). These new bursts were infrequent and irregular, had a longer duration (~150s vs. ~6s in control), a slower frequency, and a much slower decay time. This strophanthidin bursting was very stable in that it could last up to 12 hours without changing significantly, illustrating that the physiological integrity of the neurons had not been compromised. The rhythm was found to be dependent on glutamatergic transmission since blockers of glutamate receptors (NMDA, kainate, AMPA) abolished the rhythm.

The authors also explored the effects of dorsal root stimulation. Blocking the pump did not affect VR response parameters to a single DR stimulus, such as impulse conduction, action potential amplitude, or reflex threshold, suggesting that the pump does not play a role in synaptic transmission for single pulses. However, blocking the pump did affect the motoneuron response to repetitive stimulation. In control, repetitive stimulation (1 Hz, 20 pulses) causes a rapid motoneuron depolarisation, followed by a fast decay back to control.

One of the most interesting aspects of this study was the generation of a computational model for a single network that could account for both disinhibited and strophanthidin bursting, allowing the authors to ascribe a role for the pump by comparing the two outputs (Rozzo *et al.*, 2002). The results from this modelling suggested that the strophanthidin rhythm relies on glutamatergic excitation, with the eventual termination of these bursts dependent on slowly developing synaptic depression. The introduction of the pump component to their model led the authors to suggest two roles for the pump in the disinhibited rhythm. Firstly, within each disinhibited burst they suggest that the accumulation of intracellular sodium leads to pump activation, causing a hyperpolarisation that brings a significant number of neurons below firing threshold earlier to terminate bursting; and secondly, they suggest that the pump contributes an inter-burst hyperpolarisation that may activate conductances (such as Ih) responsible for the generation of the next burst (Rozzo *et al.*, 2002). These experimental and modelling data are interesting as they imply a temporal order for the mechanisms of fatigue in a spinal locomotor network in the context of spontaneous and evoked activity, with the pump-mediated hyperpolarisation generated earlier in time during a normal rhythmic burst than does synaptic depression (Rozzo *et al.*, 2002).

In a separate series of studies, the role of the sodium pump was explored in dissociated and organotypic cultured spinal neurons from the rat. Using single cell recordings directly from spinal interneurons, it was found that approximately half of the population of interneurons showed a spike-dependent hyperpolarisation during the inter-burst interval in a disinhibited rhythm, and spiking was suppressed during this hyperpolarised period of over 10 seconds (Darbon *et al.*, 2002). Moreover, they demonstrated clearly that this decrease in excitability was not due to synaptic depression (i.e. a depletion of transmitter or receptor desensitation), supporting the studies in whole-cord that suggest that pump-mediated refractory mechanisms dominate under control conditions. Finally, they also used an MEA electrode to electrically stimulate regions of cells, which generates a “bout” of rhythmic activity. The authors studied the effect that the stimulus interval had on the characteristics of the evoked output. They found

similar results to those found by Rozzo et. al (2002), whereby activity evoked too soon after a previous bursts (3-35 s) was shorter in duration and showed lower excitability (figure 8C). Overall, the authors suggest that in cultured neurons, the disinhibited rhythm depends on an unknown autoregulation mechanism that terminates bursts and lasts many seconds beyond each burst, although they do not at this point ascribe a role for the sodium pump.

The responsibility of the sodium pump for the phasic hyperpolarisations mentioned above was confirmed in a subsequent study (Darbon *et al.*, 2003). Using multi-electrode array (MEA) recordings, they found that blocking the pump with strophanthidin (10 µM) rapidly increased the frequency of disinhibition-induced bursting in both organotypic and dissociated cultures, increased the "background" activity between bursts, and decreased the amplitude of bursts. Over a longer period of time (> 10 mins), the burst rate then decreased. Using simultaneous whole-cell recordings from spinal interneurons, strophanthidin caused a depolarisation of around 20 mV. Note that the authors could replicate some of these network effects of blocking the pump simply by depolarising neurons of the network by systematically increasing extracellular potassium concentration. However, these effects were not identical, and more importantly, changing the potassium concentration is likely to have far-reaching effects beyond simply depolarising neurons.

Thus, the authors propose, like other studies, that sodium pump blockade has two effects: a depolarisation due to removal of tonic pump contribution; and the removal of a transient, inter-burst hyperpolarisation. In an attempt to differentiate these effects, the authors compared the effect of pump blockade in control conditions to the effect of pump blockade when the network is rhythmically activity (i.e. disinhibited). In control conditions, interneurons depolarised by around 12 mV. However, crucially, when they washed the strophanthidin off, and the membrane potential returned to control, the subsequent activation of disinhibited bursting caused a *hyperpolarisation* of around 8 mV that could be seen between each rhythmic burst. Moreover, when the pump blocker was then re-applied, the cells depolarised further than they did in control, this time by around 20 mV, which is the sum of the depolarisation in control plus

the hyperpolarisation caused by disinhibition (Figure 8Ai, ii). Taken together, the authors concluded that the rhythmic hyperpolarisations generated by disinhibition are entirely mediated by increased activity of the sodium pump, presumably due to the influx of sodium with each burst that resulted once the network was activated.

To corroborate these findings, the authors also simulated rhythmic activity to individual interneurons, in the absence of whole-network activity. The authors were actually investigating whether blocking the pump affected spike-frequency adaption, which it was, although indirectly due to the depolarisation described above. More interestingly, however, in performing these experiments they noted that there was a gradual hyperpolarisation of the membrane potential of around 6 mV when successive pulses were applied (Figure 8B), as long as the pulses generated repetitive spiking, but not when spiking was absent. The size of this hyperpolarisation was dependent on the number of spikes. This is a highly interesting finding, and is strong evidence that the pump contributes a dynamic component to the spinal locomotor rhythm, at least in these cultured neurons. The authors state that these dynamic pump currents induced by current injections were abolished by strophanthidin (whilst applying a holding current to compensate for the strophanthidin depolarisation), but they do not show these data. Also extremely important, but relatively understated, is the fact that the authors only observed the spike-dependent, long duration hyperpolarisation in a subset of interneurons (Darbon *et al.*, 2003), confirming the finding from the earlier study that inter-burst, spike-dependent pump hyperpolarisations were observed in roughly half of all spinal neurons (Darbon *et al.*, 2002). In light of more recent evidence on the roles of sodium pump subtypes, I suggest that it is likely that this heterogenous expression of a dynamic pump current may relate to the distribution of α3 sodium pump subtypes in the mammalian spinal cord.

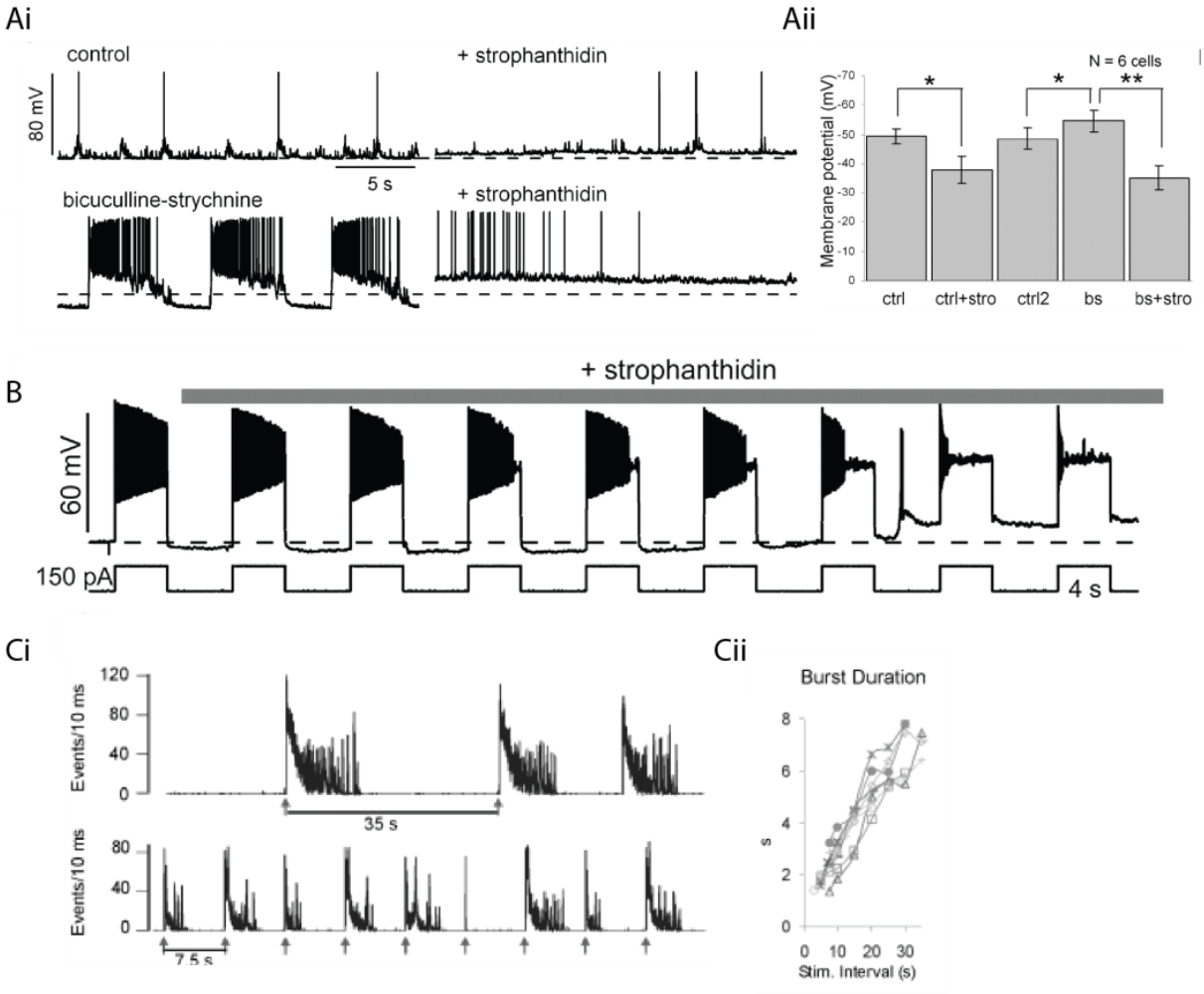

Figure 8. A rhythmic, sodium pump-mediated hyperpolarisation in rat spinal interneurons. Ai,ii. An intracellular recording from a rat spinal interneuron. The application of the sodium pump blocker strophanthidin caused a small depolarisation. Following strophanthidin washout, the subsequent induction of disinhibited bursting led to a phasic hyperpolarisation, which was removed by a second application of strophanthidin. Note that this final depolarisation is equal in value to the hyperpolarisation caused by disinhibition plus the depolarisation caused by the initial pump block, suggesting that phasic hyperpolarisations in a disinihibited rhythm are mediated by the sodium pump. Aii. Mean membrane potential values for the different conditions shown in **Ai. B.** An example of an intracellular interneuron recording showing rhythmic bursting induced by depolarising current pulses, which is removed by blocking the sodium pump. A and B taken from (Darbon *et al.*, 2003). **Ci.** Network activity plots from MEA recordings from cultured spinal interneurons showing the effect of inter-burst interval on the duration of stimulated bursts. **Cii.** Plot of the burst duration against the stimulus interval. C taken from (Darbon *et al.*, 2002).

Although there are relatively few studies on the role of the sodium pump in the mammalian locomotor CPG, the results from these initial studies provide a solid theoretical framework for this thesis. To summarise the findings, bursting in the disinhibited rhythm in the spinal locomotor CPG relies upon recurrent excitation for each burst, but the burst termination relies upon a Na^+-spike dependent pump hyperpolarisation which lasts many seconds and dictates the inter-burst interval. Synaptic depression has been shown consistently not to mediate this

decrease in excitability (Darbon *et al.*, 2002, 2003; Rozzo *et al.*, 2002). During rhythmic activity, blockade of the pump eliminates this dynamic pump current, as well as depolarises spinal neurons, to mediate an increase in the frequency of the bursting rhythm. Because of the long duration of the sodium pump current, activity evoked shortly after previous activity is shorter in duration due to the influence of the pump current on excitability.

Interactions between dopamine and the sodium pump

The involvement of the Na^+/K^+-ATPase in a range of cellular functions is accompanied by the requirement for both short- and long-term regulation to adjust to physiological and environmental changes. This is especially true for neuronal sodium pumps, where both the steady-state pump rate and the dynamic relationship between neuronal firing and pump activity have been shown to be under the modulatory control of neurotransmitters, hormones and other neuromodulators (Therien & Blostein, 2000). Earlier in this introduction I outlined a number of examples where sodium pumps are targeted by neuromodulators including pump modulation by myomodulin and 5-HT in the leech (Catarsi *et al.*, 1993; Tobin & Calabrese, 2005); by calcium at the Calyx of Held (Kim *et al.*, 2007); by NO in midbrain dopaminergic neurons (Cox & Johnson, 1998); and by ethanol in the cerebellum (Forrest, 2015). Dopamine is also a common modulator of sodium pumps, although most research so far has focused on the modulation of sodium pumps in kidney and cardiac tissue (Therien & Blostein, 2000).

Dopamine, usually acting via PKA or PKC, can enhance or inhibit pump activity depending on the species, tissue type and the dopamine receptors involved (Zhang *et al.*, 2013). In striatal neurons, for example, the activation of D2-like receptors stimulates the sodium pump by inhibiting PKA and thus dephosphorylating the α3 subunit; D1 receptor activation, on the other hand, causes long-term inhibition of α3 pump activity by increasing PKA-mediated phosphorylation (Bertorello *et al.*, 1990; Wu *et al.*, 2007). Other studies have similarly shown that changes in PKA activation in neurons can modulate the ability of a neuron to respond to changes in intracellular sodium through phosphorylation/dephosphorylation of α3 (Azarias *et*

al., 2013). Interestingly, sodium pumps in the brain are also known to form a complex (or "signalplex") with D1 and D2 dopamine receptors to allow *direct* reciprocal modulation between dopamine receptors and the pump (Hazelwood *et al.*, 2008).

Research framework

Across the main model systems for studying motor control, such as lamprey, zebrafish and mice, there is a comprehensive picture of the role of dopamine as a neuromodulator of locomotion (see earlier). However, whilst young *Xenopus* tadpoles are one of the best defined and understood vertebrate models in the motor control field, almost nothing is known about how dopamine acts as a neuromodulator at this early stage of development. Thus, the first chapter of this thesis aims to fill this gap in understanding and will use ventral root and single-cell recordings to explore the network effects of dopamine, as well as the cellular mechanisms which underlie these effects on overall locomotor output.

Secondly, I will further explore the role of the sodium pump in *Xenopus* tadpoles from what is already known (Zhang & Sillar, 2012), and particularly how the pump can be modulated by intracellular sodium, dopamine, nitric oxide, and temperature. Although the core role of the sodium pump has been defined previously, the role of these factors in influencing sodium pump activity in the *Xenopus* spinal cord remains unexplored, and this is the focus of the second chapter of this thesis. In addition, this chapter will also focus on the role of Ih current in *Xenopus* spinal neurons, which has not previously been characterised.

Thirdly, I will explore the almost completely unexplored role of the sodium pump in the locomotor network of neonatal mice. Using ventral root recordings from isolated spinal cords from neonatal mice, I will explore the effects of sodium pump manipulation on drug-induced locomotor bursting, as well as the effects on locomotor-like activity evoked by patterns of dorsal root stimulation. Finally whilst the effects of dopamine on network output are relatively well understood in this system, I will explore the possibility that dopamine underlies some of these network effects through actions on the sodium pump in the mouse spinal cord.

This thesis is somewhat unusual in that it implements two evolutionarily diverse model systems: *Xenopus* tadpoles and neonatal mice. Modern amphibians and mammals share a common ancestor that existed around 360 million years ago, and therefore comparisons between these two systems are at best, speculative. However, the evidence suggests that the amphibian and mammalian genomes are in fact surprisingly similar (Hellsten *et al.*, 2010), suggesting that whilst the two groups have obviously diverged massively since they split 360 m.y.a., the underlying nuts and bolts of the nervous system may share similar features, at least at the single cell level. Indeed, the neuronal sodium pump in particular is extremely well conserved between vertebrates (Takeyasu *et al.*, 1990; Dobretsov & Stimers, 2005), and the results presented in this thesis suggest a conserved role for the sodium pump in the spinal cord of tadpoles and mice, as well as a similar excitatory role for dopamine as a spinal modulator of the sodium pump. As humans, we split from our common ancestor with mice only 65 million years ago, and so one can speculate that the sodium pump may play a similar role in neuronal self-regulation as it does in leech, lamprey, fruit-flies, tadpoles and mice.

Chapter 1: Mechanisms underlying the endogenous dopaminergic inhibition of spinal locomotor circuit function in *Xenopus* tadpoles

Chapter 1 contributions and publications

This chapter is adapted from previously published work (Picton & Sillar (2016) Scientific Reports). All experiments were conducted by Laurence Picton.

Chapter 1 summary

Dopamine plays important roles in the development and modulation of motor control circuits, yet no previous studies have explored the role of dopamine in the modulation of *Xenopus* tadpole swimming at early stages of development. In this chapter I show that dopamine exerts potent effects on the central pattern generator circuit controlling locomotory swimming in post-embryonic *Xenopus* tadpoles. Using ventral root recordings, I show that dopamine (0.5-100 µM) reduced fictive swim bout occurrence and caused both spontaneous and evoked episodes to become shorter, slower and weaker. The D2-like receptor agonist quinpirole mimicked this repertoire of inhibitory effects on swimming, whilst the specific D4 receptor antagonist, L745,870, had the opposite effects. The dopamine reuptake inhibitor bupropion also potently inhibited fictive swimming, demonstrating that dopamine constitutes an endogenous modulatory system. Both dopamine and quinpirole also inhibited swimming in spinalised preparations, suggesting that the dopamine receptors involved in this inhibition are located in the spinal cord. Using whole-cell patch clamp recordings, I show that dopamine and quinpirole hyperpolarised identified rhythmically active spinal neurons, increased the minimum current needed to induce an action potential (rheobase), and reduced spike probability both during swimming and in response to current injection. The hyperpolarisation was TTX-resistant and was accompanied by decreased input resistance, suggesting that dopamine opens a K^+ channel. The K^+ channel blocker barium chloride (but not TEA, glybenclamide or tertiapin-Q) significantly occluded the hyperpolarisation. Overall, I show that endogenously released dopamine acts upon spinally located D2-like receptors, leading to a rapid inhibitory modulation of swimming via the opening of a K^+ channel with GIRK-like pharmacology.

Chapter 1 introduction

As outlined in the main introduction, neural circuits of the spinal cord that generate rhythmic locomotor activity (central pattern generators (CPGs)) are subject to profound modulatory influences which alter neuronal properties and synaptic strengths to confer flexibility on locomotor output and behaviour (Harris-Warrick, 2011). Sources of neuromodulators are present both intrinsically within the spinal cord and extrinsically in higher centres of the brainstem, and include classical neurotransmitters, peptides, biogenic amines and the gaseous free radical nitric oxide (for a recent review see (Miles & Sillar, 2011)). The biogenic amines serotonin, noradrenaline and dopamine, emanating primarily from brainstem nuclei, form diffuse modulatory systems that project to spinal sensory and motor circuits and are known to modulate CPG output. Many neuromodulators exert their influences by activation of more than one pharmacologically distinct subset of GPCRs with distinct physiological actions. Dopamine, which is a widely distributed and phylogenetically conserved neuromodulator, acts upon two principal classes of receptor which generally exert inhibitory (D2-like: D2,D3,D4) or excitatory (D1-like: D1,D5) influences on neural circuits (Beaulieu & Gainetdinov, 2011).

Dopaminergic fibres forming descending tracts from the brain offer a rich source of neuromodulatory input to the axial locomotor circuits in the spinal cords of aquatic vertebrates (lamprey (McPherson & Kemnitz, 1994) and zebrafish (Thirumalai & Cline, 2008; Jay *et al.*, 2015)); amphibian tadpoles (Clemens *et al.*, 2012), and the appendicular spinal circuits of mammals (Han *et al.*, 2007). The diencephalic dopaminergic tract (DDT) forms a phylogenetically conserved descending projection which is present in all vertebrates studied to date and provides the earliest developing aminergic projection to the spinal cord (McLean & Fetcho, 2004*b*). In zebrafish, endogenous dopamine plays important roles in establishing the complement of CPG neurons early in development (Reimer *et al.*, 2013). Dopamine also subsequently controls the developmental expression of motor pattern generation by acting on a range of dopamine receptors (Thirumalai & Cline, 2008; Lambert *et al.*, 2012; Jay *et al.*, 2015). In free-swimming larval *Xenopus laevis* tadpoles, dopamine has opposing,

concentration-dependent effects on swimming: low dopamine concentrations activate high affinity D2-like receptors to inhibit spontaneous locomotor activity; while high dopamine concentrations facilitate locomotion by activating lower affinity D1-like receptors (Clemens *et al.*, 2012). However, this previous research on older, pre-metamorphic free swimming stages of tadpole development was obtained using extracellular ventral root recordings and did not address the cellular mechanisms responsible for dopamine's actions in the spinal cord or the developmental onset of the dopaminergic system.

In the present chapter I have examined the role of dopamine at earlier stages of *Xenopus* development, around the time of hatching, when the animal possesses a simpler and much better defined spinal locomotor circuit (Roberts *et al.*, 2010). Neurons immunoreactive for tyrosine hydroxylase (TH) are known to be present in the mesencephalic posterior tuberculum (PT), the spinal cord and other areas of the CNS at these early stages of development (Velázquez-Ulloa *et al.*, 2011), but the role of the dopaminergic system at these stages remains unknown. I show that dopamine profoundly and rapidly inhibits swimming even at the highest concentration tested, suggesting a preponderance of D2-like receptors and a paucity of D1-like receptors early in development. These receptors are expressed on rhythmically active spinal cord neurons and can be activated by endogenously released dopamine when uptake is inhibited, or through the application of the D2-like receptor agonist quinpirole. Conversely, I show that D4 receptor antagonism has excitatory effects on the swim network, highlighting the constitutive nature of dopaminergic signalling in the *Xenopus* spinal cord. I show that the inhibition of locomotor activity is due mainly to a direct, TTX-resistant postsynaptic hyperpolarization of a range of identified spinal CPG neurons associated with an increase in membrane conductance. I provide evidence that this hyperpolarisation is due to the opening of an inwardly rectifying K^+ channel, with GIRK-like pharmacology. Thus, dopamine's rapid inhibition of the swim network occurs via a mechanism that is unlikely to involve a slower, classical G protein/2nd messenger cascade, but instead likely involves a membrane delimited coupling to K^+ channels.

Chapter 1 materials and methods

Experimental animals

All experiments conformed to UK Home Office regulations and were approved by the Animal Welfare Ethics Committee (AWEC) of the University of St Andrews. All experiments were performed on newly hatched pre-feeding *Xenopus laevis* tadpoles at developmental stage 37/38 or 42 (Nieuwkoop & Faber, 1956). Tadpoles were reared from fertilized ova obtained following breeding of adults selected from an in-house colony. Mating was induced by injections of human chorionic gonadotropin (HCG, 1000 U/ml, Sigma-Aldrich, Poole, UK) into the dorsal lymph sac of breeding pairs of adult frogs. The injection of HCG into adult frogs is a licensed procedure and was performed by myself using a personal license (personal license number: PIL 60/13743).

Electrophysiology

Xenopus tadpoles were immobilized by gashing the skin using a sharpened tungsten needle before placing in 12.5 μM α-bungarotoxin saline for approximately 30 minutes, and then mounted on a rotatable Sylgard platform in a bath of saline (in mM: 115 NaCl, 2.5 KCl, 2 $CaCl_2$, 2.4 $NaHCO_3$, 1 $MgCl_2$, 10 HEPES, adjusted with 4 M NaOH to pH 7.4). Both sides of the trunk skin overlying the myotomal muscles were removed using a finely etched needle and forceps. The dorsal parts of approximately 7 rostral myotomes were freed from the spinal cord and the roof of the hindbrain and spinal cord was opened to the neurocoel to improve drug access and provide access for patch clamp electrodes. For whole-cell current clamp recordings, exposed neuronal somata were patch clamped using borosilicate glass pipettes (Harvard Apparatus Ltd) pulled on a Sutter P97 pipette puller. Patch pipettes were filled with 0.1% neurobiotin (Vector labs, Peterborough, UK) in the intracellular solution (in mM: 100 K-gluconate, 2 $MgCl_2$, 10 EGTA, 10 HEPES, 3 Na_2ATP, 0.5 NaGTP adjusted to pH 7.3 with KOH) and had resistances of ~10 MΩ. Changes in membrane potential were recorded in current clamp mode using an Axoclamp 2B amplifier. Simultaneous extracellular recordings of fictive swimming were made with suction electrodes from ventral roots at intermyotomal clefts, and signals were

amplified using differential AC amplifiers (A-M Systems Model 1700). Simultaneous intracellular and extracellular signals were digitized using a CED Power 1401, and displayed and stored on a PC computer using Spike 2 software. Fictive swimming was initiated by stimulating through a glass suction electrode placed on the tail skin, which delivered a 1 ms current pulse via a DS2A isolated stimulator (Digitimer, Welwyn Garden City, UK).

Pharmacological agents

All drugs were obtained from Sigma-Aldrich (Poole, UK) or Tocris Bioscience (Bristol, UK) and bath-applied to the preparation. Dopamine hydrochloride (Sigma-Aldrich, Poole, UK) was always made up in distilled H_20 prior to the experiment (<1 hour) and stored on ice in the dark to minimise oxidation. All other drugs were made up to stock concentrations and frozen in aliquots, defrosted before an experiment, and diluted to final concentrations. Quinpirole hydrochloride (Tocris Bioscience, Bristol, UK) and Bupoprion hydrochloride (Tocris Bioscience, Bristol, UK) were both dissolved in distilled H_20. L745,870 trichydrochloride (Tocris Bioscience, Bristol, UK) was dissolved in DMSO.

Data analysis

Electrophysiological data were first analysed using dataview software (v 10.3.0, courtesy of Dr. W. J. Heitler) and all raw data were imported into Excel spreadsheets and analysed. Statistical analyses were conducted using PASW statistics 21. A rest time of 2 minutes was given between evoked episodes of swimming to ensure each episode was not influenced by preceding activity (Zhang & Sillar, 2012; Zhang *et al.*, 2015). For swim episode duration analysis, a mean of 3 consecutive evoked episodes in each condition was calculated. For intra-episode swim parameters (cycle frequency, burst duration, burst amplitude) a mean of the first 20 cycles of swimming across 3 episodes was calculated for each condition. For analysis of spontaneous swimming I calculated the number of spontaneously occurring swim episodes in a 20 min period in each condition. To calculate spike probability the number of action potentials in the first 50 cycles of swimming in an episode was measured and this value was divided by the number of cycles. For all experiments, values are displayed as mean ±

SEM and unless otherwise stated conditions were compared using either paired t-tests or repeated measures ANOVAs followed by Bonferonni-corrected post-hoc comparison. For patch clamp data where I obtained a wash value in only a subset of experiments, only the individual wash values are displayed but not the mean value.

Neuron identification

Following patch-clamp recordings, animals were fixed in 2% glutaraldehyde in 0.1 M phosphate buffer, pH 7.2, overnight in a refrigerator (~4°C). Animals were first rinsed with 0.1 M PBS (120 mM NaCl in 0.1 M phosphate buffer, pH 7.2), and washed in two changes of 1% Triton X-100 in PBS for 15 min with agitation. Next, animals were incubated in a 1:300 dilution of extravidin peroxidase conjugate in PBS containing 0.5% Triton X-100 for 2–3 hours with agitation, and washed again in at least four changes of PBS. Animals were then immersed in 0.08% diaminobenzidine in 0.1 M PBS (DAB solution) for 5 min, moved to a DAB solution with 0.075% hydrogen peroxide for 1-2 min, and then washed in running tap water. Finally, animals were dehydrated in 100% alcohol, cleared in methyl benzoate and xylene, and mounted whole between two coverslips using Depex. Neuronal cell bodies and axon processes were observed under a x40 objective to identify CPG neuron types.

Chapter 1 results

Dopamine inhibits the parameters of fictive swimming

In an initial set of experiments, dopamine was bath-applied to immobilized *Xenopus* tadpoles at a range of concentrations to assess its modulatory influence on spontaneous and electrically evoked episodes of fictive swimming. In keeping with a previous report on older free swimming *Xenopus* tadpoles (Clemens *et al.*, 2012), low concentrations of dopamine (0.5 – 5 µM) reduced the probability of occurrence of spontaneous swimming episodes (Figure 1Cii). In addition, and in contrast to older stages, several parameters of both spontaneous and evoked fictive swimming were also reduced in the presence of a low dose of dopamine including swim episode duration (Figure 1Ci) and cycle period (Figure 1B, Ciii). These effects of dopamine were partially reversible after approximately 30 mins return to control saline, although at this time point the recovery only reached statistical significance for swim cycle frequency. Next, higher dopamine concentrations (50 - 100 µM) were applied to address whether, as in older tadpole stages, the effects of dopamine switch to become excitatory at high doses. However, only the inhibitory effects of dopamine were observed (Figure 1A,Di-v), and even exaggerated at the higher doses, suggesting that a D2-like effect alone is present at these early stages of development. Compared to other modulators in this preparation, such as serotonin and noradrenaline (McDearmid *et al.*, 1997), the onset of the effects of dopamine on swimming activity occurred extremely rapidly (<1 minute after entering the bath). In addition to effects on the parameters of swimming, dopamine also increased the sensory threshold for evoking swimming, as evidenced by the increase in the number and intensity of stimulation pulses needed to trigger swimming in Figure 1A, middle trace. However, this aspect of dopamine modulation was not studied in more detail here.

Figure 1. Dopamine inhibits fictive swimming across a range of concentrations. Top: The experimental preparation. **A:** Raw traces showing evoked and spontaneous episodes of fictive swimming in control, in the presence of 50 µM dopamine and after dopamine wash-out. “s” denotes spontaneous swim episodes and “*” denotes tail stimulus. **B:** Raw traces showing 500 ms of activity at the start of an evoked episode in control, in dopamine (50 µM) and after dopamine washout. Note that the swimming is slower and weaker in dopamine compared to control and wash. **C:** A low concentration of dopamine (5 µM) significantly reduced episode duration (i: $p<0.05$, $n=6$); the number of spontaneous episodes of swimming (ii: $p<0.05$, $n=3$); and swim frequency (iii: $p<0.05$, $n=6$). **D:** A high concentration of dopamine (50 µM) was also inhibitory and significantly reduced episode duration (i: $p<0.05$, $n=8$); the number of spontaneous episodes of swimming (ii: $p<0.05$, $n=6$); swim frequency (iii: $p<0.05$, $n=8$); and burst durations (ii; $p<0.05$, $n=5$).

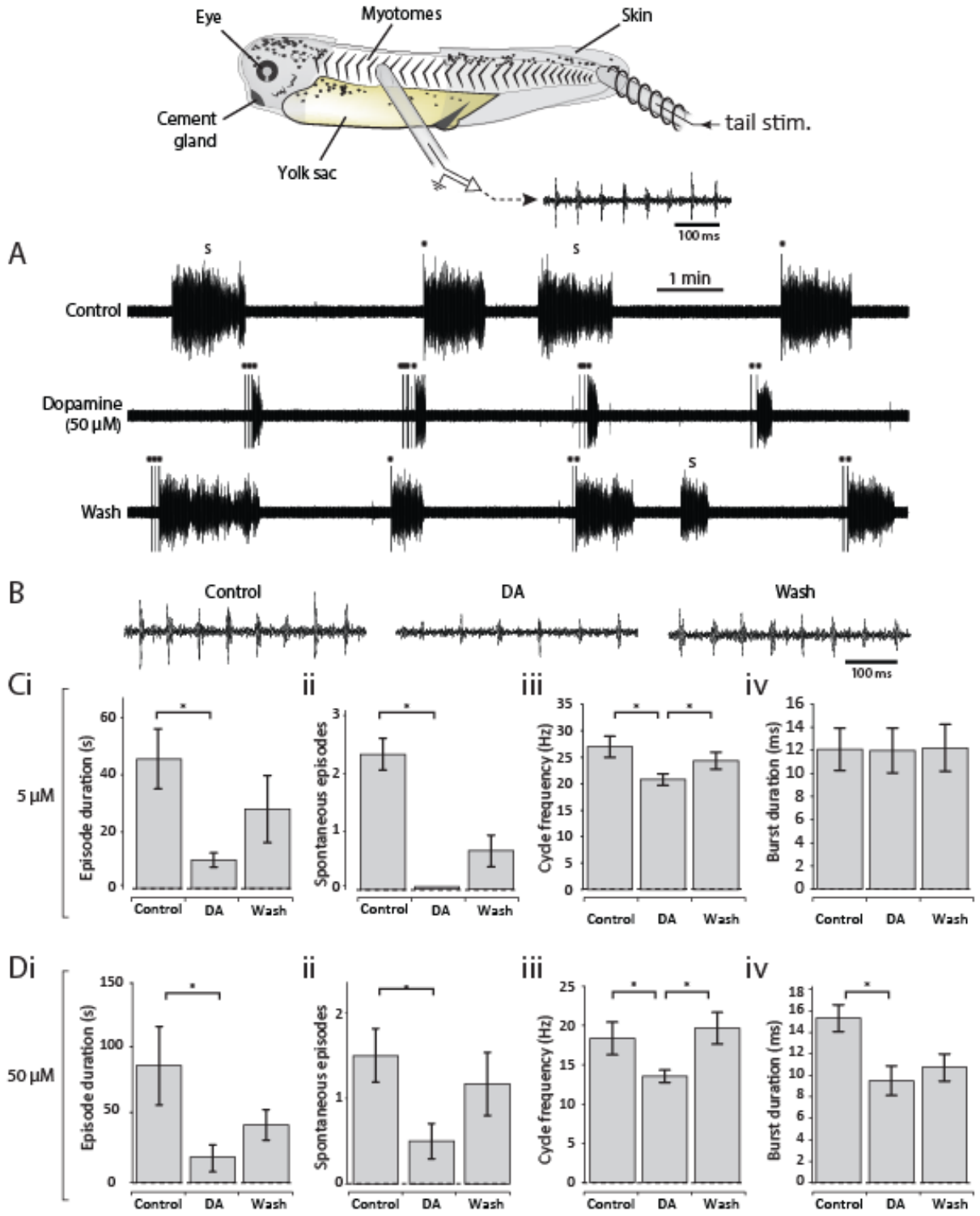
Eye
Myotomes
Skin
Cement gland
Yolk sac
tail stim.
100 ms
A
Control
Dopamine (50 µM)
Wash
1 min
B
Control
DA
Wash
100 ms
Ci
5 µM
Episode duration (s)
Spontaneous episodes
Cycle frequency (Hz)
Burst duration (ms)
Control
DA
Wash
Di
50 µM
Episode duration (s)
Spontaneous episodes
Cycle frequency (Hz)
Burst duration (ms)
Control
DA
Wash

Dopamine inhibition is mediated via D2-like receptors in the spinal cord

Dopamine acts upon two principal classes of receptor which generally exert inhibitory (D2-like: D2,D3,D4) or excitatory (D1-like: D1,D5) influences on neural circuits. To confirm that the inhibitory effects of dopamine on the *Xenopus* swim circuit are indeed mediated via actions at D2-like receptors, the broad-spectrum D2-like agonist quinpirole (25 µM) was bath applied. Quinpirole faithfully mimicked all of the effects of dopamine by rapidly reducing the occurrence of spontaneous episodes of fictive swimming and inhibiting the same parameters of motor output including cycle period, burst duration and burst amplitude (Figure 2A, Ci-iv). The fact that quinpirole and dopamine effects were qualitatively the same suggests that the effects of dopamine are exclusively mediated at D2-like receptors at this early stage of development. This conclusion is supported by the fact that the D1 agonist SKF38393 (2 µM) exerted no overall significant effects on any of the parameters of the fictive swimming rhythm at these early stages of development (Figure 2B, Di-iv).

In order to investigate whether the D2-like receptors mediating inhibitory effects on the tadpole swim CPG are located in the spinal cord and/or in higher brain centres, the immobilized preparation was spinalized at the level of the 2nd post-otic intermyotomal cleft (Figure 2Ei). This procedure leaves sufficient rhythm generating circuitry in the spinal cord to produce sustained swim episodes in response to skin stimulation (Li *et al.*, 2006), but removes the influence of descending brainstem pathways, abolishes spontaneous episodes and regularizes swim episode parameters. Quinpirole (25 µM) continued to exert as profound an inhibitory effect on fictive swimming as intact preparations (Figure 2Ei-iii), indicating that the D2-like receptors involved in dopamine modulation are located on CPG neurons of the spinal cord.

Figure 2. The inhibitory effects of dopamine on the swim network are mediated via spinal D2-like receptors. Ai: Raw trace showing the effect of the D2-like agonist quinpirole (25 µM) on fictive swimming. **Aii:** Raw trace showing a 500 ms excerpt of activity in control, in the presence of quinpirole, and after washout. **B:** Raw trace showing the lack of effects of the D1-like agonist SKF38393 (2 µM). **C:** Quinpirole (25 µM) significantly reduced episode duration (i: $p<0.05$, n=9), the number of spontaneous episodes of swimming (ii: $p<0.05$, n=4), swim frequency (iii: $p<0.001$, n=9) and burst durations (iv; $p<0.05$, n=6). **D.** Overall, SKF38393 (2 µM) had no significant effects on episode duration (i: $p>0.05$, n=11), spontaneous swimming (ii: $p>0.05$, n=10), swim frequency (iii: $p>0.05$, n=11) or burst durations (iv; $p>0.05$, n=9). **E.** Quinpirole (25 µM) still had an inhibitory effect on episode durations (ii, $p<0.05$, n=5) and cycle frequency (iii, $p<0.01$, n=5) in tadpoles that had been spinalised at the level of the 2nd post-otic intermyotomal cleft, suggesting that inhibitory D2-like receptors are present in the spinal cord. Note that spinalisation removes spontaneous swimming and shortens burst durations, and therefore data on these parameters is not shown.

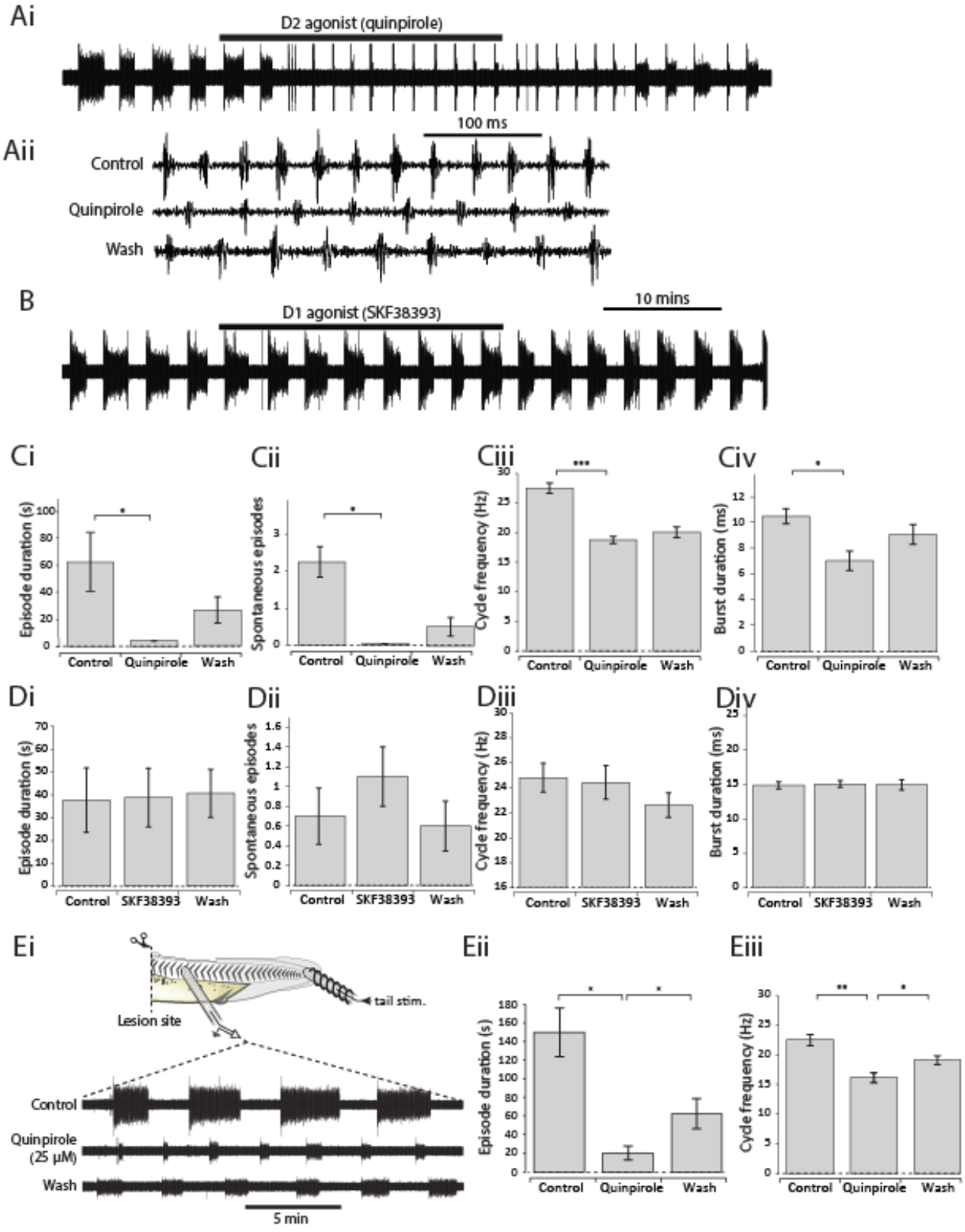
Ai
D2 agonist (quinpirole)
Aii
100 ms
Control
Quinpirole
Wash
B
D1 agonist (SKF38393)
10 mins
Ci
Episode duration (s)
Control
Quinpirole
Wash
Cii
Spontaneous episodes
Ciii
Cycle frequency (Hz)
Civ
Burst duration (ms)
Di
SKF38393
Dii
Diii
Div
Ei
tail stim.
Lesion site
Control
Quinpirole
(25 µM)
Wash
5 min
Eii
Eiii

Endogenously released dopamine inhibits swimming

To test the extent to which endogenously released dopamine can inhibit swimming, the dopamine reuptake inhibitor bupropion (100 µM, (Svensson *et al.*, 2003)) was bath-applied (Figure 3). The time to onset of bupropion effects were longer than those of dopamine or quinpirole (Figure 3Aii), as might be expected, but within 20 to 30 minutes of application there was a clear reduction in spontaneous episode occurrence (Figure 3Ai, Cii) and the range of inhibitory effects on swim parameters observed in the agonist experiments were replicated (Figure 3B-D). The effects of bupropion were partially reversible upon return to control saline. These data strongly suggest that endogenously released dopamine, acting on D2-like receptors on spinal neurons, can inhibit swimming in young *Xenopus* frog tadpoles.

D4 receptor antagonism has excitatory effects on the swim network

Next I wanted to test whether tonic release of dopamine inhibits the network constitutively. Amongst the inhibitory D2-like receptors (D2,D3,D4), the D4 receptor has been previously shown to play an especially important role in regulating spinal swim circuitry (Lambert *et al.*, 2012). Therefore, I bath-applied the specific D4 receptor antagonist L745,870 (10 µM) and assessed its effects on fictive swimming. L745,870 caused a dramatic increase in the occurrence of spontaneous swim episodes (Figure 4Ai, Bii). Moreover, swim episodes in the presence of L745,870 were both significantly longer in duration (Figure 4Ai, Bi), and had a higher swim cycle frequency (Figure 4Aii, Ci). I found no overall effect on burst duration (Figure 4Cii). Overall, however, blockade of the D4 receptor results in the opposite effects to dopamine and quinpirole on most parameters of fictive swimming, suggesting that dopamine is constituitively released onto the *Xenopus* spinal cord where it acts, at least in part, via activation of the D4 receptor.

Figure 3. Endogenously released dopamine inhibits swimming. Ai: Raw trace of fictive swimming showing an entire 2 hour experiment. The application of 100 µM bupropion clearly inhibited swimming after approximately 20 minutes. **Aii:** A comparison of the effect onset in a bupropion experiment and a dopamine experiment. **B:** Raw traces showing 500 ms of activity at the start of an evoked episode in control, 100 µM bupropion, and following drug washout. **C:** Bupropion (100 µM) significantly reduced episode duration (i: $p<0.01$, $n=13$) and the number of spontaneous episodes of swimming (ii: $p<0.05$, $n=4$). **D.** Bupropion (100 µM) also significantly reduced swim frequency (i: $p<0.001$. $n=13$) and burst durations (ii: $p<0.05$. $n=5$).

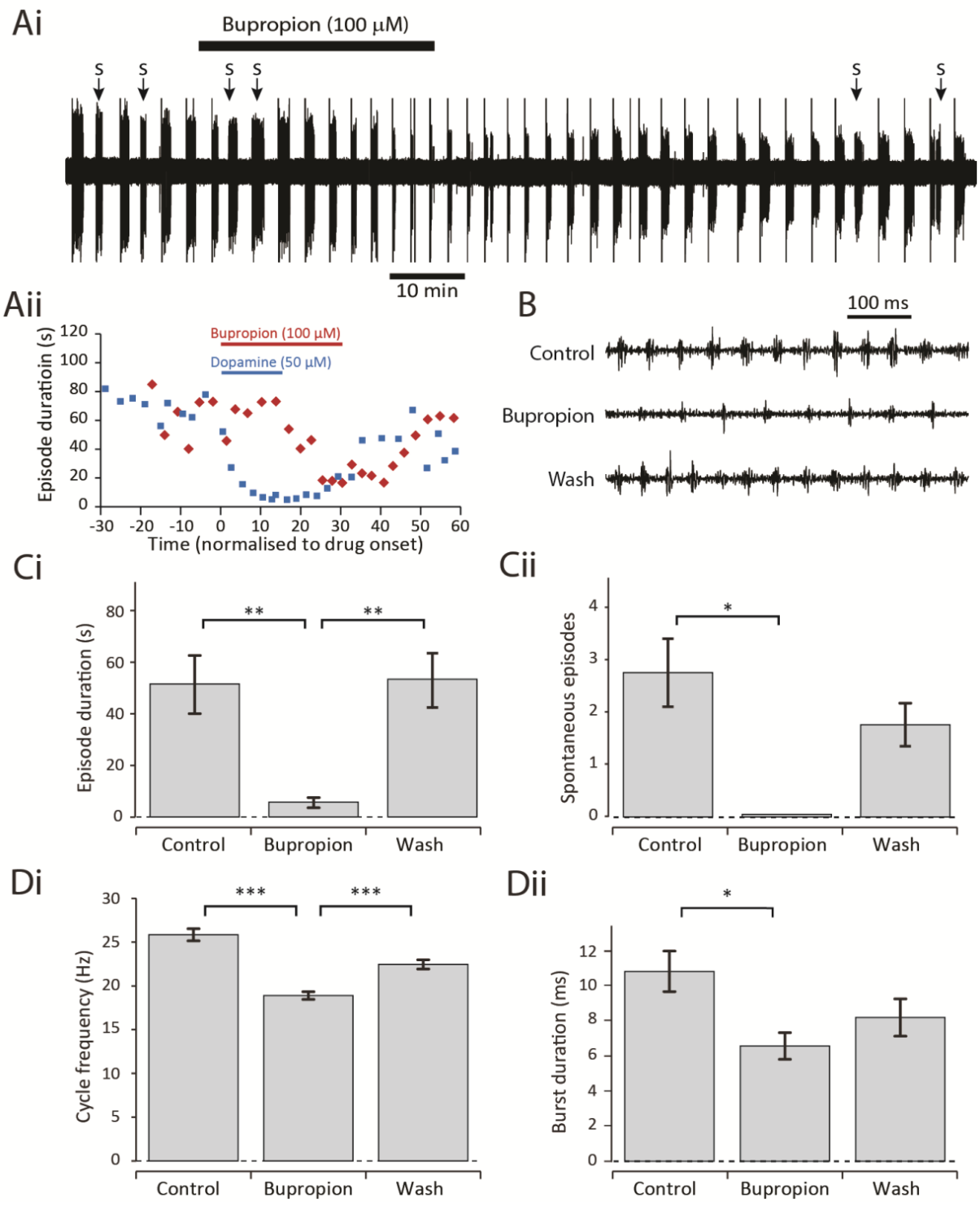
Ai
Bupropion (100 µM)
S
10 min
Aii
Episode duratioin (s)
Bupropion (100 µM)
Dopamine (50 µM)
Time (normalised to drug onset)
B
100 ms
Control
Bupropion
Wash
Ci
Episode duration (s)
Control
Bupropion
Wash
Cii
Spontaneous episodes
Control
Bupropion
Wash
Di
Cycle frequency (Hz)
Control
Bupropion
Wash
Dii
Burst duration (ms)
Control
Bupropion
Wash

Figure 4. The D4 antagonist L745,870 has the opposite effects to dopamine and quinpirole. A. Raw trace of fictive swimming showing an entire experiment. The application of 10 µM L745,870 has a clear excitatory effect on swimming. **Aii:** Raw traces showing ~500 ms of activity at the start of an evoked episode in control, 10 µM L745,870, and following drug washout. **B:** L745,870 (10 µM) significantly increased episode duration (i: $p<0.01$, n=8) and the number of spontaneous episodes of swimming (ii: $p<0.01$, n=7). **C.** L745,870 (10 µM) also significantly reduced swim frequency (i: $p<0.01$. n=8) but had no significant effect on burst durations (ii: $p>0.05$. n=7).

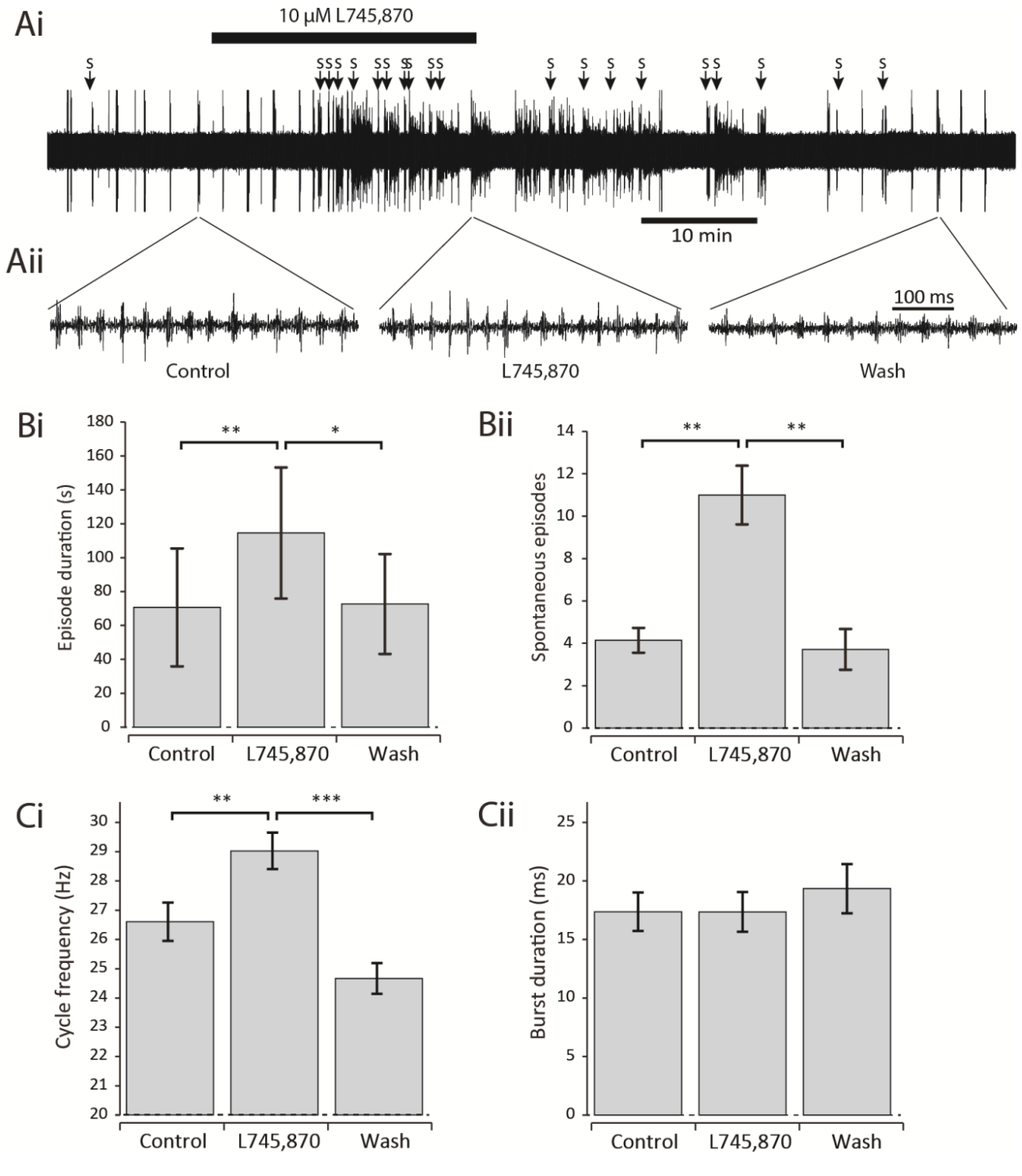
Ai
10 µM L745,870
10 min
Aii
100 ms
Control
L745,870
Wash
Bi
Episode duration (s)
Bii
Spontaneous episodes
Ci
Cycle frequency (Hz)
Cii
Burst duration (ms)

Cellular effects of D2-like receptor activation

Having established that dopamine acts via an intrinsically active pathway on D2-like receptors in the spinal cord to profoundly inhibit fictive swimming, I next wanted to explore the cellular mechanisms responsible for this network inhibition. Therefore, patch clamp recordings were made from spinal neurons that are rhythmically active during fictive swimming (e.g., Figure 5A). The most immediate effect of D2-like receptor activation was a rapid and reversible membrane potential hyperpolarization of spinal neurons. During the quiescent periods between swim episodes, dopamine (50 µM) reversibly hyperpolarized the membrane potential by up to 7 mV (Figure 5Bi,Biii, mean change = 3.6±0.4 mV; $p<0.001$, n=8). Furthermore, I found that this hyperpolarization was accompanied by an increase in membrane conductance, as evidenced by reduced voltage deflections in response to constant amplitude hyperpolarizing current pulses (Figure 5Bii,Biv, $p<0.05$, n=8), which also significantly reversed upon washout. Quinpirole (25 µM) application similarly hyperpolarized the membrane potential (Figure 5Ci,Ciii; mean change = 3.5±0.3 mV; $p<0.001$, n=18), again accompanied by an increase in membrane conductance (Figure 5Cii,Civ; $p<0.05$, n=18). The hyperpolarisation and decrease in input resistance induced by quinpirole persisted when applied in the presence of 1 µM TTX to block sodium spikes and therefore spike-mediated transmission (n=5). This in turn suggests a direct postsynaptic effect of D2 receptor activation. Overall these data strongly suggest that the dopamine hyperpolarization of spinal neurons is mediated through the D2-like receptor-coupled opening of an ion channel, most likely a K^+ channel.

Figure 5. Activation of D2-like receptors hyperpolarises rhythmically active spinal neurons and decreases their input resistance. A: The experimental preparation for making patch clamp recordings with simultaneous ventral root recordings. An intracellular recording of a rhythmically active spinal neuron is shown, with the ventral root trace shown below. The cell is the same as shown in Ci. **Bi.** Representative trace showing a hyperpolarisation caused by 50 µM dopamine in a rhythmically active spinal neuron. **Bii.** Traces showing the membrane response to a 20 pA hyperpolarising current pulse under each condition. Six responses (sweeps) are overlaid for each condition. **Biii.** Pooled data showing a significant hyperpolarisation of resting membrane potential in the presence of 50 µM dopamine ($n=8$, $p<0.001$) which significantly reversed upon washout ($p<0.001$). **Biv.** Pooled data showing a significant reduction in input resistance in the presence of dopamine ($n=8$, $p<0.05$) which significantly reversed upon washout ($p<0.05$). **Ci.** Representative trace showing a hyperpolarisation caused by 25 µM quinpirole in the presence of TTX. Note also the reduction in frequency of spontaneous synaptic potentials. **Cii.** Traces showing membrane responses to a 20 pA hyperpolarising current pulse. Six responses (sweeps) are shown overlaid for each condition. **Ciii.** Pooled data showing a significant hyperpolarisation in the presence of 25 µM quinpirole ($n=18$, $p<0.001$). **Civ.** Pooled data showing a significant reduction in input resistance in the presence of quinpirole ($n=18$, $p<0.05$).

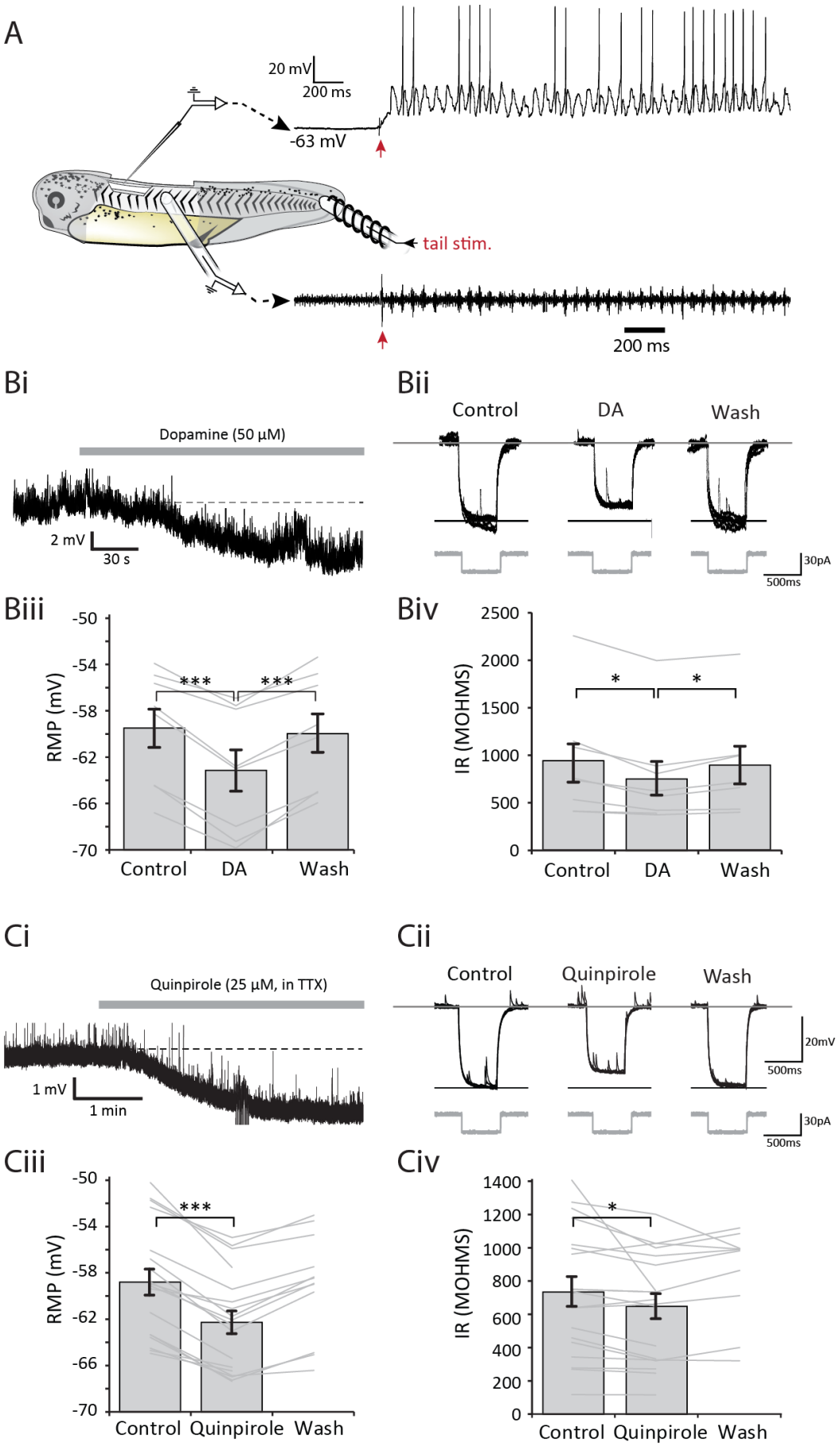
A
20 mV
200 ms
-63 mV
tail stim.
200 ms
Bi
Dopamine (50 µM)
2 mV
30 s
Bii
Control
DA
Wash
30pA
500ms
Biii
RMP (mV)
-50
-54
-58
-62
-66
-70
***
***
Control
DA
Wash
Biv
IR (MOHMS)
2500
2000
1500
1000
500
0
*
*
Control
DA
Wash
Ci
Quinpirole (25 µM, in TTX)
1 mV
1 min
Cii
Control
Quinpirole
Wash
20mV
500ms
30pA
500ms
Ciii
RMP (mV)
-50
-54
-58
-62
-66
-70
***
Control
Quinpirole
Wash
Civ
IR (MOHMS)
1400
1200
1000
800
600
400
200
0
*
Control
Quinpirole
Wash

Evidence for the activation of a GIRK-like channel by dopamine

To investigate the possibility that dopamine opens a K^+ channel in spinal neurons, a range of pharmacological blockers of different K^+ channel subtypes was applied in the presence of TTX to test which, if any, could occlude the subsequent quinpirole effect on membrane potential (Figure 6). TEA had no effect on quinpirole's ability to hyperpolarize spinal neurons (Figure 6C, n=3, $p>0.05$), suggesting that voltage- and calcium-dependent K^+ channels are unlikely to be involved. In contrast, barium chloride (BaCl), a broad spectrum blocker of inward-rectifying K^+ channels, significantly occluded quinpirole's effect on membrane potential in a dose-dependent manner (Figure 6A,B). These data suggest that a member of the inward-rectifying family of K^+ channels ($K_{ir}1$-7) is likely to be responsible for the hyperpolarising effects of dopamine on membrane potential. Within this family of K^+ channels, previous studies have shown that G protein-coupled, inward rectifying K^+ channels (GIRKs) are a common target for D2-like receptors (Yamada *et al.*, 1998). Therefore, I bath-applied tertiapin-Q, a highly selective blocker of GIRK1/4 heterodimer and ROMK1 ($Kir_{1.1}$), but this failed to occlude the effects of quinpirole (Figure 6C, n=4, $p>0.05$).

Because I was unable to directly antagonise the target channel I initially suspected to be involved in the quinpirole effects, I explored the possibility that another inward-rectifying channel may be involved. Alternative K_{ir} channels known to be targeted by dopamine are the ATP-sensitive K^+ channels ($K_{ir}6$) (e.g. (Roeper *et al.*, 1990; Lin *et al.*, 1993)). To rule these out as the target channel, I bath-applied glybenclamide (50 µM), a non-selective blocker of ATP-sensitive inward rectifier channels, but this had no effect on the quinpirole-induced hyperpolarization (Figure 6C, $p>0.05$, n=3).

Figure 6. Barium chloride (BaCl), but not other potassium channel blockers, occludes the D2-like receptor mediated hyperpolarisation of spinal CPG neurons. A. A representative intracellular recording showing the effects of 25 µM quinpirole in the presence of TTX and BaCl. Application of 200 µM BaCl depolarised the cell by approximately 4 mV before stabilising, at which point the membrane potential was corrected to control (dashed line) using DC current injection (solid black line). Quinpirole (25 µM) had only a small (< 1 mV) hyperpolarising effect when subsequently applied in the presence of BaCl. The inset shows an expansion of the main trace. The effect of quinpirole alone is illustrated as a faded trace for comparison. **Bi.** Timecourse showing the resting membrane potential, pooled and normalised into 1 minute bins, to illustrate the hyperpolarising effect of quinpirole (25 µM) under control conditions (red), in the presence of 200 µM BaCl (light green) and in the presence 1mM BaCl (dark green). **Bii:** Pooled data showing a significantly smaller hyperpolarisation in both 200 µM BaCl ($p<0.05$, $n=4$) and 1mM BaCl ($p<0.01$, $n=3$) compared to control. **Ci:** Timecourse plot showing the quinpirole hyperpolarisation in a range of other K^+ channel blockers. **Cii:** Various K^+ channel blockers, including TEA, glybenclamide and tertiapin-Q showed no significant occlusion of the quinpirole effect.

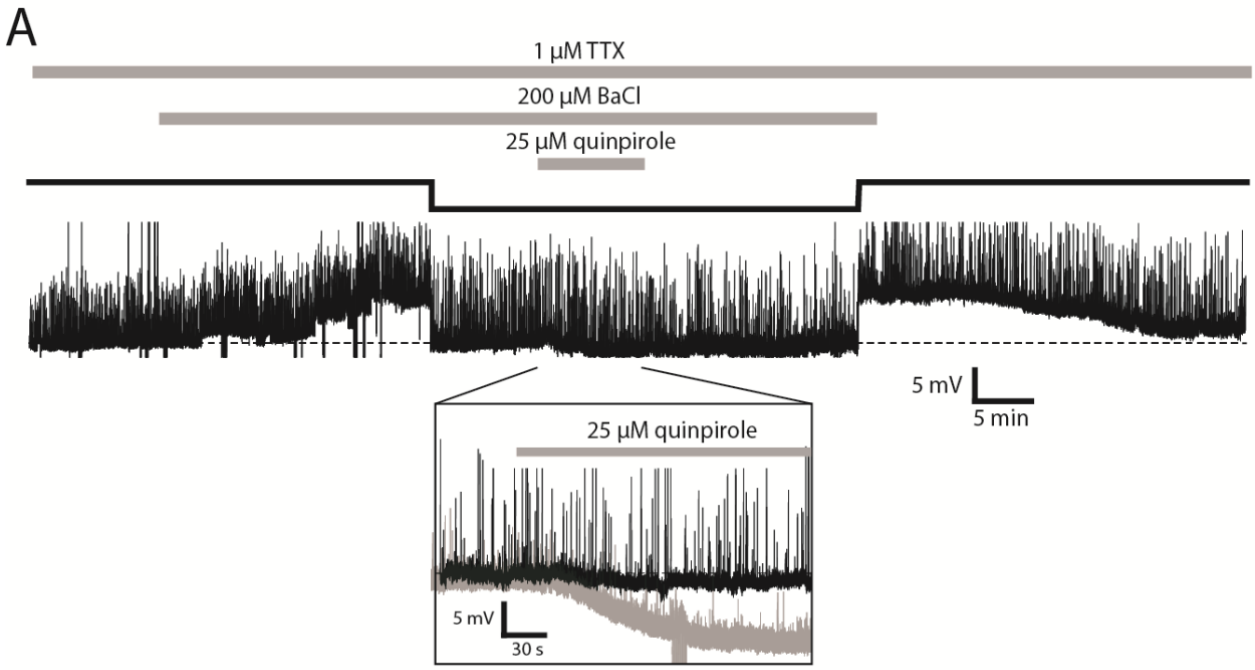
A
1 µM TTX
200 µM BaCl
25 µM quinpirole
5 mV
5 min
25 µM quinpirole
5 mV
30 s

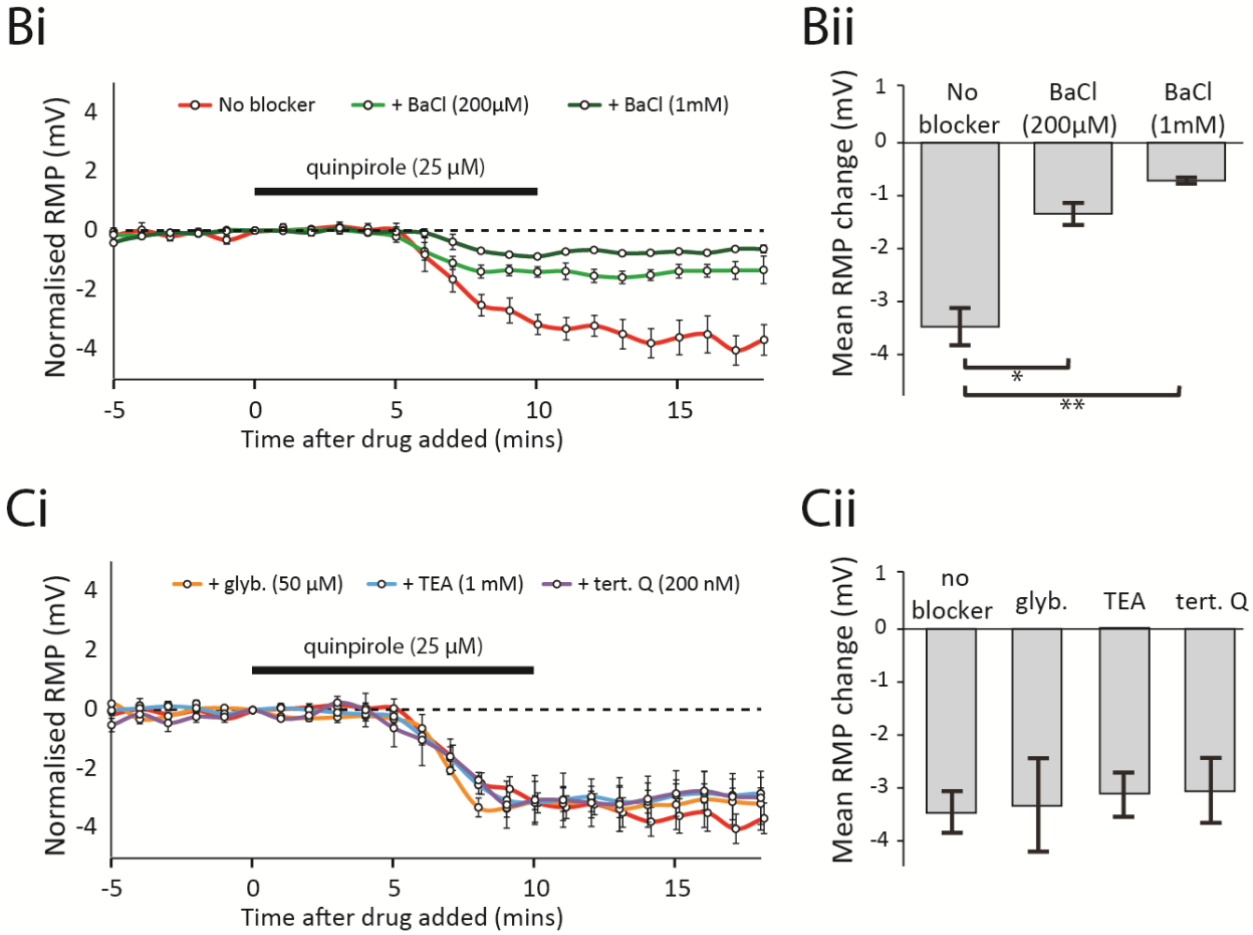
Bi
No blocker
+ BaCl (200µM)
+ BaCl (1mM)
quinpirole (25 µM)
Normalised RMP (mV)
Time after drug added (mins)
Bii
No blocker
BaCl (200µM)
BaCl (1mM)
Mean RMP change (mV)
*
**

Ci
+ glyb. (50 µM)
+ TEA (1 mM)
+ tert. Q (200 nM)
quinpirole (25 µM)
Normalised RMP (mV)
Time after drug added (mins)
Cii
no blocker
glyb.
TEA
tert. Q
Mean RMP change (mV)

Dopamine decreases the probability of neuron spiking during swimming

Next I wanted to explore the impact of D2 receptor-mediated changes in membrane potential and conductance upon neuronal firing properties. During bouts of swimming, many rhythmically active spinal neurons, with the exception of the rhythm-generating dINs, can vary in the number of spikes they generate in each swim cycle, with important consequences for the temporal dynamics of overall network output (Zhang *et al.*, 2011). Thus, I first checked whether neuron spike probability was affected when swimming was evoked following D2-like receptor activation. Dopamine (50 µM) caused a significant reduction in the firing probability of rhythmically active spinal neurons during swimming (Figure 7A,B, n=7, $p<0.05$), which reversed upon washout of the drug. The same effect was found for quinpirole (10-25 µM), which also caused a clear and significant decrease in spike reliability during swimming (Figure 7C,D n=8, $p<0.01$). This effect was observed across a range of rhythmically active cell types including motoneurons (mns: n=3 confirmed), commissural interneurons (cINs: n=6 confirmed, e.g. figure 7A) and ascending interneurons (aINs: n=3 confirmed). The firing probability remained lower during swimming even when the resting membrane potential of the neuron was artificially brought back to the pre-quinpirole value using tonic DC current injection (Figure 7C, n=4, $p<0.05$), suggesting that D2-like receptor activation affects not only the membrane potential, but also either presynaptic inputs to the recorded neurons and/or that other properties of the neuron have been affected (such as rheobase). The effects of quinpirole were significantly harder to reverse than dopamine and did not always wash within the timescale of our experiments; however, on occasions when recordings were maintained for longer periods (> 1 hour) the effects eventually washed off.

Figure 7. Activation of D2-like receptors leads to a reduction in spike reliability during swimming. Ai: Raw traces showing an intracellular recording of a cIN (black) and below that the ventral root trace (grey) in control, in the presence of dopamine (50 µM) and following dopamine washout. **Aii**: The inset shows an expansion of the trace in Ai as indicated by the black box. **B:** Pooled data shows that 50 µM dopamine significantly reduced the reliability of spiking during swimming ($p<0.05$, $n=7$), which reverses significantly upon washout of dopamine. **Ci:** Raw trace of a recording from an aIN in control, in the presence of quinpirole (10 µM) both without and with corrected RMP, and following quinpirole washout. **Cii**: The inset shows 250 ms of activity from the black box in Ci. Pooled data shows that quinpirole significantly reduced the reliability of spiking during swimming both without (Di: $p<0.01$, $n=8$) and with corrected RMP (Dii: $p<0.05$, $n=4$).

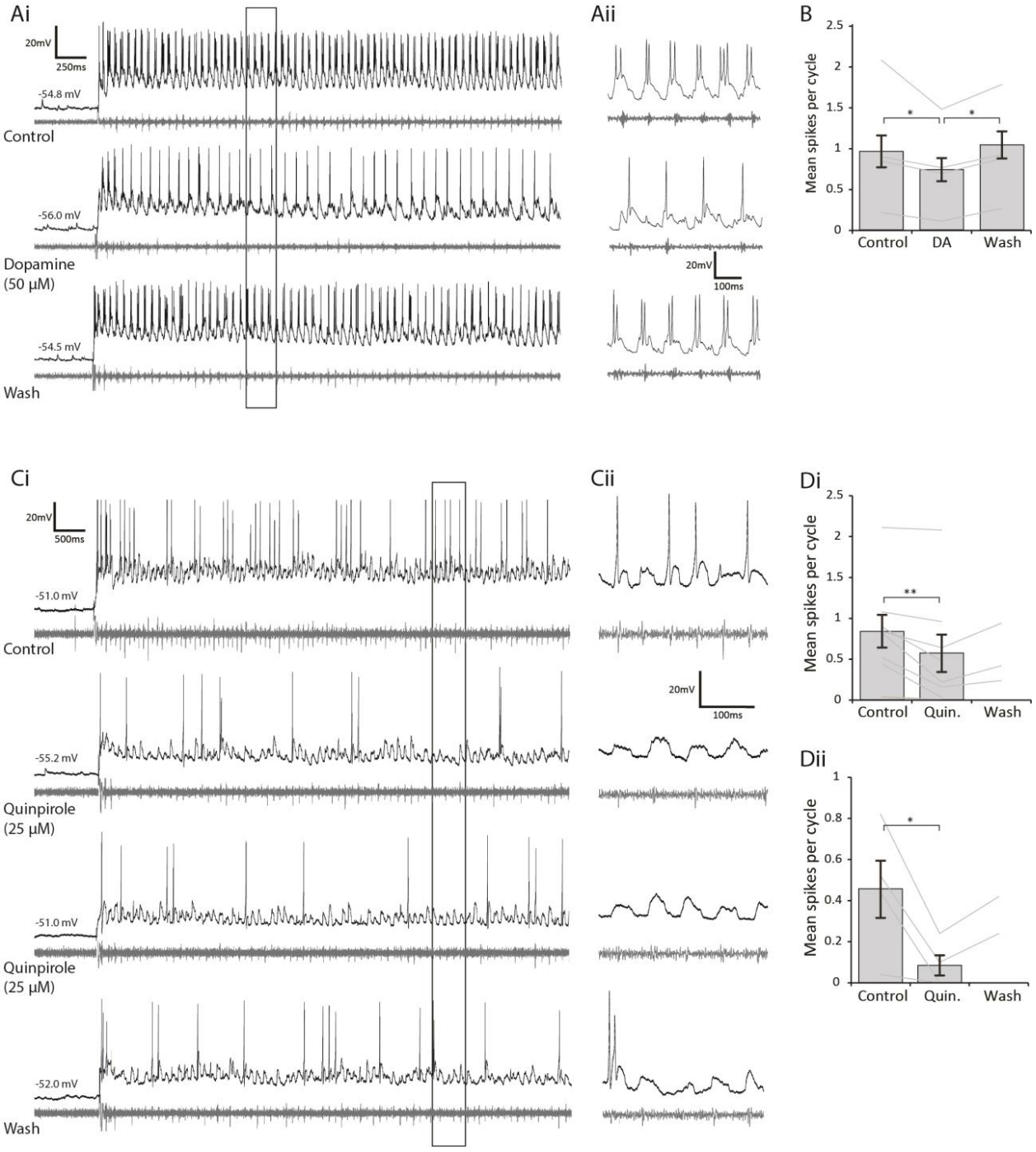
Ai
20mV
250ms
-54.8 mV
Control
-56.0 mV
Dopamine
(50 µM)
-54.5 mV
Wash
Aii
20mV
100ms
B
Mean spikes per cycle
2.5
2
1.5
1
0.5
0
*
*
Control
DA
Wash
Ci
20mV
500ms
-51.0 mV
Control
-55.2 mV
Quinpirole
(25 µM)
-51.0 mV
Quinpirole
(25 µM)
-52.0 mV
Wash
Cii
20mV
100ms
Di
Mean spikes per cycle
2.5
2
1.5
1
0.5
0
**
Control
Quin.
Wash
Dii
Mean spikes per cycle
1
0.8
0.6
0.4
0.2
0
*
Control
Quin.
Wash

Dopamine affects the intrinsic properties of spinal neurons

A reduction in firing reliability during swimming can be explained either by changes in the integrative properties of the recorded neurons, or in the efficacy of synaptic inputs from neurons elsewhere in the network, or both. To test between these hypotheses I used a protocol in which a series of depolarising current pulses (200 ms duration) with increasing amplitude (steps of 10 pA) was injected into neurons to assess any dopaminergic effects on their intrinsic excitability. In dopamine (50 µM), a larger amplitude current pulse was required to evoke action potentials (Figure 8A,Bi, n=5, $p<0.01$). Moreover, this was not simply due to the RMP being further away from spike threshold because I found the same effect when the RMP was corrected back to the control level using DC current injection (Figure 8Bii, n=5, $p<0.01$). In a number of neurons, I also observed an effect on the firing frequency in response to current injection. In 3 of 5 cells there was a clear rightward shift in the F-I relationship, indicating a decrease in neuronal excitability characterised by a reduction in spike frequency in response to the same current input (e.g. Figure 8A,Biii). As in previous experiments, I found the same effects for quinpirole (10-25 µM), with a larger amplitude current pulse needed to induce an action potential in the presence of the drug (Figure 8C,Di, n=9, $p<0.05$), which persisted when the RMP was corrected back to control (Figure 8Dii, n=5, $p<0.05$). In 6 of 9 cells I found a rightward shift in the F-I relationship (e.g. Figure 8C,Diii). This general reduction in firing probability persisted when the RMP was corrected back to the control level. Consistent with my extracellular data, these results suggest that D2-like receptors are expressed on rhythmically active spinal neurons and the receptors couple to a target which reduces the excitability of these cells by modifying their electrical properties.

Figure 8. The activation of D2 receptors modifies the integrative electrical properties of spinal CPG neurons. A: An example of the cellular response to depolarising current pulses in control, in 50 µM dopamine and following washout of dopamine. **Bi:** Pooled data showing that dopamine significantly increases rheobase ($p<0.01$, $n=5$). **Bii:** The effect persists when the RMP of the cell is corrected to control value using DC current injection ($p<0.01$, $n=5$). **Biii**: F-I plot for the cell shown in A. Dopamine shifted the FI curve to the right, demonstrating reduced firing frequency in response to the same current input. **C:** Responses to depolarising current pulses in control, in 25 µM quinpirole and following washout of quinpirole. **Di**: Pooled data showing that quinpirole also significantly increases rheobase ($p<0.05$, $n=9$), which persisted when the RMP was corrected (**Dii**, $p<0.05$, $n=5$). **Diii:** F-I plot for the cell shown in C. Quinpirole shifted the FI curve to the right, demonstrating reduced firing frequency in response to the same current input.

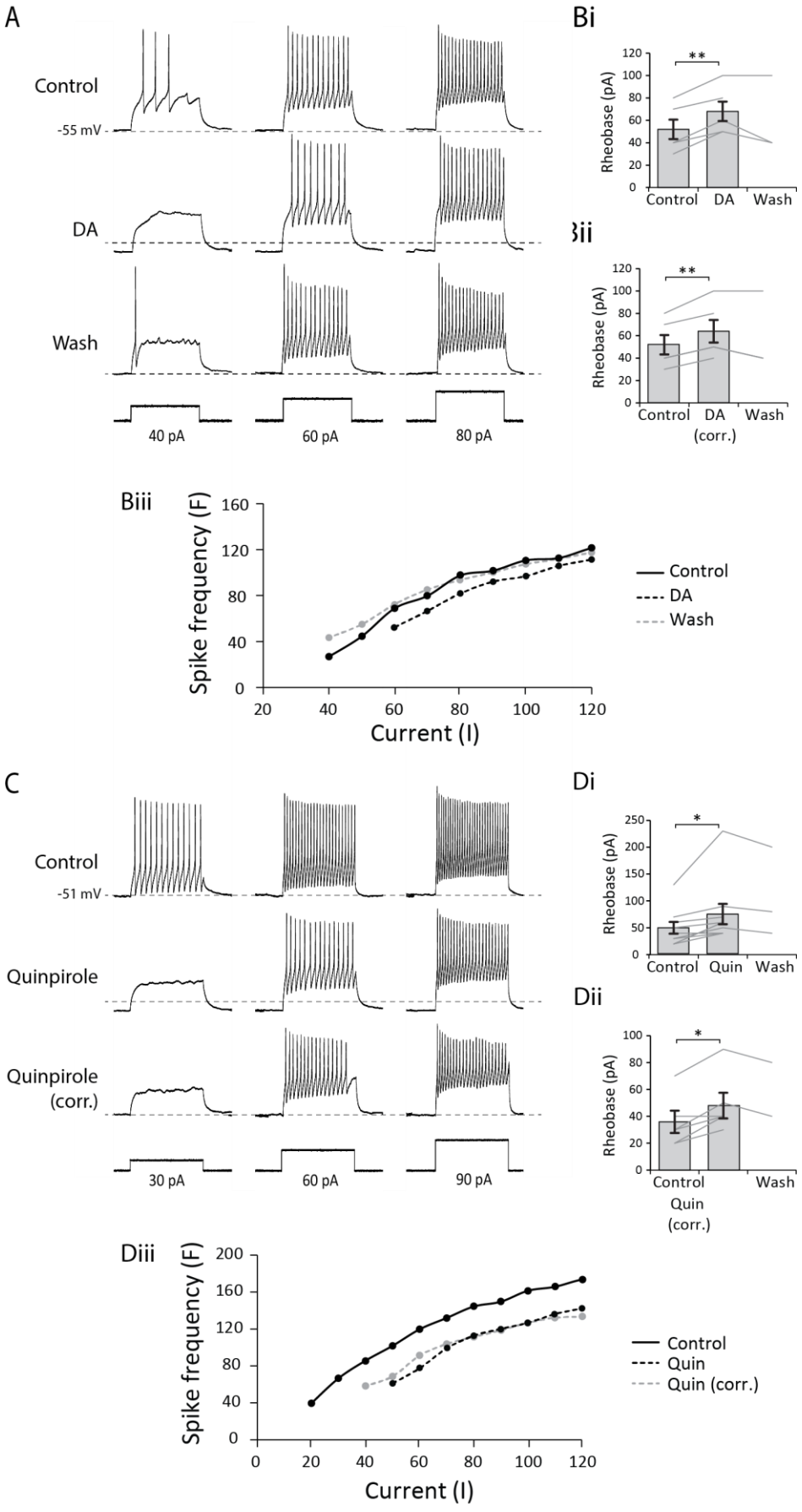
A
Control
-55 mV
DA
Wash
40 pA
60 pA
80 pA
Bi
Rheobase (pA)
Control
DA
Wash
**
Bii
Rheobase (pA)
Control
DA
Wash
(corr.)
**
Biii
Spike frequency (F)
Current (I)
Control
DA
Wash
C
Control
-51 mV
Quinpirole
Quinpirole
(corr.)
30 pA
60 pA
90 pA
Di
Rheobase (pA)
Control
Quin
Wash
*
Dii
Rheobase (pA)
Control
Wash
Quin
(corr.)
*
Diii
Spike frequency (F)
Current (I)
Control
Quin
Quin (corr.)

Chaper 1 discussion

Dopamine is a widely distributed and phylogenetically conserved modulator of central neural circuits. In vertebrates, the dopamine system has long been associated with motor control, largely due to the Parkinsonian symptoms that accompany the loss of dopaminergic neurons in the substantia nigra (Dauer & Przedborski, 2003). However, there is also growing evidence that descending pathways to the spinal cord release dopamine to modify ongoing locomotor output produced by spinal CPGs (see (Sharples *et al.*, 2014) for a recent review). In the spinal cord, dopamine acts on receptors belonging to two broad classes: D1-like receptors, which are typically excitatory; and D2-like receptors, which are typically inhibitory. In free swimming larval stages of *Xenopus laevis,* dopamine has opposing actions depending upon which of these receptor classes is activated: low dose dopamine selectively activates higher affinity D2-like receptors to reduce spontaneous swim bout occurrence, while higher doses activate lower affinity D1-like receptors to increase swimming (Clemens *et al.*, 2012). The present chapter of this thesis sought to address two related and unanswered questions regarding dopamine modulation: firstly, what are the effects of dopamine on swimming at earlier stages of *Xenopus* development when much more is known of the CPG circuit and when the tadpole is normally sessile until stimulated to swim; and secondly, what are the cellular consequences of dopamine receptor activation in this model system?

My extracellular ventral root recordings show that dopamine, acting solely via D2-like receptors at all concentrations tested, exerts strong inhibitory effects on the full range of locomotor parameters including the occurrence of spontaneous swimming, episode duration as well as the frequency, duration and amplitude of individual locomotor bursts (Figure 1 and 2). Moreover, consistent with studies in zebrafish (Thirumalai & Cline, 2008), and lamprey (Schotland *et al.*, 1995; Svensson *et al.*, 2003), the application of bupropion to block the reuptake of dopamine potently mimicked these inhibitory effects on the swim network (Figure 3), suggesting that the effects of dopamine constitute a behaviourally relevant and functioning modulatory system. In support of this hypothesis, antagonising the D4 receptor led to a block

of inhibition, presumably resulting from the tonic release of dopamine, resulting in excitatory effects on the swim network (Figure 4). This also suggests that the D4 receptor underlies the majority of the inhibitory effects of dopamine on the *Xenopus* swim network.

Interestingly, however, a low concentration of dopamine had no significant effect on burst durations, whereas a high concentration of dopamine reduced burst durations. All other parameters of swimming were inhibited at both concentrations, and all parameters were inhibited by the D2-like agonist quinpirole. One possible explanation for the lack of effect of low dopamine on burst durations could be that different D2-like receptor subtypes are expressed in motoneurons vs. interneurons. Dopamine binds with a higher affinity to the D4 (and D3) receptor compared to the D2 receptor (Lee & Wong, 2010). Thus, it is possible that low concentrations of dopamine may have been acting on D4 receptors in interneurons, to slow burst frequency, but is insufficiently high to activate D2 receptors in motoneurons, which are only activated by the higher dopamine concentration. In support of this hypothesis, the highly specific D4 receptor antagonist L745,870 had excitatory effects on all the swim parameters that were affected by dopamine *except* for burst durations. Thus, overall, these results suggest that dopamine predominantly acts on D4 receptors in the spinal cord to inhibit most of the parameters of swimming (frequency, episode duration, spontaneous swim occurence), whilst D2 receptors on motoneurons mediate a decrease in burst durations. There is increasing evidence that the D4 receptor plays an especially important role in the actions of dopamine in the spinal cord, including in zebrafish (Boehmler *et al.*, 2007; Lambert *et al.*, 2012; Reimer *et al.*, 2013) and lampreys (Pérez-Fernández *et al.*, 2015). Interestingly, there is also evidence that mRNA encoding D4 receptors is especially high in human spinal cord, compared to the brain (Matsumoto *et al.*, 1996).

The effects of dopamine on a rhythmic network depends upon the species (Miles & Sillar, 2011); the developmental stage (Thirumalai & Cline, 2008); the drug concentration (Clemens *et al.*, 2012); and even the cell type being targeted ((Harris-Warrick *et al.*, 1998); see introduction for a detailed overview). This heterogeneity of action has often made the precise

role of dopamine in rhythmic networks difficult to precisely characterise. In zebrafish, dopaminergic input to the spinal cord is known to derive exclusively from the descending dopaminergic diencephalic tract (DDT) (McLean & Fetcho, 2004*a*), which plays diverse roles in establishing the complement of spinal CPG cell types, in modulating ongoing swimming, and controlling developmental changes in swim pattern (Thirumalai & Cline, 2008; Lambert *et al.*, 2012; Reimer *et al.*, 2013; Jay *et al.*, 2015). For example, dopamine acts on D2-like receptors to inhibit spontaneous swimming episodes (Thirumalai & Cline, 2008), similar to our observed effect on spontaneous swimming in *Xenopus* tadpoles. However, in contrast to the current data in this chapter, dopamine had no effects on the specific parameters of fictive swimming in zebrafish. A further, and likely related difference, is that no effects were observed on the integrative properties of zebrafish spinal neurons, with the effects appearing to be mediated by supraspinal D2-like receptors at centres controlling the initiation of movement. In contrast, I found that the effects of dopamine occur directly on spinal neurons, although a possible contribution of additional supraspinal receptors to the inhibition of spontaneous swimming cannot be ruled out, as spontaneous bouts are not observed in spinalized animals.

Dopamine modulation of mammalian locomotor networks is also, unsurprisingly, complex, in part due to the heterogenous patchwork of all the receptor subtypes (including D1-D5) expressed in the ventral horn of the spinal cord (Miles & Sillar, 2011; Sharples *et al.*, 2014). For drug-induced locomotor activity in rodents, dopamine slows the bursting rhythm through actions on D2-like receptors, while stabilising the rhythm through D1-like receptors (Barrière *et al.*, 2004; Sharples *et al.*, 2015). The mechanisms are not fully understood but in mice, at least, dopamine increases the excitability of motoneurons via a D1 receptor mediated depolarisation and a decrease in at least two potassium conductances: I_A and SK_{CA} (Han *et al.*, 2007). Activation of D1 receptors also facilitates glutamatergic synaptic transmission through an increase in AMPA-mediated currents (Han & Whelan, 2009). Thus, for drug-induced locomotor activity dopamine acts at multiple levels on a combination of D1-like and D2-like receptors to mediate complex effects on the locomotor network. Further complexity

derives from the fact that dopamine has been shown to have different effects depending on the method of evoking locomotion. For example, whilst dopamine applied to a drug-induced locomotor rhythm has overall excitatory effects (see earlier), the same concentrations applied to a preparation using ventral-root stimulation strongly inhibits activity (Humphreys & Whelan, 2012).

Various lines of evidence from the intracellular recordings in this chapter suggest that in *Xenopus* tadpoles, dopamine acts primarily through the D2-like receptor coupled opening of a potassium channel with GIRK-like pharmacology expressed heterogeneously on various spinal neuron types (Figure 5 and 6). Firstly, I consistently found a TTX-resistant membrane potential hyperpolarisation with relatively fast onset that was associated with a decrease in input resistance, consistent with the opening of either a chloride, or more likely, a potassium channel. Secondly, I ruled out most voltage-dependent K^+ channels, another common target for dopamine, as TEA was unable to reduce the hyperpolarisation. Thirdly, barium chloride significantly occluded the hyperpolarisation in a dose-dependent manner, strongly suggesting an inward-rectifying K^+ channel, such as a GIRK, as the target. Fourthly, although I was unable to occlude the hyperpolarisation with one specific GIRK blocker (tertiapin-Q), I was able to rule out another commonly coupled inward-rectifier, the ATP-dependent K^+ channel, because glybenclamide was ineffective in occluding the quinpirole effect. Although TEA had no significant effect on the hyperpolarisation of spinal neurons, it is possible that other BaCl-sensitive, TEA-insensitive K^+ channels, such as flickering potassium channels (Koh *et al.*, 1992) or Na^+-dependent K^+ channels (Kaczmarek, 2013), may be involved. However, these are rarely found to be coupled to D2-like receptors, whereas GIRK channels are a common target for D2-like receptors across a range of tissue types (Neve, n.d.). Moreover the D4 receptor, which I expect to mediate the effects of dopamine in this chapter, have been consistently shown to couple to GIRK channels (e.g. (Pillai *et al.*, 1998; Wedemeyer *et al.*, 2007)), and these D4-coupled GIRK currents are blocked by the same selective D4 antagonist used in this study (L745,870, (Pillai *et al.*, 1998)). Thus, while it is possible that other K^+

channels may contribute to the effects of dopamine in this chapter, the weight of evidence suggests that the most prominent target is a constitutively active GIRK channel.

Tertiapin-Q is a highly selective blocker of the GIRK1/4 heterodimer (Jin *et al.*, 1999), yet it failed to occlude the membrane hyerpolarisation. In mammals, there are four distinct genes encoding GIRK channels (GIRK1–GIRK4 or Kir3.1–Kir3.4) and neuronal GIRK channels are comprised of homo- or hetero-tetramers containing GIRK1–GIRK3 subunits, whereas GIRK4 expression is low (Mark & Herlitze, 2000). Therefore I suggest that a dimer involving GIRK 2 or 3, or a homologous amphibian GIRK that is not sensitive to tertiapin-Q, may be involved in dopamine modulation of *Xenopus* swimming. The direct coupling of GPCRs to GIRK channels occurs via a membrane-delimited pathway (Sadja *et al.*, 2003), therefore responses are particularly fast compared to GPCR pathways relying on changes in second messenger concentrations. Indeed, the onset of dopaminergic effects on swimming were about an order of magnitude faster than other modulators in this preparation such as serotonin and noradrenaline (McDearmid *et al.*, 1997).

A hyperpolarisation caused by the opening of a K^+ channel shifts neurons away from firing threshold, and hence they showed reduced spiking during swimming and in response to current injection (Figures 7 and 8). These effects persisted even when the membrane potential change was corrected for by tonic DC current injection, thus the accompanying conductance increase is also likely to shunt the membrane and reduce the responsiveness of neurons to excitatory inputs. Indeed, a decrease in input resistance is known to shift F-I curves to the right (Holt & Koch, 1997). It is possible that these effects on firing could be due to an indirect effect mediated by the activation of D2-like receptors located elsewhere in the network. However, this is unlikely because the hyperpolarisation and decrease in input resistance persisted in TTX, suggesting a direct effect on CPG neurons. Moreover, the data presented here show that D2-like receptors are located in the spinal cord, as the effects of dopamine persisted even when the brain was removed. One way to test this hypothesis would be to make recordings in the presence of blockers of synaptic transmission to distinguish between direct effects on the

properties of recorded neurons versus changes in synaptic inputs to that neuron. It is possible, even in TTX, that the effects on recorded cells could be propagated by gap junction coupling from elsewhere in the spinal network (Song *et al.*, 2016). Again, however, this is unlikely, because electrical coupling is thought to be restricted to the dIN (Li *et al.*, 2009) and motoneuron (Zhang *et al.*, 2009) populations, whereas I observed consistent effects in a range of CPG neuron types.

Can the effects of dopamine on overall network output be explained by the effects on the spiking properties of specific spinal neuron subtypes? In the lamprey, dopamine (10-100 µM) decreases the frequency of glutamate-induced fictive swimming through the D2 receptor-mediated depression of low-voltage activated (LVA) calcium channels on spinal commissural interneurons (cINs) (McPherson & Kemnitz, 1994; Schotland *et al.*, 1995; Svensson *et al.*, 2003; Wang *et al.*, 2011). These LVA channels contribute to the post-inhibitory rebound (PIR) property of cINs which normally hastens the onset of swim cycles, so their inhibition by dopamine slows swimming. Here I also observed that dopamine had a strong inhibitory effect on both swim frequency and the cINs (e.g. the cell shown in Figure 7Ai). A reduction in cIN firing in *Xenopus* tadpoles is known to reduce PIR in the descending interneuron (dIN) population, also slowing the onset of the next bout of excitatory drive, slowing swim frequency (Li & Moult, 2012). Thus, the cINs are likely to be the locus of the inhibitory effects on swim frequency. For the motoneuron population, the reduction in firing observed during swimming in the presence of dopamine leads to a reduction in the duration of locomotor bursts, and in turn reduced excitatory output to axial swim muscles (Zhang *et al.*, 2011). I also observed inhibitory effects on identified aINs, and the effect of inhibiting this interneuron population is less easy to interpret. The aINs play two main roles in the swim network. Firstly, aINs provide phasic, glycinergic inhibition to dorsolateral ascending (dla) and commissural (dlc) cells. This phasic inhibition prevents these sensory interneurons from firing from tail stimulation if the stimulation happens to coincide with flexion on the same side, thus providing a form of sensory gating that prevents the interruption of ongoing swimming (Sillar & Roberts, 1988; Li *et al.*,

2002). Secondly, aINs also provide phasic inhibition to motoneurons, cINs and dINs, which is thought to help synchronise the firing of these CPG neurons (Li *et al.*, 2004*a*). A reduction in the excitability of the aIN population may thus desynchronise neuronal firing, which could completely compromise the functional integrity of a swim episode.

In contrast to older free-swimming *Xenopus* tadpoles (Clemens *et al.*, 2012; Currie, 2014), I found no evidence for an excitatory, D1-mediated effect of high dopamine concentration, suggesting that developmental changes in *Xenopus* motor behaviour may be mediated by an increase in D1 receptor expression. Although a systematic, developmental analysis of dopamine receptor expression is yet to be performed in *Xenopus* tadpoles, findings from other model systems support this overall developmental pattern of receptor expression. For example, a recent study in mice showed that high levels of inhibitory D2-like receptors are found in the spinal cord throughout development, whilst excitatory D1 receptor expression is low at early stages but increases with development, leading to an age-dependent increase in excitatory drive in the spinal cord (Keeler *et al.*, 2015). Similarly, there is abundant expression of inhibitory D2 receptors in the motoneurons and interneurons of young larval lamprey (Fernandez-Lopez *et al.*, 2015), which remains high in the adult lamprey (Perez-Fernandez *et al.*, 2014), although less is known about spinal D1 receptor expression in this system. In zebrafish, some studies have shown that D2-like receptors mostly mediate the inhibitory effects of dopamine early in development (Thirumalai & Cline, 2008); although subsequent studies have shown that dopaminergic modulation in this species is more complex than first thought ((Lambert *et al.*, 2012; Jay *et al.*, 2015); see introduction).

It is also interesting that in this thesis I described potent effects on not only spontaneous swim bout occurrence, but also on parameters of swimming including episode duration, cycle frequency and burst durations. The previous studies using older *Xenopus* tadpoles (Clemens *et al.*, 2012; Currie, 2014) found no significant effects on these parameters of swimming. However, one important difference is that I used electrical stimulation to evoke swimming, whereas the previous study used entirely spontaneous swimming, thus potentially missing

important dopaminergic effects on these parameters. Alternatively, there may be a developmental loss of inhibitory D2-like receptors, at least in subpopulations of neurons such as cINs and motoneurons, as has been proposed in zebrafish (Thirumalai & Cline, 2008). Future studies exploring the expression levels of dopamine receptor subtypes will be able to more fully explain these developmental differences. An important additional point to explore in future will be the physiological levels of dopamine that are present endogenously at spinal synapses in young and developing *Xenopus* tadpoles. For example, whilst dopamine applied in the micromolar range may have excitatory effects on swimming in older tadpoles, the animal may only experience nanomolar synaptic concentrations of dopamine under normal physiological conditions.

In addition to the developmental onset of this D1 excitation in *Xenopus* tadpoles, the mechanism of excitation by D1 activation is also an avenue for future research. Interestingly, barium chloride depolarised spinal neurons by ~4 mV (Figure 8A), suggesting that the suspected GIRK channels are likely to be open at rest. This is supported by the excitatory effects of the D4 receptor antagonist on the swim network. Thus, one possibility is that these K^+ channels become a target for the later developing spinal D1 receptors, which may close, rather than open them.

Chapter 1 conclusions

Dopamine is a well-established and important modulator of locomotor circuits. In this chapter I have shown that in early *Xenopus* tadpole development, when the network remains relatively simple, dopamine acts at all concentrations tested as an endogenous inhibitory neuromodulator that reduces the occurrence, frequency and intensity of swimming activity. The mechanism of inhibition involves the activation of D2-like receptors present on spinal neurons, which directly couple to K^+ channels with GIRK-like pharmacology. The activation of this pathway leads to membrane hyperpolarisation associated with an increase in membrane conductance, and a subsequent reduction in the excitability of specific CPG neuron classes. Thus, at these early stages of development when the animal is predominantly sessile, the dopaminergic signalling is predominantly inhibitory and likely contributes to this behavioural state. During development this inhibitory D2-like pathway persists (Clemens *et al.*, 2012; Currie, 2014), but at some developmental stage, likely around the onset of free-feeding and free-swimming (Currie *et al.*, 2016), there is a switch to excitation by high dopamine concentrations, presumably through the introduction of excitatory D1-like receptors to the swim network.

Chapter 2: Modulatory interactions between sodium pumps and ionic conductances in the Xenopus tadpole swim network

Chapter 2 contributions and publications

Some data from this chapter is adapted from previously published work (Zhang et al., 2015, Scientific Reports). All data shown are from experiments conducted by Laurence Picton.

Chapter 2 summary

In this chapter I explore the roles of the sodium pump mediated afterhyperpolarisation, its modulation by nitric oxide, dopamine, and temperature, and describe an Ih current in a subset of spinal neurons. I first outline the pump-mediated ultra-slow afterhyperpolarisation (usAHP) and the effects of raising intracellular sodium, using the sodium ionophore monensin. Monensin (10 µM) caused a significant decrease in swim episode duration and swim cycle frequency. At the cellular level, monensin caused a membrane hyperpolarisation, but only in central pattern generator (CPG) neurons which displayed a usAHP under control conditions; moreover, the amplitude of the membrane hyperpolarisation caused by monensin was proportional to the size of the usAHP displayed in control, and occurred without a change in conductance. Together, this suggests that monensin is acting by converting a dynamic, spike-dependent pump potential into a tonic membrane hyperpolarisation. Consistent with previous studies, I found no evidence of a usAHP in the rhythm-generating descending interneurons (dINs). However, for the first time in *Xenopus* tadpoles, I found strong evidence for an Ih current, with dINs displaying a prominent sag potential in response to hyperpolarisation, the hallmark of Ih current activation. A proportion of non-dIN neurons also displayed sag potentials, but only at very hyperpolarised, and physiologically irrelevant membrane potentials. These sag potentials were blocked by ZD7288 (50 µM) in both dINs and non-dINs, providing evidence that they are mediated by the voltage-dependent HCN channels known to underlie Ih activation. At the network level, ZD7288 (50 µM) significantly decreased episode duration and disrupted the fast swimming rhythm, causing bursts to become slower, longer and more variable. Upon washout of ZD7288, a spontaneous swimming rhythm emerged, reminiscent of the swim pattern at later stages of *Xenopus* development. ZD7288 had no effect on the RMP or input resistance of non-dINs, but caused their firing during swimming to become sporadic, with occasional bouts of high intensity spikes accompanying large ventral root bursts. Unlike non-dINs, ZD7288 clearly hyperpolarised dINs by ~10 mV, with an accompanying decrease in membrane conductance. ZD7288 also caused dIN spike failures

during swimming, suggesting that Ih may contribute to the post-inhibitory rebound mechanism that generates dIN spikes during each swim cycle. I also explored the effects of raising temperature on swimming. Consistent with previous studies, raising the temperature of the bath saline shortened swim episodes and increased their cycle frequency. Raising the temperature depolarised CPG neurons and decreased their input resistance, suggesting the opening of a temperature-sensitive sodium channel, leading to a higher spike probability during swimming. In some neurons, I also found evidence for increased sodium pump activity and enhanced Ih currents at high temperatures. Finally, I also explored whether the sodium pump could be modulated by nitric oxide and dopamine. The nitric oxide donors SNAP (200 µM) and DEA-NO (200 µM) both reversibly reduced the amplitude of the pump-mediated usAHP. The D1-like agonist SKF38393 (2 µM), but not the D2-like agonist quinpirole (25 µM), increased the amplitude of the usAHP. These results contribute to our understanding of the roles of Ih, temperature and sodium pumps in the swim network of *Xenopus* tadpoles.

Chapter 2 introduction

The sodium pump has previously been shown to play an important role in the *Xenopus* tadpole swim network (Zhang & Sillar, 2012). Following intense spiking, intracellular sodium accumulates in a subset of CPG neurons. This causes an increase in sodium pump activity, resulting in a net hyperpolarisation due to the 3/2 ratio of positive ion exchange across the cell membrane. The hyperpolarisation recovers slowly, over a period of around a minute and has been termed the ultra-slow hyperpolarisation (usAHP). In other systems where sodium pumps play an important role in contributing to cellular excitability, a number of factors including intracellular sodium concentration, temperature, Ih currents and neuromodulators have been shown to interact with the sodium pump (e.g. (Kang *et al.*, 2004; Tobin & Calabrese, 2005; Kim & von Gersdorff, 2012; Gulledge *et al.*, 2013)). In this chapter I explore the roles of these factors in influencing the *Xenopus* swim network and whether these effects involve interactions with the sodium pump.

Whilst there are no known direct pharmacological activators of the sodium pump, a number of studies have used monensin, as a Na^+/H^+ ionophore, to mediate the electroneutral exchange of internal H^+ for external Na^+ as a means of flooding neurons with sodium. This has been shown to mimic the rise in intracellular Na^+ caused by intense firing, which in turn triggers a rise in sodium pump activity (Lichtshtein *et al.*, 1979; Haber *et al.*, 1987). For example, suprachiasmatic nucleus (SCN) neurons display a prominent pump-mediated hyperpolarisation in response to repetitive spiking (Wang & Huang, 2006). Monensin applied to these neurons causes a tonic hyperpolarisation of the membrane potential due to increased sodium pump activity - an effect which was shown, using ratiometric Na^+ imaging, to be due to a monensin-induced increase in intracellular Na^+ ions (Wang *et al.*, 2012). Similar results have been found in hippocampal and striatal neurons (Azarias *et al.*, 2013), as well as in thalamic neurons (Senatorov *et al.*, 2000). Thus, the first aim of this chapter is to explore the effects of monensin on the *Xenopus* tadpole swim network and explore the cellular basis for these effects.

Secondly, this chapter focuses on the previously unexplored role for Ih currents at these early stages of *Xenopus* development. Ih currents (or *hyperpolarisation-activated cation currents*) were first characterised in the rabbit heart sinoatrial node (Noma & Irisawa, 1976) but have since been shown to be present in many cell and tissue types and often play an important role in contributing to the rhythmic properties of networks (Pape, 1996; Moosmang *et al.*, 2001; Robinson & Siegelbaum, 2003). Ih currents usually contribute to the resting membrane potential and conductance of a cell, with their presence making a neuron more depolarised and have a higher membrane conductance (Robinson & Siegelbaum, 2003). They are mediated by hyperpolarisation-activated cyclic nucleotide-modulated (HCN) channels, of which there are four mammalian subunit isoforms (HCN1-4) that become activated by hyperpolarisation of the membrane potential, usually at values more negative than -40 to -50 mV (Craven & Zagotta, 2006). Ih is known to perform a number of important roles in neurons, such as stabilising the membrane potential and input resistance, but arguably the most important is in its dynamic contribution to the pacemaker properties of certain neurons, which in turn contributes to network rhythm generation. Ih is especially well studied in invertebrate rhythmic networks. For example, Ih activation contributes to the rhythmic firing of leech heart interneurons (HNs), whereby within each rhythmic cycle, inhibitory inputs hyperpolarise the membrane potential to activate Ih, which in turn causes rebound excitation that depolarises HNs to initiate the next phase of spiking (Angstadt & Calabrese, 1989). Ih plays a similar role in various rhythmically active neurons of the pyloric network of the lobster stomatogastric ganglion (STG), and here, Ih is also a known target for a range of neuromodulators (Harris-Warrick, 1995; Peck *et al.*, 2006). Ih currents are also known to play an important, albeit more complex, role in a range of mammalian networks including the rhythmically active brainstem respiratory network (Thoby-Brisson *et al.*, 2000); the thalamus (McCormick & Pape, 1990); and the hippocampus (Maccaferri & McBain, 1996).

There is also evidence that Ih can contribute to maintaining rhythmicity in networks controlling locomotor behaviours (Harris-Warrick & Marder, 1991). In the marine gastropod, *Clione*, for

example Ih currents contribute to the post-inhibitory rebound mechanism that maintains rhythmic activity in the swim interneurons that coordinate its wing-like parapodia during swimming (Pirtle & Satterlie, 2007). Ih currents are also found in spinal interneurons of the turtle spinal cord (Smith & Perrier, 2006), as well as in mouse motoneurons and interneurons, although their role here is not fully understood (Takahashi, 1990; Kiehn *et al.*, 2000; Butt *et al.*, 2002). Across species, Ih generally performs the same role in rhythmic networks of providing an "escape from inhibition" in response to phasic hyperpolarisation, and blocking Ih subsequently disrupts the rhythmicity of the network. The swimming rhythm in *Xenopus* tadpoles relies on a post-inhibitory rebound mechanism in dINs, following phasic inhibition from cINs (Moult *et al.*, 2013). The specific mechanism of post-inhibitory rebound remains unclear, although the de-inactivation of sodium channels is thought to be involved (Li *et al.*, 2010; Hull *et al.*, 2016); however, other ionic conductances, such as Ih, could also contribute to PIR. The role of Ih in the swim network of young *Xenopus* tadpoles is yet to be explored and so this is one of the main aims of this chapter.

Neural circuits respond to abiotic stress; for example, they perform differently at different temperatures. This is especially true for poikilotherms, as homeotherms are usually able to effectively counteract environmental changes in temperature, except in cases of disease, illness or injury. Increased temperature usually results in an increase in the activity of specific proteins, with the effects usually being described by a Q_{10} relationship: the change in the rate of a biochemical process for a 10 °C increase in temperature. For example, increased temperature can result in the opening of HCN channels or 2-pore-domain K^+ channels such as TASK and TREK. In addition, it has been shown in a number of cell types that raising the temperature causes a net depolarisation, which is in large part due to an increase in the activation of Ih current (Angstadt & Calabrese, 1989; Kim & von Gersdorff, 2012). Moreover, other proteins that contribute to the membrane potential, such as ion pumps, increase their activity as temperature is raised (Kim & von Gersdorff, 2012; Gulledge *et al.*, 2013).

The effects of raising temperature on the *Xenopus* tadpole swim network have already been described using ventral root recordings (Sillar & Robertson, 2009; Robertson & Sillar, 2009). Raising the temperature of bath saline caused a decrease in episode duration and an increase in swim frequency (Sillar & Robertson, 2009). If the temperature is raised beyond ~30 °C there is eventually *hyperthermic failure* – the swim network is no longer able to generate normal swimming, but instead initiates bouts of presumed Mauthner-mediated escape swimming. Recovery from this hyperthermic failure has been shown to involve nitric oxide signalling, with nitric oxide donors slowing recovery and nitric oxide scavengers speeding recovery (Robertson & Sillar, 2009). The cellular effects of raising the temperature in *Xenopus* tadpoles have not yet been explored, and so is the third main focus of this chapter; in particular, focussing on whether temperature affects the sodium pump and HCN channels.

Finally, the sodium pump is a well-established target for modulators in both non-nervous and nervous tissue, including by nitric oxide, dopamine, serotonin and noradrenaline (Therien & Blostein, 2000). The gaseous molecule nitric oxide has been shown modulate sodium pumps in a variety of tissues. For example, nitric oxide increases sodium pump activity in ventricular myocytes via a PKC-dependent mechanism (William *et al.*, 2005; Pavlovic *et al.*, 2013). Conversely, in other tissue types, nitric oxide donors have been shown to decrease sodium pump activity including in kidney cells (Liang & Knox, 1999), in choroid plexus (Ellis *et al.*, 2000), and at the renal medulla (McKee *et al.*, 1994). In the spinal cord, nitric oxide decreases sodium pump activity in mammalian spinal neurons (Ellis *et al.*, 2003). However, this spinal sodium pump inhibition in mammals has not been explored further, and the significance of this finding, given the key role of nitric oxide as a modulator of locomotor circuits (McLean & Sillar, 2004; Foster *et al.*, 2014), remains to be explored. The effects of nitric oxide on the sodium pump, in most cases, is linked to the activation of the cGMP/PKG pathway. Other than nitric oxide, a lot of research on neuronal sodium pump modulation has also focused on dopaminergic pathways. For example, dopamine, usually acting via PKA or PKC, can enhance or inhibit pump activity depending on the species, tissue type and dopamine receptors involved

(Zhang *et al.*, 2013). In striatal neurons, D2-like receptor activation stimulates sodium pumps by inhibiting PKA, thus dephosphorylating the α3 subunit (Bertorello *et al.*, 1990; Wu *et al.*, 2007). Other studies have similarly shown that changes in PKA activity can modulate the ability of a neuron to respond to changes in intracellular sodium through phosphorylation/dephosphorylation of the α3 isoform (Azarias *et al.*, 2013). Neuronal sodium pumps can even form a complex ("signalplex") with D1 and D2 dopamine receptors, to allow direct reciprocal modulation between dopamine receptors and the pump (Hazelwood *et al.*, 2008). In the fourth main section of this chapter I will explore whether nitric oxide and dopamine are able to modulate the sodium pump-mediated usAHP.

Chapter 2 materials and methods

Experimental animals

All experiments conformed to UK Home Office regulations and were approved by the Animal Welfare Ethics Committee (AWEC) of the University of St Andrews. All experiments were performed on newly hatched pre-feeding *Xenopus laevis* tadpoles at developmental stage 37/38 or 42 (Nieuwkoop & Faber, 1956). Tadpoles were reared from fertilized ova obtained following breeding of adults selected from an in-house colony. Mating was induced by injections of human chorionic gonadotropin (HCG, 1000 U/ml, Sigma-Aldrich, Poole, UK) into the dorsal lymph sac of breeding pairs of adult frogs.

Electrophysiology

All electrophysiological recordings on *Xenopus* tadpoles were performed in the same way as described in the methods section in chapter 1.

Temperature experiments

For raising the temperature of the bath saline for extracellular ventral root recording experiments, I used the same methods and equipment as described in (Robertson & Sillar, 2009). Saline was perfused through a piece of glass tubing which had a heating element wrapped around it. Temperature ramps from room temperature (~22 °C) to ~32 °C were obtained by turning on the heating element, with passive cooling upon turning the heating element off. The temperature of the bath saline was measured at 0.1°C resolution using a temperature probe (VWR international, Stockholm, Sweden) which was placed directly next to the tadpole in the bath. Due to issues with high noise using this method for heating the saline, I used an alternative, more controlled heating device for making whole-cell patch clamp recordings. For these experiments I used a PTC03 proportional temperature controller (Digitimer, Welwyn Garden City, UK). Due to the cooling of the saline during the short distance between the outlet from the heater to the tadpole in the bath, I found that the optimum protocol using this device involved setting the heater to 50 °C. This rapidly raised the temperature,

which peaked around 32 °C and remained stable until the heater was turned off. The temperature of the bath saline was measured using the same temperature probe as described above.

Pharmacological agents

All drugs were obtained from Sigma-Aldrich (Poole, UK) or Tocris Bioscience (Bristol, UK) and bath-applied to the preparation.

Data analysis

Electrophysiological data were first analysed using dataview software (v 10.3.0, courtesy of Dr. W. J. Heitler) and all raw data were imported into Excel spreadsheets and analysed. Statistical analyses were conducted using PASW statistics 21. A rest time of 2 minutes was given between evoked episodes of swimming or between protocols for inducing a usAHP, to ensure that activity was not influenced a previous sodium pump current (Zhang & Sillar, 2012; Zhang *et al.*, 2015). For swim episode duration analysis I calculated a mean of 3 consecutive evoked episodes in each condition. For intra-episode swim parameters (cycle frequency, burst duration) a mean of the first 20 cycles of swimming across 3 episodes was calculated for each condition. For analysis of spontaneous swimming I calculated the number of spontaneously occuring swim episodes in a 20 min period in each condition. To calculate spike probability, I measured the number of action potentials in the first 50 cycles of swimming in an episode and divided this value by the number of cycles. For all experiments, values are displayed as mean ± SEM and unless otherwise stated conditions were compared using either paired t-tests or repeated measures ANOVAs followed by Bonferonni-corrected post-hoc comparison.

Neuron identification

Following patch-clamp recordings, animals were fixed in 2% glutaraldehyde in 0.1 M phosphate buffer, pH 7.2, overnight in a refrigerator (~4°C). Animals were first rinsed with 0.1 M PBS (120 mM NaCl in 0.1 M phosphate buffer, pH 7.2), and washed in two changes of 1% Triton X-100 in PBS for 15 min with agitation. Next, animals were incubated in a 1:300 dilution

of extravidin peroxidase conjugate in PBS containing 0.5% Triton X-100 for 2–3 hours with agitation, and washed again in at least four changes of PBS. Animals were then immersed in 0.08% diaminobenzidine in 0.1 M PBS (DAB solution) for 5 min, moved to a DAB solution with 0.075% hydrogen peroxide for 1-2 min, and then washed in running tap water. Finally, animals were dehydrated in 100% alcohol, cleared in methyl benzoate and xylene, and mounted whole between two coverslips using Depex. Neuronal cell bodies and axon processes were observed under a x40 objective to identify CPG neuron types.

Chapter 2 results

The usAHP and the effects of sodium loading with monensin

Firstly, I wanted to characterise the usAHP in CPG neurons, and because it is hypothesised that the usAHP is triggered by spike-dependent rises in intracellular sodium ions, I also wanted to explore the effects of raising intracellular sodium using a pharmacological method. To generate the usAHP I used one of two protocols to induce intense spiking, in order to generate an accumulation of intracellular sodium that triggers the activation of the sodium pump. Firstly, I injected a series of depolarising current pulses (200 ms) of increasing amplitude (10 pA steps) into each neuron (e.g. Figure 1Ai). After several suprathreshold pulses, repetitive spiking starts to drive the membrane potential to a more hyperpolarised level, which is mediated by increased activation of the sodium pump (Zhang & Sillar, 2012). Once the protocol has ceased, the membrane potential gradually recovers back to control levels over a period of around a minute. Different neurons respond differently to this protocol due to variations in their electrical properties such as spike threshold and the FI relationship of the neuron. Moreover, some CPG neurons types do not fire multiple action potentials in response to depolarising pulses. Therefore, I also used a second protocol which involved the injection of 500 high amplitude (400 pA), short duration (2 ms) depolarising pulses. Across all neurons tested, this reliably generated 500 action potentials and therefore I could compare the usAHP generated by this protocol across neurons. I compared the characteristics of the usAHP in each respective protocol in a sample of recordings. There were no overall differences in the amplitude or duration of the usAHP resulting from these two protocols (Figure 1B,C; n=23 for protocol 1, n=11 for protocol 2, $p>0.05$). Therefore, for subsequent measurements of the usAHP, data were pooled using these two protocols.

Figure 1. The usAHP. Ai. An intracellular recording of a cIN showing the induction of a usAHP using suprathreshold pulses of increasing amplitude. **Aii.** An alternative method used for inducing a usAHP involving a series of 500, short duration, suprathreshold depolarising pulses. **B.** Mean amplitude of the hyperpolarisation induced by the two protocols. Note that there were no significant differences in the amplitude or the duration of the usAHP between the two protocols. **C.** Mean duration of the hyperpolarisation induced by the two protocols. Again, there were no differences between the protocols. **D.** The anatomy of the commissural interneuron shown in A. The cell body is on the right side of the spinal cord, the axon crosses the midline (dashed line) and heads both caudally and rostrally. Note that in this example the cell body and axonal projection has been traced for clarity. FB = forebrain, PE = pineal eye, MB = midbrain, OC = otic capsule, SC = spinal cord.

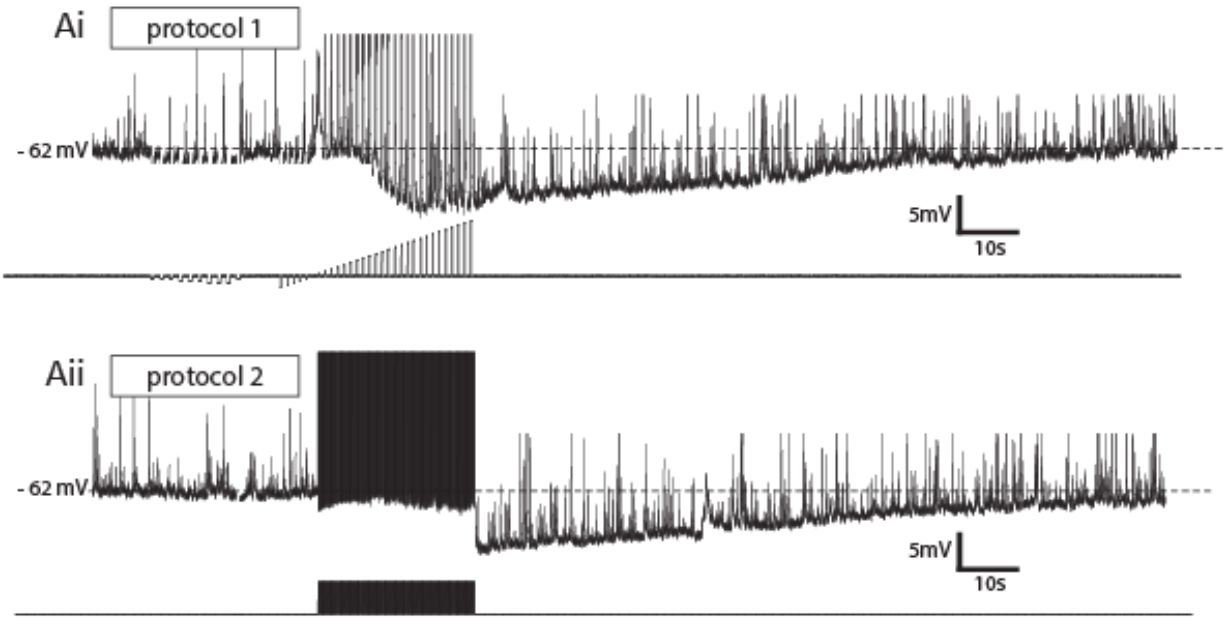
Ai
protocol 1
- 62 mV
5mV
10s
Aii
protocol 2
- 62 mV
5mV
10s

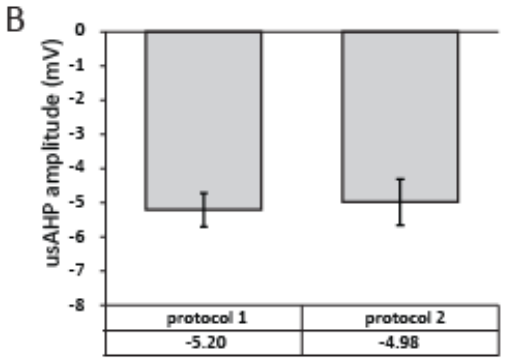
B
usAHP amplitude (mV)
0
-1
-2
-3
-4
-5
-6
-7
-8
protocol 1
protocol 2
-5.20
-4.98

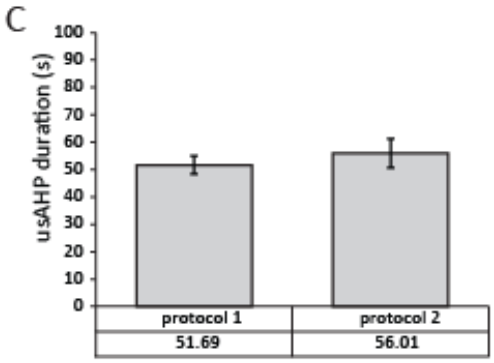
C
usAHP duration (s)
100
90
80
70
60
50
40
30
20
10
0
protocol 1
protocol 2
51.69
56.01

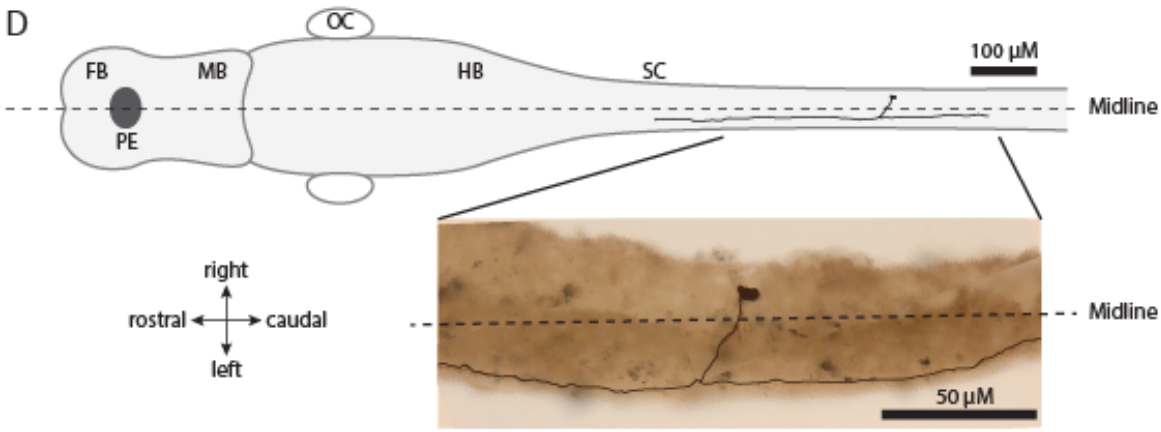
D
OC
FB
MB
HB
SC
PE
100 µM
Midline
right
rostral
caudal
left
Midline
50 µM

Sodium pumps increase their ion exchange activity during periods of high activity due to the accumulation of intracellular sodium that accompanies repetitive action potentials. Indeed, the main limiting factor for the sodium pump is not ATP or K^+, which are generally at saturating concentrations at rest, but intracellular sodium concentration (Therien & Blostein, 2000). Therefore, I wanted to test the effects of increasing the intracellular sodium concentration in CPG neurons. Previous studies have demonstrated that monensin, a one-for-one H^+/Na^+ antiporter, is an effective method of increasing intracellular sodium in an electroneutral manner (Haber *et al.*, 1987; Wang *et al.*, 2012). This in turn has been shown to increase the activity of the sodium pump. Firstly, I assessed the overall effects of monensin on the swim network. Monensin (10 µM) added to the recording bath shortened the swimming episode duration (Fig. 2A,C, n=6; $p<0.001$) and significantly slowed swimming frequency (Fig. 2B,D; $p<0.05$), although the effects were not reversible in the time course of the wash period of more than 30 minutes. The effects of monensin, triggered by an increase in intracellular Na^+ concentration, therefore closely mimic the adaptation of the motor network following intense swimming, resulting in a less excitable motor network.

Figure 2. Increasing intracellular sodium concentration using the ionophore monensin. **A.** Bath applying 10 µM monensin irreversibly reduced episode duration. **B**. Swimming bursts at the beginning of a swim episode in control and in monensin. **C.** Mean swim episode duration. **D.** Time series measurements showing swimming frequencies of an episode in control and in the presence of monensin. Inset bar graph shows the average normalized swim frequency.

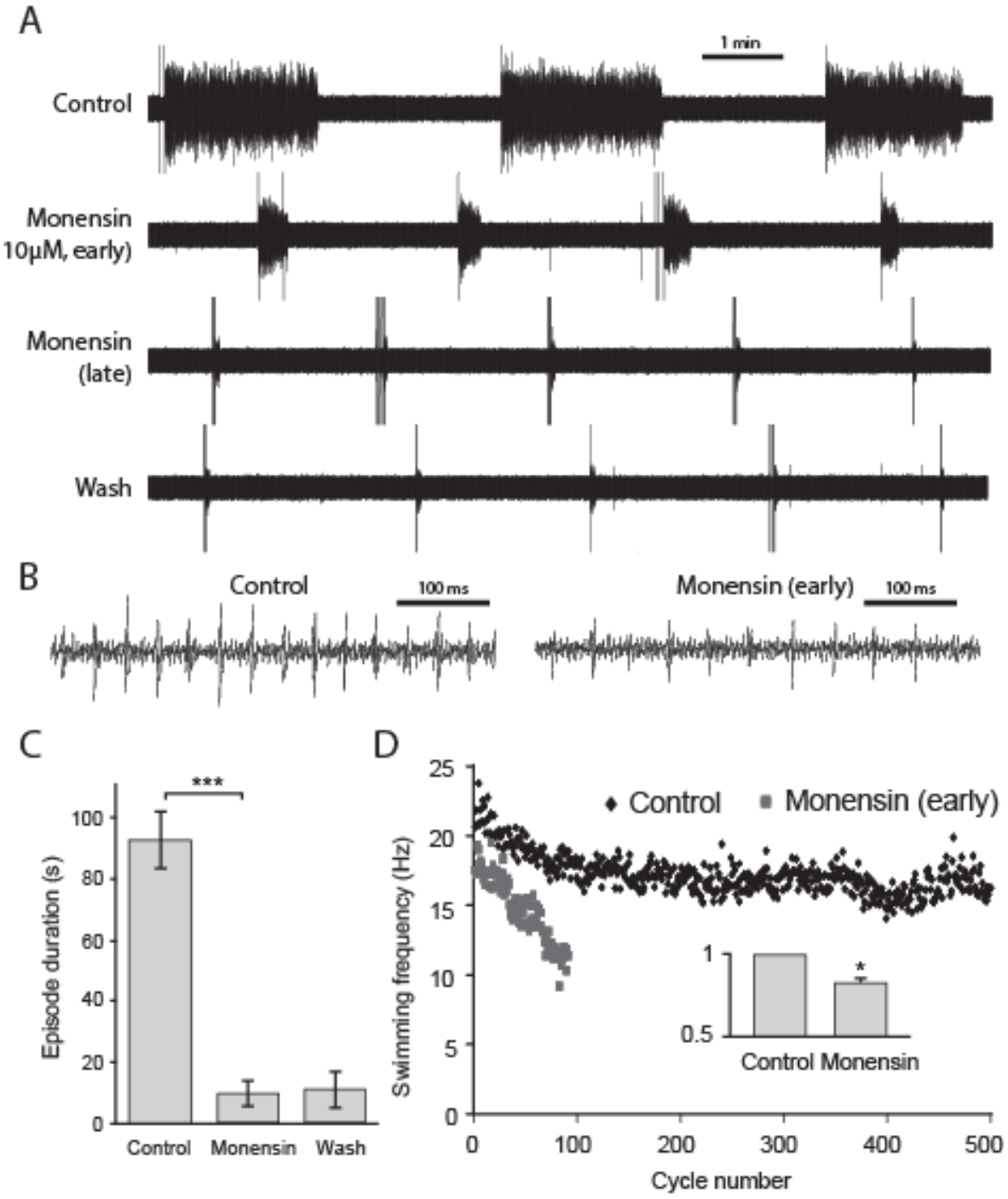
A
1 min
Control
Monensin
10µM, early)
Monensin
(late)
Wash
B
Control
100 ms
Monensin (early)
100 ms
C
***
Episode duration (s)
100
80
60
40
20
0
Control
Monensin
Wash
D
Control
Monensin (early)
Swimming frequency (Hz)
25
20
15
10
5
0
1
0.5
*
Control Monensin
0
100
200
300
400
500
Cycle number

Next, I explored the effects of monensin on the properties of individual CPG neurons. Firstly, monensin was applied to neurons which did not display a usAHP under control conditions. Interestingly, in these neurons, monensin (10 μM) had no clear effect on the membrane potential (Figure 3Ai, Aii, n=2). However, because effects are expected to be mediated by actions on the sodium pump, monensin was next applied to neurons displaying a prominent usAHP in control. In these neurons, monensin (10 μM) caused a clear membrane hyperpolarisation (Figure 3Bi, Bii, n=4, $p<0.05$). Moreover, after this hyperpolarisation, monensin affected the responses to the spiking protocols described at the start of this chapter. In neurons where there was a clear usAHP observed in control in response to high intensity spiking protocols, this could no longer be induced after the tonic membrane hyperpolarisation (Figure 3Ci, Cii, $p<0.01$, n=4). Importantly, this was not due to an effect on the ability to generate action potentials, which was unchanged by monensin. The amplitude of the membrane hyperpolarisation by monensin was not the same across all neurons, and correlated with the amplitude of the usAHP observed in control for each neuron (Figure 3Di, $p<0.05$, $R^2 = 0.79$, n=6). Because CPG neurons only hyperpolarised in monensin if they displayed a pump-mediated hyperpolarisation in control conditions, and the amplitude of the hyperpolarisation was proportional to the amplitude of the usAHP, these results suggest that the change in membrane potential induced by monensin is likely mediated by the potentiation of sodium pump activity. To confirm that the hyperpolarisation was not mediated by a secondary effect of monensin, such as the opening or closing of an ion channel, hyperpolarising current pulses were injected before and after the monensin hyperpolarisation. I found no evidence of a change in conductance, as indicated by the similar voltage response to constant current pulses in control and in monensin (Figure 3Diii, Div, $p>0.05$, n=4). Finally, in one recording I was able to hold a patch recording for long enough to apply the sodium pump blocker ouabain to the neuron (1 μM) after the initial membrane hyperpolarisation caused by monensin. This caused the membrane potential to depolarise back to the pre-monensin level, before stabilising briefly (Figure 3E). However, the animal swam

spontaneously, which caused a prolonged depolarisation of the neuron until the neuron reached around -3mV. One possible explanation for this large depolarisation may involve an off-target effect of monensin on intracellular Ca^{2+} concentration (see discussion).

One of the interesting features of the usAHP is that whilst it is found in a proportion of almost all CPG neuron subtypes, it has been shown to be absent in the rhythm-generating dIN neurons (Zhang & Sillar, 2012). dINs are characterised by an ipsilateral descending axon projection (Figure 4A), fire only a single action potential in response to continuous depolarising pulses (Figure 4B), and fire only a single action potential per swim cycle (Figure 4C). Consistent with previous findings, our recordings from dINs found no evidence for a usAHP in response to high frequency action potentials (Figure 4D, n=3, $p>0.05$).

Whilst our recordings from dINs support previous findings showing that they do not display a usAHP, one notable feature that I observed that has not been previously identified is the evidence of the presence of a prominent Ih current. Therefore, in the next section I explore the role of Ih in the locomotor network of *Xenopus* tadpoles.

Figure 3. The effects of increasing intracellular sodium on spinal CPG neurons. Ai: Raw trace of a CPG neuron which did not display a usAHP in control. In this neuron, monensin had no clear effect on the RMP. **Aii:** Pooled data showing no significant effect of monensin on RMP in neurons without a usAHP. **Bi:** Raw trace of a CPG neuron which displayed a usAHP of around 5 mV in control. Around 5 minutes after the application of monensin, (10 µM) the neuron hypepolarised by approximately 5 mV. **Bii:** Pooled data showing a significant membrane hyperpolarisation by monensin. **Ci:** Example of a usAHP in the same neuron as B. In control, there was a prominent and consistent usAHP in response to intense firing. Early in monensin, the usAHP reduced to around 2 mV in amplitude and did not recover. Eventually, the usAHP was abolished altogether. In order to test whether the loss of a usAHP was related to the change in RMP, I corrected the RMP back to control using holding current, but the usAHP was still absent. **Cii:** Pooled data showing a significant decrease in the usAHP in monensin. **Di:** The amplitude of the hyperpolarisation by monensin significantly correlates with the amplitude of the usAHP displayed by the neuron ($p<0.05$, $R^2 = 0.79$, $n=6$). **Dii:** A comparison of the RMP change caused by monensin in cells displaying a usAHP versus those without a usAHP. **Diii:** A comparison of the membrane responses to hyperpolarising pulses in control (black) and in the presence of monensin (grey). **Div:** Monensin had no significant effect on input resistance. **E:** An example of a neuron where 1 µM ouabain was applied after the monensin hyperpolarisation. This caused a depolarisation back to the pre-monensin RMP, followed by a large depolarisation to approximately -3 mV after the animal swam spontaneously.

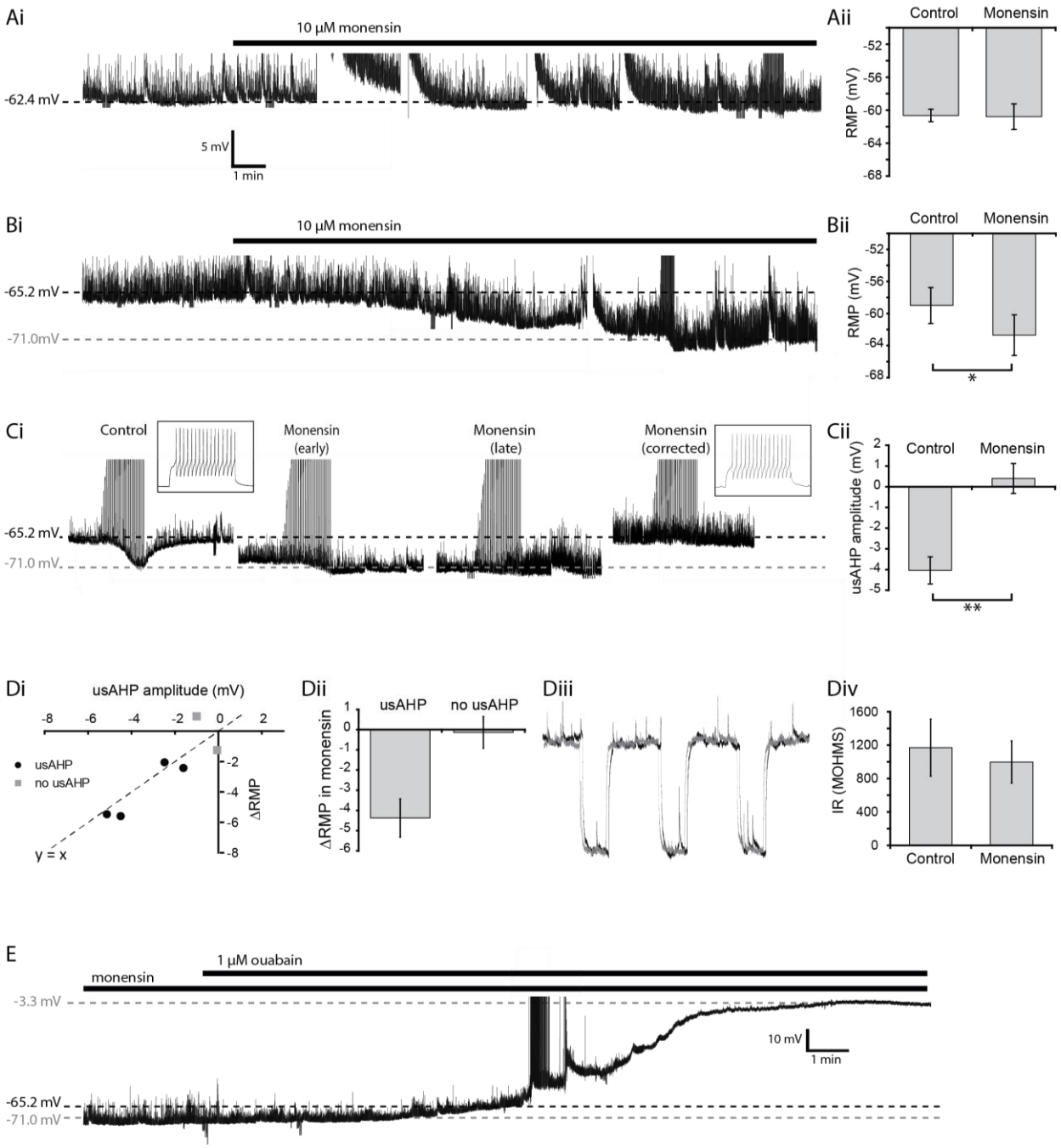
Ai
10 µM monensin
-62.4 mV
5 mV
1 min
Aii
Control
Monensin
RMP (mV)
Bi
10 µM monensin
-65.2 mV
-71.0mV
Bii
Control
Monensin
RMP (mV)
*
Ci
Control
Monensin (early)
Monensin (late)
Monensin (corrected)
-65.2 mV
-71.0 mV
Cii
Control
Monensin
usAHP amplitude (mV)
**
Di
usAHP amplitude (mV)
usAHP
no usAHP
y = x
ΔRMP
Dii
usAHP
no usAHP
ΔRMP in monensin
Diii
Div
IR (MOHMS)
Control
Monensin
E
1 µM ouabain
monensin
-3.3 mV
10 mV
1 min
-65.2 mV
-71.0 mV

Figure 4. dINs do not display a usAHP. **A.** The anatomy of a dIN. Anatomy of the neuron shown in A and B. The axon heads ventrally and then caudally. **B.** Responses of a dIN to depolarising pulses of increasing amplitude. Unlike non-dINs, suprathreshold pulses produce only a single spike. **C.** During swimming, dINs also only fire a single spike per cycle. **D.** Unlike all other neuron types in the *Xenopus* spinal cord, dINs do not display a usAHP in response to our protocols or after swimming. **Ei.** A comparison of the mean RMP of dINs and non-dINs. dINs were significantly more depolarised compared to non-dINs. **Eii.** A comparison of the input resistance of dINs and non-dINs. dINs had a significantly lower input resistance compared to non-dINs.

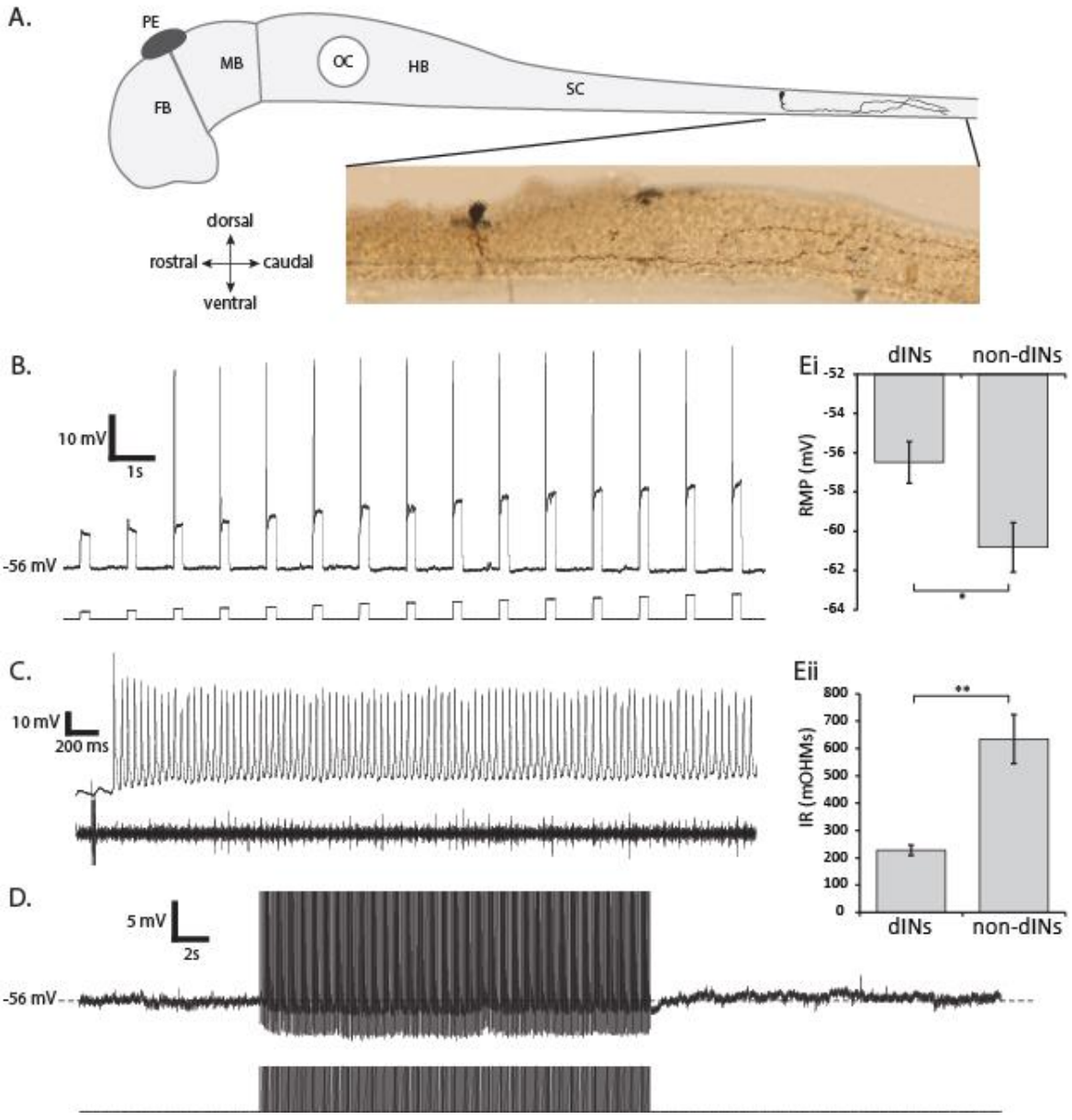
A.
PE
MB
OC
HB
SC
FB
dorsal
rostral
caudal
ventral
B.
10 mV
1s
-56 mV
Ei
dINs
non-dINs
RMP (mV)
-52
-54
-56
-58
-60
-62
-64
*
C.
10 mV
200 ms
Eii
**
IR (mOHMs)
800
700
600
500
400
300
200
100
0
dINs
non-dINs
D.
5 mV
2s
-56 mV

Ih current

Ih currents (or *hyperpolarisation-activated cation currents*) are slowly developing inward currents that are activated by hyperpolarisation of the membrane potential beyond around -40/ to -50 mV (Pape, 1996; Robinson & Siegelbaum, 2003; Craven & Zagotta, 2006). Ih currents are known to contribute to rhythm generation in motor control networks (see introduction). Moreover, a number of studies have found that Ih currents can become activated by a hyperpolarisation mediated by the sodium pump (Trotier & Døving, 1996; Rozzo *et al.*, 2002; Kim & von Gersdorff, 2012; Gulledge *et al.*, 2013). For example, in hippocampal pyramidal cells, recovery from a sodium pump mediated hyperpolarisation is accelerated by the activation of Ih (Gulledge *et al.*, 2013). HCN channels that mediate Ih are slowly activating, and therefore a common test for Ih is to apply a long hyperpolarising current pulse in current clamp mode, which results in a depolarising sag potential. It has previously been shown, using this method, that Ih currents are widespread in spinal CPG neurons in older, pre-metamorphic larval *Xenopus* tadpoles (Currie, 2014). However, neither the existence, nor the function of Ih has been documented in the young *Xenopus* tadpole swim CPG. Therefore, I tested for Ih in a number of different neuron types in the CPG swim network.

Compared to the other CPG neurons in the *Xenopus* swim network, dINs are known to have a depolarised resting membrane potential and a lower input resistance, suggesting that a depolarising ionic conductance, such as Ih, might be more active at rest in dINs than in other spinal cell types (Sautois *et al.*, 2007). Indeed, I also found that dINs were significantly more depolarised (dIN = -56.5 mV +/- 1.06, n=3 vs. non-dIN = -60.82 mV +/- 1.25, n=15, $p<0.05$) and had a lower input resistance (dINs = 227.9MΩ +/- 19.4, n=3 vs. non-dINs = 635.1MΩ, n=15, $p<0.01$) compared to a random sample of non-dIN neurons (Figure 4Ei,ii). Therefore, I firstly looked for evidence of Ih currents in dINs, and whether Ih could account for these differences in intrinsic properties. To test for this characteristic hallmark of Ih, long, hyperpolarising current pulses (3s duration) of increasing amplitude (10 pA incremental steps) were injected into the neuron. In all dIN recordings (3/3) there was a prominent sag potential

in response to these hyperpolarising pulses (Figure 5B,C). Importantly, these sag potentials occurred even at moderately hyperpolarised potentials, close to the resting membrane potential (mean sag appearance: -57.5 mV, n=3), and persisted in the presence of TTX. To confirm that these sag potentials are indeed mediated by the activation of Ih channels following membrane hyperpolarisation, I applied the selective blocker of Ih channels, ZD7288 at a concentration which is thought to specifically block HCN channels, with little or no off-target effects (50 µM; e.g. (Darbon *et al.*, 2004; Kim & von Gersdorff, 2012)). ZD7288 clearly blocked the sag current at all membrane potentials (Figure 3D, Eii). Moreover, ZD7288 shifted the I-V relationship to the right (Figure 5Ei), indicating that block of Ih enhances the voltage response to a given current step. This in turn indicates an increase in input resistance (also see figure 7Biii), and provides further evidence that ZD7288 blocks Ih in these neurons.

Finally, because sag currents appeared even at only moderately hyperpolarised membrane potentials, I wanted to test the possibility that Ih currents may be active at resting membrane potential in dINs. Therefore dINs were held depolarised by approximately 10 mV and the protocol of hyperpolarising current pulses was repeated. In all three dIN recordings, when the neuron was held at a depolarised level (~-46-48mV), hyperpolarising pulses produced clear and prominent sag potentials around the resting membrane potential (~-59mV, Figure 3Fi). Moreover, in response to higher amplitude hyperpolarising current pulses, the neuron produced a post-inhibitory rebound depolarisation that was sufficient to generate a single action potential (Figure 3Fii). Thus, it is clear that there is an Ih current in the rhythm-generating dINs that is active at rest, contributes to the RMP and increases resting conductance, and may be involved in the coordination of the swimming rhythm.

Figure 5. Ih currents in dINs. A. The anatomy of a dIN showing the axon heading caudally. **B.** An example of the responses of a dIN to hyperpolarising current pulses (3s duration) of increasing amplitude (10 pA incremental steps). Note the induction of a slow depolarising sag current after approximately the fifth current pulse. **C.** An expanded trace from B showing responses to hyperpolarising pulses. The peak and steady state membrane potential responses are indicated by dotted lines. **D.** An overlay of several membrane responses to a current pulse in control and in the presence of the Ih blocker ZD7288 (50 µM), which abolished the sag currents observed at hyperpolarised membrane potentials. Note that in the presence of ZD7288, the membrane potential is more hyperpolarised (see later, Figure 9). **Ei.** The current-voltage (I-V) relationship for the dIN shown in A and the **e**ffect of 50 µM ZD7288. For both control (circles) and in ZD7288 (triangles), the peak and the steady-state Vm are plotted against each injected current step. **Eii.** The amplitude of the sag currents plotted against the membrane potential (mV). **Fi.** When the neuron was held depolarised (~-48 mV) relative to rest, I observed sag currents when the membrane potential was hyperpolarised at around the level of the original RMP (~-59 mV), indicating that Ih current is active at rest. **Fii.** At even more hyperpolarised membrane potentials, the dIN showed post-inhibitory rebound spiking upon removal of the hyperpolarising pulse when it is held depolarised.

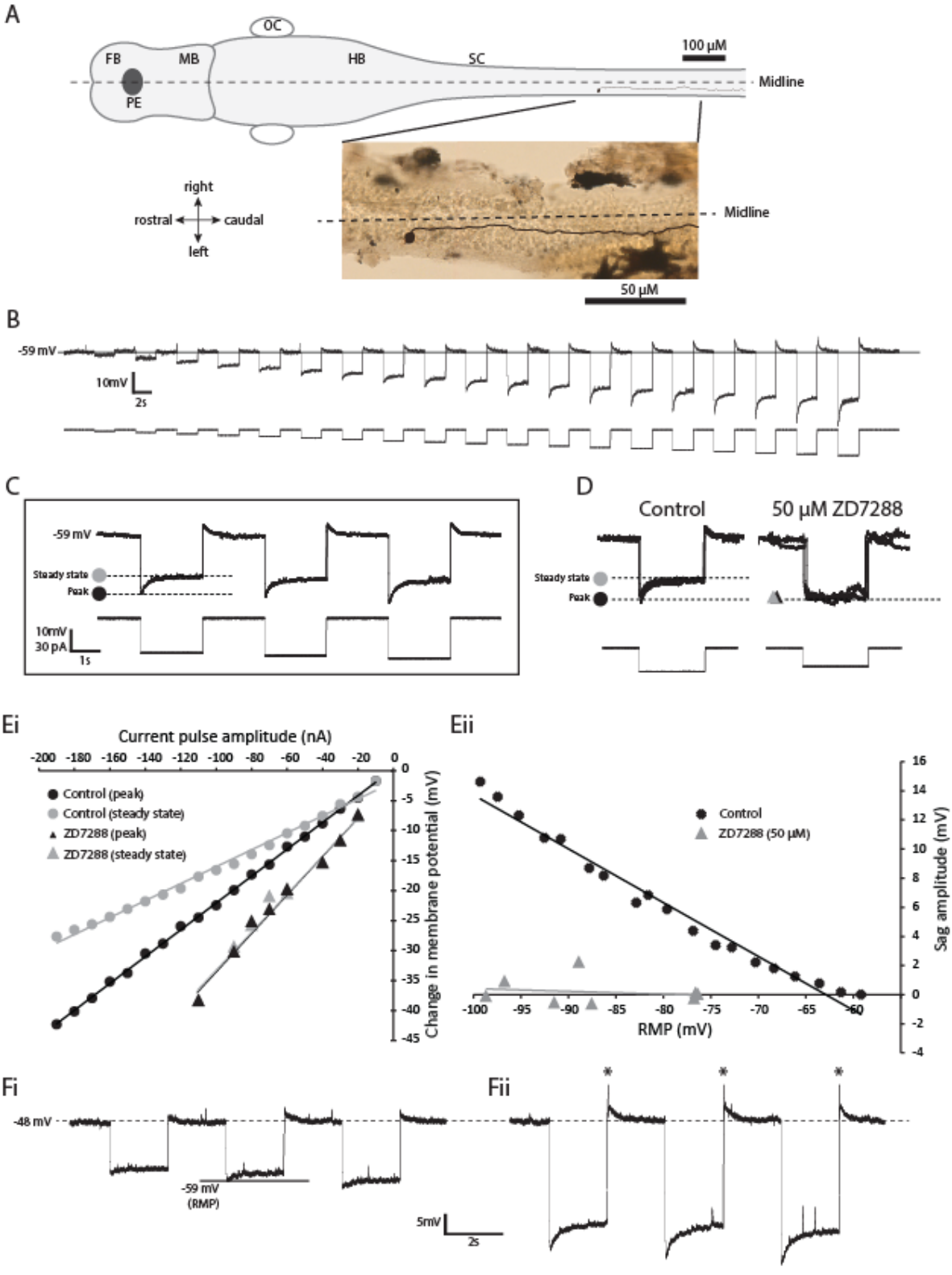
A
OC
FB
MB
HB
SC
PE
100 µM
Midline
right
rostral
caudal
left
Midline
50 µM
B
-59 mV
10mV
2s
C
-59 mV
Steady state
Peak
10mV
30 pA
1s
D
Control
50 µM ZD7288
Steady state
Peak
Ei
Current pulse amplitude (nA)
-200 -180 -160 -140 -120 -100 -80 -60 -40 -20 0
Control (peak)
Control (steady state)
ZD7288 (peak)
ZD7288 (steady state)
0 -5 -10 -15 -20 -25 -30 -35 -40 -45
Change in membrane potential (mV)
Eii
Control
ZD7288 (50 µM)
-100 -95 -90 -85 -80 -75 -70 -65 -60
RMP (mV)
16 14 12 10 8 6 4 2 0 -2 -4
Sag amplitude (mV)
Fi
-48 mV
-59 mV
(RMP)
5mV
2s
Fii
*
*
*

Whilst dINs displayed a prominent and large Ih current, even at resting membrane potentials, I found a different pattern in non-dIN neurons. In a sample of 45 non-dINs tested, around a quarter of neurons showed no evidence of a sag current within the membrane potential range tested (from rest to around -120 mV, n=11/45; 24%). For the other three quarters of non-dIN neurons, (n=34/45; 76%), sag potentials did appear in response to the protocol of hyperpolarising pulses, but only at extremely hyperpolarised membrane potentials not normally experienced by the neurons (mean sag appearance: -85.9 mV +/- 1.7, n=34, e.g. Figure 6Ai.). Indeed, when comparing the sag current at -80 mV between dINs and non-dINs (excluding those without a sag), there was a significantly smaller sag amplitude in non-dINs, with the mean sag amplitude close to 0 mV for these cells (Figure 6C, $p<0.01$, dINs: 6.38 mV +/- 0.3, n=3; non-dINs: 0.63 mV +/- 0.2; n=34). Nevertheless, the sag potentials that did appear at these hyperpolarised membrane potentials were clearly and significantly blocked by 50 µM ZD7288 (Figure 6Aii, D, Eii, $p<0.01$, n=4) demonstrating that they are likely mediated by HCN channels. Again, this resulted in a shift in the I-V relationship to the right (Figure 6Ei), but this was only clear at hyperpolarised membrane potential, supporting the idea that Ih is not active at rest in non-dINs. Overall, while dINs show a consistent Ih current at rest, a proportion of non-dINs show no evidence of Ih at any membrane potential, while the majority show small Ih current only at very hyperpolarised membrane potential ranges.

Figure 6. Ih currents in non-dINs. Ai. An example of the responses of a non-dIN to hyperpolarising current pulses of increasing amplitude. Compared to dINs, sag currents only appear at very hyperpolarised membrane potentials. **Aii.** The sag currents observed at hyperpolarised membrane potentials were abolished by the blocker of Ih currents, ZD7288 (10 µM). **B.** An expanded trace from Ai showing responses to hyperpolarising pulses. The peak and steady state membrane potential responses are indicated by dotted lines. **C.** A comparison of the sag amplitude at -80 mV in dINs and non-dINs. **D.** ZD7288 (50 µM) significantly abolished the sag potential at -90 mV. **Ei.** The current-voltage (I-V) relationship of the non-dIN shown in A and the effect of 50 µM ZD7288. In both control (circles) and in ZD7288 (triangles), both the peak and the steady-state Vm are plotted against each injected current step. **Eii.** The amplitude of the sag currents plotted against the membrane potential (mV).

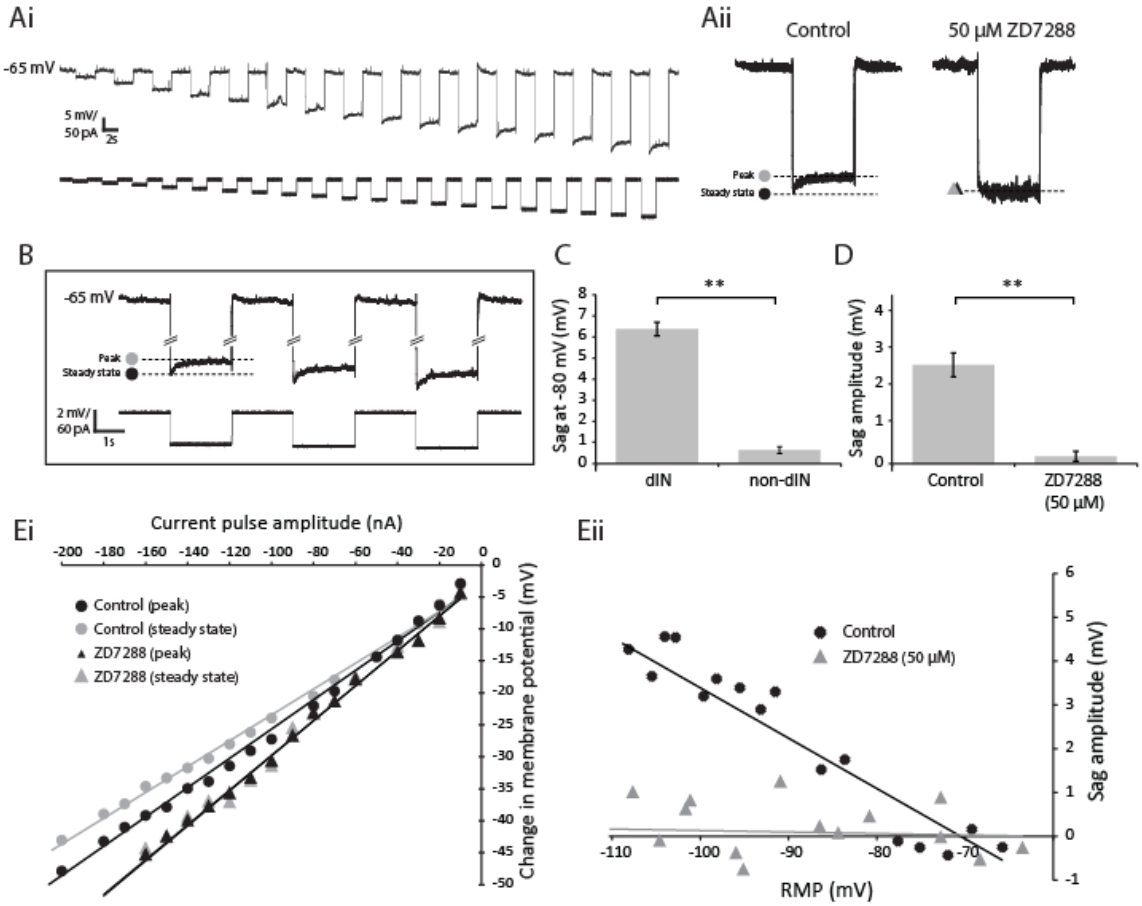
Ai
-65 mV
5 mV/
50 pA
2s
Aii
Control
50 µM ZD7288
Peak
Steady state
B
-65 mV
Peak
Steady state
2 mV/
60 pA
1s
C
Sag at -80 mV (mV)
**
dIN
non-dIN
D
Sag amplitude (mV)
**
Control
ZD7288
(50 µM)
Ei
Current pulse amplitude (nA)
-200 -180 -160 -140 -120 -100 -80 -60 -40 -20 0
Control (peak)
Control (steady state)
ZD7288 (peak)
ZD7288 (steady state)
Change in membrane potential (mV)
Eii
Control
ZD7288 (50 µM)
Sag amplitude (mV)
-110 -100 -90 -80 -70
RMP (mV)

Thus, Ih currents appears to be present in dINs at physiologically relevant membrane potential ranges, and are also present in around three quarters of non-dINs, but only at very hyperpolarised and physiologically irrelevant membrane potentials. Because dINs play a fundamental role in coordinating the swimming rhythm in *Xenopus* tadpoles, block of Ih should affect the swimming rhythm. To test this hypothesis, I explored the effects of blocking Ih currents on the swim network using ventral root recordings. Blockade of Ih currents had a clear effect on a number of parameters of swimming. Firstly, ZD7288 shortened evoked episode duration (Figure 5A, Bi, $p<0.05$, $n=6$). Secondly, although there was no significant effect on the number of spontaneous swim episodes in the presence of ZD7288, upon washout there was a clear increase in spontaneous swim episodes (Figure 5Aiii, Bii, $p<0.01$ compared to control, $p<0.05$ compared to drug, $n=6$). Finally, ZD7288 also affected the individual parameters of the swimming rhythm itself. There was a clear loss of the stability of the rhythm; the bursts became highly unstable and variable in terms of both cycle frequencies and burst durations (Figure 7A, Ci, Di) which manifested itself overall as a significant decrease in swim frequency (Figure 7Cii, $p<0.05$, $n=6$) and increase in burst durations (Figure 7Dii $p<0.05$, $n=6$).

Figure 7. The effects of ZD7288 on the *Xenopus* swim network. A. Raw traces showing evoked swim episodes in control (Ai) in the presence of the Ih current blocker ZD7288 (10 µM, Aii) and after washout (Aiii). The insets show an expansion of swimming with the rectified and integrated trace shown below. **Bi.** ZD7288 (10 µM) significantly shortened episode duration. **Bii.** Following washout of ZD7288 (10 µM), there was a significant increase in the number of spontaneous swim episodes. **Ci.** Timeplot showing mean swim cycle frequency across 3 evoked episodes in control, ZD7288 and after washout. Note that the swim frequency is lower and more variable. **Cii.** ZD7288 (10 µM) caused a significant decrease in cycle frequency($p<0.05$, $n=6$). **Di.** Timeplot showing mean burst durations across 3 evoked episodes in control, ZD7288 and following washout. **Dii.** ZD7288 (10 µM) caused a significant increase in burst duration ($p<0.05$, $n=6$).

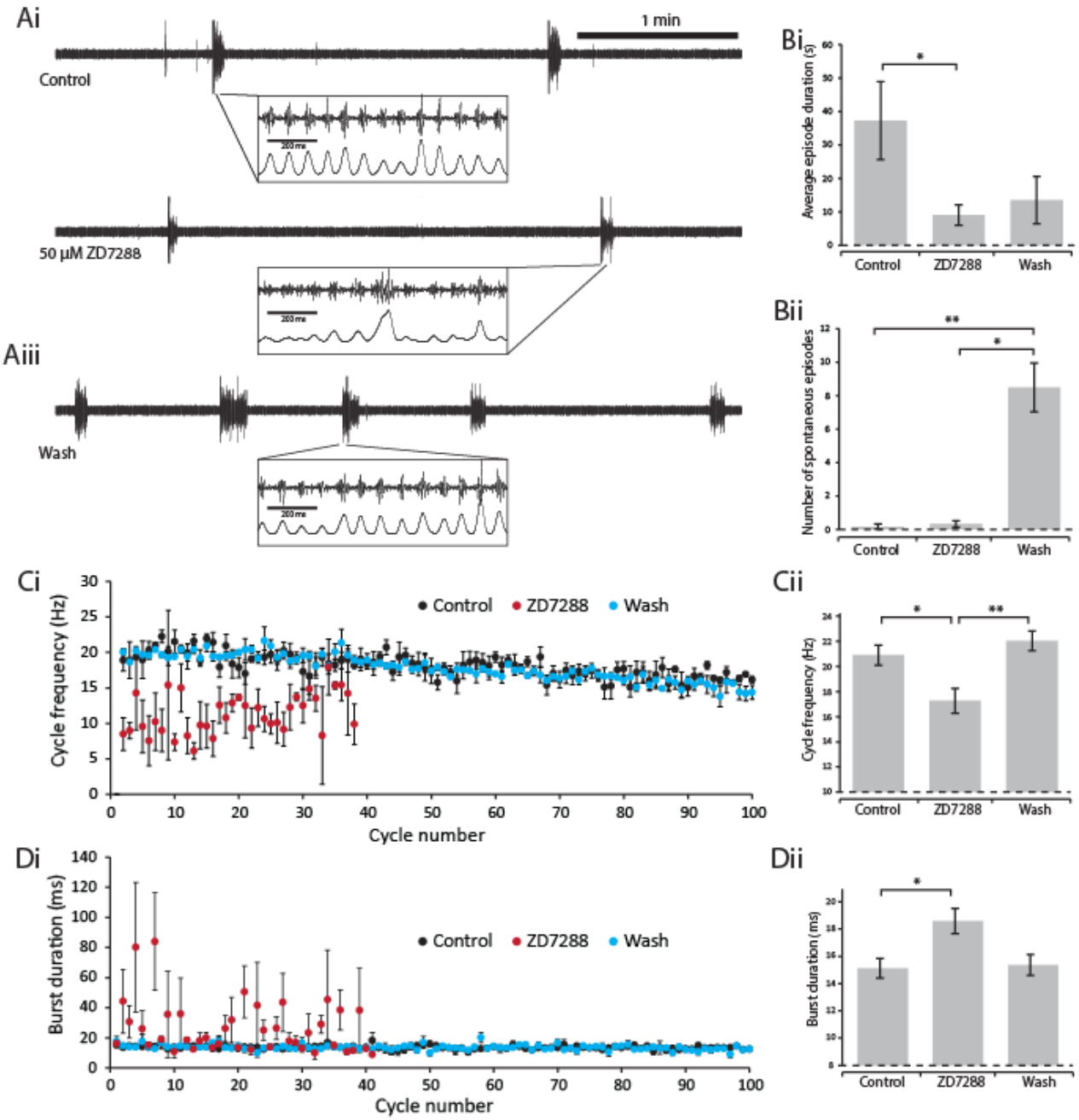
Ai
1 min
Control
50 µM ZD7288
Aiii
Wash
Bi
Average episode duration (s)
Control
ZD7288
Wash
Bii
Number of spontaneous episodes
Control
ZD7288
Wash
Ci
Cycle frequency (Hz)
Control
ZD7288
Wash
Cycle number
Cii
Cycle frequency (Hz)
Control
ZD7288
Wash
Di
Burst duration (ms)
Control
ZD7288
Wash
Cycle number
Dii
Burst duration (ms)
Control
ZD7288
Wash

Blockade of Ih currents using ZD7288 clearly had disruptive effects on the CPG network controlling swimming. Therefore, I next wanted to explore the effects of blocking Ih currents on cellular properties of individual CPG neurons. Because there were differences in the Ih currents in non-dINs and dINs, I treated these separately and explored the effects of ZD7288 on the properties and spiking of these two groups of neurons. For non-dINs, I found no clear effects of ZD7288 (50 µM) on resting membrane potential (Figure 8A, Bi, Bii, $p>0.05$, $n=4$). Similarly, there was no clear change in input resistance (Figure 8Bii, $p>0.05$, $n=4$). Despite a lack of direct effect on the intrinsic properties of non-dINs, I found that spiking during swimming activity was significantly affected, with uncoordinated and variable spiking (Figure 8C). Overall, across all experiments there was no apparent increase, or decrease in spiking, but less consistent numbers of spikes during the swim episodes. For instance, in some cycles, neurons would not spike at all but then would suddenly fire several action potentials in quick succession, coincident with large ventral root bursts (e.g. Figure 8Dii). Thus, despite a lack of effect of ZD7288 on the intrinsic properties of non-dINs, changes in their spiking patterns during swimming appear to correlate well with the deficits observed at the ventral root level. Thus, the overall conclusion from recordings in non-dINs is that they are not directly affected by Ih block but instead there appears to be an effect on the presynaptic excitatory CPG drive – i.e. the dIN population.

Figure 8. ZD7288 affects the spiking, but not RMP or input resistance, of non-dIN neurons. **A.** Raw trace of a non-dIN neuron show the lack of effect of ZD7288 (10 µM) on membrane potential. **B.** The resting membrane and input resistance plotted against experiment time. **Bii.** There was no overall effect of ZD7288 on RMP ($p>0.05$, $n=4$). **Bii.** There was no overall effect of ZD7288 on input resistance ($p>0.05$, $n=4$). **C.** Despite a lack of effect on RMP and input resistance, the spiking of non-dIN neurons during swimming was profoundly affected. **D.** Under control conditions (Di) the number of spikes per cycle (blue) was relatively constant and this was accompanied by a constant burst duration (red). In the presence of ZD7288 the number of spikes per cycle varied. Moreover, long burst durations coincided periods when spiking increased. These effects on spiking and burst duration returned to normal upon washout (Dii).

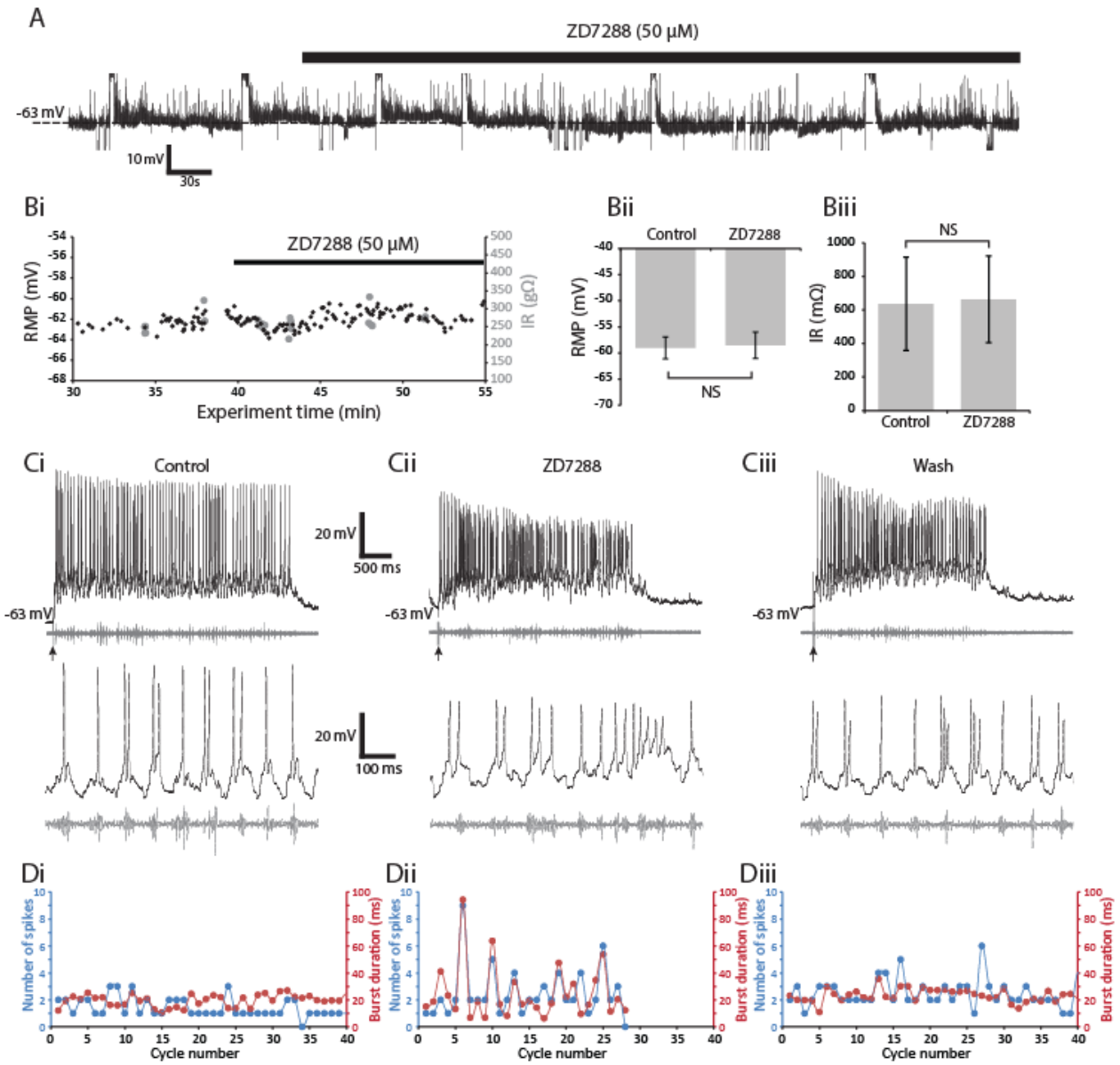
A
ZD7288 (50 µM)
-63 mV
10 mV
30s
Bi
ZD7288 (50 µM)
RMP (mV)
IR (gΩ)
Experiment time (min)
Bii
Control
ZD7288
RMP (mV)
NS
Biii
NS
IR (mΩ)
Control
ZD7288
Ci
Control
Cii
ZD7288
Ciii
Wash
20 mV
500 ms
-63 mV
20 mV
100 ms
Di
Dii
Diii
Number of spikes
Burst duration (ms)
Cycle number

The lack of a direct effect of ZD7288 on the intrinsic properties of non-dIN CPG neurons is not surprising in light of my earlier experiments suggesting that Ih only becomes activated at very hyperpolarised membrane potentials. However, the clear effect on spiking during swimming suggests that other neuron subtypes in the swim network must be affected, with dINs being the likely candidate. Unfortunately, using blind patch I only occasionally recorded from dINs; nevertheless in one dIN recording I applied ZD7288 and found clear effects. For this recording, ZD7288 (50 µM) significantly hyperpolarised the membrane potential (Figure 9A, Bi, Bii), and caused a clear increase in input resistance (Figure 9Bi, Biii). There was also an effect on spiking during swimming. ZD7288 caused multiple spike failures during swimming (Figure 9C). Finally, during the wash period there were clear membrane oscillations, usually triggering spontaneous swim episodes, but sometimes just leading to a small depolarisation (Figure 9D).

Figure 9. ZD7288 affects the spiking, RMP and input resistance of dIN neurons. A. Raw trace showing a clear membrane hyperpolarisation of approximately 10 mV following the application of ZD7288 (10 µM). **Bi.** Resting membrane potential and input resistance plotted against experiment time. **Bii.** ZD7288 (10 µM) caused a clear hyperpolarisation of the RMP for this dIN **Bii.** ZD7288 (10 µM) also caused a clear increase in input resistance. **C,D.** During swimming, dINs normally spike once per swim cycle (Ci, Di) but in the presence of ZD7288 there were frequent spike dropouts (Cii, Dii) which returned to normal after washout of the drug (Ciii, Diii). **D.** After washout of ZD728 there were clear membrane oscillations which were usually accompanied by spontaneous swim episodes, but occasionally there was only a small membrane depolarisation (asterisks).

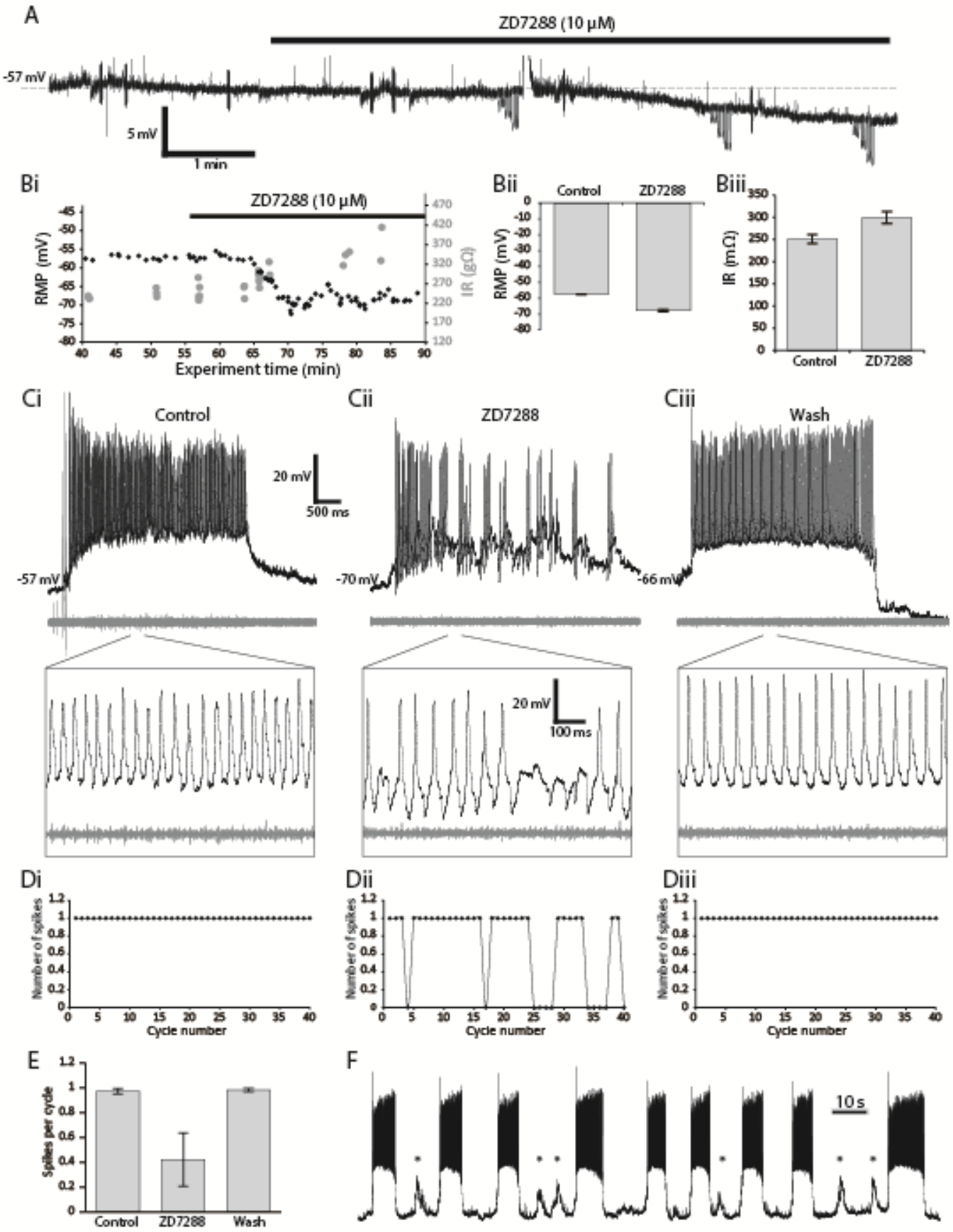
A
ZD7288 (10 µM)
-57 mV
5 mV
1 min
Bi
ZD7288 (10 µM)
RMP (mV)
IR (gΩ)
Experiment time (min)
Bii
Control
ZD7288
RMP (mV)
Biii
IR (mΩ)
Control
ZD7288
Ci
Control
20 mV
500 ms
-57 mV
Cii
ZD7288
-70 mV
Ciii
Wash
-66 mV
20 mV
100 ms
Di
Dii
Diii
Number of spikes
Cycle number
E
Spikes per cycle
Control
ZD7288
Wash
F
10 s

The effects of temperature on the Xenopus swimming and interactions with Ih and the sodium pump

I next wanted to explore the effects of manipulating the temperature on the *Xenopus* swim network and whether Ih and sodium pumps are affected in such a way as to contribute to the known temperature effects on swim output in *Xenopus* tadpoles. Using ventral root recordings, and consistent with previous studies on the effects of raising the temperature on the *Xenopus* swim network (Robertson & Sillar, 2009), raising the temperature of the bath saline caused a clear and significant decrease in swim episode duration (Figure 10A, Ci, $p<0.05$, $n=8$), which reversed upon return to control temperature. Secondly, there was also a significant increase in swim frequency at high temperature (Figure 10B, Cii, $p<0.001$, $n=8$) which again returned to normal when the temperature returned to baseline.

I next wanted to explore the effects of raising the temperature on the intrinsic properties of CPG neurons, which has not been documented previously. However, there were a number of technical difficulties using the previous heating method (Robertson & Sillar, 2009) whilst I attempted to make simultaneous patch-clamp recordings. For example, the device produced considerable noise in the recording, and whilst useful for producing a temperature ramp, it was very difficult to maintain high temperature for long enough periods to properly measure cellular properties. Nevertheless, preliminary recordings using this method showed that neurons consistently depolarised, accompanied by a decrease in input resistance (data not shown). However, to more carefully analyse these parameters in a more stable environment I used a Digitimer heating device (see methods). Consistent with my preliminary recordings, raising the temperature of the bath saline using the Digitimer saline heater caused a significant depolarisation of membrane potential (Figure 11A, B, C, $p<0.01$, $n=6$). Secondly, this depolarisation was accompanied by a significant decrease in input resistance (Figure 11B, Cii, $p<0.01$, $n=6$). These effects on both RMP and input resistance returned to normal after temperature was left to return to the control level.

Figure 10. The effects of raising the temperature on swim network. A. Raw trace showing the effects of raising saline temperature on swimming. **B.** Timeplots showing the mean swim cycle frequency for all experiments against swim cycle at control temperature (20 °C), after raising the temperature (30 °C) and upon return to control temperature (20 °C). **Ci.** Raising the temperature caused a significant decrease in swim episode duration ($p<0.05$, $n=8$). **Cii.** Raising the temperature also significantly increase swim cycle frequency ($p<0.001$, $n=8$).

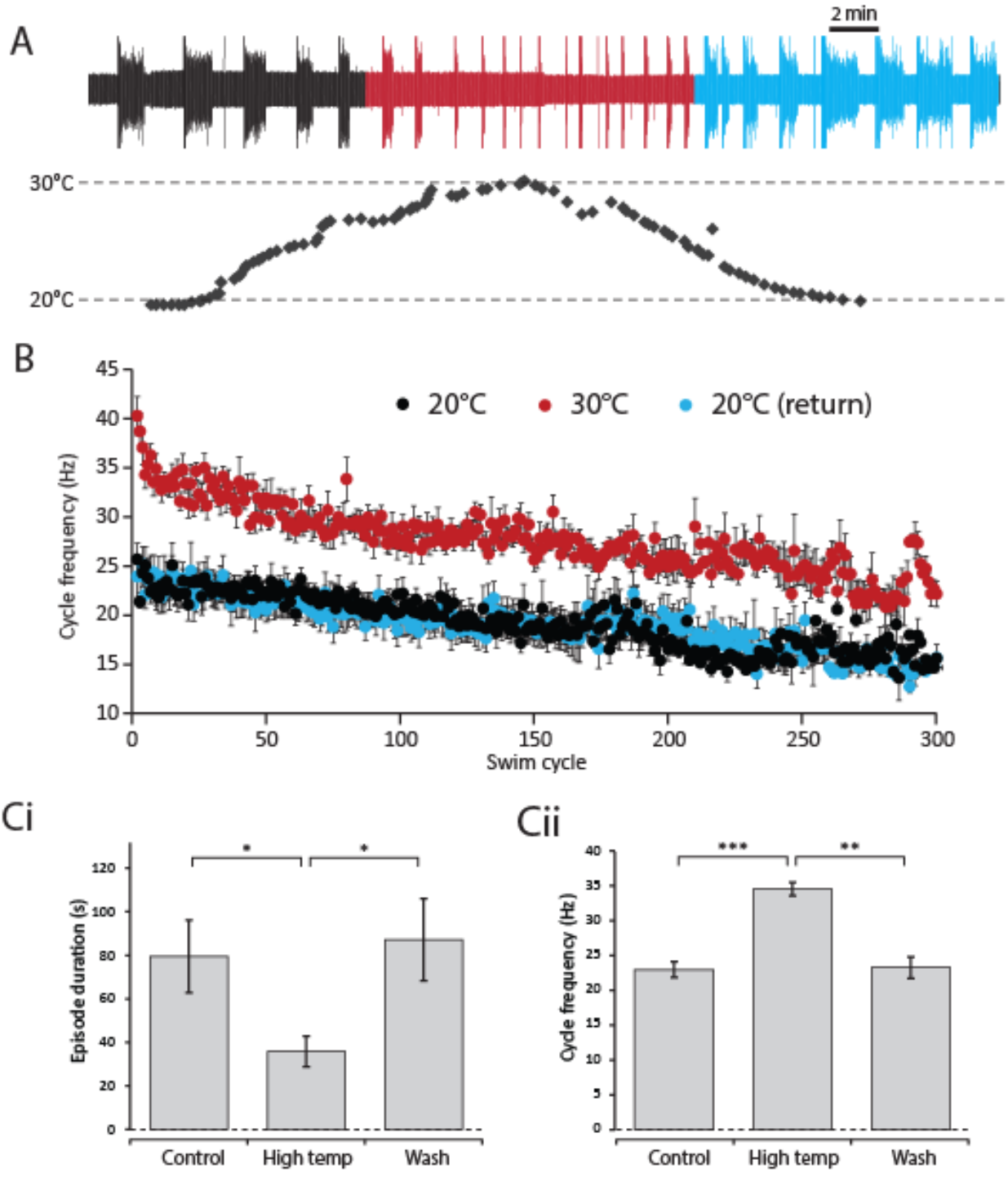
A
2 min
30°C
20°C
B
20°C
30°C
20°C (return)
Cycle frequency (Hz)
Swim cycle
Ci
Episode duration (s)
Control
High temp
Wash
Cii
Cycle frequency (Hz)
Control
High temp
Wash

Figure 11. The effects of raised temperature on the cellular properties of CPG neurons in *Xenopus* tadpoles. **A.** Raw trace showing a depolarisation as the temperature of the bath saline is raised, which returns as the temperature returns to control. **B.** Timeplot of the experiment shown in A showing the temperature, the RMP and the input resistance of the neuron. **Ci.** The RMP is significantly depolarised in response to an increase in the temperature of bath saline ($p<0.01$, $n=6$). **Cii.** The input resistance of CPG neurons is significantly decreasd in response to increased temperature ($p<0.01$, $n=6$).

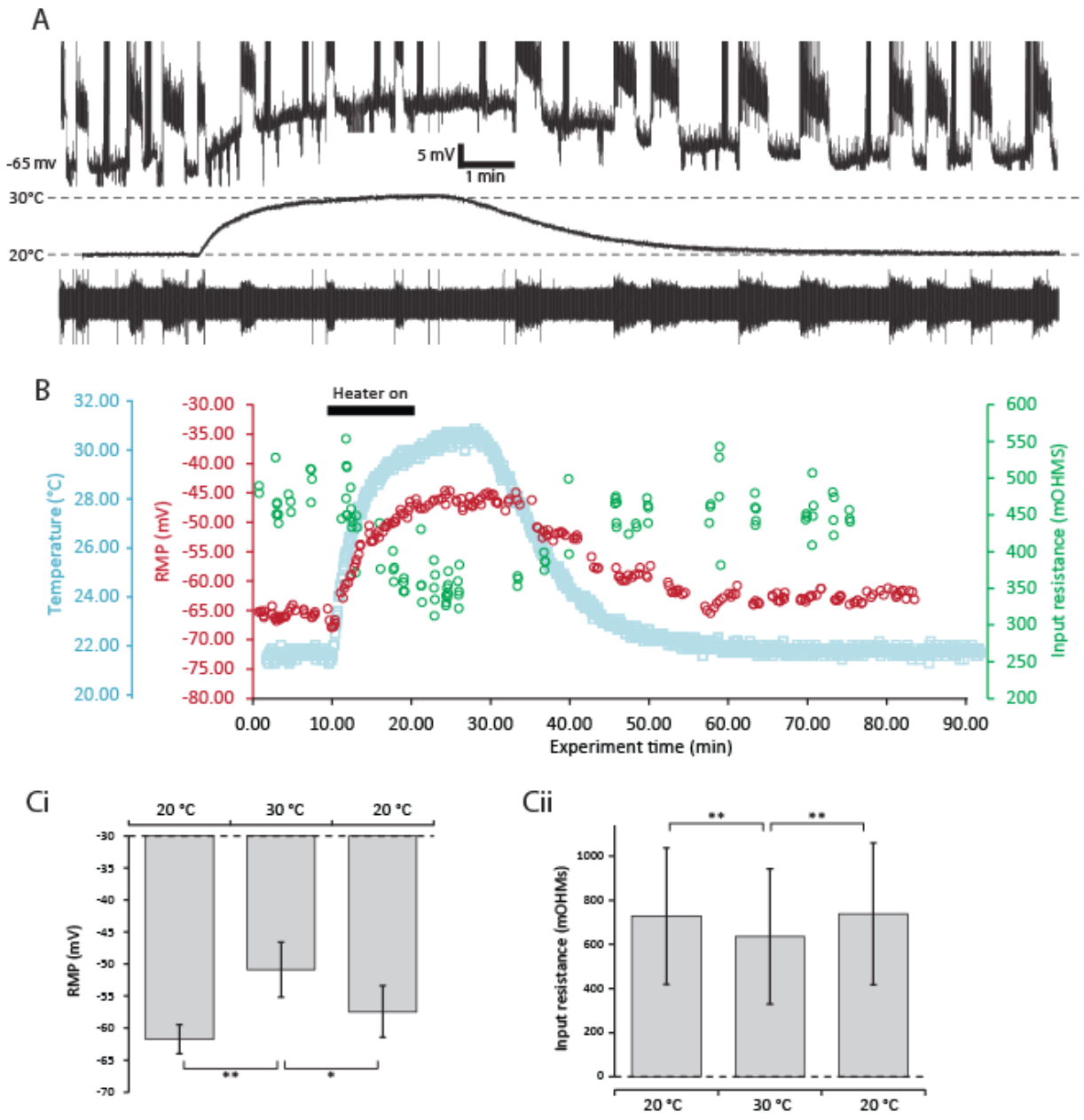
A
-65 mv
5 mV
1 min
30°C
20°C
B
Heater on
Temperature (°C)
RMP (mV)
Input resistance (mOHMS)
Experiment time (min)
Ci
20 °C
30 °C
20 °C
RMP (mV)
Cii
Input resistance (mOHMs)
20 °C
30 °C
20 °C

Next I wanted to explore the effects of temperature on the spiking of neurons during swimming. For non-dINs, most neurons fired between one and three action potentials per swim cycle at control temperature (e.g. Figure 12Ai). Once the temperature was raised, the probability that non-dINs would spike significantly increased (Figure 12A, Bi, $p<0.01$, $n=5$). In one experiment, the neuron only very occasionally spiked during swimming at all temperatures tested and therefore this neuron was excluded from the analysis. For dINs, which consistently fire only a single action potential per swim cycle, there was no change in spike probability at high temperature (Figure 12Bii, $p>0.05$, $n=2$).

The activity of the sodium pump has been shown to be sensitive to changes in temperature, therefore I also assessed whether there was a change in the usAHP after raising the temperature of the saline. Only 2/6 of our neurons showed a prominent post-swim usAHP. However, for both of these neurons there was an increase in the amplitude of the usAHP in response to a swim episode (Figure 13A, Dii, $n=2$). However, as shown above, CPG neurons fire more action potentials during swimming at higher temperatures. Therefore this increase in usAHP amplitude may not be a direct effect of raised temperature on the pump, but may be due to higher sodium influx from greater spike number per swim episode. Consequently, I used the protocols described earlier in the chapter to induce a usAHP in each condition. Interestingly 5/6 neurons showed a larger amplitude usAHP at raised temperature compared to control (Figure 13B, C, Di), whilst in one neuron the raised temperature unexpectedly caused a *decrease* in the amplitude of the usAHP (arrowed in Di). If this neuron is excluded from the analysis, there is a significant increase in the usAHP amplitude ($p<0.05$, $n=5$) which significantly returns after the temperature is decreased back to control. It is unclear why one CPG neuron responded differently to the others, but one possibility is that raising the temperature also increases the release of neuromodulators, some of which may act to decrease sodium pump activity, which could mask any increase in the usAHP (e.g. nitric oxide; see later results and discussion).

Figure 12. The effects of raised temperature on CPG spiking during swimming. A. Raw trace showing an intracellular recording of a non-dIN during swimming, with the ventral root trace showing below (grey). The inset on the right shows an expansion of the raw trace as marked by the black box. At control temperature (20 **°C**) the neuron occasionally spiked during swimming. After raising the temperature to approximately 30 **°C** the neuron spiked more regularly during swimming and occasionally fired multiple action potentials per swim cycle (Aii). Spike probability returned to normal after return to control temperature (Aiii). **Bi.** Raising the temperature caused a significant increase in spike probability in non-dINs ($P<0.01$, $n=5$). **Bii.** There was no effect of temperature on the spike probability of dINs ($p>0.05$, $n=2$) which consistently fired a single action potential per swim cycle at all temperatures. **C.** dIN firing during periods of escape swimming.

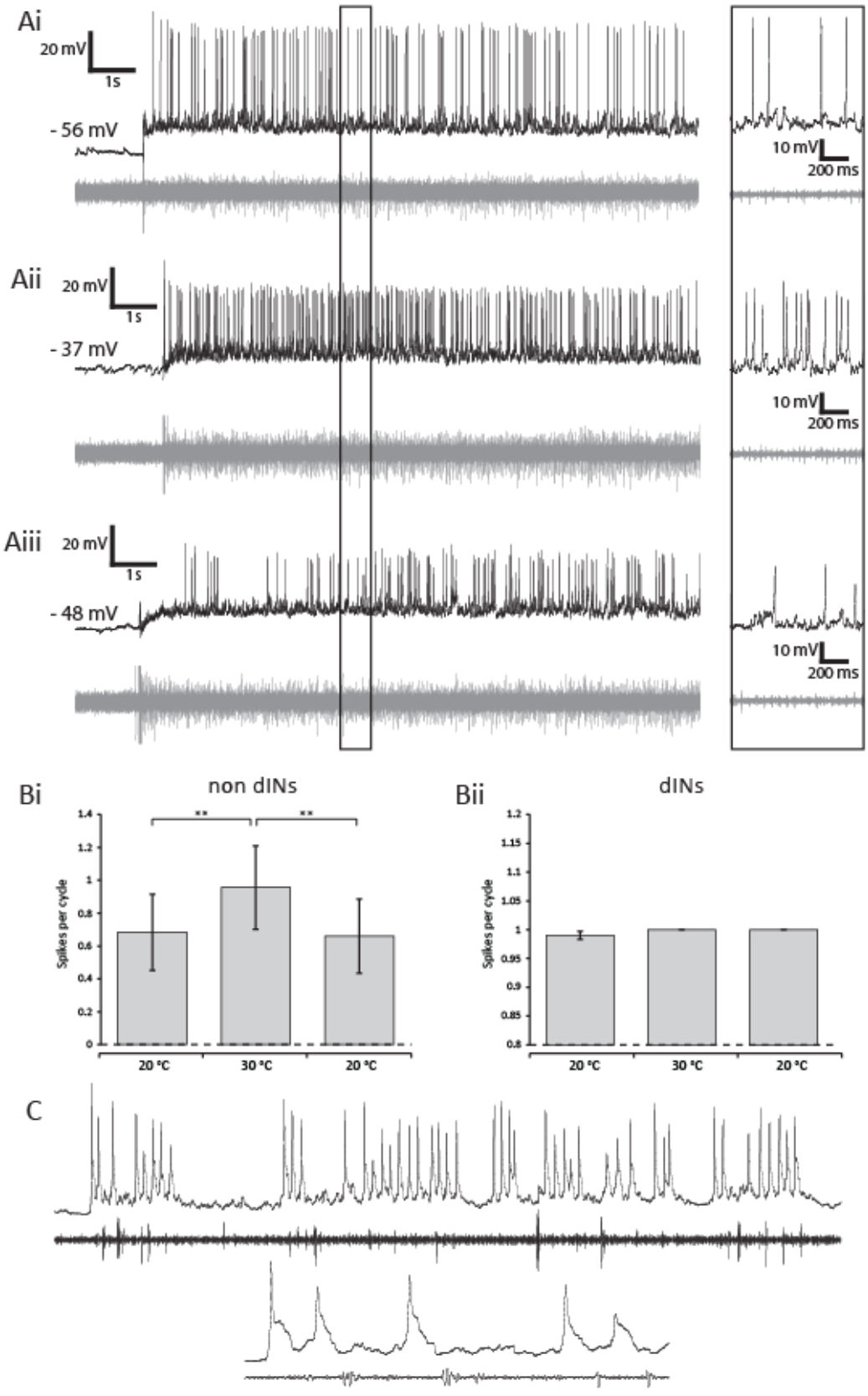
Ai
20 mV
1s
- 56 mV
10 mV
200 ms
Aii
20 mV
1s
- 37 mV
10 mV
200 ms
Aiii
20 mV
1s
- 48 mV
10 mV
200 ms
Bi
non dINs
Spikes per cycle
20 °C
30 °C
20 °C
Bii
dINs
Spikes per cycle
20 °C
30 °C
20 °C
C

Figure 13. The effects of raised temperature on the usAHP in CPG neurons. A. Raw traces showing episodes of swimming at different temperatures. Both the intracellular recording and the ventral root recording (grey) are shown. **B.** Examples of the usAHP at different temperatures in response to depolarising current pulses of increasing amplitude. **C.** Examples of the usAHP in response to a second protocol involving the induction of 500 action potentials. **Di.** Pooled data showing that in 5/6 neurons, raising the temperature caused a reversible increase in the amplitude of the usAHP in response to our protocols. However, in 1/6 neurons there was a reversible decrease in the amplitude (red arrow). **Dii.** In neurons which consistently displayed a usAHP following swimming, the amplitude of the post-swim usAHP was increased.

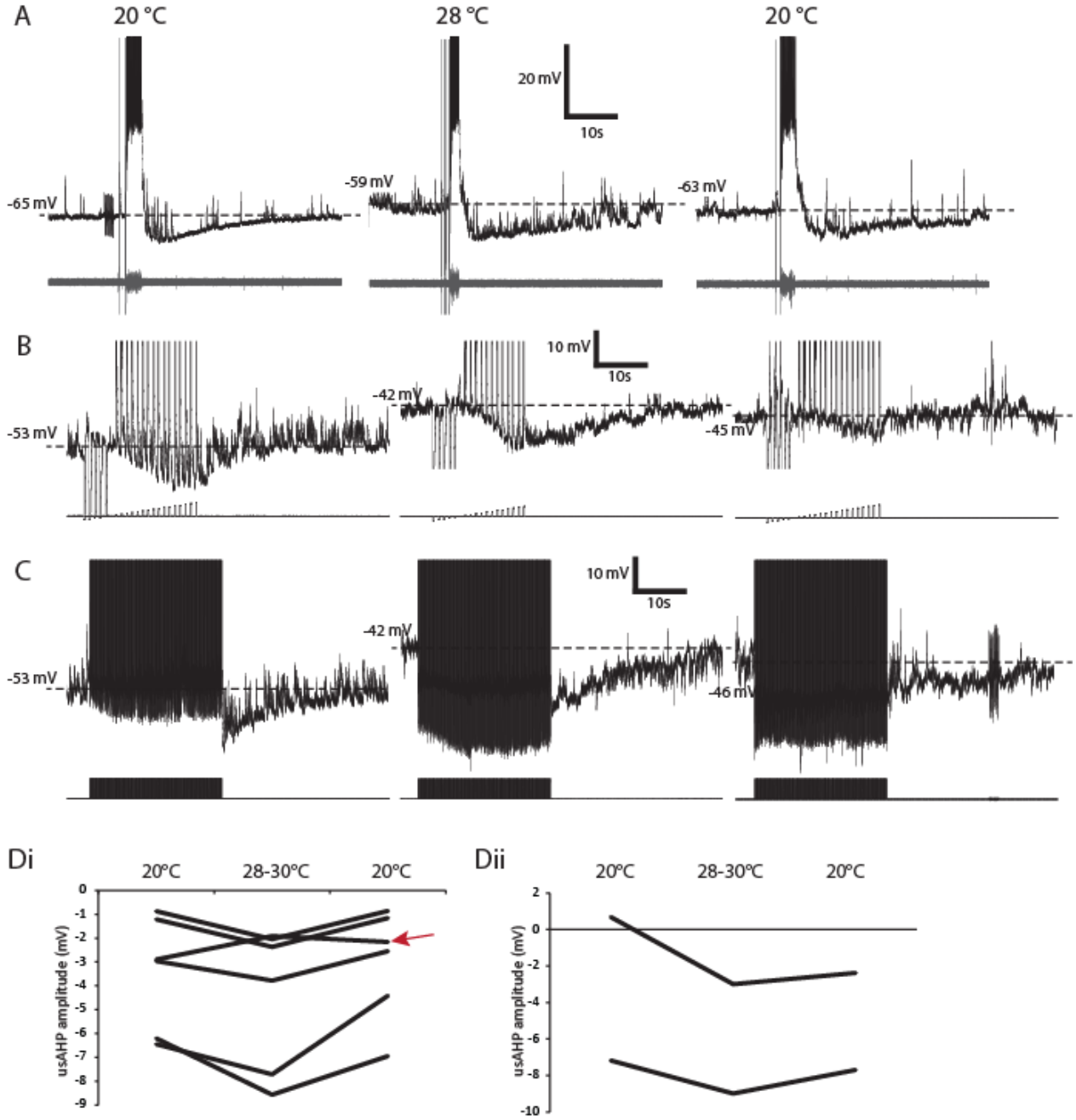
A
20 °C
28 °C
20 °C
20 mV
10s
-65 mV
-59 mV
-63 mV
B
10 mV
10s
-53 mV
-42 mV
-45 mV
C
10 mV
10s
-53 mV
-42 mV
-46 mV
Di
20°C
28-30°C
20°C
usAHP amplitude (mV)
0
-1
-2
-3
-4
-5
-6
-7
-8
-9
Dii
20°C
28-30°C
20°C
usAHP amplitude (mV)
2
0
-2
-4
-6
-8
-10

Finally, I explored whether temperature affected the Ih currents characterised in the previous section. After correcting for changes in RMP, raising the temperature of bath saline caused a clear decrease in the amplitude of sag potentials (Figure 14A, Bii). When comparing the steady state and peak components of these sag potentials (Figure Bi) it appears that the peak component at high temperature was shifted towards, and fairly closely matched, the steady state component, at control and high temperature. This result suggests that the decrease in sag potential amplitude could be explained by increased tonic activation of Ih, which in turn could explain the membrane depolarisation.

Figure 14. The effect of raised temperature on Ih currents. A. Responses of a dIN to hyperpolarising current pulses of increasing amplitude at control temperature (Ai) and at raised temperature (Aii). Note that in Ai the neuron is held depolarised to approximately -48 mV using DC current injection, whilst in Aii the neuron is depolarised due to raised temperature. **Bi.** The current-voltage (I-V) relationship of the dIN shown in A and the **e**ffect of raised temperature. **Cii.** The amplitude of the sag currents plotted against the membrane potential (mV).

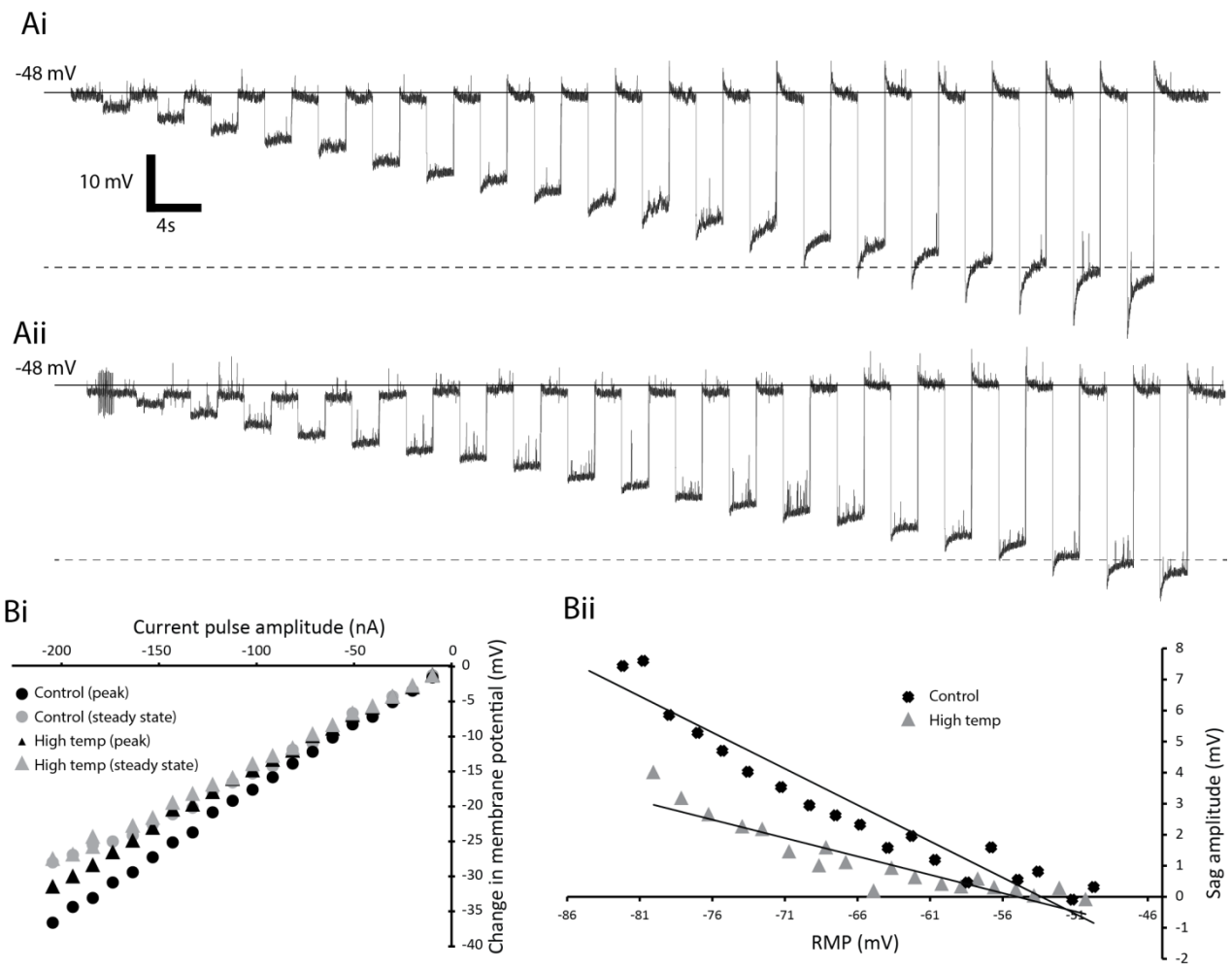
Ai
-48 mV
10 mV
4s
Aii
-48 mV
Bi
Current pulse amplitude (nA)
-200
-150
-100
-50
0
Control (peak)
Control (steady state)
High temp (peak)
High temp (steady state)
0
-5
-10
-15
-20
-25
-30
-35
-40
Change in membrane potential (mV)
Bii
Control
High temp
-86
-81
-76
-71
-66
-61
-56
-51
-46
RMP (mV)
8
7
6
5
4
3
2
1
0
-1
-2
Sag amplitude (mV)

Extrinsic modulation of the sodium pump by nitric oxide and dopamine

In addition to temperature, it is well established that a number of neuromodulators are able to modulate the activity of the sodium pump (Therien & Blostein, 2000). Nitric oxide and dopamine both play important roles in vertebrate motor control (Miles & Sillar, 2011), and specifically in this preparation (dopamine, this thesis; NO, (McLean & Sillar, 2004)), so I next tested whether these two neuromodulators had an effect on the usAHP. Firstly, I tested the effects of the nitric oxide donor S-nitroso-N-acetylpenicillamine (SNAP). Compared to control, SNAP (200 µM) caused a clear and significant decrease in the amplitude of the usAHP (Figure 15B, C, D, $p<0.01$, $n=7$) which returned upon washout of the drug.

To confirm this finding I used an alternative nitric oxide donor, 1,1-diethyl-2-hydroxy-2-nitroso-hydrazine (DEA-NO), which is known to more potently stimulate guanylate cyclase activity (Ferrero *et al.*, 1999). Compared to control, DEA-NO (200 µM) caused a significant decrease in the amplitude of the usAHP (Figure 16B, C, D, $p<0.01$, $n=5$), which returned to control levels upon washout. The effects of DEA-NO and SNAP were similar, with the main difference being the speed and potency of the effect on the pump current, with DEA-NO being more rapid and potent (Figure 16Di).

Finally, I wanted to test whether agonists at dopamine receptors were also capable of modulating the activity of the sodium pump. Firstly, I assessed the effects of the D2 agonist quinpirole. Quinpirole (25 µM) had no clear effects on the amplitude of the usAHP (Figure 19A, D). On the other hand, surprisingly, the D1 agonist SKF38393 caused a significant *increase* in the amplitude of the usAHP (Figure 19B, C, E, $p<0.05$, $n=7$), the opposite effects of the NO donors.

Figure 15. The effects of the nitric oxide donor SNAP on the activity-dependent sodium pump current. A. Anatomy of a cIN recorded in these experiments. **Bi.** An example of a sodium pump current (usAHP) generated by a rhythmically active spinal neuron in response to depolarising pulses of increasing amplitude. **Bii.** An example of the lack of usAHP generated by the same protocol in the presence of the nitric oxide donor SNAP. **Ci.** An example of a usAHP generated in response to 500 high frequency action potentials. **Cii.** A small usAHP is generated in response to the same protocol in the present of SNAP (200 µM). **Ciii.** An example of a recovered usAHP in the wash. **Di:** A timecourse plot showing the usAHP amplitude of the neuron shown in A and B illustrating the effect of SNAP. **Dii:** Pooled data across multiple experiments showing a significant reduction in usAHP by SNAP (200 µM) with a significant washout ($N=5$, $p<0.01$).

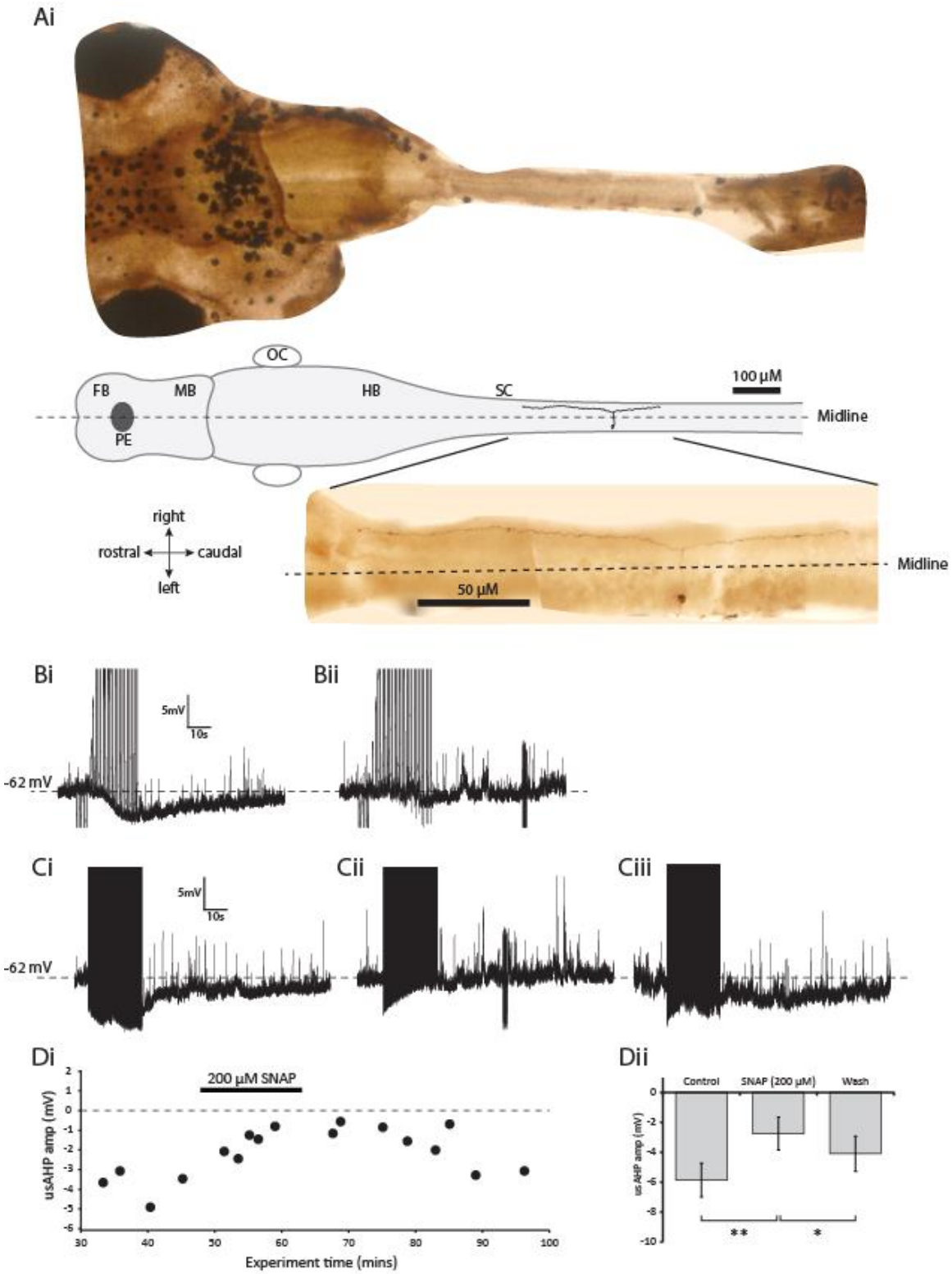
Ai
OC
FB
MB
HB
SC
PE
100 µM
Midline
right
rostral
caudal
left
50 µM
Midline
Bi
Bii
5mV
10s
-62 mV
Ci
Cii
Ciii
5mV
10s
-62 mV
Di
200 µM SNAP
usAHP amp (mV)
Experiment time (mins)
Dii
Control
SNAP (200 µM)
Wash
usAHP amp (mV)
**
*

Figure 16. The effects of the nitric oxide donor DEA-NO on the activity-dependent sodium pump current. A. Anatomy of the interneuron for B,C and D. **Bi.** An example of a sodium pump current (usAHP) generated by a rhythmically active spinal neuron in response to depolarising pulses of increasing amplitude. **Bii.** An example of the lack of usAHP generated by the same protocol in the presence of the nitric oxide donor DEA-NO (200 µM). **Biii.** An example of a recovered usAHP following drug washout. **Ci.** An example of a usAHP generated in response to 500 high frequency action potentials. **Cii.** A small usAHP is generated in response to the same protocol in the present of DEA-NO (200 µM). **Ciii.** An example of a recovered usAHP in the wash. **Di:** A timecourse plot showing the usAHP amplitude of the neuron shown in A and B illustrating the effect of DEA-NO. **Dii:** Pooled data across multiple experiments showing a significant reduction in usAHP by DEA-NO (200 µM) with a significant washout ($N=5$, $p<0.01$).

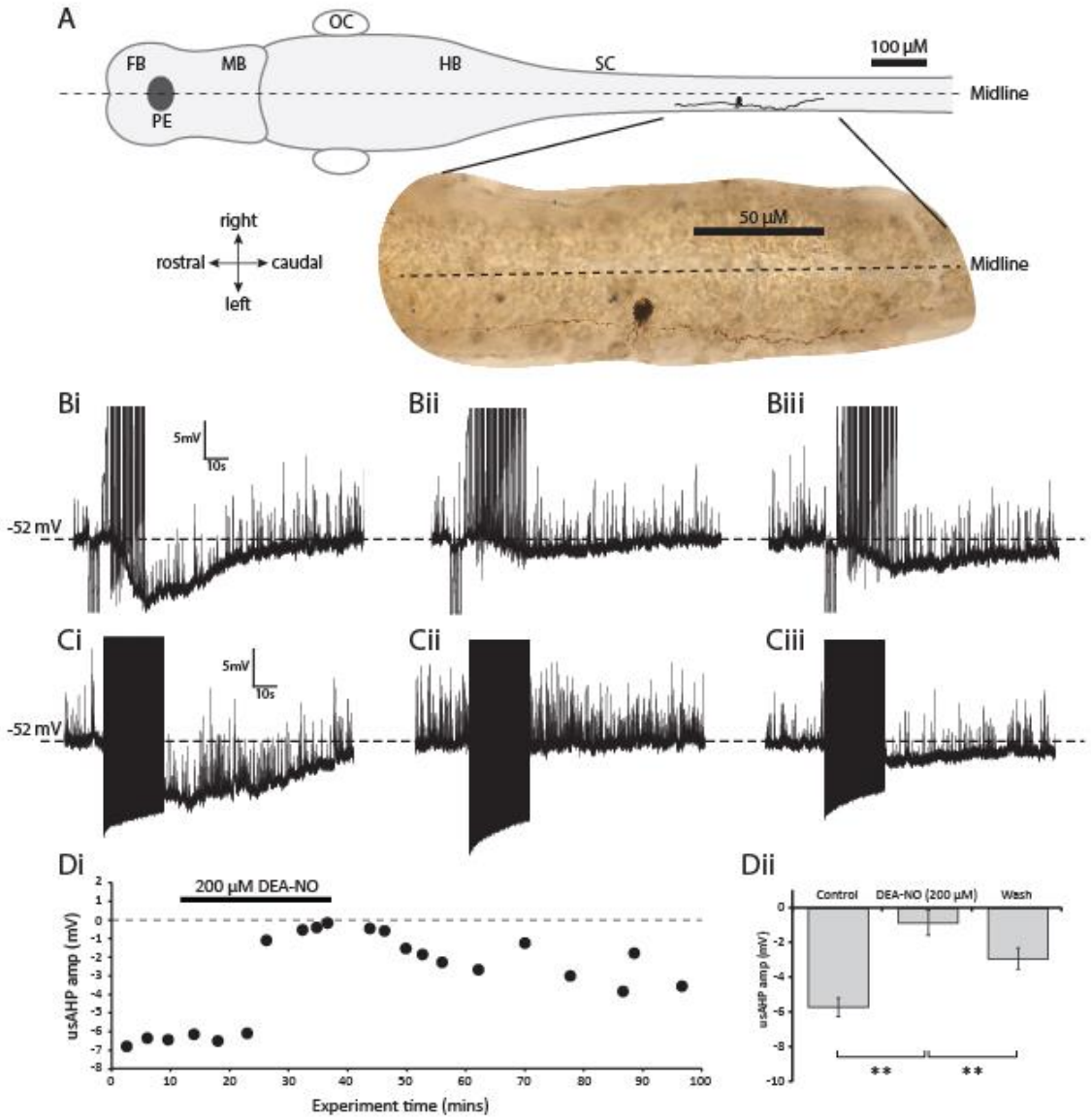
A
OC
FB
MB
HB
SC
PE
100 µM
Midline
right
rostral
caudal
left
50 µM
Midline
Bi
Bii
Biii
5mV
10s
-52 mV
Ci
Cii
Ciii
5mV
10s
-52 mV
Di
200 µM DEA-NO
usAHP amp (mV)
Experiment time (mins)
Dii
Control
DEA-NO (200 µM)
Wash
usAHP amp (mV)
**
**

Figure 17. The effects of the D2 and D1 receptor activation on the usAHP. A. D2-like receptor activation using quinpirole has no effect on the usAHP. **B.** D1-like receptor activation. **C.** A timecourse plot showing the usAHP amplitude of the neuron shown in F illustrating the effect of D1 receptor activation. **D.** Overall there was no significant increase in usAHP amplitude by quinpirole. **E.** Overall SKF38393 caused a significant increase in usAHP amplitude ($p<0.05$, $n=7$). **F.** Anatomy of a cIN used for the experiment shown in B.

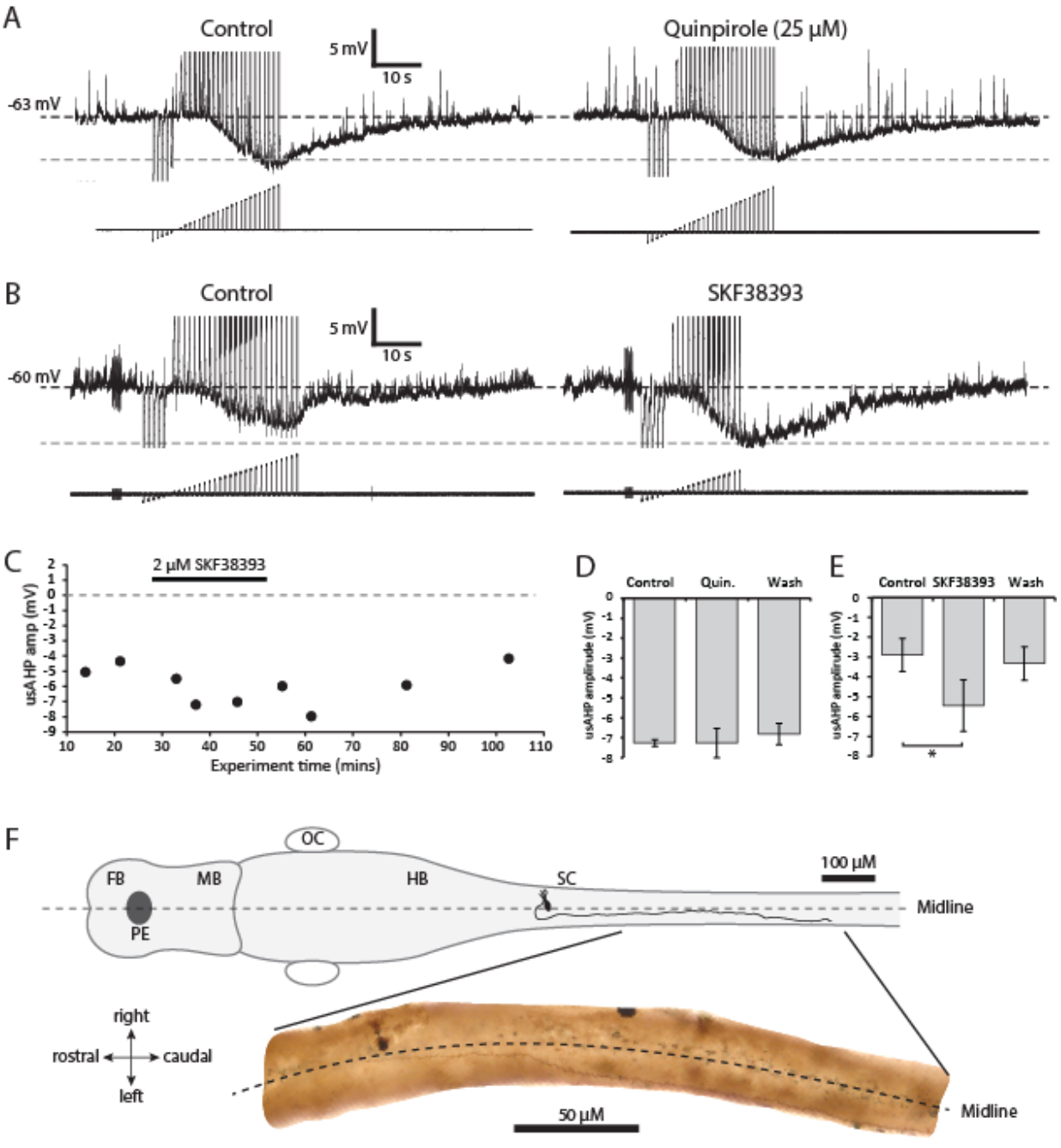
A
Control
5 mV
10 s
Quinpirole (25 µM)
-63 mV
B
Control
5 mV
10 s
SKF38393
-60 mV
C
2 µM SKF38393
usAHP amp (mV)
Experiment time (mins)
D
Control
Quin.
Wash
usAHP amplitude (mV)
E
Control
SKF38393
Wash
usAHP amplitude (mV)
*
F
OC
FB
MB
HB
SC
PE
100 µM
Midline
right
rostral
caudal
left
50 µM
Midline

Chapter 2 discussion

The usAHP and changes in intracellular sodium

In this chapter I have further characterised the pump-mediated usAHP and explored the effects of increasing activation of the pump current using monensin to flood CPG neurons with Na^+ ions. Raising intracellular sodium using monensin had clear inhibitory effects on the swim network; causing episodes to become shorter and slower. This is consistent with what would be expected from increased sodium pump activation, as blocking the sodium pump results in longer bouts and more intense swim activity (Zhang & Sillar, 2012). Moreover, I previously showed that swim episodes evoked after a short interval from a previous swimming episode, when the usAHP is still active, are shorter and slower; highly similar to swim episodes observed in monensin (Zhang *et al.*, 2015). Thus, monensin appears to act as a proxy for intense spiking activity by increasing intracellular sodium and in turn activating the sodium pump. Consistent with this hypothesis I found that the response to monensin differed depending on whether or not a neuron displayed a usAHP in control saline. Neurons with no obvious usAHP showed no change in RMP or IR in the presence of monensin, whereas those with a usAHP hyperpolarised to a value that matched the amplitude of the usAHP observed in control. This hyperpolarisation occurred without any clear changes in input resistance, further supporting the theory that it is mediated by an increase in ion pump activity, which involves no change in conductance. Furthermore, when I applied a usAHP-inducing protocol in these neurons after the monensin hyperpolarisation I no longer observed any clear pump-induced voltage change, suggesting that there is now a reduced capacity to respond to raised sodium, presumably because the pumps are fully active. This strongly suggests that the main effect of monensin on CPG neurons is to maximise sodium pump activity, essentially converting a dynamic, spike-dependent hyperpolarisation of the membrane potential into a tonic one. The effects of raising intracellular sodium levels are perhaps counterintuitive, as increasing intracellular Na^+ ions may initially be expected to depolarise neurons, and therefore exert excitatory effects on swimming. However, because monensin acts in an electroneutral

manner, only the inhibitory effects are observed, and this illustrates how powerful the sodium pumps are in homeostatically rebalancing the intracellular sodium concentration.

In one of the monensin experiments, the sodium pump blocker ouabain (1 µM) was applied after the monensin hyperpolarisation. Initially, this caused the neuron to depolarise back to the pre-monensin RMP, which stabilised for a few minutes, supporting the hypothesis that the monensin hyperpolarisation is mediated by the sodium pump. After a few minutes in ouabain, the tadpole started to fictively swim spontaneously, and this caused the neuron to fire intensely for a brief period, the RMP continued to depolarise, and eventually this appeared to cause a depolarising block on spiking before stabilising at approximately -3 mV. This depolarisation beyond the pre-monensin value is surprising as ouabain (at 1 µM) usually has no effect on the RMP (Zhang & Sillar, 2012), and monensin is known to be electroneutral as it exchanges positive Na^+ ions for H^+ ions in a 1:1 ratio (see later discussion). Therefore, one possibility, is that in this particular cell the recording was no longer viable and I had lost the cell.

Previous studies have explored the effects of monensin in a range of neuron types. For example, in neurons of the suprachiasmatic nucleus (SCN), monensin increases intracellular sodium and hyperpolarises the membrane potential due to increase sodium pump activity; an effect which is reversed by blocking the sodium pump (Wang *et al.*, 2012). Similar results have been found in hippocampal and striatal neurons (Azarias *et al.*, 2013). In these neuron types, the focus has also been on exploring which specific sodium pump subtypes are responsible for responding to increased sodium. The authors demonstrate that expression of the $\alpha 3$ sodium pump subtype is responsible for Na^+-induced hyperpolarisations, such as those described for monensin.

It is important to mention that previous studies have also found some side effects of monensin beyond sodium pump activation, including changes in membrane conductance (Inabayashi *et al.*, 1995) and changes in synaptic strength (Meiri *et al.*, 1981; Atwood *et al.*, 1983). To further explore the underlying causes of these off-target effects, one previous study carefully

monitored the effects of monensin on various ionic concentrations, membrane potential and pH in neurons and synaptosomes (Erecińska *et al.*, 1991). Consistent with all other studies using this drug, the authors found that monensin dramatically increased intracellular sodium - by around two-fold (from ~25mM to ~50mM) - which was accompanied by an approximate doubling of sodium pump activity. The authors also observed a small hyperpolarisation in neurons (~3 mV), presumably due to the known increase in sodium pump activity. In support of this hypothesis, when the sodium pump was blocked using ouabain in the presence of monensin, there was a large depolarisation (~24 mV), similar to our results after ouabain block, accompanied by a further rise in intracellular sodium (to around 75 mM). As mentioned above, monensin is expected to be electroneutral, and so the authors propose a number of possible explanations for this depolarization in monensin after block of the sodium pump. Although the primary effects of monensin involve changes in Na^+ and H^+ ion flux, a number of secondary ionic conductances and properties could also be affected. For example. the authors measured a small alkalinisation effect from monensin (~0.1.-0.4 unit increase in pH), due to a decrease in extracellular H^+ ions, but this was considered too small to mediate the large changes in RMP. Instead, the authors suggest that a likely explanation is the activation of Na^+-dependent outward ionic conductances. Another possible explanation is that increased intracellular sodium could reduce the driving force for the Na^+/Ca^{2+} exchanger, leading to increased intracellular calcium that could depolarise the neurons directly, or indeed activate Ca^{2+}-activated cation channels such as SK channels. However, (Erecińska *et al.*, 1991) measured only a “small and slow” increase in intracellular calcium following monensin application, and more importantly, the membrane potential changes were not occluded when calcium was excluded, suggesting that calcium is not involved in their observed depolarisation. On the other hand, these neurons were not spontaneously active, whereas in my experiments the large depolarization observed in monensin and ouabain occurred only after swimming, when calcium entry would occur during spiking in CPG neurons. In my experiments, therefore, it may be the inability to extrude increased calcium during swimming that could contribute to the

depolarisation. One way in future experiments to at least exclude the possibility of SK channels being involved would be to apply monensin in the presence of the SK channel blocker apamin.

The data in this thesis broadly support the overall theoretical framework for the effects of monensin based on the above studies. In summary, spike-dependent increases in intracellular sodium generate a usAHP that lasts around a minute after spiking has ceased. If intracellular sodium concentration is artificially raised using monensin to mimic spiking, sodium pumps become maximally active and generate a tonic hyperpolarisation. I suggest that the initial hyperpolarisation I observed under monensin in CPG neurons is therefore due to increased sodium pump activation, which is also responsible for the effects at the level of the swim network. Upon block of the sodium pump, the hyperpolarisation is abolished and the neuron returns to pre-monensin levels. At this point, intracellular sodium is high, but the net effect on membrane potential is mitigated by the equal and opposite exchange of H^+ ions. When the animal swims, however, spike-depenedent Ca^{2+} that enters the neurons may be prevented from being extruded due to decreased activity of the Na^+/Ca^{2+} exchanger, as a result of sodium imbalance. Moreover, there is some evidence that extracellular protons can also inhibit the Na^+/Ca^{2+} exchanger (Egger & Niggli, 2000), providing another possible mechanism for depolarisation in these conditions.

Ih currents

Ih currents are present in a range of rhythmic networks and are a target for neuromodulators; moreover, their activation can influence the rhythm of motor networks (Harris-Warrick & Marder, 1991). In this chapter I have documented the presence of an Ih current in tadpole swim CPG neurons, explored the impact of this current and the effects of blocking Ih on the swim network, as well as on individual CPG neuron properties. I found that blocking Ih using ZD7288 had clear and substantial effects on the swimming rhythm in *Xenopus* tadpoles. The most dramatic effects were observed on the fast swimming rhythm, whereby rhythmic swim episodes were generally characterised as having slower, longer bursts, which displayed more variable properties compared to the typically stable rhythm recorded in control conditions.

These disrupted swimming episodes terminated earlier than under control conditions. Previous studies have found similar slowing and/or disruptive effects of Ih blockade on rhythmic patterns of bursting activity. For example, the leech heartbeat network is disrupted by Ih block, causing tonic spiking to occur in heartbeat interneurons, interspersed with periods of inconsistent, unstable bursting (Angstadt & Calabrese, 1989). Moreover, enhancing Ih currents using the neuromodulator myomodulin has the opposite effect on the leech heartbeat and results in an increase in the frequency of the rhythm (Tobin & Calabrese, 2005). Similarly, blockade of Ih currents in stomatogastric ganglion (STG) neurons of the pyloric lobster network causes a slowing of rhythm frequency, suggesting that Ih also accelerates pacemaker activity in this system (Peck *et al.*, 2006). Injection of cRNA encoding Ih channels into rhythmically active neurons of the lobster STG enhances Ih current and increases cycle frequency (Zhang *et al.*, 2003). The presence of an Ih current has also been shown to slow the cycle frequency of molluscan motor networks. For example, in *Clione* (the sea angel), blocking Ih current causes a disruption and slowing of swim frequency (Pirtle & Satterlie, 2007). This is due to the introduction of a delay to post-inhibitory rebound spiking in swim interneurons, which is normally mediated by Ih current activation. Thus, an increase in Ih current appears to play a common role in rhythmic networks of stabilising the rhythm and increasing cycle frequency, and our effects of Ih blockade on the tadpole swim network are consistent with this contribution of Ih.

Can the disruptive effects of Ih blockade on the swim network be explained by the effects on specific CPG neurons described in this chapter? Non-dINs (cINs, aINs, MNs) are unlikely to be directly involved, simply because Ih appeared to be active only at very hyperpolarised membrane potentials, and therefore are likely not to play any major role; at least at this stage of development (stage 37-42), either at rest or during swimming. Moreover, Ih block (using ZD7288) had no effect on the membrane potential or input resistance of the non-dINs described here. Whilst they are unlikely to play a role at this stage of development under control conditions, their activation range may shift to more physiological membrane potentials

later in development, when Ih currents have been shown to be expressed more widely (Currie, 2014). It is also possible that their activation range in these neurons may be shifted, for example by the action of certain neuromodulators. However at this earlier stage of development, and under control conditions, I found that Ih currents predominate only in the dIN population at physiologically relevant membrane potentials. In dINs, Ih is active at rest and block of Ih caused a clear and large hyperpolarisation of ~10 mV, with an accompanying decrease in membrane conductance, demonstrating that Ih contributes to the resting properties of the rhythm-generating neurons of the tadpole swim network. Therefore the source of the effects on the swim network is likely to be these rhythm-generating dINs, although I cannot completely rule out additional contributions of Ih block outwith the CPG network. It is interesting that I found Ih to be active at rest in only a subset of CPG neurons (dINs), but not in others, although this heterogeneity is not unusual. For example, specific neurons of the leech heartbeat network, such as HNs and p-type mechanosensory neurons show a prominent Ih at rest; but other neuron subtypes, such as Retzius neurons only display a small sag current at very hyperpolarised levels (>-70mV) (Gerard *et al.*, 2012). Again, the HNs in this network are the excitatory rhythm-generating interneurons, and so it it is possible that Ih plays a common role in CPG networks in contributing to the rhythmicity of excitatory interneurons. Interestingly, it is well-documented (but not fully explained) that dINs are significantly more depolarised and have a lower input resistance than other CPG neurons in the *Xenopus* swim network (Sautois *et al.*, 2007), which is supported by our recordings. Thus, it is likely that the presence of an active Ih current in dINs could contribute to these differences in intrinsic properties.

If Ih current contributes towards the firing pattern of dINs during swimming then an important question is whether (and when) Ih becomes active during a swim bout. When I used DC current injection to hold dINs depolarised to ~-40 mV, I observed sag currents between -50mV and -55 mV in response to hyperpolarisation. During swimming, the membrane potential of dINs reaches around -55 mV at its most negative peak, and therefore will be just

within the range of Ih, as predicted by sag potentials. However, whilst sag potentials were only small (~1 mV) at around -50-55 mV, our dIN recording hyperpolarised by at least 10 mV in response to ZD7288, suggesting that the measure of Ih using sag potentials is likely to be an underestimation. Indeed, some studies have found that the “signature” sag component can sometimes even be partially masked by a leak potassium current at certain membrane potentials (Debanne *et al.*, 2006).

Overall it seems highly likely that Ih currents are active in dINs during swimming, but how do they contribute towards spiking? One possibility is that Ih currents provide a *dynamic* depolarising force that contributes towards post-inhibitory rebound (PIR) in each swim cycle. Indeed, for most studies on the role of Ih in rhythmic networks, the presence of an Ih current accelerates and stabilises the rhythm frequency (as discussed earlier) through a mechanism involving an enhancement of the amplitude or rate of PIR. For example, this is the mechanism through which Ih increases cycle frequency in *Clione* swimming (Pirtle *et al.*, 2010); in the lobster pyloric network (Harris-Warrick, 1995); and in CPG interneurons in the turtle spinal cord (Smith & Perrier, 2006). In *Xenopus* tadpoles, each cycle of swimming is driven by a single, synchronous spike in each member of the dIN population, which activates various CPG interneurons, including the inhibitory cIN population. The cINs provide glycinergic, mid-cycle inhibition to the contralateral dIN population, which not only ensures that when one side of the CPG is active the other side is silent, but this mid-cycle inhibition also causes PIR in the contralateral dIN population that triggers the next swim cycle (Roberts *et al.*, 2010; Li & Moult, 2012). Thus, one possible explanation for the effects of ZD7288 is that Ih current activation contributes to the cyclical PIR mechanism in the dINs that maintains swimming. Thus, blocking Ih weakens dIN spike depolarisation, causes dINs to drop out of the rhythm, ultimately leading to a destabilisation of swimming rhythm generation. However, it is important to note that at rest, whilst hyperpolarisation does generate sag potentials, this does not result in PIR spiking upon removal of the hyperpolarisation. However, when I held dINs depolarised close to the membrane potential reached by dINs during swimming (~-48mV), PIR spiking does occur in

response to even relatively small hyperpolarisations (Figure 5Fii). Thus, these results suggest that during swimming a dynamic Ih current is active and may contribute to the fast rhythm during swimming, possibly through a contribution of Ih to PIR in dINs. The spike pattern of non-dINs was also disrupted, despite Ih not being active at rest. This is likely a secondary effect of the Ih block in dINs, whose dropout during swimming presumably weakens cIN mid-cycle inhibition, in turn leading to periods of sporadic, intense firing in other CPG neurons which rely on mid-cycle inhibition to become switched off midway through each swim cycle.

Whilst one explanation is that Ih contributes to swimming on a cycle by cycle basis, the kinetics of Ih channels are often slow (several seconds), and therefore it could be questioned whether changes in Ih can occur fast enough to modulate fast spiking. On the other hand, Ih kinetics vary greatly between different cells, with Ih in cardiac cells activating slowly (several seconds), but relatively rapidly in CA1 neurons (~30 ms) (Robinson & Siegelbaum, 2003). These differences generally reflect different HCN channel expression, with the HCN1 channel subtype having the fastest time constant (Bois *et al.*, 2011). Even within a neuron type, there can be huge variation in activation kinetics; in spiral ganglion neurons in the auditory system, the activation kinetics of HCN channels show both fast components (~20 ms time constant) as well as slow components (~ 550 ms time constant) (Liu *et al.*, 2014), with the fast end of the range equating to approximately half a swim cycle in *Xenopus* tadpoles. Thus, the range of time constants that can be involved in Ih activation mean that it is plausible that Ih could be dynamically activating and deactivating on a cycle by cycle basis in *Xenopus* dINs.

Others have also argued that even if Ih activation is unchanging (i.e. not turning on and off during rhythmic activity), the presence of a *tonically* active Ih current can also affect spike shape by contributing to both spike depolarisation and repolarisation phases. For example, in trigeminal sensory neurons, blockade of Ih using ZD7288 increases action potential half-width duration, with the authors suggesting that Ih facilitates both depolarisation and repolarisation during an action potential, depending on the membrane potential relative to the Ih reversal potential (~-37.5 mV) (Tanaka, 2002; Cho *et al.*, 2011). In other words, tonic Ih current

contributes to depolarising the cell until the spike crosses -37.5 and then contributes an outward current that helps repolarise the cell. In turn, these effects on spike shape in trigeminal neurons have been shown to diminish the ability of neurons to maintain repetitive spiking (Hogan & Poroli, 1999; Tanaka, 2002). Indeed, block of Ih has also been shown to result in action potential failures in other systems, such as in the cerebellum (Baginskas *et al.*, 2009).

In other systems, Ih appears to play a role in the network, but doesn't directly affect either spike shape, or the intrinsic properties of the neurons in which it is expressed. For example, in the respiratory network, blocking Ih unexpectedly increases the burst frequency, but has no effect on the membrane potential of rhythm-generating neurons (pacemaker type 2 neurons) (Thoby-Brisson *et al.*, 2000). However, this effect of increasing rhythm frequency, and the lack of effect on RMP, suggests that Ih plays a specialised role here that differs from most other systems, where the rhythm frequency is typically decreased by a block of Ih.

Finally, it is likely that the spontaneous bouts of swimming I consistently observed upon washout of ZD7288 can also be explained by an effect on the dIN population. Upon washout, I observed dIN membrane potential oscillations, providing evidence that not only does Ih contribute to the fast swimming rhythm in *Xenopus*, but that it may also contribute to the slower pattern of rhythmic episodes of swimming which emerges during development. It seems likely that the spontaneous rhythm during the washout of ZD7288 is due to hyperactivation of Ih, which seems to cause dINs to enter a rhythm of slow depolarisation and hyperpolarisation. At this point it is unclear whether these are synaptic or intrinsic in origin. Future experiments using blockers of synaptic transmission would need to be performed in order to distinguish these possibilities. It is interesting that during *Xenopus* development, Ih appears to become more widespread (Currie, 2014) in conjunction with increased spontaneous swimming (Currie *et al.*, 2016), and it may be that the stable spontaneous rhythm observed upon washout of ZD7288 resembles a more mature swim network with overexpression of Ih.

Overall, based on my findings in this chapter I hypothesise that Ih is activated in dINs during swimming, and block of Ih reduces a depolarising force that facilitates dIN spiking during swimming. Future experiments will seek to determine whether Ih is more dynamically activated by mid-cycle inhibition from cINs, or whether the contribution from Ih persists throughout a swim episode. Moreover, future experiments will need to more carefully define exactly the extent to which Ih is active during swimming, as well as which HCN channels are involved. Finally, I also provide evidence that hyperactivation of Ih, during washout of ZD7288, causes the swim network to enter a pattern of regular spontaneous swim episodes, suggesting that Ih may also be involved in the transition from an irregular, evoked swimming pattern to regular, spontaneous swimming as development proceeds.

Temperature

I also explored the effects of manipulating temperature on the *Xenopus* swim network, including exploring the effects on the usAHP and Ih current. Temperature plays a particularly important role in the physiology of cold-blooded animals (poikilotherms) such as *Xenopus* tadpoles, which are unable to regulate their internal temperature, and temperature can thus have a profound effect on the functioning of CPG circuits. Changing the temperature of a CPG circuit can affect a whole range of processes, from ion diffusion rates, to the rate of conformational changes in proteins. Ultimately, this will affect spike conduction and synaptic delays.

Raising the temperature had a clear effect on the overall swim network, causing episodes to have a higher swim frequency but become shorter in duration. This is consistent with a previous study which focused on effects of raised temperature on the *Xenopus* swim network (Sillar & Robertson, 2009). In this study, once the temperature was raised to above ~34 °C, it also became impossible to evoke swimming (hyperthermic failure), and in a subsequent study it was shown that the threshold and time to recovery from hyperthermic failure was tuned by nitric oxide modulation (Robertson & Sillar, 2009). Activating the nitric oxide/cGMP pathway either using the nitric oxide donor SNAP or 8-bromo-cGMP caused the recovery from

hypothermic failure to take longer, whilst inhibitors of the pathway (CPTIO, ODQ, L-NAME) had the opposite effects. The mechanisms underlying the temperature effects on the swim pattern in *Xenopus* are not fully understood, although they are likely to be the consequence of Q_{10} relationships of specific, temperature-sensitive proteins, including ion channels and pumps (Robertson, 2004). An acceleration of cycle frequency is a common effect of raising temperature in poikilotherms, and is likely due to the well-established effect of a temperature-induced decrease in synaptic and conduction delays (Robertson, 2004; Robertson & Money, 2012). This effect of increasing cycle frequency in response to raised temperature has been shown in a wide range of CPG networks, including the mouse respiratory network (Tryba & Ramirez, 2003); the leech heartbeat network (Arbas & Calabrese, 1984); the network controlling crawling in *Drosophila* larvae (Barclay *et al.*, 2002); and the crab pyloric network (Tang *et al.*, 2010). It is less well understood why episode durations get shorter at higher temperatures in *Xenopus* tadpoles. One possibility is that nitric oxide, which decreases episode durations, contributes to this effect. However, (Robertson & Sillar, 2009) state in their discussion a number of factors "…*lead us to believe that most of the temperature-induced shortening of swim episodes is not mediated via NO*".

My results using intracellular recordings provide clues as to why raising the temperature increases swim frequency and shortens episode duration. I found clear evidence that when the temperature of the bath saline is increased it causes a depolarisation of CPG neurons, which is accompanied by a decrease in input resistance. This, in turn, caused an increase in spike probability in non-dIN CPG neurons. These recordings included a number of cINs, whose spiking activity has been shown to determine the cycle frequency of the *Xenopus* swimming rhythm (Li & Moult, 2012). Therefore, it is likely that the temperature-induced increase in swim frequency relates to an increase in the firing of cINs, which in turn will increase PIR in dINs, leading to an earlier dIN spike onset in the subsequent cycle, reducing the cycle period.

The profound decrease in episode duration could be due to a number of factors. However, based on the finding that spike probability increases as the temperature is raised, the explanation is likely to involve a spike-dependent mechanism such as that ascribed to the sodium pump, whose role in restricting the duration of swimming in *Xenopus* tadpoles is described earlier in this chapter, (Zhang & Sillar, 2012). The usAHP amplitude is proportional to the number of spikes discharged by a neuron and therefore it is reasonable to assume that raising the temperature will result in the generation of a usAHP during swimming at a faster rate than at control temperature. Indeed, in neurons that displayed a usAHP following swimming in control, I found that this post-swim usAHP was larger at higher temperatures, even for a shorter swim episode.

This suggests that one possible explanation for shorter episode durations at higher temperature is simply that the swim circuit is more excitable - CPG neurons fire more spikes per cycle and with a faster cycle frequency, and this results in more rapid intracellular sodium accumulation and the accumulation of a usAHP earlier, that contributes to premature swim termination. Moreover, the sodium pump protein itself is also highly temperature sensitive, with a Q_{10} value measured at around 2 for temperatures between 20-37 °C (Glitsch & Pusch, 1984; Nakamura *et al.*, 1999). Thus, it would also be expected that the sodium pump ion exchange rate would increase when the temperature is raised, independent of spike number. Using protocols to induce a usAHP, I found evidence in support of this hypothesis. Importantly, the larger usAHP in response to these protocols is not due to higher spike number, as I utilised a protocol that consistently triggers 500 action potentials in each condition. However, the increase in usAHP amplitude was only significant when one outlier experiment was excluded in which the usAHP reversibly *decreased* in amplitude at the higher temperature. Although it is difficult to explain the result of this single experiment, one possibility is that this specific neuron was targeted by a neuromodulator that decreased the activity of the sodium pump; and increased temperature resulted in an increase in this negative pump neuromodulation which masked any increase in the usAHP. One possible candidate for this neuromodulation

is nitric oxide, which I show in this chapter to decrease the usAHP. Whilst in this one experiment the usAHP amplitude decreased, 5/6 neurons showed a reversible increase in usAHP amplitude with temperature. Increases in sodium pump mediated hyperpolarisations in response to raised temperature have been observed in other systems. For example, in neurons at the calyx of Held it was shown that the amplitude of a spike-dependent pump current (described as a "post-tetanic hyperpolarisation (PTH)" in that study) was increased when the temperature was raised from 22 to 35 °C (Kim & von Gersdorff, 2012), similar to our experiments. Similarly, pump-mediated AHPs in CA1 pyramidal neurons are enhanced at raised temperatures (Gulledge *et al.*, 2013). Interestingly, in this study the authors also found that at room temperatures, AHPs produced by spike trains had calcium-dependent contributions, whilst at 35 °C the calcium contribution was negligible and the hyperpolarisation was entirely mediated by the sodium pump.

Beyond the sodium pump, other mechanisms are also likely to be involved in the shorter episode durations in *Xenopus* tadpoles, due to the fact that raising the temperature will have widespread effects on the CPG network. An alternative, activity-dependent run-down mechanism known to play a role in swim episode durations involves purinergic signalling (Dale & Gilday, 1996). At the start of swim episodes, ATP levels are high and are known to block specific K^+ channels, therefore maintaining a high level of excitability at the start of swimming. As swimming proceeds, ATP is broken down into adenosine, which blocks Ca^{2+} channels, impairing synaptic transmission and reducing excitability, slowing swim frequency, and contributing to the run-down and eventual termination of swimming. Thus, one possible additional contributor to the shortened swim episodes at high temperature could be that adenosine accumulates faster in the network, leading to premature episode termination.

Overall, I suggest that increased cycle frequency and shortened episode durations are likely due to a temperature-induced depolarisation, which leads to more spikes during swimming, which raises cycle frequency but also accelerates the development of a usAHP, as well as other activity-dependent mechanisms. Membrane depolarisations are a common response to

temperature in a number of neuron types, but the identity of the ion channels responsible for such effects varies. For example raising the temperature depolarises neurons in the octopus cochlear nucleus through effects on Ih currents and a low-voltage activated potassium current (Cao *et al.*, 2011). Similarly, in both pre- and post-synaptic neurons at the calyx of Held, raising the temperature also depolarises cells but it was shown that this was predominantly mediated by an increase in Ih current, due to the accompanying decrease in input resistance and the partial occlusion of the depolarisation by ZD7288 (Kim & von Gersdorff, 2012). Indeed, Ih channels appear to be commonly involved in temperature-induced depolarisations, an observation originally made in the heart (DiFrancesco & Ojeda, 1980). Other temperature induced changes in ion channel activation include the closure of leak K^+ conductances, such as 2-pore-domain potassium channels including TASK and TREK. In my recordings I observed a decrease in input resistance, therefore it is unlikely to involve the closure of a K^+ channel, but is more likely to predominantly involve the opening of a temperature-sensitive Na^+ channel. Other possible ion channels that are known to be opened by increased temperature include transient receptor potential (TRP) channels. Indeed, a TRP channel has been shown to mediate a depolarisation similar to mine in cultured *Xenopus* spinal neurons (Wang & Poo, 2005).

Together, my results contribute to our understanding of the effects of temperature on the neural circuit controlling swimming in *Xenopus* tadpoles. I found evidence supporting previous studies that swimming frequency increases with temperature, in parallel with a decrease in the duration of swim bouts. The recordings suggest that raising the temperature reversibly depolarises a range of CPG neuron types, accompanied by a decrease their input resistance, suggesting the opening of a temperature-sensitive sodium channel. The identity of these channels is unknown, although are likely to include HCN channels, at least for dINs, where Ih is active at rest. This depolarisation across CPG types leads to increased spike probability during swimming, causing greater and faster sodium influx, which in turn leads to greater sodium pump activation. This leads to the more rapid generation of a usAHP by the sodium

pump, whose exchange activity is also directly increased by temperature, which contributes to the premature termination of swimming.

Extrinsic modulation of the sodium pump

In addition to changes in intracellular sodium and temperature, sodium pump activity is also under the control of a range of modulators in a number of different tissue types (Therien & Blostein, 2000). This is particularly well-studied in kidney and cardiac tissue, where sodium pumps have been shown to be modulated by adrenaline, noradrenaline, dopamine and peptide hormones via complex and varied downstream pathways. Neuronal sodium pumps are also subject to regulation by neuromodulators, although this is less well studied. Serotonin has been shown to have clear inhibitory effects on the amplitude of the pump-dependent AHP observed in tactile sensory neurons of the leech (Catarsi *et al.*, 1993), whilst serotonin enhances glial sodium pump activity in the cerebellum and hippocampus (Peña-Rangel *et al.*, 1999). Sodium pump modulation has also been studied in the context of rhythm-generating CPG networks. In the network controlling the leech heartbeat, the neuropeptide myomodulin inhibits pump activity which results in an increase in the heartbeat rhythm (Tobin & Calabrese, 2005).

One of the most common modulators of sodium pump activity, especially in cardiac tissue, is nitric oxide - a diatomic molecule produced by the enzyme nitric oxide synthase (NOS) that is involved in the regulation of a wide range of cellular functions. Nitric oxide most commonly has an inhibitory effect on sodium pump activity (McKee *et al.*, 1994; Liang & Knox, 1999; Ellis *et al.*, 2000, 2003); although it has also been shown to have excitatory effects in some tissues (Cox & Johnson, 1998; William *et al.*, 2005; Pavlovic *et al.*, 2013). In my experiments, the application of the nitric oxide donors SNAP and DEA-NO caused a clear and reversible decrease in the usAHP across a range of neuron types; consistent with the majority of previous studies that show that nitric oxide inhibits sodium pump activity. There are a number of possible mechanisms through which nitric oxide could be acting on the pump. However, the effects most likely involve the nitric-oxide mediated increase in guanylate cyclase activity,

which leads to an increase in cGMP. The rise in cGMP in turn activates PKG, leading to the phosphorylation of a range of proteins, including the sodium pump (McKee *et al.*, 1994; Lincoln & Komalavilias, 2000). Indeed, in cases where nitric oxide has been shown to inhibit the sodium pump, the mechanism involved has often been shown to involve facilitation of the cGMP/PKG pathway (McKee *et al.*, 1994; Liang & Knox, 1999; Ellis *et al.*, 2000). Moreover, whilst the role of nitric oxide modulation of sodium pumps in the spinal cord has only been reported in one study previously (Ellis *et al.*, 2003), in this case it was also shown to involve the cGMP/PKG pathway. In *Xenopus* tadpoles, the role of nitric oxide in the control of swimming is well described and involves the cGMP/PKG pathway (McLean & Sillar, 2000, 2004). In young *Xenopus* tadpoles*,* potentiation of nitric oxide signalling causes a reduction episode duration by directly facilitating GABA release from mid-hindbrain reticulospinal (MHR) neurons; whilst simultaneously slowing the swim frequency indirectly, by facilitating noradrenergic neuromodulation to potentiate glycinergic inhibition. The role of the sodium pump inhibition described in this chapter was explored at the single cell level, rather than at the level of the overall swim network. It is difficult to link this nitric oxide pump inhibition, which would be expected to be excitatory, with the known inhibitory effects of nitric oxide on swimming. However, bath application of nitric oxide will affect many physiological targets in the swim network, and some of the nuanced effects on swimming could potentially be masked. Indeed, it has indeed been shown that nitric oxide depolarises CPG neurons, which is also unexpected given the network effects of nitric oxide (McLean & Sillar, 2002, 2004). Thus, nitric oxide targeted to motoneurons specifically, without the activation of MHR neurons, could conceivably lengthen the duration of swimming through the removal of the usAHP mechanism, without the GABAergic inhibition responsible for reducing swim episode duration.

Another neuromodulator known to target the sodium pump in a range of tissue types is dopamine (Therien & Blostein, 2000). Similar to nitric oxide, dopamine, acting via PKA or PKC, can enhance or inhibit pump activity depending on the species, tissue type and dopamine receptors involved (Zhang *et al.*, 2013). In striatal neurons, D2-like receptor activation

stimulates sodium pumps by inhibiting PKA, thus dephosphorylating the α3 subunit; (Bertorello *et al.*, 1990; Wu *et al.*, 2007). Other studies have similarly shown that changes in PKA activity can modulate the ability of a neuron to respond to changes in intracellular sodium through phosphorylation/dephosphorylation of the α3 sodium pump subtype (Azarias *et al.*, 2013). My experiments revealed that the activation of D1 receptors, but not D2 receptors, led to an increase in the amplitude of the usAHP. It is slightly unexpected that the activation of D1-like receptors modulates the usAHP in *Xenopus* spinal neurons, yet overall has no significant effects on the swim network (see chapter 1, Figure 2). It is possible that the change in usAHP amplitude may be too small, or may be masked by other D1 mediated effects on the network, such that D1-like agonists have no clear effects on overall network output. An alternative, and more likely explanation, is that the protocols used to induce a usAHP when testing the effects of the D1 agonist may involve higher intensity spiking than is normally experienced by CPG neurons during normal swimming at these developmental stages. Indeed, the number of spikes per swim cycle increases during development, and therefore the subtle increase in the usAHP amplitude by D1 modulation may become more important as development progresses. It will be interesting to see the importance of this sodium pump modulation by D1-like receptor activation later in development when D1-like agonists have clear effects on spontaneous swimming (Clemens *et al.*, 2012; Currie, 2014).

Overall, these results demonstrate that the usAHP can be toggled up (D1 activation) and down (nitric oxide) to give a wide dynamic range of pump-mediated network output configurations. Moreover, it is likely that other neuromodulators not studied in this thesis, but which are known to influence *Xenopus* swimming, may be acting at least in part through modulation of the sodium pump.

Chapter 2 conclusions

In this chapter I have explored the roles of the usAHP, temperature, Ih currents, and sodium pump modulation. I have demonstrated, at the network and cellular levels, the consequences of raising intracellular sodium in spinal CPG neurons, using the sodium ionophore monensin. Monensin acts as a proxy for intense spiking, essentially "fatiguing" the network and causing swimming to become shorter in duration and slower in frequency. These effects are due to the potentiation of sodium pump activity – the dynamic, spike-dependent usAHP present in subsets of neurons becomes tonically activated, leading to a pump-mediated hyperpolarisation without any changes in membrane conductance. I have also explored the role of the Ih current in the *Xenopus* swim network. Ih currents are differentially expressed across CPG neurons, with non-dINs displaying Ih only at non-physiological membrane potentials, whilst the rhythm-generating dINs show Ih activation at rest. I show that Ih is blocked by ZD7288, which disrupts the swimming rhythm and leads to slower, shorter swim episodes. This network effect appears to be due to a disruption of the core rhythm-generating role of dINs, which become hyperpolarised when Ih is blocked, accompanied by a decrease in input resistance; this leads to uncharacteristic dIN spike failures during swimming. This effect on dINs also appears to have knock-on effects for firing in other CPG neurons during swimming, despite the intrinsic properties of these neurons being unaffected by Ih block. Firing in non-dINs becomes irregular, leading to periods of erratic spiking which accompany intense ventral root output. I have also explored the effects of raising the temperature on the *Xenopus* swim network. Increasing the temperature of the bath saline led to shorter swim episodes with higher cycle frequency. This appears to be due to a heat-induced depolarisation of multiple CPG neuron types, which is accompanied by a decrease in input resistance, suggesting the opening a temperature-sensitive sodium channel. As a result of this depolarisation, neurons spike at higher frequency, which likely activates a number of activity-dependent run-down mechanisms, including the pump-mediated usAHP, providing a likely explanation for shorter episode durations at high temperatures. Finally, I also explored the role of extrinsic

neuromodulation of the sodium pump, using the parameters of the usAHP to demonstrate that sodium pump activity can be both reduced (by nitric oxide) and enhanced (by dopamine) in the *Xenopus* swim network.

Chapter 3: The role of sodium pumps in mammalian locomotor networks

Chapter 3 contributions and publications

This chapter is adapted from previously published work (Picton, Nascimento, Broadhead, Sillar & Miles (2017) Journal of Neuroscience). All experiments were conducted by Laurence Picton except for patch clamp data presented in figure 8 and 9, which was collected by Filipe Nascimento. Laurence Picton designed all experiments, interpreted all data and constructed all figures.

Chapter 3 summary

As outlined in chapter 2 and the overall introduction, sodium pumps play an important role in invertebrate and vertebrate motor control. However, very little is known about the contribution of sodium pumps to mammalian locomotion. In this chapter, I explore the effects of manipulating sodium pump activity on the output of the locomotor network in the spinal cord of neonatal mice, using both pharmacological and electrical stimulation. The sodium pump inhibitor, ouabain, increased the frequency and decreased the amplitude of drug-induced locomotor bursting, and these effects were found to be highly dependent on the presence of the neuromodulator dopamine. Conversely, activating the pump using the sodium ionophore monensin significantly decreased burst frequency. In addition, monensin caused a decoupling of the left and right sides of the spinal cord, but synchronised the normally alternating flexor-extensor relationship. When more “natural” locomotor output was evoked using dorsal-root stimulation, ouabain increased burst frequency and extended locomotor episode duration, whilst monensin slowed and shortened episodes. I also manipulated the interval between evoked episodes of locomotor activity. Decreasing the time between dorsal-root stimulation, and therefore inter-episode interval, shortened and slowed activity, suggesting that pump activity may encode information about past network output and contribute to feedforward control of subsequent locomotor bouts. Indeed, this was confirmed by blocking the sodium pump, which abolished the relationship between evoked episodes of locomotor activity. Finally, using whole-cell patch-clamp recordings, a long duration (~60s), activity-dependent, TTX and ouabain-sensitive, hyperpolarising current (~5mV), is also described. The duration of this dynamic pump current is enhanced by dopamine**.** These results therefore reveal sodium pumps as dynamic regulators of mammalian spinal motor networks and as targets for neuromodulatory control.

Chapter 3 Introduction

In chapter 2 I explored how activation of the sodium pump through spike- or drug-dependent increases in intracellular sodium can contribute a large hyperpolarisation to the membrane potential of neurons that can have important consequences for locomotor networks. Activity-dependent sodium pump currents have been found in a range of cell types across diverse species (outlined in detail in the introduction to this thesis). These include sensory neurons in leech and lamprey (Parker *et al.*, 1996; Scuri *et al.*, 2002); pre- and post-synaptic neurons at the Calyx of Held synapse (Kim *et al.*, 2007); and in various neuron subtypes in the mammalian brain including cerebellar Purkinje fibres (Forrest *et al.*, 2012), CA1 pyramidal neurons (Gulledge *et al.*, 2013), dopaminergic midbrain neurons (Johnson *et al.*, 1992), and neurons of the suprachiasmatic nucleus (Wang & Huang, 2006). Pump currents play an especially important role in regulating rhythmically active networks, such as those involved in the coordination of locomotion. As described in the previous chapter on *Xenopus* tadpoles, sodium pumps generate a spike-dependent hyperpolarisation of spinal neurons that both weakens and terminates swimming, and impairs future activity for around a minute, acting as a short-term motor memory mechanism linking past to future network activity (Zhang & Sillar, 2012; Zhang *et al.*, 2015). Similarly, *Drosophila* larvae motoneurons generate a pump current which regulates the frequency of crawling locomotor behaviour (Pulver & Griffith, 2010).

There are relatively few studies exploring the role of sodium pumps in mammalian networks of the spinal cord and brainstem. However, compared to other classes of animal a considerable amount is known about the distribution of sodium pump subtypes in the mammalian nervous system, so it is worth providing an overview of the current state of understanding in the context of studies in mammalian rhythmic networks. There are four catalytic α-subunit isoforms (α1 - α4) in mammals, with neurons predominantly expressing α1 and α3 (Hieber *et al.*, 1991). As described in detail in the introduction, the α3 subtype has a lower Na^+ affinity and is sub-maximally active in resting neurons, allowing it to act as a sensor for activity-dependent rises in intracellular Na^+ (Dobretsov & Stimers, 2005; Azarias *et al.*,

2013). The subsequent increase in α3-pump activity not only restores intracellular Na^+ levels, but can also generate a membrane hyperpolarisation that reduces the excitability of the neuron for tens of seconds. A recent study characterised the distribution of α1 and α3 in the mouse spinal cord (Edwards *et al.*, 2013). They found that α1 sodium pumps were present in cervical, thoracic and lumbar spinal cord, but its expression was relatively restricted to mainly ependymal cells and large ventral horn neurons, including α-motoneurons. On the other hand, α3 sodium pumps were found to be more widespread throughout the spinal cord, including in motoneurons and interneurons of differing sizes and locations across cervical, thoracic and lumbar regions. However, α3 immunofluorescence was especially high in medium and small spinal neurons, and especially high in γ-motoneurons, where α1 expression was low. Overall, this study illustrates that α3 sodium pumps, the subtype thought to be responsible for activity-dependent pump currents, are widespread in the mouse spinal cord and found in a number of spinal neuron types that contribute to locomotion; the functional relevance of this remains to be explored. Importantly, the frequency of locomotor bursts *in vivo* has been shown to fall within the 0.5-2Hz range in mice, which is ideally placed to be influenced by a dynamic usAHP (Meehan *et al.*, 2012).

There is a need to understand the role of sodium pumps in mammalian networks as their functional impairment has been linked to a range of disorders. There are currently three rare neurological disorders in humans known to be caused specifically by mutations in the *ATP1A3* gene encoding the α3 sodium pump protein. These including Alternating Hemiplegia of Childhood (AHC, (Heinzen *et al.*, 2012)); Rapid-onset Dystonia Parkinsonism (RDP, (De Carvalho Aguiar *et al.*, 2004)); and Cerebellar ataxia, Areflexia, Pes cavus, Optic atrophy and Sensorineural hearing loss (CAPOS) syndrome (Demos *et al.*, 2014). Furthermore, dysfunction of the α3 sodium pump subtype is also known to contribute to Amyotrophic Lateral Sclerosis (Ellis *et al.*, 2003; Ruegsegger *et al.*, 2015); epilepsy (Krishnan *et al.*, 2015) and bipolar disorder (Kirshenbaum *et al.*, 2012*a*). Because of the importance of the α3 sodium

pump to a number of disorders of the nervous system, currently four mouse models have been created to study the *in vivo* effects of changes in α3 expression and/or activity (reviewed in (Holm & Lykke-hartmann, 2016)). For example, *Myshkin* (Mysk) mice carry an inactivating mutation (I810N) which reduces neuronal α3 sodium pump activity by about 40% in heterozygotes (Homozygote *Myshkin* mice die shortly after birth (Clapcote *et al.*, 2009)). These mice show a number of symptoms related to manic bipolar episodes, epileptic seizures as well as dystonia symptoms similar to those observed in RDP (Clapcote *et al.*, 2009; Kirshenbaum *et al.*, 2012, 2012*a*, 2013). Importantly, *Myshkin* mice also show several motor deficits, with the most obvious being an increase in locomotor activity (hyperambulation), which is faster compared to wild type mice and involved longer distances travelled. They also show gait problems (an "…unsteady, tremorous gait, with occasional splaying of hindlimbs": (Kirshenbaum *et al.*, 2013)), and unusually short stride lengths with wide stride widths. Indeed, the mutant mice with defective α3 sodium pumps in all four lines of mutants so far generated show severe motor deficits. Interestingly, they consistently show hyperactivity (Moseley *et al.*, 2007; DeAndrade *et al.*, 2010; Kirshenbaum *et al.*, 2011; Ikeda *et al.*, 2013; Sugimoto *et al.*, 2014; Hunanyan *et al.*, 2015). Given the role of the α3 sodium pump in spinal cord described in this thesis so far, as a mechanism of neuronal self-regulation that limits the speed and duration of locomotor bouts, it is highly likely that spinal sodium pumps contribute to the motor deficit observed in these α3 mutant mice. However, so far, no study has tested this hypothesis.

Whilst few studies have explored the functional significance of the α3 sodium pump in mice, much more is known about the importance of sodium pump function in rat spinal cord. For example, around 50% of cultured rat spinal interneurons have been shown to display a spike-dependent hyperpolarisation mediated by sodium pump activity (Darbon *et al.*, 2002). Moreover, in a disinhibited rhythm generated by blocking fast inhibitory synaptic inputs ($GABA_A$ and glycine receptors), this dynamic hyperpolarisation was shown to become active in interneurons during the inter-burst interval, which suppressed spiking until the next rhythmic burst of activity. A number of other studies have also focused on blocking the pump during a

disinhibited bursting rhythm (Ballerini *et al.*, 1997; Rozzo *et al.*, 2002; Darbon *et al.*, 2003). Complete blockade of the sodium pump disrupts disinhibited bursting in rat whole cord preparations, causing activity to become sporadic and cease altogether (Ballerini *et al.*, 1997; Rozzo *et al.*, 2002). However, if sodium pumps are kept blocked for long periods (>1 hour), a new, irregular rhythm involving longer and slower bursts emerges, which was termed "strophanthidin bursting" (Rozzo *et al.*, 2002). The role of the pump hyperpolarisation in spinal neurons has also been explored in the context of the interval relationship between bouts of evoked activity (Rozzo *et al.*, 2002; Darbon *et al.*, 2003). If the interval between evoked activity was decreased, this resulted in shorter bouts of evoked locomotor activity. Importantly, the authors demonstrate that this "fatigued" activity is not due to mechanisms of synaptic depression (depletion of transmitter or receptor desensitation), but is instead due to the activity being evoked with the period of a pump hyperpolarisation. It is not currently known whether the spinal interneurons described in these studies which displayed a pump hyperpolarisation express the $\alpha 3$ subtype or not. Moreover, these studies often used relatively high concentrations of ouabain (>10 µM), and therefore some of the effects may be related to effects on both the $\alpha 1$ and $\alpha 3$ subtypes.

To the best of my knowledge, no previous study has explored the effects of sodium pump manipulation on locomotor-related activity in the mouse, which is the focus of this chapter. Here I show that sodium pump blockade increases the frequency of drug-induced locomotor activity in neonatal mice, whilst activating the sodium pump using monensin has the opposite effects. Interestingly, the effects of pump blockade using ouabain are dependent on the presence of dopamine, suggesting that dopamine may be modulating sodium pump activity to mediate its effects on the locomotor network. I also test the effects of removing extracellular potassium from the recording solution, in order to block the sodium pump by removing a key substrate for its activity. However, zero K^+ solution produced complex and multi-phasic effects on the locomotor network, suggesting, not surprisingly, that there are effects beyond the blockade of the sodium pump. Using a more physiological method for evoking locomotor

activity, dorsal root stimulation, I show that blocking the sodium pump using ouabain increases the duration and frequency of sensory-evoked locomotor bouts, whilst monensin again has the opposite effects. The interval between these evoked locomotor episodes also influenced the properties of locomotor activity, with shorter inter-episode intervals resulting in a decrease in evoked episode duration and burst frequency. Finally, using whole-cell patch-clamp recordings, a spike-dependent sodium pump hyperpolarisation in motoneurons and interneurons is also identified, which is abolished in a dose-dependent manner by ouabain, blocked by TTX, and enhanced by dopamine. These results highlight the importance of the sodium pump both as a dynamic regulator of the mammalian locomotor CPG, and as an important spinal target for dopaminergic modulation.

Chapter 3 materials and methods

Experimental animals

All experimental procedures were conducted in accordance with the UK Animals (Scientific Procedures) Act 1986, approved by the Animal Welfare Ethics Committee (AWEC) of the University of St Andrews and conformed to UK Home Office regulations. Whole spinal cord preparations in which ventral root recordings were performed were obtained from post-natal day 1-4 C57BL/6 mice. Spinal cord slice preparations used for whole-cell patch-clamp recordings were obtained from post-natal day 2-15 C57BL/6 mice. Cre-Lox recombination was used to target Pitx2+ interneurons by crossing Pitx2::Cre mice (Liu *et al.*, 2003) with homozygous ROSA-loxP-STOP-loxP-tdTomato fluorescent reporter animals (Madisen *et al.*, 2010). The Pitx2::Cre: ROSA-loxP-STOP-loxP-tdTomato animals exhibited fluorescence in Pitx2+ cells (Zagoraiou *et al.*, 2009) which were targeted in a subset of single cell electrophysiology experiments.

Spinal cords were isolated using techniques similar to those described in (Jiang *et al.*, 1999). In summary, animals were killed via cervical dislocation, decapitated and eviscerated. Then, the spinal column, pelvic girdle and hindlimbs were transferred and pinned, ventral side up, to the bottom of a chamber containing aCSF (equilibrated with 95% oxygen, 5% carbon dioxide, ~4 °C). Under a dissecting microscope, vertebral bodies from mid-cervical to upper sacral segments were carefully removed to reveal the spinal cord. Spinal cord tissue was then floated out of the spinal canal by snipping spinal roots on both sides, and removing further connective tissue. The dorsal and ventral roots were then trimmed on both sides. For ventral root recordings, the preparation was transferred to a recording chamber superfused with oxygenated aCSF (flow rate 8-12 ml/min). The spinal cord was then pinned onto Sylgard resin inside this chamber with the ventral side up, ready for electrophysiological recordings.

For single cell recordings, P2-P15 mouse spinal cords were isolated as above using dissecting aCSF (equilibrated with 95% oxygen, 5% carbon dioxide, ~4 °C). Spinal cord slices (300 µm thickness) from lumbar segments were obtained using a vibratome (VT1200, Leica, Wetzlar,

Germany) and transferred to recovery aCSF, which was kept at ~34ºC and continuously bubbled with 95% oxygen, 5% carbon dioxide for at least 1h. Slices were then transferred to a beaker containing aCSF (equilibrated with 95% oxygen, 5% carbon dioxide, RT).

Pharmacological agents and solutions

All drugs were supplied by Sigma-Aldrich (Poole, UK), dissolved in H_20 and stored in aliquots at -20 °C before use. The artifical cerebrospinal fluid (aCSF) used for dissections contained (in mM): 127 NaCl, 3 KCl, 1.25 NaH2PO4, 1 MgCl2, 2 CaCl, 26 NaHCO3, 10 glucose. For zero K^+ solution experiments 3mM KCl was replaced by 3mM NaCl. The dissecting aCSF (in mM): 25 NaCl, 188 sucrose, 1.9 KCl, 1.2 NaH_2PO_4, 10 $MgSO_4$, 1 CaCl, 26 $NaHCO_3$, 25 glucose and 1.5 kynurenic acid. The recovery aCSF contained (in mM): 119 NaCl, 1.9 KCl, 1.2 NaH_2PO_4, 10 $MgSO_4$, 1 CaCl, 26 $NaHCO_3$, 20 glucose and 1.5 kynurenic acid. Intracellular solution used for single-cell recordings contained (in mM): 140 $KMeSO_4$, 10 NaCl, 1 CaCl, 10 HEPES, 1 EGTA, 3 Mg-ATP and 0.4 GTP-Na_2.

Electrophysiological recordings

Ventral root experiments

For experiments in which locomotor-related activity was induced pharmacologically, glass suction electrodes were attached to the first or second lumbar ventral roots (L_1, L_2) on both the left and right side of isolated spinal cords to record left-right alternating, flexor-related activity. In the majority of experiments, a third electrode was also attached to the fifth lumbar ventral root (L_5) to record extensor-related activity (Figure 1Ai). N-methyl-D-aspartic acid (NMDA; 5 µM), 5-hydroxytryptamine (5-HT; 10 µM) and dopamine (DA; 50 µM) were added to the aCSF in order to induce rhythmic bursts of locomotor-related ventral root activity that alternated between the left and right sides of the spinal cord and between ipsilateral flexor ($L_{1/2}$) and extensor (L_5) related ventral roots. For a subset of experiments, only NMDA and 5-HT were used to induce locomotor-related activity, with dopamine omitted. Consistent with previous studies (e.g. (Foster *et al.*, 2014; Sharples *et al.*, 2015)), the frequency of bursting was faster and the rhythm less stable in the absence of dopamine. Drugs used to manipulate

Na^+ pump activity were applied once the observed amplitude, frequency and duration of rhythmic bursting had stabilised (usually after ~1 hour). For dorsal root stimulation experiments, glass suction electrodes were attached to the first or second lumbar ventral roots (L_1, L_2) on both the left and right side of isolated spinal cords, while a stimulating electrode was attached to the third, fourth or fifth lumbar dorsal root (L_3,L_4 or L_5) on either the left or right side. A series of 40 current pulses (4 Hz) was delivered to the caudal stimulating electrode every 2 minutes, using a Master-8 pulse generator and iso-flex pulse stimulator (Master-8, AMPI, Jerusalem, Israel), in order to evoke episodes of locomotor-like activity (as in (Whelan *et al.*, 2000)). The amplitude of the pulses was set to 50-100 µA. In an initial set of experiments, dopamine (50 µM) was found to stabilise sensory-evoked motor output and therefore was added to the aCSF for the remaining dorsal root stimulation experiments. For both drug- and sensory-induced activity, signals were amplified and filtered (30–3,000 Hz; Qjin Design, ON, Canada) and then acquired at a sampling frequency of 6 kHz using a Digidata 1440A A/D board and AxoScope software (Molecular Devices, Sunnyvale, CA, USA). Simultaneous online rectification and integration was performed on each raw ventral root signal during the recording.

Patch-clamp experiments

Spinal cord slices were immersed in a recording chamber with aCSF continuously re-perfused (50mL) at a constant rate (1 mL per second). Whole-cell patch-clamp recordings were performed from ventral horn interneurons and motoneurons using glass microelectrodes (2.5-5MΩ) filled with intracellular solution. Signals were amplified and filtered (4-kHz low-pass Bessel filter) with a MultiClamp 700B amplifier (Molecular Devices, Sunnyvale, CA, USA) and acquired at ≥10 kHz using a Digidata 1440A A/D board and pClamp software (Molecular Devices, Sunnyvale, CA, USA). Gigaseals (>2GΩ) were obtained prior to the establishment of whole-cell mode and neurons with RMP between -40 mV and -80 mV were used for experiments. All recordings were performed in current-clamp mode. The dynamic, activity-dependent pump potential was elicited by either applying a 10 second supramaximal continuous depolarizing pulse, or if the neuron exhibited single spike or adaptive spiking

behavior, high-frequency stimulation (100Hz) was utilized. A hyperpolarizing, bias current (≤ -50pA) was sometimes injected into the neuron if it depolarized following drug perfusion. This prevented any significant differences in firing frequency during stimulation, allowing us to fairly compare pump potentials between control and drug conditions. To evaluate input resistance pre- and post-stimulation, 20pA hyperpolarizing pulses were injected (see results section). All experiments were conducted at room temperature (approximately 20 °C).

Data analysis

Extracellular electrophysiological data were first analysed using Dataview software (v 10.3.0, courtesy of Dr. W. J. Heitler) and all raw data were imported into Excel spread sheets and analysed. Statistical analyses were conducted using PASW statistics 21 or Excel. The means of each condition were compared using paired student's *t*-tests or repeated-measures ANOVAs followed by bonferonni-corrected t-tests, unless otherwise stated. Results are reported as mean ± SEM. For determination of left-right phase values, 50 bursts recorded from the left and right second lumbar root (L_2) were analysed, and circular statistics were applied. Phase values were calculated by dividing the latency between a consecutive left and right burst by the cycle period on the side of the leading burst (see (Kjaerulff & Kiehn, 1996) for details). Phase values for flexor-extensor alternation were calculated using the same method as above but using bursts from the second lumbar root (L_2) and fifth lumbar root (L_5) on the same side. Where relevant, the phase values from a sample individual experiment are plotted on a circular plot for each condition, with the mean phase indicated by an arrow and the length of the arrow indicating the strength of coupling. Mean phase values for the full set of experiments are also shown on a circular plot, with crosses indicating mean phase values and the colour indicating the condition. Rayleigh's test for uniformity was used to statistically assess whether any of the drug conditions affected left-right or flexor-extensor coupling.

For patch-clamp experiments data were analysed using ClampFit software (Molecular Devices, Sunnyvale, CA, USA) then exported to Excel spreadsheets for statistical analysis. Pre-stimulation resting voltage was compared with immediate post-stimulation voltage to

address the pump potential amplitude. The time between the end of the stimulation and the end of the hyperpolarizing phase was used to calculate the duration of the pump potential. Due to its slow kinetics (e.g. (Zhang & Sillar, 2012)), the pump potential was defined as a slow hyperpolarization lasting 20 seconds or more. Paired student's t-tests were used to determine statistically significant changes between control and drug conditions.

Chapter 3 results

Sodium pump inhibition increases locomotor frequency

The role of the sodium pump within mouse spinal motor networks was first investigated by applying the cardiac glycoside inhibitor of the pump, ouabain, to isolated spinal cord preparations while recording locomotor-related activity from the ventral roots (Figure 1A,B). Stable locomotor activity was induced by the bath application of NMDA (5µM), 5-HT (10µM) and DA (50µM) (Figure 1Aii). Since different subtypes of the sodium pump are differentially sensitive to ouabain (Lichtstein & Rosen, 2001), a range of concentrations of ouabain was used, from 300 nM to 30 µM (Figure 1C,D). Ouabain concentrations below 30 µM would be expected to exclusively block the α3 subtype, as the ouabain inhibition constant (K_i) for α1 is around 40 - 140 µM (Blanco & Mercer, 1998; Hamada *et al.*, 2003; Dobretsov & Stimers, 2005; Kim *et al.*, 2007). No significant effects were found for 300 nM ouabain ($p>0.05$, n=7). However, bath application of 1 µM ouabain caused a rapid, clear and significant increase in the frequency of locomotor bursts of around 15% (15.8% ± 4.1%, $p<0.05$, n=7) with no significant change in burst amplitude. A higher concentration of ouabain (3µM; Figure 1B,C) elicited a similar, but more pronounced increase in locomotor burst frequency of around 40% (39.5% ± 5.2%, $p<0.01$, n=7), but also significantly reduced the amplitude of bursts by around 20% (22.6% ± 4.3%, $p<0.05$, n=7). Finally, I bath-applied a high dose of ouabain (30µM), which rapidly increased the frequency (reaching a peak of around a 200% increase) but then quickly abolished activity altogether (data not shown, n=2). At all concentrations tested, ouabain had no effect on the left-right alternating pattern of locomotor bursting, which was found to be significantly clustered around a mean phase value of approximately 0.5 in both control ($p<0.01$), and drug ($p<0.01$), conditions (Figure 1B, Ei,ii). Flexor and extensor alternation was similarly unaffected (Figure 1B). These results demonstrate that decreasing the activity of the sodium pump in the spinal cord accelerates the frequency of drug-induced locomotor bursting.

Figure 1. Ouabain increases the frequency and reduces the amplitude of drug-induced locomotor activity in a dose-dependent manner. Ai. Schematic illustrating glass suction electrodes on first or second lumbar ventral roots (L_1, L_2) on left and right sides of an isolated spinal cord to record flexor-related activity, and third electrode on the fifth ventral root (L_5) to record extensor-related activity. **Aii**. Raw and rectified/integrated traces showing drug-induced activity on the left and right L_2 root and the right L_5 root. **B.** Equivalent traces showing activity on the left and right L_2 root and the right L_5 root, illustrating the effects of 3 µM ouabain. **Ci.** Time course plot showing normalised frequency values averaged into 30 s bins. Ouabain causes a concentration-dependent increase in locomotor frequency. **Cii.** Time course plot showing normalised amplitude values. Ouabain causes a concentration-dependent decrease in the amplitude of locomotor activity. **Di.** Mean change in locomotor burst frequency at three different concentrations of ouabain (300 nM, n=7; 1 µM, n=7; 3 µM, n=7). *$p<0.05$, **$p<0.01$. **Dii.** Mean change in locomotor burst amplitude at the same concentrations described above. *$p<0.05$. **Ei.** Circular plots illustrating the relative phase of bursts recorded from the left L_2 ventral root relative to the right L_2 ventral root. The plots depict 50 bursts recorded in control and 50 bursts recorded in the presence of 3 µM ouabain (taken from the same experiment shown in parts A and B). Data points are clustered around 0.5 in both conditions, illustrating left-right alternation in both conditions ($p<0.05$). **Eii.** Circular plot depicting mean left-right values in control (black crosses) and 3 µM ouabain (red crosses) across several experiments (n=5, $p<0.05$).

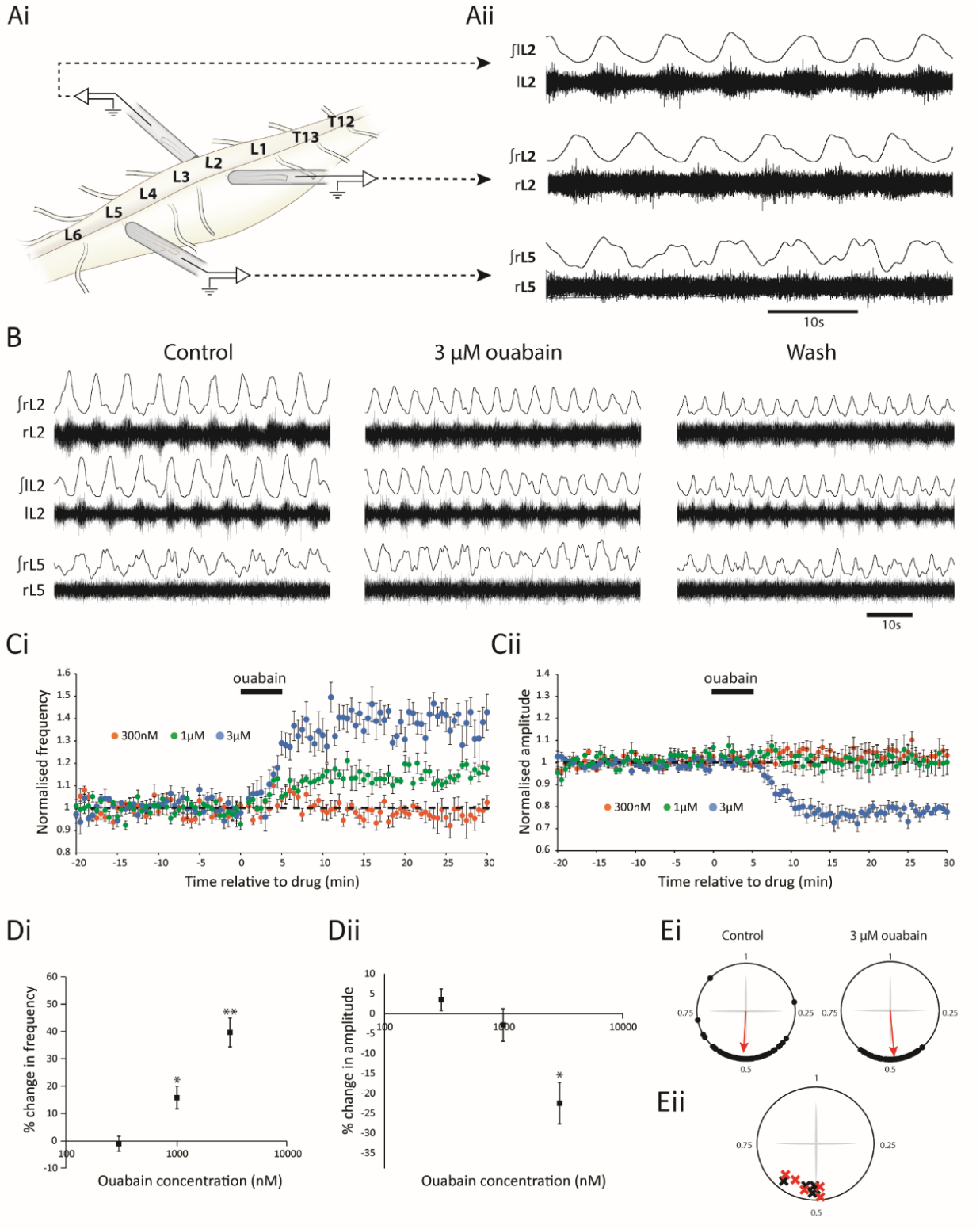
Ai
Aii
T12
T13
L1
L2
L3
L4
L5
L6
∫lL2
lL2
∫rL2
rL2
∫rL5
rL5
10s
B
Control
3 μM ouabain
Wash
∫rL2
rL2
∫lL2
lL2
∫rL5
rL5
10s
Ci
Cii
ouabain
300nM
1μM
3μM
Normalised frequency
Normalised amplitude
Time relative to drug (min)
Di
Dii
% change in frequency
% change in amplitude
Ouabain concentration (nM)
Ei
Eii
Control
3 μM ouabain

In addition to ouabain, another effective way to block the sodium pump is to remove K^+ ions from the extracellular solution, thereby removing the driving force for the pump. This has been shown to be effective in blocking sodium pump activity and removing a pump-mediated usAHP in a range of neuron types including *Xenopus* spinal neurons (Zhang & Sillar, 2012); lizard motoneurons (Morita *et al.*, 1993); SCN neurons (Wang & Huang, 2006; Wang *et al.*, 2012); crayfish stretch receptor neurons (Sokolove & Cooke, 1971); and leech tactile sensory neurons (Catarsi *et al.*, 1993). However, in this preparation, I found that switching from normal aCSF to zero K^+ had complex effects on the drug-induced locomotor rhythm (Figure 2). Initially, the locomotor burst frequency rapidly, and significantly, dropped to around 20% of control after around 5 minutes (Figure 2A,B,C, n=6, $p<0.05$). After 5 minutes, but while still in zero K^+ solution, this effect then reversed and the burst frequency significantly increased, more similar to the effects of ouabain (n=6, $p<0.05$). Upon washout, the effects then occurred in reverse; there was an initial drop in frequency (n=6, $p<0.05$), followed by a final increase late in the wash. However, this final increase in burst frequency was not significant ($p>0.05$), which is likely because the locomotor pattern was severely disrupted during the late wash phase. Instead of continuous, stable bursting, the activity occurred in several, high frequency locomotor bursts interspersed with delays (Figure 2B). Overall, this complex effect on locomotor frequency suggests that there are multiple mechanisms at play in response to the removal of K^+ ions (see discussion). The effects on burst amplitude were more straightforward. There was a clear and significant decrease in burst amplitude, which appeared similar to the effects of 3 µM ouabain (Figure 2A, D, $p<0.05$).

Figure 2. The effects of K^+-free aCSF on the locomotor network. A. Raw (top) and rectified/integrated (bottom) recordings from the left L2 root, showing an entire experiment to illustrate the effects of zero K^+ extracellular solution. **B.** Enlarged panels from A showing the raw (top) and rectified/integrated (bottom) traces for both the left and right L2 root, illustrating the effect of zero K^+ solution at different timepoints. **Ci.** Timecourse plot showing normalised frequency values averaged into 30s bins. Switching to zero K+ solution had a biphasic effect on locomotor frequency, with an initial decrease followed by an increase. **Cii.** Mean locomotor burst frequency during control, around 5 mins after swapping to zero K+ solution, around 10 minutes after the washout, and around 40 mins after the washout (n=6). *p<0.05, ***p<0.001. **Di.** Timecourse plot showing normalised amplitude values. Switching to zero K+ solution caused a reduction in locomotor burst amplitude (n=6). **Dii.** Mean locomotor burst amplitude during control, 25 mins after switching to zero K+ solution, and 45 mins after washing normal solution back (n=6). *p<0.05.

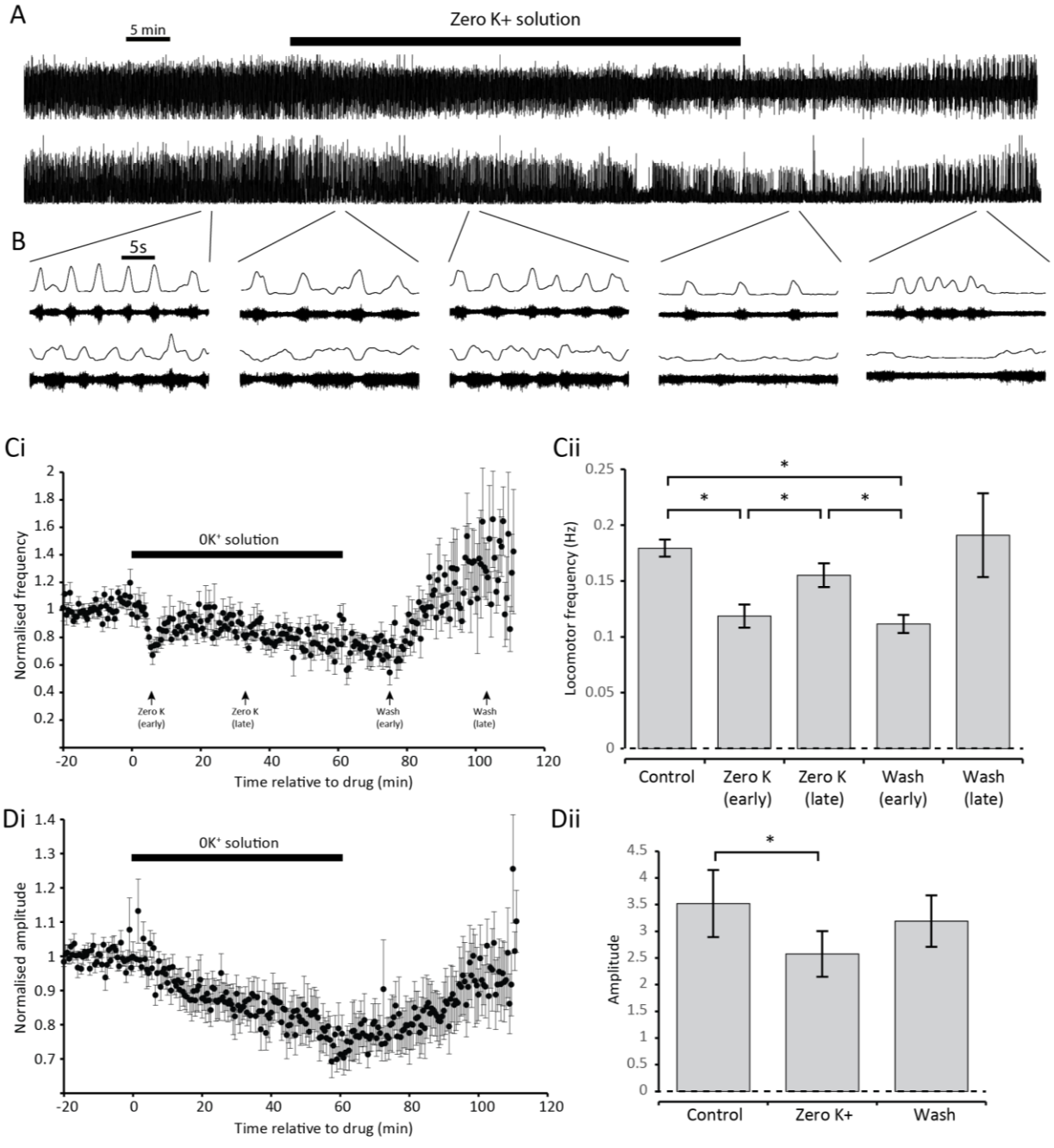
A
5 min
Zero K+ solution
B
5s
Ci
0K⁺ solution
Normalised frequency
Zero K (early)
Zero K (late)
Wash (early)
Wash (late)
Time relative to drug (min)
Cii
Locomotor frequency (Hz)
Control
Zero K (early)
Zero K (late)
Wash (early)
Wash (late)
Di
0K⁺ solution
Normalised amplitude
Time relative to drug (min)
Dii
Amplitude
Control
Zero K+
Wash

Sodium pump activation decreases locomotor frequency

Next, I wanted to explore the effects of increasing the activity of the sodium pump on drug-induced locomotor activity. There are no known direct pharmacological activators of the sodium pump, but as described in the previous chapter, the sodium ionophore monensin is often used to increase intracellular Na^+ concentration, which has been shown to trigger an increase in sodium pump activation (e.g. (Wang *et al.*, 2012; Zhang *et al.*, 2015; Kueh *et al.*, 2016)). Bath application of 10 µM monensin to isolated spinal cord preparations led to a significant decrease in locomotor frequency of around 70%, the opposite effect to ouabain (-70.6% ± 4.3%, Figure 3A,B,C; $p<0.001$, n=7). There was no significant effect of monensin on burst amplitudes (Figure 2D, $p>0.05$, n=7). However, monensin disrupted left-right and flexor-extensor coupling (Figure 3B,E,F). I observed normal left-right alternation in control conditions, with a mean phase value significantly clustered around a value of 0.5 ($p<0.001$, n=6). In monensin, phase values became uniformly distributed ($p=0.2$, n=6), indicating a loss of this left-right coupling. I also observed normal flexor-extensor alternation in control (Figure 3B,F, $p<0.05$, n=4). However, in monensin, although significant coupling remained ($p<0.01$, n=4), the mean values were clustered around a value of 1, indicating flexor-extensor synchrony. These results suggest that activation of the sodium pump in the spinal cord, by raising intracellular sodium, decelerates the frequency of a drug-induced locomotor bursting rhythm, causes a decoupling of the left and right sides of the spinal cord, and switches the normally alternating flexor-extensor relationship into synchronous bursting activity.

Figure 3. Activation of the sodium pump using the sodium ionophore monensin slows the frequency of drug-induced locomotion and disrupts left-right and flexor-extensor coupling. A. Raw (top) and rectified/integrated (bottom) recordings from the left L2 root, showing an entire experiment to illustrate the effects of 10 µM monensin. **B.** Raw (top) and rectified/integrated (bottom) traces showing activity on the left and right L2 root and the right L5 root, illustrating the effect of the sodium ionophore monensin (10 µM) **Ci.** Timecourse plot showing normalised frequency values averaged into 30s bins. Monensin (10 µM) causes a decrease in locomotor frequency. **Cii.** Mean locomotor burst frequency during control, 25 mins after the addition of 10 µM monensin, and 45 mins after drug washout (n=7). ***p<0.001. **Di.** Timecourse plot showing normalised amplitude values. Monensin (10 µM) had no significant effect on locomotor burst amplitude (n=7). **Dii.** Mean locomotor burst amplitude during control, 25 mins after the addition of 10 µM monensin, and 45 mins after drug washout (n=7). **Ei.** Circular plots for the experiment shown in A depicting left-right phase values. Monensin caused a loss of left-right alternation. **Eii.** Left-right phase values for individual experiments in control (black crosses), monensin (red crosses) and wash (blue crosses) (n=6; 50 bursts for each L2 root). **Fi.** Circular plots for the experiment shown in A depicting flexor-extensor relationship. Monensin caused flexor and extensor activity to become synchronous. **Fii.** Flexor-extensor phase values for individual experiments in control (black crosses), monensin (red crosses) and wash (blue crosses) across experiments (n=4).

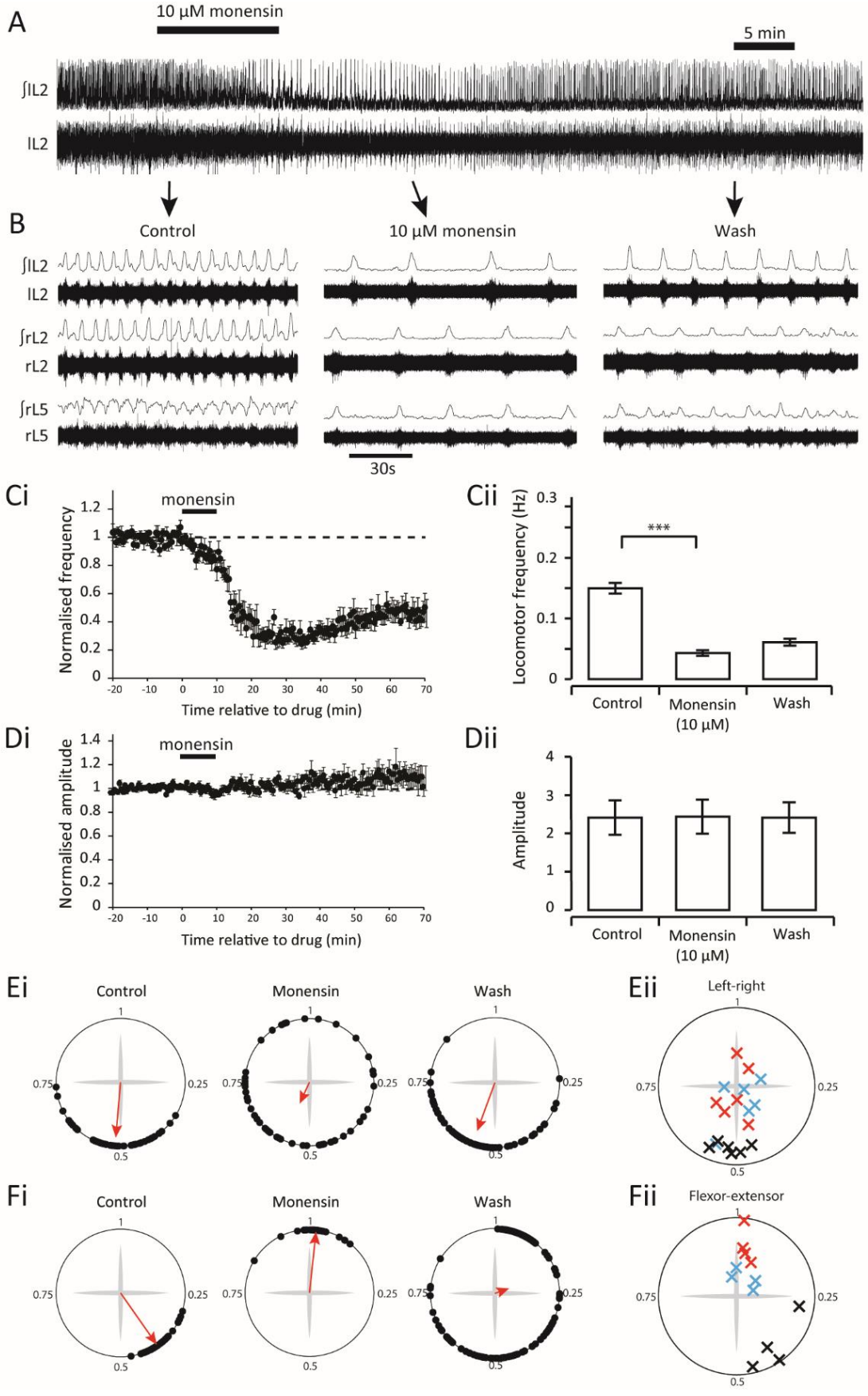
A
10 µM monensin
5 min
∫IL2
IL2
B
Control
10 µM monensin
Wash
∫IL2
IL2
∫rL2
rL2
∫rL5
rL5
30s
Ci
monensin
Normalised frequency
Time relative to drug (min)
Cii
Locomotor frequency (Hz)
***
Control
Monensin (10 µM)
Wash
Di
monensin
Normalised amplitude
Time relative to drug (min)
Dii
Amplitude
Control
Monensin (10 µM)
Wash
Ei
Control
Monensin
Wash
Eii
Left-right
Fi
Control
Monensin
Wash
Fii
Flexor-extensor

Dopamine-mediated modulation of locomotor activity involves effects on the sodium pump

Dopamine lowers the frequency and increases the amplitude of locomotor bursting induced by NMDA and 5-HT (Sharples *et al.*, 2015), but the mechanisms through which dopamine acts remain largely unknown. One possibility is that dopamine modulation could include the activation of the sodium pump, for which precedents exist ((Therien & Blostein, 2000), also see chapter 2 in *Xenopus* tadpoles). To test this possibility, I conducted a series of experiments in which ouabain (3 µM) was bath-applied to preparations and in which dopamine had been excluded from the combination of drugs used to induce locomotor-related activity. Consistent with previous findings, the locomotor pattern in the absence of dopamine displayed a higher frequency of bursting, with reduced amplitude (Figure 4Ai), reminiscent of activity in the presence of a sodium pump blocker. Importantly, in the absence of dopamine, bath-applied ouabain no longer had a significant effect on burst frequency ($p>0.05$, $n=7$, Figure 4A,B). Without dopamine present, ouabain still significantly decreased burst amplitude ($p<0.05$, $n=7$, Figure 4A,C), however there was a clear and significant difference between the magnitude of the amplitude effect when compared with experiments in the presence of dopamine (22.6 ± 11.4% (dopamine) vs. 8.6% ± 7.7% (without dopamine), $p<0.001$). These results demonstrate that the effects of ouabain are substantially dependent on the presence of dopamine, suggesting that dopamine's actions as a neuromodulator in the spinal cord may include activation of the sodium pump.

Figure 4. The effects of ouabain on locomotor output are dependent on the presence of dopamine. Ai. Raw (top) and rectified/integrated (bottom) traces showing locomotor-like activity in the absence of dopamine in control and in the presence of 3 µM ouabain. **Aii.** Raw (top) and rectified/integrated (bottom) traces showing locomotor activity recorded in the presence of 50 µM dopamine in control and in the presence of 3 µM ouabain. **B.** Pooled locomotor burst frequency data. In the absence of dopamine, 3 µM ouabain no significant effect on the locomotor burst frequency. However, in the presence of 50 µM dopamine, 3 µM ouabain caused a clear and significant increase in the frequency of locomotor bursts. **C.** Pooled locomotor burst amplitude data. 3 µM ouabain had a larger effect on burst amplitude when applied in the presence of dopamine, however the change was significant both with and without dopamine. Overall, these data suggest that the effects of sodium pump blockade are dependent on the presence of dopamine. *p<0.05. **p<0.01. ***p<0.001.

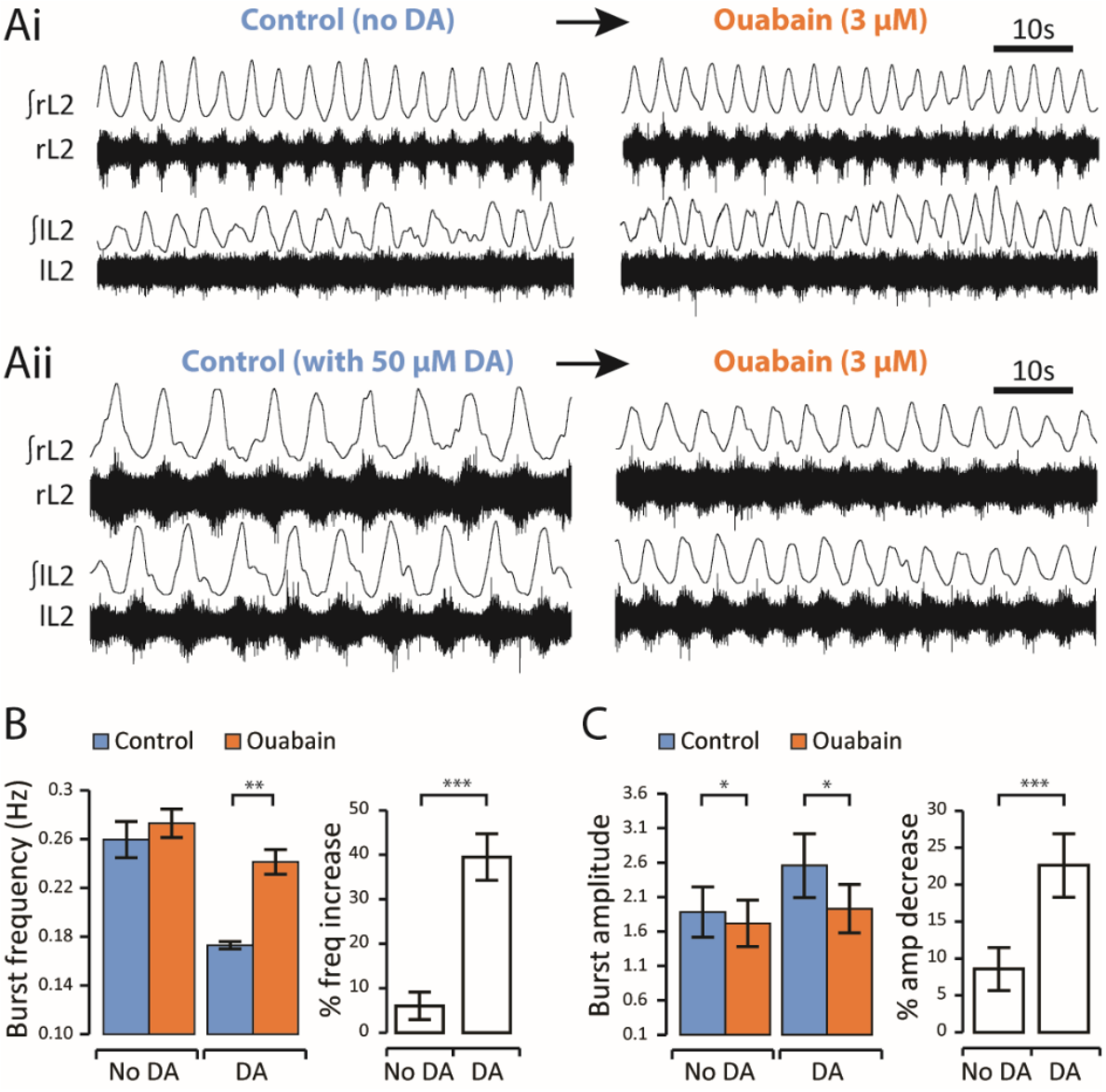
Ai
Control (no DA)
Ouabain (3 µM)
10s
∫rL2
rL2
∫lL2
lL2
Aii
Control (with 50 µM DA)
Ouabain (3 µM)
10s
∫rL2
rL2
∫lL2
lL2
B
Control
Ouabain
Burst frequency (Hz)
0.3
0.26
0.22
0.18
0.14
0.10
**
No DA
DA
% freq increase
50
40
30
20
10
0
***
No DA
DA
C
Control
Ouabain
Burst amplitude
3.6
3.1
2.6
2.1
1.6
1.1
0.6
0.1
*
*
No DA
DA
% amp decrease
30
25
20
15
10
5
0
***
No DA
DA

Sodium pump activity modulates sensory-induced locomotor bouts

Next, I wanted to explore whether the effects of sodium pump manipulation also occur using an alternative, and potentially more physiological method for generating motor output. Therefore, in the absence of the normal locomotor cocktail, I used dorsal root stimulation to induce brief episodes (~20s long) of locomotor-like activity (see methods section for details). Given that sodium pumps have a greater influence on locomotor network activity when dopamine is present, the following dorsal root stimulation experiments were all performed with 50 µM dopamine included in the aCSF. Ouabain (3 µM) significantly extended the duration of sensory-evoked locomotor episodes by approximately 70% (66.7% ± 15.8% Figure 5C,E; $p<0.01$, n=7), and also led to a small but significant increase in the frequency of locomotor activity of around 6% (5.9% ± 1.7%, Figure 5C,D,F; $p<0.05$, n=7). These data suggest that the duration and frequency of sensory-evoked locomotor episodes is somehow restricted by a pump-dependent mechanism. If so, then increased pump activity would be expected to decrease episode durations and slow the frequency. To test this hypothesis, we next used the sodium ionophore to increase intracellular sodium and activate the sodium pump.

As predicted, monensin (10 µM) reduced the duration of sensory-evoked locomotor episodes by approximately 24% (23.7% ± 4.5%, Figure 6A, C; $p<0.05$, n=7), before eventually abolishing activity altogether. In addition, the frequency of locomotor bursts within the shortened episodes of activity was significantly slowed by around 20% (18.8% ± 5.2%, Figure 6B,D; $p<0.05$, n=7); opposite to the effects of ouabain. Collectively, these results illustrate that changes in sodium pump activity in the spinal cord modulate the duration and frequency of sensory-induced bouts of locomotor activity.

Figure 5. The sodium pump blocker ouabain increases the duration and frequency of sensory-evoked locomotor activity. Ai. Schematic illustrating the experimental setup. Glass suction electrodes were attached to the first or second lumbar ventral roots (L_1, L_2) on the left and right side of an isolated spinal cord to record flexor-related activity. A third electrode was also attached to the fifth dorsal root (L_5) on either the left or right side and used to deliver a series of current pulses to initiate locomotion (see methods). **Aii.** An example of the locomotor output recorded in response to the stimulus delivered to the dorsal root. Inset shows left-right alternation. **B**. Raw (top) and rectified/integrated (bottom) traces showing 3 consecutive stimulus-evoked episodes of locomotor activity in control; in the presence of 3 µM ouabain; and following washout of the drug. **C**. Expanded raw traces showing several locomotor bursts in each condition to illustrate the effect of ouabain on locomotor burst frequency. **D**. Pooled data showing the effects of ouabain on sensory-evoked episode duration (n=7). **E**. Pooled data showing the effect of ouabain on locomotor burst frequency (n=7). *$p<0.05$. **$p<0.01$.

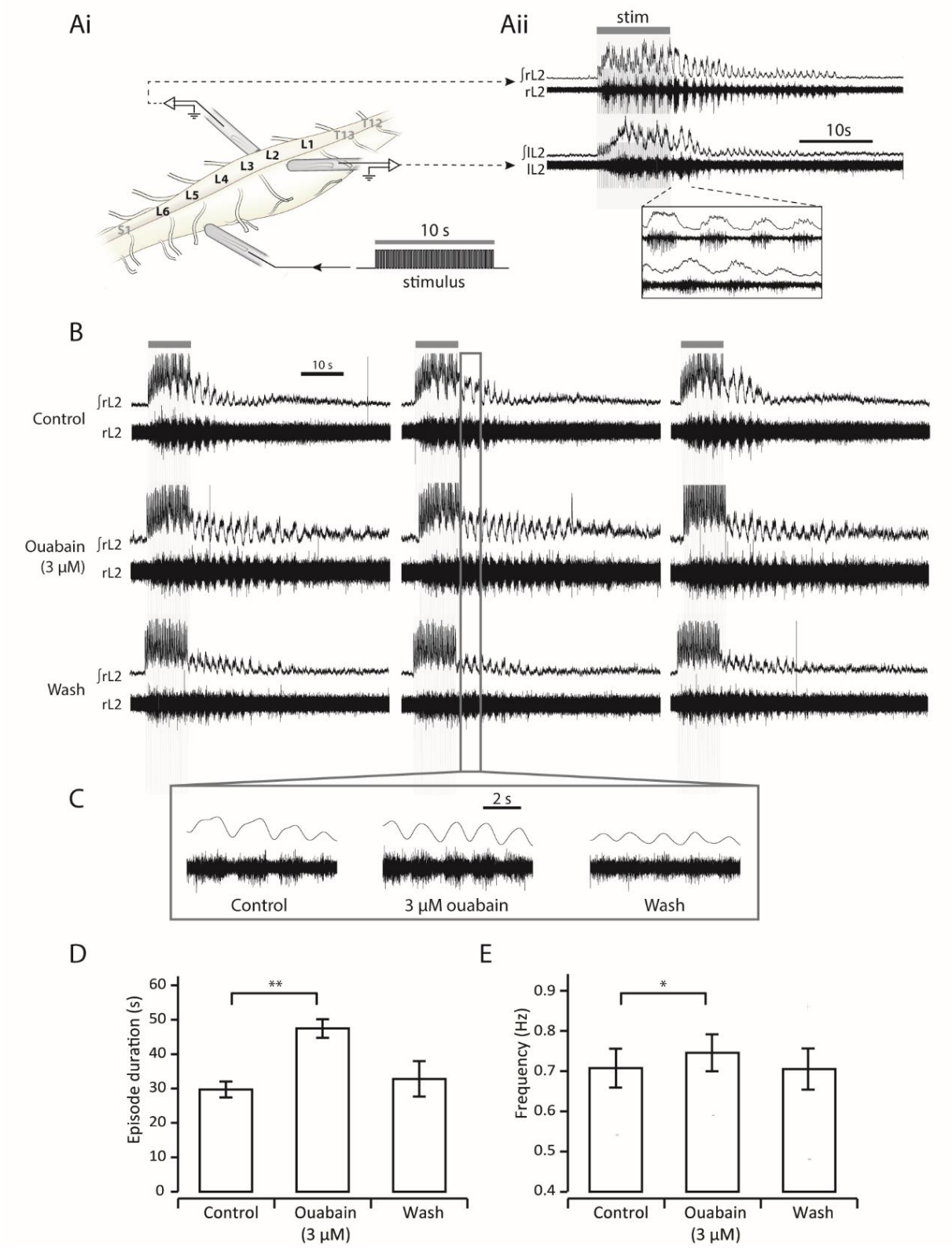
Ai
Aii
stim
∫rL2
rL2
∫lL2
lL2
10s
T12
T13
L1
L2
L3
L4
L5
L6
S1
10 s
stimulus
B
10 s
Control
Ouabain
(3 µM)
Wash
C
2 s
Control
3 µM ouabain
Wash
D
Episode duration (s)
**
Control
Ouabain
(3 µM)
Wash
E
Frequency (Hz)
*
Control
Ouabain
(3 µM)
Wash

Figure 6. Activation of the sodium pump using the sodium ionophore monensin decreases both the duration and frequency of evoked locomotor activity. A. Raw (top) and rectified/integrated (bottom) traces showing three sensory-evoked episodes of locomotor activity in control and in the presence of 10 µM monensin. **B.** Expanded raw traces showing several locomotor bursts in each condition to illustrate the effect of monensin on locomotor burst frequency. **C.** Pooled data showing the effects of monensin on sensory-evoked episode duration (n=7). **D.** Pooled data showing the effect of monensin on locomotor burst frequency (n=7). *$p<0.05$.

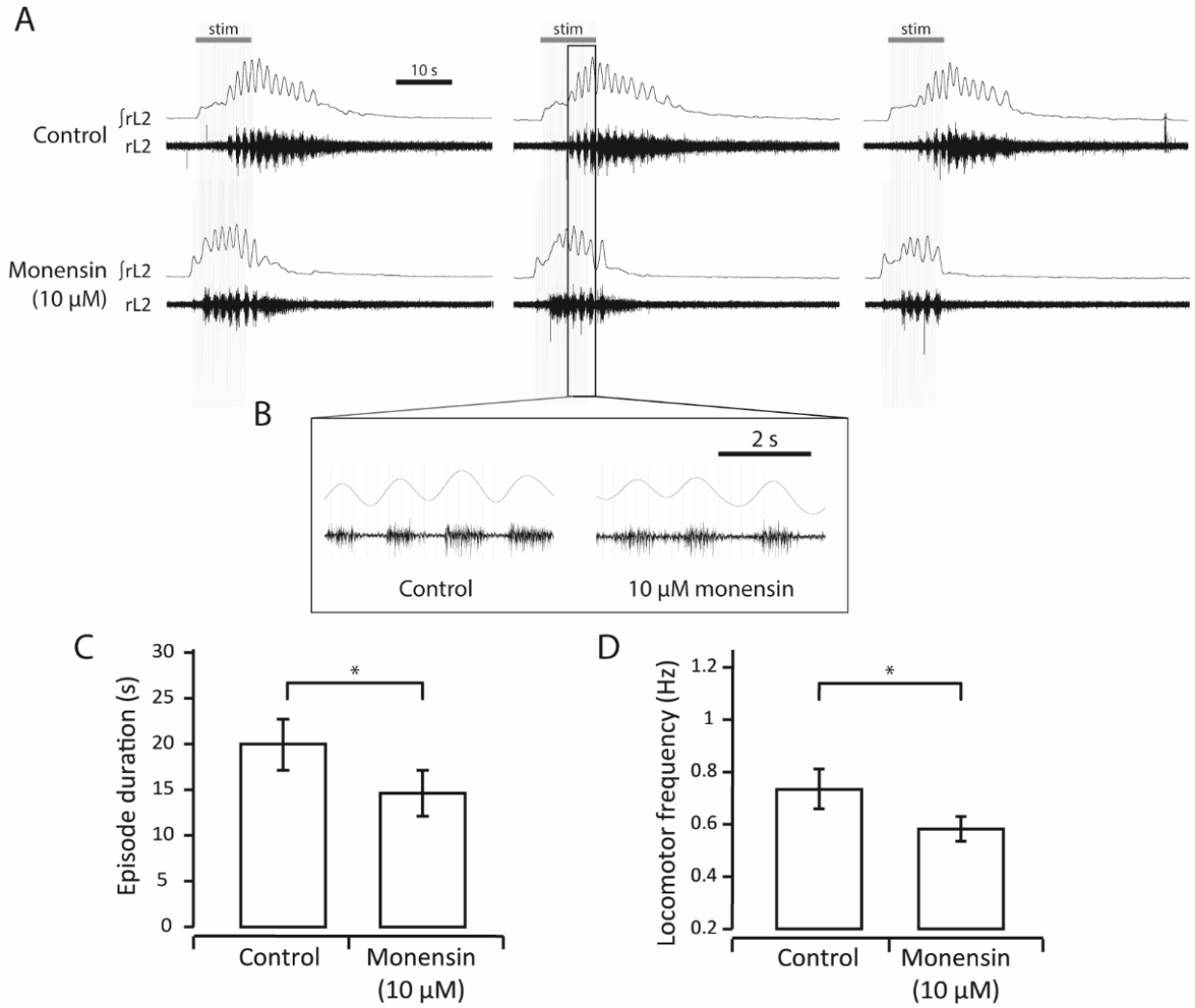
A
stim
stim
stim
10 s
Control
∫rL2
rL2
Monensin
(10 µM)
∫rL2
rL2
B
2 s
Control
10 µM monensin
C
Episode duration (s)
30
25
20
15
10
5
0
*
Control
Monensin
(10 µM)
D
Locomotor frequency (Hz)
1.2
1
0.8
0.6
0.4
0.2
*
Control
Monensin
(10 µM)

Effects of inter-episode interval on sensory-evoked locomotor activity

In other preparations, including *Xenopus* tadpoles and *Drosophila* larvae, the amplitude and duration of a pump hyperpolarisation generated by CPG neurons during locomotion encodes information about locomotor network output in an activity-dependent manner. This allows the network to retain a short-term memory of recent activity, enabling future network output to be influenced in an interval-dependent fashion. In *Xenopus* tadpoles, this “motor memory” can last up to 1 minute; if swimming is evoked within this minute, the unrecovered pump hyperpolarisation inhibits spinal neurons, causing the second episode to be slower, weaker and shorter in duration (Zhang & Sillar, 2012; Zhang *et al.*, 2015).

To test whether an activity-dependent pump potential may play a similar role in mice, I manipulated the interval between sensory-evoked episodes of locomotor-like activity using a protocol in which locomotor episodes were evoked with a two minute separation. After at least three consistently similar control episodes, the interval was reduced to either 30 or 15 seconds. Compared with episodes evoked with a two minute interval, episodes were significantly shorter in duration for both the 30 s interval (-31.4% ± 5.1%, Figure 7A, Bi; $p<0.001$, n=7) and the 15 s interval (-36.2% ± 4.9, Figure 7C, Di; $p<0.05$, n=7). Moreover, the locomotor bursts were significantly slower for both the 30 s (-16.1% ± 3.9, Figure 7A, Bii, $p<0.05$; n=7) and 15 s interval (-16.4% ± 4.5%, Figure 7C, Dii, $p<0.05$; n=7). These results suggest that the locomotor network encodes information about its own previous output and that this information is retained for at least 30 seconds. Locomotor activity evoked within this period is inhibited in a manner reminiscent of, and consistent with, increased sodium pump activity.

Figure 7. The interval between evoked episodes of fictive locomotor activity affects both the duration and frequency of locomotor output. A. Raw (top) and rectified/integrated (bottom) traces showing a series of sensory-evoked episodes, with expanded traces below. The first three episodes are separated by a two minute stimulation interval. Between the third and fourth episodes shown the interval is set to 30 seconds, before returning to a 2 minute stimulation interval. **Bi**. Episodes evoked after a 30 s interval were significantly shorter in duration compared with episodes evoked after a 2 minute interval. **Bii.** Episodes evoked after a 30 s interval had significantly slower frequency compared with episodes evoked after a 2 minute interval. **C.** Raw (top) and rectified/integrated (bottom) traces showing a series of sensory-evoked episodes, with inset showing expanded traces. The first three episodes are separated by a 2 minute stimulation interval. Between the third and fourth episode shown the interval is set to 15 seconds. **Di**. Episodes evoked after a 15 s interval were significantly shorter in duration compared with episodes evoked after a 2 minute interval. **Dii.** Episodes evoked after a 15 s interval had significantly slower frequency compared with episodes evoked after a 2 minute interval. **Ei.** An example of two evoked episodes of locomotor episodes separated by a 15 s interval, prior to the application of ouabain. Similar to the results shown in D, both episode duration (**Eii**, $p<0.01$, $n=5$) and burst frequency (**Eiii**, $p<0.05$, $n=5$) were significantly reduced in episode 2 (EP2) compared to episode 1 (EP1). **Fi.** An example of two evoked episodes from the same experiment as Ei in the presence of 3 µM ouabain but still separated by a 15s interval, In the presence of ouabain, there was no significant difference in episode duration (**Fii**, $p>0.05$, $n=5$) or burst frequency (**Fiii**, $p>0.05$, $n=5$) between EP1 and EP2. *$p<0.05$, **$p>0.01$, ***$p<0.001$.

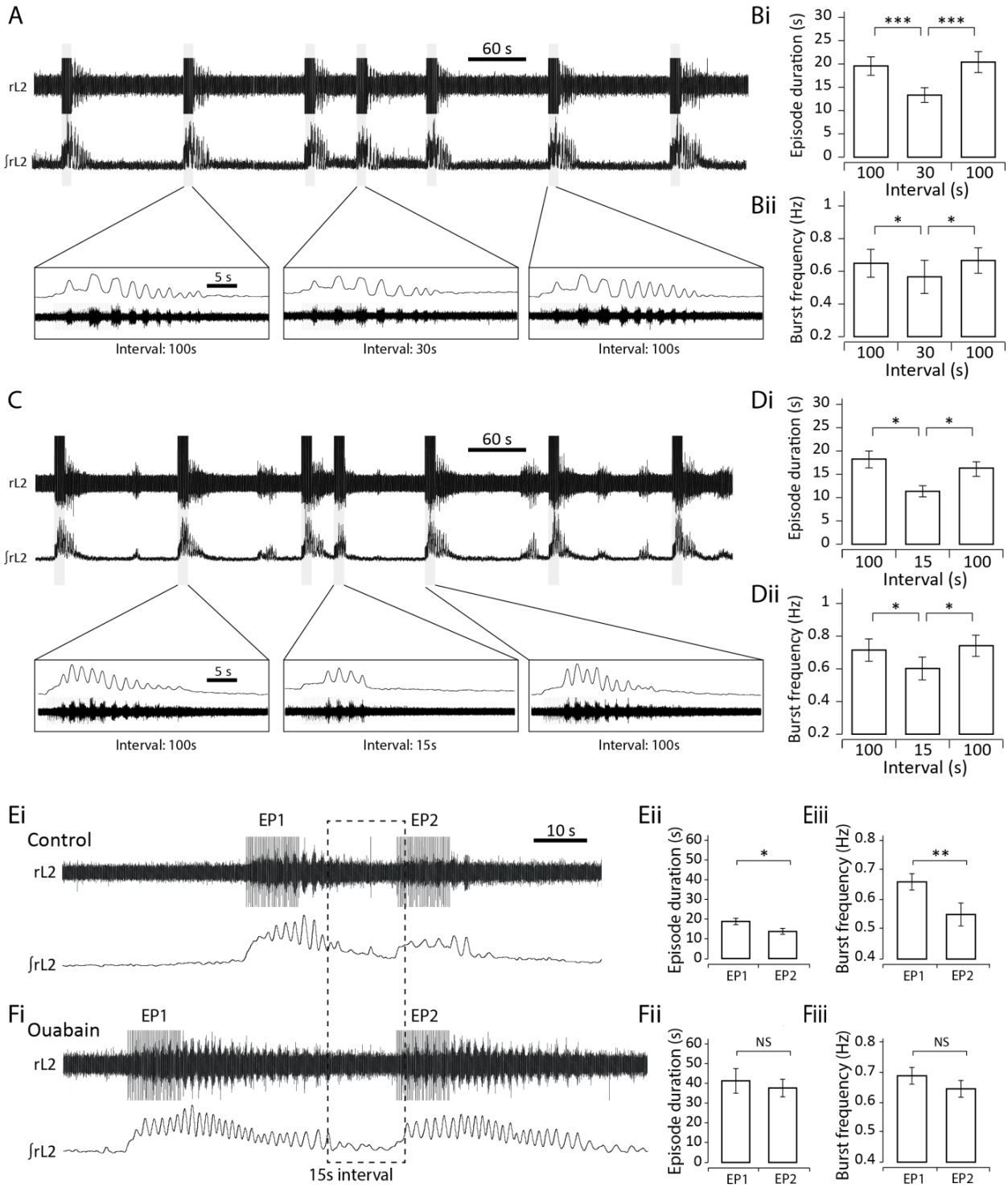
A
60 s
rL2
∫rL2
5 s
Interval: 100s
Interval: 30s
Interval: 100s
Bi
Episode duration (s)
***
***
100
30
100
Interval (s)
Bii
Burst frequency (Hz)
*
*
100
30
100
Interval (s)
C
60 s
rL2
∫rL2
5 s
Interval: 100s
Interval: 15s
Interval: 100s
Di
Episode duration (s)
*
*
100
15
100
Interval (s)
Dii
Burst frequency (Hz)
*
*
100
15
100
Interval (s)
Ei
Control
EP1
EP2
10 s
rL2
∫rL2
Eii
Episode duration (s)
*
EP1
EP2
Eiii
Burst frequency (Hz)
**
EP1
EP2
Fi
Ouabain
EP1
EP2
rL2
∫rL2
15s interval
Fii
Episode duration (s)
NS
EP1
EP2
Fiii
Burst frequency (Hz)
NS
EP1
EP2

To more specifically test whether the sodium pump contributes to this interval effect, I tested the effects of ouabain (3 μM) on the relationship between evoked episodes separated by an interval of 15 seconds. Under control conditions, I replicated the effects described earlier, whereby the second episode (EP2) of a pair of evoked episodes, separated by a 15 s interval, is significantly shorter (Figure 6Ei, Eii, $p<0.01$, n=5) and slower (Figure 6Ei, Eiii, $p<0.05$, n=5) when compared to the first episode (EP1). However, the application of ouabain disrupted the relationship between interval and episode duration as well as between interval and locomotor burst frequency. Following the application of ouabain, episodes were not only longer, and higher in frequency compared to control (Figure 6Fi, same as Figure 4), but the second episode of a pair was no longer significantly shorter (Figure 6Fi, Fii, $p>0.05$, n=5) or slower (Figure 6Fi, Fiii, $p>0.05$, n=5) compared to the first episode. In other words, blockade of the sodium pump disrupted the interval relationship between locomotor activity, suggesting that the main mechanism responsible for this feedforward control of activity involves the activity-dependent enhancement of sodium pump activity.

A sodium pump-mediated afterhyperpolarisation in spinal neurons

The preceding ventral root recordings suggest that sodium pumps play an important role in shaping locomotor output, but what are the effects, if any, at the cellular level? To address this question, whole-cell patch-clamp recordings were made from spinal cord slices. Sodium pump activity can modify neuronal firing via a *tonic* contribution to the RMP and/or via a *dynamic*, transient, activity-dependent afterhyperpolarisation (AHP). The presence of a dynamic sodium pump potential was tested by inducing repetitive spiking in neurons in one of two ways: either by applying a large, continuous depolarising current pulse (10s duration); or, if a cell showed pronounced spike adaptation, using a 10s train of short duration (10ms) depolarising current pulses. A range of different post-stimulation responses were observed. In some cells, there was no post-tetanic change in membrane potential. In some motoneurons (62/126 cells), and interneurons (25/43 cells), there was a short duration afterhyperpolarisation, with the membrane potential returning to baseline after around 5-10 seconds (Figure 8Ai). However,

in a large proportion of motoneurons (>40%; 52/126 cells), and a smaller proportion of unidentified ventral horn interneurons (~24%; 5/21 cells), there was a prominent, long duration AHP, approximately 5 mV in amplitude (4.80±0.3mV for motoneurons, n=52; 5.9±0.6mV for interneurons, n=5; Figure 8Aii), where the membrane potential gradually returned to baseline over a period of around 1 minute (76.8s ± 3.2s for motoneurons, n=52; 57.4±5.2s for interneurons, n=5). The amplitude and duration of this long, post-activity AHP is reminiscent of the minute-long usAHP generated by sodium pump activity in *Xenopus* spinal neurons (see Chapter 2 and (Zhang & Sillar, 2012)), so this terminology is adopted here. Whilst a large proportion of motoneurons (~40%) displayed a usAHP, it was found in only around 25% of unidentified ventral horn interneurons, suggesting more restricted expression of the usAHP in specific interneuron subtypes. One interneuron subtype known to contribute to spinal locomotor control and which exhibits activity phase locked to motoneuron output are Pitx2-positive interneurons (Zagoraiou *et al.*, 2009). It is therefore hypothesised that a higher proportion of this cell type might display a usAHP. Using spinal cord slices from Pitx2::Cre: ROSA-loxP-STOP-loxP-tdTomato mice, over half of PitX2-positive interneurons (13/22 cells) displayed a usAHP.

Figure 8. A spike-dependent, pump-mediated usAHP in motoneurons and interneurons **Ai.** An example of a motoneuron displaying a short duration AHP that lasts only around 5s**. Aii.** An example of an ultra-slow afterhyperpolarisation (usAHP) in a motoneuron in response to a high frequency train of action potentials, which lasts around 60s. **Aiii:** Summary of the proportion of motoneurons and interneurons displaying a usAHP. **Aiv.** Summary of the amplitude of the usAHP in motoneurons and interneurons. **B.** Responses to short duration current pulses in a motoneuron before and after the induction of a usAHP. Inset shows measurements of conductances before and after stimulation (stim.). **C.** The sodium channel blocker tetrodotoxin (TTX, 0.5 µM) reduces both the amplitude (Aii) and duration (Aiii) of the usAHP (n=4). **D.** The sodium pump blocker ouabain reduced the usAHP amplitude (Bii) and duration (Biii) in a dose-dependent manner (1 µM: n=3, 3 µM: n=6). **E.** Bath application of 50 µM dopamine increased the duration (Ciii) but not the amplitude (Cii) of the usAHP (n=9). *p<0.05. **p<0.01.

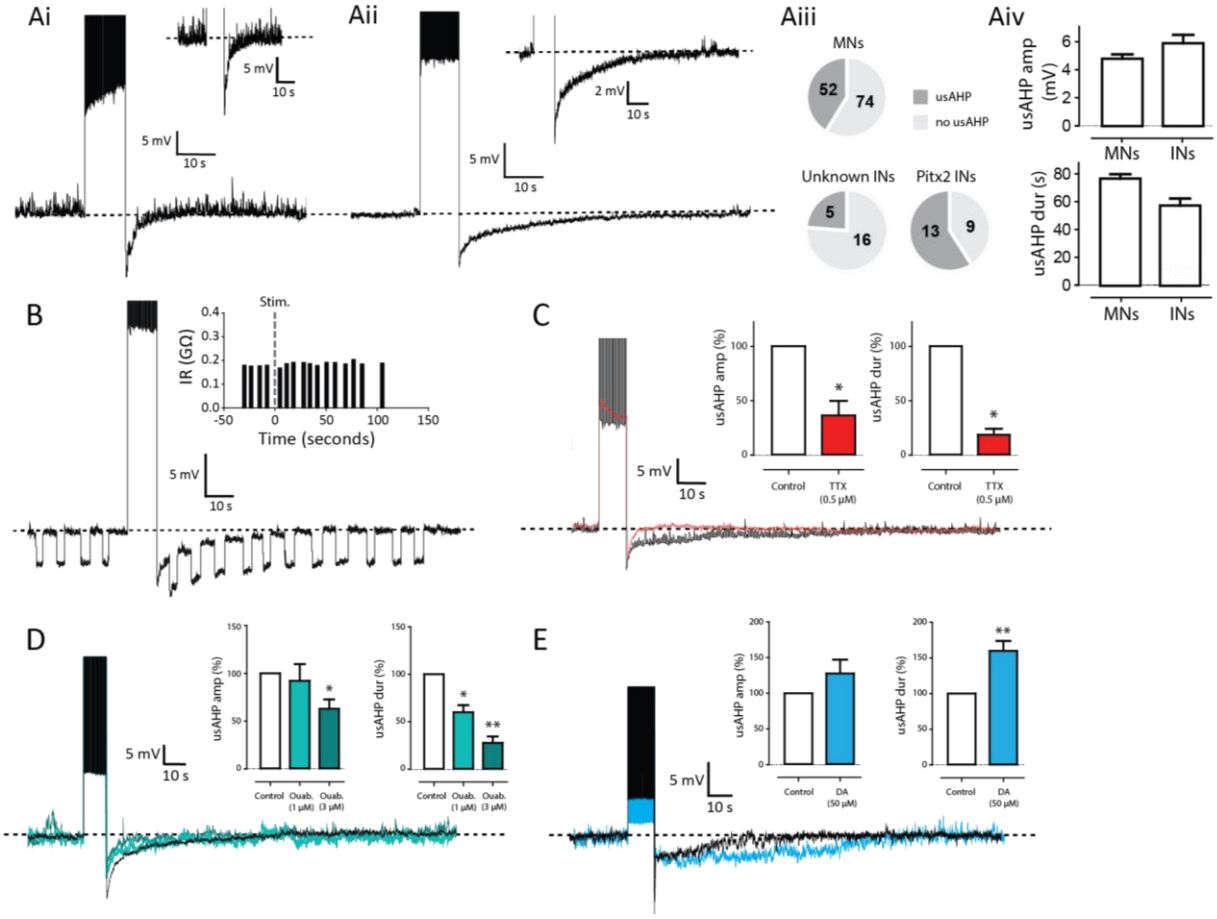
Ai
5 mV
10 s
5 mV
10 s
Aii
2 mV
10 s
5 mV
10 s
Aiii
MNs
52
74
usAHP
no usAHP
Unknown INs
5
16
Pitx2 INs
13
9
Aiv
usAHP amp (mV)
MNs
INs
usAHP dur (s)
MNs
INs
B
Stim.
IR (GΩ)
Time (seconds)
5 mV
10 s
C
usAHP amp (%)
usAHP dur (%)
Control
TTX (0.5 μM)
5 mV
10 s
D
usAHP amp (%)
usAHP dur (%)
Control
Ouab. (1 μM)
Ouab. (3 μM)
5 mV
10 s
E
usAHP amp (%)
usAHP dur (%)
Control
DA (50 μM)
5 mV
10 s

Sodium pump AHPs produce no measurable change in membrane conductance (Pulver & Griffith, 2010; Zhang & Sillar, 2012); therefore hyperpolarising current pulses were injected into the cell to measure the input resistance of the cell before, during and after the usAHP. No significant change in input resistance was found (Figure 8B). Moreover, the application of 0.5 µM TTX irreversibly blocked sodium spikes and abolished the usAHP ($p<0.05$, n=4, Figure 8C). The short duration hyperpolarisation was resistant to both TTX and ouabain and therefore is likely to be a Ca^{2+}-dependent K^+ current (K_{Ca}, SK), which is known to be expressed in mammalian motoneurons (Miles *et al.*, 2005). Finally, to more directly confirm that the usAHP is produced by sodium pump activity ouabain (1-3 µM) was applied, which decreased both the usAHP amplitude (1µM: -7.85% ± 17.60%, n=3, $p>0.05$; 3µM: -37.06% ± 9.76%, n=6, $p<0.05$) and duration (1µM: -39.92% ± 7.44%, n=3; 3µM: -72.89% ± 6.67%, n=6, $p<0.05$) in a dose-dependent manner (Figure 8D). Overall, these data demonstrate that a significant proportion of both motoneurons and ventral horn interneurons, including Pitx2-positive interneurons, exhibit a spike-dependent, minute-long usAHP. Given that this usAHP is sensitive to both ouabain and TTX, and occurs without changes in membrane conductance, it is most likely mediated by an activity-dependent sodium pump potential.

The facilitatory effects of 3 µM ouabain on locomotor burst frequency were dependent on the presence of 50 µM dopamine (Figure 3), suggesting that dopamine may modulate sodium pumps in mouse spinal neurons. The effects of 50 µM dopamine on the usAHP were therefore tested. Dopamine initially depolarised cells and increased spiking (not shown), so a direct holding current was applied to return the RMP back to control levels. After repeating the protocol to induce repetitive spiking in the presence of dopamine, the duration of the usAHP was significantly increased by around 60% (59.91% ± 13.96%, n=9, $p<0.05$; Figure 8E). Dopamine had no significant effect on the peak amplitude of the usAHP immediately after cessation of spiking (n=9, $p>0.05$); however, such measurements were likely complicated by the presence in some cells of short duration, non-pump related AHPs (Figure 8Ai). These data demonstrate that in motoneurons which express a pump-mediated outward,

hyperpolarising potential, dopamine modulates the sodium pump to increase the duration of this usAHP.

Monensin converts a dynamic usAHP into a tonic hyperpolarisation

To test whether the usAHP could be enhanced by increasing intracellular sodium, monensin was used as a proxy for intense network activity. For motoneurons which displayed a large usAHP in control conditions (e.g. Figure 9Ai), the first and most obvious effect of monensin (10 µM) was a membrane hyperpolarisation (Figure 9A,C, $n=5$, $p<0.01$), which was concurrent with a loss of the dynamic usAHP in response to high frequency spiking (Figure 9Aii,iii; $n=5$, $p<0.05$). Similar to the situation in *Xenopus* tadpoles, the amplitude of the hyperpolarisation was proportional to the usAHP amplitude observed during control conditions (Figure 9D), strongly suggesting that increased pump activity is mediating the change in membrane potential. Indeed, for neurons which showed no usAHP (e.g. Figure 9Bi), there was no effect of monensin on membrane potential ($n=4$, Figure 9B,C, $p>0.05$). These data suggest that monensin mimics high activity by increasing intracellular sodium, which in turn activates the sodium pump and generates a hyperpolarisation. Unlike sodium influx induced by discontinuous intense spiking, the pumps are presumably unable to fully counteract the continuous monensin-induced sodium influx and so pump activity remains high; hence further sodium influx driven by spiking no longer generates a usAHP. Overall, monensin appears to convert a *dynamic* pump potential into a *tonic* hyperpolarisation by maximising pump activity.

Figure 9. Increasing intracellular sodium using monensin converts a dynamic usAHP into a tonic hyperpolarisation. A. The effect of monensin (10 µM) on a motoneuron displaying a usAHP. Ai: Motoneuron displaying a usAHP. Aii: The same cell in the presence of monensin, which caused the membrane potential to hyperpolarise and the usAHP to be abolished. Aiii: Monensin significantly reduced the amplitude of the usAHP (n=5). **B.** Monensin has no effect on the membrane potential of neurons which lack the usAHP. Bi: Motoneuron exhibiting no usAHP. Bii: The same cell in the presence of monensin, which did not cause a hyperpolarisation. **C.** In motoneurons displaying a usAHP, monensin caused a significant hyperpolarisation of the resting membrane potential (n=5), whereas there was no significant change in cells lacking a usAHP (n=4). **D.** For neurons which did express a usAHP, the size of the hyperpolarisation induced by monensin was proportional to the size of the usAHP displayed in control. *$p<0.05$.

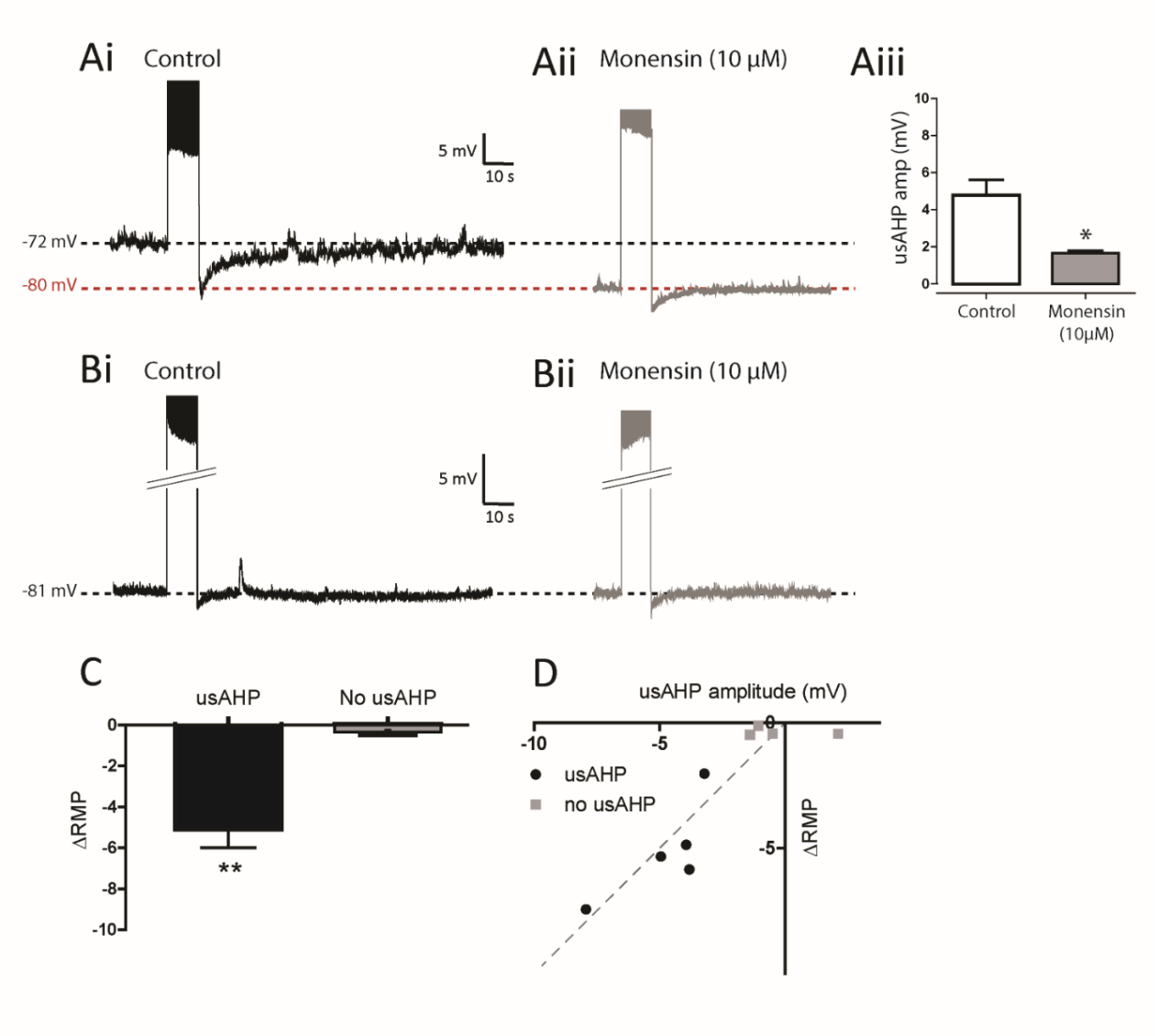
Ai
Control
Aii
Monensin (10 µM)
Aiii
5 mV
10 s
-72 mV
-80 mV
usAHP amp (mV)
10
8
6
4
2
0
*
Control
Monensin
(10µM)
Bi
Control
Bii
Monensin (10 µM)
5 mV
10 s
-81 mV
C
usAHP
No usAHP
ΔRMP
0
-2
-4
-6
-8
-10
**
D
usAHP amplitude (mV)
-10
-5
0
usAHP
no usAHP
-5
ΔRMP

Chapter 3 discussion

In this chapter I show that manipulating the sodium pump using ouabain (to block the pump), and monensin (to activate the pump) regulates locomotor activity generated by the mouse spinal cord. Using two different methods to evoke locomotor-like activity (pharmacological and sensory stimulation), blockade of the sodium pump increased the frequency of rhythmic output, whilst activating the pump had the opposite effect. Similar accelerations in rhythm frequency with ouabain have been reported in the leech heartbeat CPG (Tobin & Calabrese, 2005); the rat respiratory CPG (Tsuzawa *et al.*, 2015); and networks of dopaminergic midbrain neurons in the rat (Johnson *et al.*, 1992). The effect of pump blockade on rhythm frequency could be due to removal of a *tonic,* negative contribution of the pump to the RMP, thereby depolarising specific CPG neurons involved in pattern generation. For example, in the mammalian respiratory CPG, ouabain is thought to accelerate the rhythm in part by depolarising specific CPG neurons (Tsuzawa *et al.*, 2015), although effects on a dynamic pump component have also been shown (Krey *et al.*, 2010). In many systems, however, the contribution of α3 to the maintenance of RMP is both negligible, and slow, such that low concentrations of ouabain that selectively block α3 but not α1 have little effect on membrane potential (e.g. (Pulver & Griffith, 2010; Zhang & Sillar, 2012)). Blocking the sodium pump may instead be acting on the network by abolishing a *dynamic,* activity-dependent pump current, which can contribute to setting rhythm frequency. For example in rhythmically active midbrain dopaminergic neurons (Johnson *et al.*, 1992), and in cultured rat spinal neurons (Darbon *et al.*, 2003), each recurring burst is terminated by a pump-mediated hyperpolarisation of several millivolts. Blocking the α3 pump accelerates the rhythm by abolishing this intrinsic inter-burst delay. Similar effects of ouabain also occur in the locomotor networks underlying *Xenopus* tadpole swimming, *Drosophila* larva crawling and, as shown here, neonatal mouse locomotion. Importantly, there is evidence that the α3 subunit is widely expressed in motoneurons and interneurons throughout the dorsal and ventral horn in neonatal mice,

although the specific neuron subtypes expressing this subtype is yet to be fully explored (Edwards *et al.*, 2013).

I also observed a decrease in the amplitude of bursts following the application of 3 µM ouabain, but not with 1 µM or lower. This difference may relate to distinct effects on tonic and dynamic pump components at the single cell level. The dynamic pump potential (the usAHP) characterised in spinal neurons was reduced by both 1 and 3 µM ouabain, suggesting that its inhibition underlies frequency effects. However 3 µM, but not 1 µM ouabain, also depolarised spinal neurons, suggesting that the 3 µM amplitude effect may be due to an inhibitory effect on the tonic pump contribution. Raising intracellular Na^+ concentration with the Na^+ ionophore monensin exerted the opposite effects to ouabain on the rhythm, consistent with the activation of a Na^+-dependent hyperpolarizing dynamic pump potential. As described in chapter 2, monensin acts as a proxy for intense, sustained neuronal firing and rather than depolarizing neurons, drives their membrane potential towards the most hyperpolarised levels attained by the usAHP. Monensin also profoundly affected rhythm coordination, severely disrupting left-right alternation and synchronising flexor-extensor phase values. Although the mechanisms underlying these coupling effects remain to be determined, monensin presumably suppresses the activity of interneurons mediating half-center alternation. These results thus provide indirect evidence that the neuronal populations controlling left-right and flexor-extensor alternation, such as the commissural V0 population (Talpalar *et al.*, 2013), and reciprocal Ia inhibitory neurons (rIa-INs) (Talpalar *et al.*, 2011), respectively, are likely to display a usAHP. Whilst the exact identity of the interneurons involved remains to be investigated, the switch from flexor-extensor alternation to synchrony in monensin is intriguing, and offers potential insight into activity-dependent changes in unit burst generator coupling such as those accompanying speed related changes in gait (Bellarditta & Kiehn, 2015).

The experiments using K^+-free extracellular solution did not precisely match the data using ouabain, suggesting that multiple mechanisms are likely to be involved upon removal of extracellular K^+, which is not surprising. The amplitude was reduced, similar to our ouabain

experiments, but the locomotor burst frequency showed a complex, biphasic pattern of change over the course of an experiment. Initially, the frequency rapidly dropped over a period of around 5 minutes, but this was quickly followed by an increase in burst frequency. The frequency then remained relatively stable throughout the hour long period in zero K^+ solution. Upon washout of zero K^+ solution, the burst frequency again showed a biphasic response: an initial decrease, followed by an increase. Although in some studies (e.g. (Zhang & Sillar, 2012)), the major effects of zero potassium solution have generally been restricted to effects on the sodium pump, other studies have found the effects to be more complex due to effects on ionic gradients. Indeed, one would expect the potassium gradient to be severely disrupted, with the removal of extracellular K^+ causing an enhancement of potassium currents. A number of previous studies have also found biphasic responses to zero K^+ solution, similar to our results. In tactile sensory neurons of the leech, zero K^+ solution caused an initial hyperpolarisation, which increased over a period of around 15 mins, followed by a large depolarisation beyond control RMP (Catarsi *et al.*, 1993). The authors propose that the initial hyperpolarisation relates to the increased K^+ outflow due to the increase in ionic gradient, with the latter depolarisation mediated by decreased sodium pump activity. Similar results have been found for SCN neurons, whereby removal of extracellular K^+ causes an initial inhibitory effect on spontaneous spike rate, followed by a delayed excitatory effect that resembles the effects of ouabain (Wang & Huang, 2006). Again, this was proposed to be due to a rapid effect on the potassium concentration gradient, followed by a slightly slower, blockade of the sodium pump. It is likely that these mechanisms could also explain the biphasic effect on frequency observed by zero K^+ aCSF in the mouse spinal locomotor network. I also observed an unusual, irregular rhythm late in the washout period, which involved “bouts” of high frequency bursting. It is possible that this rhythm may be due to a loss of tissue integrity over the long timecourse of the experiment (>3 hours). Alternatively, this rhythm may reflect a mixture of an enhanced sodium pump usAHP (responsible for the large inter-burst delays) combined with a depolarisation from a reduction in K^+ current (responsible for the high frequency bursts), which would both be expected to occur upon washout of the zero K^+ solution.

The usAHP was present only in a subset of motoneurons and interneurons. This matches the heterogeneous distribution of the usAHP both between and within spinal neuron subtypes documented previously, and indeed the proportions of neuron types expressing the usAHP in mice is highly similar to the situation in *Xenopus* tadpoles (Chapter 2; see also (Darbon *et al.*, 2003; Pulver & Griffith, 2010; Zhang & Sillar, 2012)). Activity-dependent pump mediated AHPs are thought to be generated by increases in the activity of the α3 sodium pump subtype, and one possibility is that the amplitude and duration of a dynamic pump potential is mediated by differences in the expression level of the α3 sodium pump subtype relative to α1. This suggests that pump potentials are not a generic neuronal phenomenon, but rather a carefully orchestrated feature of rhythmic networks whose distribution is likely correlated with α3 isoform expression, which has been shown throughout the mammalian spinal cord, but restricted to some cells and not others (Edwards *et al.*, 2013). Many spinal interneuron types contribute to mammalian locomotor rhythm generation, and in this study usAHP expression was found in the relatively small population of Pitx2-positive interneurons clustered around the central canal. However, the usAHP was also found in a number of unidentified spinal interneurons. It will be important in future work to identify these interneuron subtypes and establish the impact of the usAHP upon their contribution to rhythm generation. Moreover, the animals used in this study were very young (P0-P4), and so it would be interesting to see how the distribution of the α3 subtype changes with development, and how changes in usAHP distribution contribute to the functional developmental of the locomotor network. For example, during development in *Xenopus* tadpoles, the usAHP is expressed in a similar proportion of each neuron type in the swim network, but older animals appear to have a shorter duration usAHP (Currie, 2014). Interestingly, it has been shown in rats that a pump-mediated usAHP at the Calyx of Held synapse is smaller in younger rats, which are known to express lower levels of the α3 sodium pump than older animals (Kim *et al.*, 2007).

A number of disorders of the nervous system are known to relate to sodium pump dysfunction (Arnaiz & Ordieres, 2014; Holm & Lykke-hartmann, 2016). Homozygous α1 knock-out mice

are embryonic lethal (James *et al.*, 1999), whilst α3 dyfunction is implicated in a range of neurological disorders, with at least three neurological disorders caused by mutation in the *ATP13* gene that encodes the α3 subunit (De Carvalho Aguiar *et al.*, 2004; Heinzen *et al.*, 2012; Demos *et al.*, 2014). Moreover, a number of other more common disorders are also known to involve α3 sodium pump dysfunction. In a recent study misfolded SOD1 protein was shown to aggregate with α3 in an ALS mouse model, impairing its exchange activity (Ruegsegger *et al.*, 2015). Given that dysfunction of α3 also contributes to epilepsy (Krishnan *et al.*, 2015) and bipolar disorder (Kirshenbaum *et al.*, 2012*a*), it is possible that the inability to respond dynamically and homeostatically to activity-induced rises in intracellular sodium may be a general feature of pump disorders involving the α3 subtype. Recently, a number of α3 mutant mice lines have been developed, all of which show severe motor deficits (Moseley *et al.*, 2007; DeAndrade *et al.*, 2010; Kirshenbaum *et al.*, 2011; Ikeda *et al.*, 2013; Sugimoto *et al.*, 2014; Hunanyan *et al.*, 2015). The hyperactivity phenotype in these mice is especially pronounced, with mutant mice showing almost continuous locomotor activity which is also much faster than control mice. The α3-mutation affects sodium pumps throughout the nervous system, including presumably the spinal cord, and therefore this phenotype may relate to the role of the α3 sodium pumps explored in this chapter. Indeed, this behavioural phenotype would be predicted by the effects described in this chapter using low concentrations of ouabain; namely, longer duration bouts of locomotion with a higher frequency of limb movements.

In a normal physiological context, pump-mediated AHPs can be generated by spinal neurons as they spike rhythmically during locomotor episodes. They can then not only contribute to the termination of bouts of locomotion, but can also influence future activity if it occurs within the timescale of an unrecovered pump hyperpolarisation (Pulver & Griffith, 2010; Zhang & Sillar, 2012; Zhang *et al.*, 2015). When I decreased the interval between sensory-evoked locomotor episodes to less than 1 minute, within the timescale of the usAHP, locomotor episodes became significantly shorter and slower. Moreover, blockade of the sodium pump using

ouabain disrupted this relationship; strongly suggesting that changes in sodium pump activity track ongoing locomotor activity and provides a form of short term motor memory that could function to prevent damage from overexertion. Indeed, there is increasing evidence that fatigue – defined as an activity-induced decrease in maximum motor output – involves not only limb muscles but also *central* mechanisms, such as a reduction in motoneuron drive (Meeusen *et al.*, 2006; Ranieri & Di Lazzaro, 2012). The mechanisms underlying central fatigue are poorly understood, but there is evidence even in humans that increased sodium pump activity contributes to motor axon hypoexcitability following intense motor activity (Kiernan *et al.*, 2004). Again, it is of particular interest that *Myshkin* mice, with reduced α3 sodium pump activity, are known to be hyperactive (Kirshenbaum *et al.*, 2012*b*). These mutant mice locomote almost constantly, showing far fewer breaks in activity. This behavioural phenotype would be predicted by the results shown in this chapter, and the infatiguability of these mutant mice may relate to the role of the α3 sodium pump in the spinal cord as a central fatigue mechanism that regulates, and restricts, bouts of locomotor activity.

The effects of ouabain on the frequency of locomotor output were dependent on the presence of dopamine, with no significant increase in locomotor burst frequency observed in the absence of dopamine. One possible explanation for this lack of effect may relate to a frequency ceiling effect, as the locomotor frequency is higher without dopamine. It is possible that ouabain is unable to further increase locomotor frequency, due to an upper frequency limit of the network being reached. However, this is highly unlikely as the mouse locomotor network has been shown to be capable of producing locomotor bursting at frequencies as high as high as 0.5 Hz under similar conditions (Talpalar & Kiehn, 2010), which is approximately double the frequency observed in the absence of dopamine. Instead, the more likely explanation is that dopamine is acting on the usAHP, whose enhancement could reveal an effect of blocking the sodium pump in the presence of dopamine, which is diminished without dopamine. Indeed, in support of this hypothesis, dopamine significantly enhanced the usAHP in spinal neurons. Dopamine initially depolarised motoneurons, which has been shown to be

due to the inhibition of resting, leak potassium currents (Han *et al.*, 2007). When this change was corrected for, the usAHP was still found to be enhanced, which suggests that the modulation by dopamine is likely to be targeted to the α3 sodium pumps, which do not usually contribute to the RMP.

Dopamine is a well-established modulator of locomotor circuits (Miles & Sillar, 2011; Sharples *et al.*, 2014), and indeed dopamine is released into the spinal cord during stepping activity in mammals (Gerin & Privat, 1998). Moreover, intense motor activity has been shown to result in an increase in monoamine release, including dopamine, which is thought to contribute to central fatigue (Meeusen *et al.*, 2006). However, to the best of my knowledge, this is the first evidence that the effects of dopamine on spinal motor circuits may involve the facilitation of sodium pump activity.

In fact, the sodium pump is a well-established target for modulators in both non-nervous and nervous tissue, and dopaminergic modulation of sodium pumps is especially well-described in some tissues (Therien & Blostein, 2000). Dopamine, usually acting via PKA or PKC, can enhance or inhibit pump activity depending on the species, tissue type and dopamine receptors involved (Zhang *et al.*, 2013). In striatal neurons, D2-like receptor activation stimulates sodium pumps by inhibiting PKA, thus dephosphorylating the α3 subunit; (Bertorello *et al.*, 1990; Wu *et al.*, 2007). Other studies have similarly shown that changes in PKA activity can modulate the ability of a neuron to respond to changes in intracellular sodium through phosphorylation/dephosphorylation of α3 (Azarias *et al.*, 2013). Neuronal sodium pumps can even form a complex (“signalplex”) with D1 and D2 dopamine receptors to allow direct reciprocal modulation between dopamine receptors and the pump (Hazelwood *et al.*, 2008).

Dopaminergic pump modulation in rhythmic circuits has not been studied previously, but the effects of other pump modulators are much better understood. For example, the neuropeptide myomodulin inhibits pump activity in the leech heartbeat CPG to speed up the rhythm (Tobin

& Calabrese, 2005), whilst serotonin decreases the amplitude of a pump-dependent AHP in tactile sensory neurons (Catarsi *et al.*, 1993). The gaseous molecule nitric oxide has been shown to decrease sodium pump activity in mammalian spinal neurons (Ellis *et al.*, 2003), although the significance of this finding, given the key role of nitric oxide as a modulator of locomotor circuits (McLean & Sillar, 2004; Foster *et al.*, 2014), remains to be explored.

Chapter 3 conclusions

Na^+/K^+ exchange pumps are ubiquitously distributed, abundantly expressed and phylogenetically conserved proteins that are often viewed as molecular automata engaged exclusively in the maintenance of ionic distributions across cell membranes. However, in this chapter I have shown that they respond dynamically to changes in intracellular sodium that accompany intense neuronal firing. This capacity endows networks of the mammalian spinal cord with a homeostatic control mechanism to shape motor output in an activity-dependent manner. Moreover, these data reveal a novel link between dopamine modulation of the pump and locomotor output, a finding that is relevant to diseases of the motor system in which both the pumps and dopamine have been implicated.

Concluding remarks

In order to survive, animals require flexibility from the circuits controlling their movements so that they can generate complex behaviours and interact with their environment. Although the CPG networks in the spinal cords of vertebrates that generate locomotor behaviours are able to autonomously generate and sustain rhythmic activity, the output of these networks is constantly being reconfigured through the actions of descending neuromodulators from the brain, as well as through changes in the activity of the proteins embedded within the network. The work described in this thesis has partly focused on how one neuromodulator, dopamine, acts on the CPG networks controlling locomotion, and how the activity of one particular protein, the sodium pump, can mediate important changes in the output of these networks through activity-dependent changes in its ion exchange activity.

The first chapter of this thesis focussed specifically on dopaminergic modulation of the spinal network of *Xenopus* tadpoles that controls their swimming behaviour. The dopaminergic neuromodulatory system is one of the most widespread and evolutionarily conserved systems, and the role of dopamine as a modulator of spinal locomotor circuits is receiving increasing attention (reviewed in (Sharples *et al.*, 2014)). However, whilst the network controlling swimming in *Xenopus* tadpoles is one of the most completely understood CPGs, the role of dopaminergic signalling in this system at these early stages of development was completely unknown prior to this work. The experiments in this chapter were therefore intended to fill this gap in the literature on dopaminergic signalling in locomotor systems. I have shown that dopamine acts at these early stages of *Xenopus* development as a potent inhibitory modulator of swimming, and its effects are mediated through a D2-like receptor coupled to the opening of particular potassium channels in swim CPG neurons. The use of ventral root recordings in combination with simultaneous path-clamp recordings has allowed me to define the mechanism of dopaminergic inhibition at the level of individual swim neurons, whilst relating these effects to the changes in overall network output. The *Xenopus* tadpoles used in this chapter are very young (2-3 days old), which has both advantages and disadvantages. At these stages the nervous system is relatively simple, and incredibly well-defined (Roberts *et*

al., 2010), thus avoiding some of the complex and often conflicting effects of bath-applying dopamine in other, more complex systems. Hence I have been able to trace the effects of dopamine to a specific receptor subtype, link the activation of this receptor to the opening of individual ion channel type, and relate these cellular effects to changes in swimming behaviour. At the same time, these results do not necessarily tell us very much about the mechanisms of dopaminergic signalling in the older, more mature swimming network, or indeed how dopamine is involved through the switch from tail-based swimming to limb-based walking, as the animal enters metamorphosis. Nevertheless, the results in this chapter contribute to our understanding of the role of dopamine at a specific stage of *Xenopus* tadpole development, and provide a solid framework with which to study dopaminergic signalling in the later developing animal. It will be interesting to see which aspects of dopaminergic signalling are carried right through development; which aspects are modified to achieve behavioural flexibility; and which aspects are lost altogether.

In the second chapter of this thesis I focused on the roles of the sodium pump, Ih currents and temperature in young *Xenopus* tadpoles. Again, using simultaneous patch clamp and ventral root recordings, I have been able to explore the consequences of an artificially induced usAHP at the cellular and network level. The effect of increasing sodium pump activity using monensin results in a “fatigue” of the swim network, which is mediated through the conversion of a dynamic sodium pump current in a range of CPG neuron types into a tonic hyperpolarisation. A recent study (Kueh *et al.*, 2016) has shown highly similar effects of enhancing sodium pump activity (using monensin) in the CPG neurons controlling the leech heartbeat, highlighting the importance of these findings for rhythmic networks across species. The pump current in the leech heartbeat network has also been shown to be subject to neuromodulation, and in this thesis I have provided evidence that the sodium pumps in *Xenopus* tadpoles are also subject to modulation, albeit with different neuromodulators in the leech. I have shown that the amplitude of the usAHP can be shifted in opposite directions, with D1 receptor activation enhancing the usAHP and nitric oxide reducing it. The results in this chapter have also

furthered our understanding of the effects of temperature on the *Xenopus* swim network, focusing mainly on the cellular effects which had not been studied previously. Raising the temperature has widespread effects, but mostly results in a net increase in excitation of the swim network, which in turn increases the activation of self-regulation mechanisms, leading to more intense, but shorter, locomotor episodes. I have also uncovered a previously unidentified Ih current, which is expressed mostly in the population of rhythm-generating excitatory descending interneurons (dINs). Again, it will be interesting to explore in future work the role of Ih current later in development, and also whether it becomes a target for some of the descending neuromodulators discussed in this thesis. Interestingly, the recent study in the leech heartbeat CPG (Kueh *et al.*, 2016) also showed a complex and dynamic interaction between Ih and sodium pump currents. In this thesis, I show that Ih appears to only be present in the one cell type in the network that does not display dynamic pump currents, therefore such an interaction appears to be absent, at least at this stage of development. However, as Ih becomes expressed more widely in the network during development, it is highly likely that similar interactions between Ih and the sodium pump will become apparent; it will be interesting to explore the consequences of this interaction in future work.

In the final chapter, the exploration of the role of sodium pumps in locomotion was extended to the mammalian CPG controlling walking in the neonatal mouse. Sodium pumps are receiving increasing attention in mammalian systems, in part due to their relevance to ageing and in a range of debilitating diseases in humans (Arnaiz & Ordieres, 2014; Holm & Lykke-hartmann, 2016), but also because of an increasing realisation of their importance in network function across many brain areas and in a range of species. Despite this, almost nothing was known about the role of the sodium pump in the regulation of the locomotor network in mice, and a number of clear questions were yet to be answered: what happens to locomotor activity in mice when you block or activate the sodium pump? Does the locomotor interval relationship shown for *Xenopus* tadpoles, and other species, also hold true in mice? Do modulators, such as dopamine, interact with spinal sodium pumps, and how does this affect locomotor activity?

In this final chapter I have addressed these questions and shown that changes in sodium pump activity, using ouabain (to block the sodium pump) and monensin (to activate the pump), have potent and behaviourally relevant effects on the parameters of both drug- and sensory-evoked locomotor activity generated by the mammalian spinal cord. The use of two methods for evoking locomotor activity (pharmacological and electrical stimulation) has allowed me to reveal addition roles of for the sodium pump not only in controlling the frequency of locomotor bursting, but also the duration of electrically-evoked bouts. Moreover, the use of this often overlooked method for evoking activity has allowed me to more directly compare the effects seen in *Xenopus* tadpoles with those in mice, and also allowed me to explore the role of the pump under behaviourally relevant conditions, especially compared to a number of previous studies on mammalian pumps which have relied on disinhibited bursting rhythms (see introduction). The *in vitro* results in this thesis also appear broadly to match the *in vivo* motor deficits observed in a number of recent α3 mutant mouse models, thus highlighting the importance of spinal sodium pumps in the range of disorders associated with the sodium pump.

As in chapters 1 and 2, I have also shown that dopamine plays an important role in the function of mammalian locomotor output via actions on sodium pumps. The effects of sodium pump manipulation were found to be dependent on the presence of dopamine, suggesting that dopamine is acting on the locomotor network through pump modulation. Indeed, the intracellular recordings shown here support this hypothesis. Overall, this chapter has demonstrated a clear role for the sodium pump as a sensor for activity-dependent changes in intracellular sodium that contributes to the frequency and duration of ongoing locomotor activity. Future studies will explore whether neuromodulators, aside from dopamine, also act on the sodium pump in the mammalian spinal CPG network to fine tune its contribution to locomotion. For instance, it will be interesting to see whether nitric oxide, which I showed to modulate sodium pump activity in the *Xenopus* spinal cord, also has an effect on the mammalian usAHP. Moreover, it will be fascinating to utilise the many α3 mutant mouse

models which have recently been established to more specifically test the *in vivo* significance of the findings presented in this thesis.

Finally, what comparisons can be made between my results in *Xenopus* tadpoles with those in neonatal mice? Modern amphibians and mammals share a common ancestor that lived approximately 400 million years ago (MYA). Around 340 MYA, amphibians entered the land and fully terrestrial amniotes emerged[12]. After several million years, the amniote linages split into the synapsid reptiles, which evolved to become mammals; and sauropsids, which became snakes, lizards, dinosaurs and birds. Synapsid evolution involved massive morphological transformations, including dramatic skeletal changes and a switch to an endothermic lifestyle. The earliest known mammal is thought to be *Morganucodon*[13], which emerged around 200 MYA. Finally, mice evolved only around 10-15 MYA. Thus, many major evolutionary changes occurred during the transition from amphibians to land-based reptiles, through synapsid evolution, and to the emergence of mice. The nervous system similarly underwent drastic changes to accommodate changes in lifestyle and morphology, not least with the number of neurons increasing from around 16 million in adult frogs to around 70 million in adult mice.

However, evidence suggests that compared to many of the morphological changes that have occurred over evolutionary time, many components of the nervous system are in fact highly conserved (Katz & Harris-Warrick, 1999; O'Connell & Hofmann, 2012; Strausfeld & Hirth, 2013; Katz, 2016; Keifer & Summers, 2016). The evidence suggests that the basic architecture of many neural circuits have been retained through evolutionary time, and extant species display "variations on a theme", rather than completely new circuits. Thus, we can often identify conserved principles of circuit function, and this appears to be true for the circuits controlling locomotor behaviours. Whilst the CPGs underlying swimming in tadpoles, and walking is mice, have many obvious differences, they also share a number of core features

[12] There is little fossil evidence for the first true amniotes/reptiles. However, fossils found in Scotland suggest two species of lizard-like amphibians, *Casineria* ("Cheese bay", Edinburgh) and *Westlothiana* ("Animal from West Lothian") may represent these crucial transition species.
[13] Named after the county of Glamorgan in south Wales.

such as reciprocal inhibition, a range of specific intrinsic properties and ion channels in motoneurons and interneurons. Moreover, an increasing number of studies are utilising genetic markers to identify similar neuron types in different animal models, which is revealing a conserved theme of gene expression and neural connectivity across diverse species (Goulding & Pfaff, 2005).

This functional conservation appears to be especially true for the dopaminergic system of vertebrates. In fact, recent evidence suggests that there is extensive homology between the dopaminergic systems in the central complex of arthropods, and the basal ganglia of humans, groups separated by hundreds of millions of years (Strausfeld & Hirth, 2013). The substructures of these diverse groups both involve dopaminergic signalling pathways that shape and configure the network to control motor behaviours, attention, sleep and affective processes through highly conserved mechanisms. It is therefore perhaps not surprising that dopamine is an important neuromodulator in the spinal networks of *Xenopus* tadpoles (this thesis) and of mice (previous work; summarised in (Sharples *et al.*, 2014)), as well as many other, if not all, vertebrates. The role of dopamine in the modulation of spinal CPG networks is likely to share a number of highly conserved features, and as more diverse species are studied we will likely discover conserved principles of dopaminergic modulation in the spinal cord. One emerging principle appears to be the bidirectional control of excitability in the locomotor networks of adult species, with changes in the direction of modulation mediated through differential, concentration-dependent activation of either D1-like, or D2-like receptors. Furthermore, there is growing evidence for the importance of the D4 receptor specifically in the inhibitory effects of dopamine, especially at early stages of development (Boehmler *et al.*, 2007; Lambert *et al.*, 2012; Reimer *et al.*, 2013; Pérez-Fernández *et al.*, 2015).

The sodium pump, the second major topic of this thesis, is highly conserved, with genomic analysis suggesting that the neuronal sodium pump in particular displays around 96% cross-species similarity in vertebrates (Dobretsov & Stimers, 2005). This implies that the sodium pump plays an important and conserved function for neurons in the nervous system. In this

thesis, I have performed similar experiments, using similar techniques, on both young *Xenopus* tadpoles and young mice, and a number of the findings have produced very similar results, both at the network level and at the single neuron level. For example, changes in neuronal sodium pump activity potently influences the duration of bouts of locomotor activity, in both cases with an increase in sodium pump activity "fatiguing" the locomotor network. Moreover, this network fatigue plays a role in the feedforward control of future locomotor bouts. Similarly, increased sodium pump activity also results in slower, less intense locomotor activity in both systems. The cellular substrate for these effects also appears to be extremely similar. In both cases, raising intracellular sodium through intense spiking, or using pharmacological tools, results in the generation of a usAHP, with comparable amplitude (~5 mV) and comparable duration (~1 minute). One limitation to this comparative approach is the sheer complexity of cell types in the mammalian spinal cord compared to *Xenopus* tadpoles. Thus, it will be particularly important in the future to determine the precise neuronal subtypes of the mammalian spinal cord whose sodium pump modulation is responsible for the network effects described here.

The diversity of species in which the sodium pump has been shown to play a role essentially as a spike rate device that regulates ongoing and future activity, from fruitflies to tadpoles to mice, suggests that the neuronal form of this protein may have a conserved function across a wide range of species. Humans split from the common ancestor we shared with mice only 65 million years ago, and so it will be interesting in future studies, especially with a rise in the use of human induced pluripotent stem cells (iPSCs), to study whether the sodium pumps embedded in human spinal motoneurons and interneurons also play a similar role in neuronal self-regulation. Moreover, if dopamine also shows a conserved role in the modulation of sodium pump activity, it may also lead us to understand, and ultimately develop treatments, for disorders associated with dysfunctional sodium pumps (e.g. RDP, ALS and epilepsy) as well as dopaminergic system dysfunction (e.g. Parkinson's Disease).

References

Angstadt JD & Calabrese RL (1989). A hyperpolarization-activated inward current in heart interneurons of the medicinal leech. *J Neurosci* **9,** 2846–2857.

Angstadt JD & Friesen WO (1991). Synchronized oscillatory activity in leech neurons induced by calcium channel blockers. *J Neurophysiol* **66,** 1858–1873.

Arbas EA & Calabrese RL (1984). Rate modification in the heartbeat central pattern generator of the medicinal leech. *J Comp Physiol A* **155,** 783–794.

Arnaiz GRDL & Ordieres MGL (2014). Brain Na+, K+-ATPase activity in aging and disease. *Int J Biomed Sci* **10,** 85–102.

Atwood HL, Charlton MP & Thompson CS (1983). Neuromuscular transmission in crustaceans is enhanced by a sodium ionophore, monensin, and by prolonged stimulation. *J Physiol* **335,** 179–195.

Aydemir-Koksoy A (2002). Na+, K+–ATPase: a review. *J Ankara Med Sch* **24,** 73–82.

Azarias G, Kruusmägi M, Connor S, Akkuratov EE, Liu XL, Lyons D, Brismar H, Broberger C & Aperia A (2013). A specific and essential role for Na,K-ATPase α3 in neurons co-expressing α1 and α3. *J Biol Chem* **288,** 2734–2743.

Baginskas A, Palani D, Chiu K & Raastad M (2009). The H-current secures action potential transmission at high frequencies in rat cerebellar parallel fibers. *Eur J Neurosci* **29,** 87–96.

Ballerini L, Bracci E & Nistri A (1997). Pharmacological block of the electrogenic sodium pump disrupts rhythmic bursting induced by strychnine and bicuculline in the neonatal rat spinal cord. *J Neurophysiol* **77,** 17–23.

Barclay JW, Atwood HL & Robertson RM (2002). Impairment of central pattern generation in *Drosophila* cysteine string protein mutants. *J Comp Physiol A Neuroethol Sensory, Neural, Behav Physiol* **188,** 71–78.

Barrière G, Mellen N & Cazalets JR (2004). Neuromodulation of the locomotor network by dopamine in the isolated spinal cord of newborn rat. *Eur J Neurosci* **19,** 1325–1335.

Baylor DA & Nicholls JG (1969). After-effects of nerve impulses on signalling in the central nervous system of the leech. *J Physiol* **203,** 571–589.

Beaulieu J-M & Gainetdinov RR (2011). The physiology, signaling, and pharmacology of dopamine receptors. *Pharmacol Rev* **63,** 182–217.

Bellarditta C & Kiehn O (2015). Phenotypic Characterization of Speed-Associated Gait Changes in Mice Reveals Modular Organization of Locomotor Networks. *Curr Biol* **2,** 1426–1436.

Bertorello AM, Hopfield JF, Aperia A & Greengard P (1990). Inhibition by dopamine of (Na+ K+) ATPase activity in neostriatal neurons through D1 and D2 dopamine receptor synergism. *Nature* **345,** 386–388.

Bjorklund A & Skagerberg G (1979). Evidence for a major spinal cord projection from

the diencephalic A11 dopamine cell group in the rat using transmitter-specific fluorescent retrograde tracing. *Brain Res* **177,** 170–175.

Blanco G & Mercer RW (1998). Isozymes of the Na-K-ATPase: heterogeneity in structure, diversity in function. *Am J Physiol* **275,** F633–F650.

Boehmler W, Carr T, Thisse C, Thisse B, Canfield VA & Levenson R (2007). D4 Dopamine receptor genes of zebrafish and effects of the antipsychotic clozapine on larval swimming behaviour. *Genes, Brain Behav* **6,** 155–166.

Bois P, Chatelier A, Bescond J & Faivre J-F (2011). Pharmacology of hyperpolarization-activated cyclic nucleotide-gated (HCN) channels.

Boothby KM & Roberts A (1992). The stopping response of *Xenopus laevis* embryos: pharmacology and intracellular physiology of rhythmic spinal neurones and hindbrain neurones. *J Exp Biol* **169,** 65–86.

Botta P, de Souza FMS, Sangrey T, De Schutter E & Valenzuela CF (2010). Alcohol excites cerebellar Golgi cells by inhibiting the Na+/K+ ATPase. *Neuropsychopharmacology* **35,** 1984–1996.

Bøttger P, Tracz Z, Heuck A, Nissen P, Romero-Ramos M & Lykke-Hartmann K (2011). Distribution of Na/K-ATPase alpha 3 isoform, a sodium-potassium P-type pump associated with rapid-onset of dystonia parkinsonism (RDP) in the adult mouse brain. *J Comp Neurol* **519,** 376–404.

Brown TG (1911). The Intrinsic Factors in the Act of Progression in the Mammal. *Proc R Soc B Biol Sci* **84,** 308–319.

Brown TG (1914). On the nature of the fundamental activity of the nervous centres; together with an analysis of the conditioning of rhythmic activity in progression, and a theory of the evolution of function in the nervous system. *J Physiol* **48,** 18–46.

Bublitz M, Morth JP & Nissen P (2011). P-type ATPases at a glance. *J Cell Sci* **124,** 2515–2519.

Butt SJB, Harris-Warrick RM & Kiehn O (2002). Firing properties of identified interneuron populations in the mammalian hindlimb central pattern generator. *J Neurosci* **22,** 9961–9971.

Calabrese RL, Norris BJ & Wenning A (2016). The neural control of heartbeat in invertebrates. *Curr Opin Neurobiol* **41,** 68–77.

Cao X, Oertel D, Carter BC, Bean BP, Cao X & Oertel D (2011). Temperature affects voltage-sensitive conductances differentially in octopus cells of the mammalian cochlear nucleus. 821–832.

Carlsson A, Falck B & Hillarp N-A (1962). Cellular localization of brain monoamines. *Acta Physiol Scand* **54,** 1–28.

De Carvalho Aguiar P, Sweadner KJ, Penniston JT, Zaremba J, Liu L, Caton M, Linazasoro G, Borg M, Tijssen M a J, Bressman SB, Dobyns WB, Brashear A &

Ozelius LJ (2004). Mutations in the Na+/K+-ATPase α3 gene ATP1A3 are associated with rapid-onset dystonia parkinsonism. *Neuron* **43,** 169–175.

Catarsi S, Scuri R & Brunelli M (1993). Cyclic AMP mediates inhibition of the Na(+)-K+ electrogenic pump by serotonin in tactile sensory neurones of the leech. *J Physiol* **462,** 229–242.

Cho HJ, Furness JB & Jennings EA (2011). Postnatal maturation of the hyperpolarization-activated cation current, Ih, in trigeminal sensory neurons. *J Neurophysiol* **106,** 2045–2056.

Clapcote SJ, Duffy S, Xie G, Kirshenbaum G, Bechard AR, Rodacker Schack V, Petersen J, Sinai L, Saab BJ, Lerch JP, Minassian B, Ackerley C, Sled JG, Cortez M, Henderson JT, Vilsen B & Roder JC (2009). Mutation I810N in the alpha3 isoform of Na+,K+-ATPase causes impairments in the sodium pump and hyperexcitability in the CNS. *Proc Natl Acad Sci U S A* **106,** 14085–14090.

Clemens S, Belin-Rauscent A, Simmers J & Combes D (2012). Opposing modulatory effects of D1- and D2-like receptor activation on a spinal central pattern generator. *J Neurophysiol* **107,** 2250–2259.

Clemens S, Rye D & Hochman S (2006). Restless legs syndrome: Revisiting the dopamine hypothesis from the spinal cord perspective. *Neurology* **67,** 125–130.

Combes D, Merrywest SD, Simmers J & Sillar KT (2004). Developmental segregation of spinal networks driving axial- and hindlimb-based locomotion in metamorphosing *Xenopus laevis*. *J Physiol* **559,** 17–24.

Connelly C (1959). Post-tetanic hyperpolarization in frog nerve. *Proc natn Biophys Conf,*.

Coombs J, Eccles J & Fatt P (1955). The electrical properties of the motoneurone membrane. *J Physiol* **130,** 291–325.

Cox B a. & Johnson SW (1998). Nitric oxide facilitates N-methyl-D-aspartate-induced burst firing in dopamine neurons from rat midbrain slices. *Neurosci Lett* **255,** 131–134.

Craven KB & Zagotta WN (2006). CNG and HCN channels: two peas, one pod. *Annu Rev Physiol* **68,** 375–401.

Crisp KM, Gallagher BR & Mesce KA (2012). Mechanisms contributing to the dopamine induction of crawl-like bursting in leech motoneurons. *J Exp Biol* **215,** 3028–3036.

Crisp KM & Mesce KA (2004). A cephalic projection neuron involved in locomotion is dye coupled to the dopaminergic neural network in the medicinal leech. *J Exp Biol* **207,** 4535–4542.

Crone SA, Quinlan KA, Zagoraiou L, Droho S, Restrepo CE, Lundfald L, Endo T, Setlak J, Jessell TM, Kiehn O & Sharma K (2008). Genetic Ablation of V2a Ipsilateral Interneurons Disrupts Left-Right Locomotor Coordination in Mammalian Spinal Cord. *Neuron* **60,** 70–83.

Currie SP (2014). *The development and neuromodulation of motor control systems in pro-metamorphic Xenopus laevis frog tadpoles* (thesis). PhD thesis: University of St Andrews.

Currie SP, Combes D, Scott NW, Simmers J & Sillar KT (2016). A behaviourally-related developmental switch in nitrergic modulation of locomotor rhythmogenesis in larval *Xenopus tadpoles*. *J Neurophysiol* **115,** 1446–1457.

Dahlstroem A & Fuxe K (1964). Evidence for the existence of monoamine-containing neurons in the central nervous system. I. Demonstration of monoamines in the cell bodies of brainstem neurons. *Acta Physiol Scand* **62,** SUPPL 232:1-55.

Dale N & Gilday D (1996). Regulation of rhythmic movements by purinergic neurotransmitters in frog embryos. *Nature* **383,** 259–263.

Dale N & Roberts A (1985). Dual-component amino-acid-mediated synaptic potentials: excitatory drive for swimming in Xenopus embryos. *J Physiol* **363,** 35–59.

Danner SM, Hofstoetter US, Freundl B, Binder H, Mayr W, Rattay F & Minassian K (2015). Human spinal locomotor control is based on flexibly organized burst generators. *Brain* **138,** 577–588.

Darbon P, Scicluna L, Tscherter A & Streit J (2002). Mechanisms controlling bursting activity induced by disinhibition in spinal cord networks. *Eur J Neurosci* **15,** 671–683.

Darbon P, Tscherter A, Yvon C & Streit J (2003). Role of the electrogenic Na/K pump in disinhibition-induced bursting in cultured spinal networks. *J Neurophysiol* **90,** 3119–3129.

Darbon P, Yvon C, Legrand JC & Streit J (2004). INaP underlies intrinsic spiking and rhythm generation in networks of cultured rat spinal neurons. *Eur J Neurosci* **20,** 976–988.

Dauer W & Przedborski S (2003). Parkinson's Disease: Mechanisms and Models. *Neuron* **39,** 889–909.

DeAndrade MP, Yokoi F, van Groen T, Lingrel JB & Li Y (2010). Characterisation of ATP1a3 mutant mice as a model of rapid-onset dystonia with parkinsonism. **48,** 1–6.

Debanne D, Gastrein P & Campanac E (2006). Queer channels in hippocampal basket cells: h-current without sag. *J Physiol* **574,** 2.

Demos MK, van Karnebeek CD, Ross CJ, Adam S, Shen Y, Zhan SH, Shyr C, Horvath G, Suri M, Fryer A, Jones SJ & Friedman JM (2014). A novel recurrent mutation in ATP1A3 causes CAPOS syndrome. *Orphanet J Rare Dis* **9,** 15.

DiFrancesco D & Ojeda C (1980). Properties of the current if in the sino-atrial node of the rabbit compared with those of the current iK, in Purkinje fibres. *J Physiol* **308,** 353–367.

Dimitrijevic MR, Gerasimenko Y & Pinter MM (1998). Evidence for a spinal central

pattern generator in humans. *Ann N Y Acad Sci* **860,** 360–376.

Dobretsov M & Stimers JJR (2005). Neuronal function and alpha3 isoform of the Na/K-ATPase. *Front Biosci* **10,** 2373–2396.

Drapeau P, Saint-Amant L, Buss RR, Chong M, McDearmid JR & Brustein E (2002). Development of the locomotor network in zebrafish. *Prog Neurobiol* **68,** 85–111.

Dyck J, Lanuza GM & Gosgnach S (2012). Functional characterization of dI6 interneurons in the neonatal mouse spinal cord. *J Neurophysiol* **107,** 3256–3266.

Edwards IJ, Bruce G, Lawrenson C, Howe L, Clapcote SJ, Deuchars SA & Deuchars J (2013). Na+/K+ ATPase α1 and α3 isoforms are differentially expressed in α- and γ-motoneurons. *J Neurosci* **33,** 9913–9919.

Egger M & Niggli E (2000). Paradoxical block of the Na+-Ca2+ exchanger by extracellular protons in guinea-pig ventricular myocytes. *J Physiol* **523 Pt 2,** 353–366.

Ellis DZ, Nathanson J a, Sweadner KJ & Dorette Z (2000). Carbachol inhibits Na+-K+-ATPase activity in choroid plexus via stimulation of the NO / cGMP pathway. **2129,** 1685–1693.

Ellis DZ, Rabe J & Sweadner KJ (2003). Global loss of Na,K-ATPase and its nitric oxide-mediated regulation in a transgenic mouse model of amyotrophic lateral sclerosis. *J Neurosci* **23,** 43–51.

Engl E & Attwell D (2015). Non-signalling energy use in the brain. *J Physiol* **593,** 3417–3429.

Erecińska M, Dagani F, Nelson D, Deas J & Silver IA (1991). Relations between intracellular ions and energy metabolism: a study with monensin in synaptosomes, neurons, and C6 glioma cells. *J Neurosci* **11,** 2410–2421.

Fernandez-Lopez B, Romaus-Sanjurjo D, Cornide-Petronio ME, Gomez-Fernandez S, Barreiro-Iglesias A & Rodicio MC (2015). Full anatomical recovery of the dopaminergic system after a complete spinal cord injury in lampreys. *Neural Plast*.

Ferrero R, Rodríguez-Pascual F, Miras-Portugal MT & Torres M (1999). Comparative effects of several nitric oxide donors on intracellular cyclic GMP levels in bovine chromaffin cells: correlation with nitric oxide production. *Br J Pharmacol* **127,** 779–787.

Flamm RE & Harris-Warrick RM (1986). Aminergic modulation in lobster stomatogastric ganglion. II. Target neurons of dopamine, octopamine, and serotonin within the pyloric circuit. *J Neurophysiol* **55,** 866–881.

Forrest MD (2014). The sodium-potassium pump is an information processing element in brain computation. *Front Physiol*; DOI: 10.3389/fphys.2014.00472.

Forrest MD (2015). Simulation of alcohol action upon a detailed Purkinje neuron model and a simpler surrogate model that runs >400 times faster. *BMC Neurosci* **16,** 27.

Forrest MD, Wall MJ, Press DA & Feng J (2012). The Sodium-Potassium Pump Controls the Intrinsic Firing of the Cerebellar Purkinje Neuron. *PLoS One* **7,** e51169.

Foster JD, Dunford C, Sillar KT & Miles GB (2014). Nitric oxide-mediated modulation of the murine locomotor network. *J Neurophysiol* **111,** 659–674.

French AS (1989). Ouabain selectively affects the slow component of sensory adaptation in an insect mechanoreceptor. **504,** 112–114.

Genet S & Kado RT (1997). Hyperpolarizing current of the Na/K ATPase contributes to the membrane polarization of the Purkinje cell in rat cerebellum. *Pflugers Arch Eur J Physiol* **434,** 559–567.

Gerard E, Hochstrate P, Dierkes P-W & Coulon P (2012). Functional properties and cell type specific distribution of Ih channels in leech neurons. *J Exp Biol* **215,** 227–238.

Gerin C & Privat A (1998). Direct evidence for the link between monoaminergic descending pathways and motor activity: II. A study with microdialysis probes implanted in the ventral horn of the spinal cord. *Brain Res* **794,** 169–173.

Glanzman DL (2010). Ion pumps get more glamorous. *Nat Neurosci* **13,** 4–5.

Glitsch HG (2001). Electrophysiology of the sodium-potassium-ATPase in cardiac cells. *Physiol Rev* **81,** 1791–1826.

Glitsch HG & Pusch H (1984). On the temperature dependence of the Na pump in sheep Purkinje fibres. *Pflugers Arch Eur J Physiol* **402,** 109–115.

Gocht D & Heinrich R (2007). Postactivation inhibition of spontaneously active neurosecretory neurons in the medicinal leech. *J Comp Physiol A Neuroethol Sensory, Neural, Behav Physiol* **193,** 347–361.

Godoy R, Noble S, Yoon K, Anisman H & Ekker M (2015). Chemogenetic ablation of dopaminergic neurons leads to transient locomotor impairments in zebrafish larvae. *J Neurochem* **135,** 249–260.

Gosgnach S, Lanuza GM, Butt SJ, Saueressig H, Zhang Y, Velasquez T, Riethmacher D, Callaway EM, Kiehn O & Goulding M (2006). V1 spinal neurons regulate the speed of vertebrate locomotor outputs. *Nature* **440,** 215–219.

Goulding M (2009). Circuits controlling vertebrate locomotion: moving in a new direction. *Nat Rev Neurosci* **10,** 507–518.

Goulding M & Pfaff SL (2005). Development of circuits that generate simple rhythmic behaviors in vertebrates. *Curr Opin Neurobiol* **15,** 14–20.

Grillner S (1981). Control of Locomotion in Bipeds, Tetrapods and Fish. In *Handbook of Physiology*, ed. Brooks V, pp. 1179–1236. American Physiological Society, Bethesda, MD.

Grillner S (2003). The motor infrastructure: from ion channels to neuronal networks.

Nat Rev Neurosci **4,** 573–586.

Grillner S (2006). Biological Pattern Generation: The Cellular and Computational Logic of Networks in Motion. *Neuron* **52,** 751–766.

Guertin PA (2009). The mammalian central pattern generator for locomotion. *Brain Res Rev* **62,** 45–56.

Gulledge AT, Dasari S, Onoue K, Stephens EK, Hasse JM & Avesar D (2013). A sodium-pump-mediated afterhyperpolarization in pyramidal neurons. *J Neurosci* **33,** 13025–13041.

Haber RS, Pressley TA, Loeb JN & Ismail-Beigi F (1987). Ionic dependence of active Na-K transport: “clamping” of cellular Na+ with monensin. *Am J Physiol* **253,** F26–F33.

Hamada K, Matsuura H, Sanada M, Toyoda F, Omatsu-Kanbe M, Kashiwagi A & Yasuda H (2003). Properties of the Na+/K+ pump current in small neurons from adult rat dorsal root ganglia. *Br J Pharmacol* **138,** 1517–1527.

Han P, Nakanishi ST, Tran MA & Whelan PJ (2007). Dopaminergic modulation of spinal neuronal excitability. *J Neurosci* **27,** 13192–13204.

Han P & Whelan PJ (2009). Modulation of AMPA currents by D1-like but not D2-like receptors in spinal motoneurons. *Neuroscience* **158,** 1699–1707.

Harris-Warrick RM (1995). Dopamine modulation of two subthreshold currents produces phase shifts in activity of an identified motoneuron. *J Neurophysiol* **74,** 1404–1420.

Harris-Warrick RM (2011). Neuromodulation and flexibility in Central Pattern Generator networks. *Curr Opin Neurobiol* **21,** 685–692.

Harris-Warrick RM & Johnson BR (2010). Checks and balances in neuromodulation. *Front Behav Neurosci* **4,** 1–9.

Harris-Warrick RM, Johnson BR, Peck JH, Kloppenburg P, Ayali A & Skarbinski J (1998). Distributed effects of dopamine modulation in the crustacean pyloric network. *Ann N Y Acad Sci* **860,** 155–167.

Harris-Warrick RM & Marder E (1991). Modulation of neural networks for behavior. *Annu Rev Neurosci* **14,** 39–57.

Hazelwood LA, Free RB, Cabrera DM, Skinbjerg M & Sibley DR (2008). Reciprocal modulation of function between the D1 and D 2 dopamine receptors and the Na+,K+-ATPase. *J Biol Chem* **283,** 36441–36453.

Heinzen EL, Swoboda KJ, Hitomi Y, Gurrieri F, Vries B De, Tiziano FD, Fontaine B, Walley NM, Sweney MT, Newcomb TM, Viollet L, Huff C, Lynn B, Reyna SP, Murphy KJ, Shianna K V & Gumbs CE (2012). De novo mutations in ATP1A3 cause alternating hemiplegia of childhood. **44,** 1030–1034.

Hellsten U et al. (2010). The Genome of the Western Clawed Frog *Xenopus tropicalis*.

Science (80-) **328,** 633–636.

Hieber V, Siegel GJ, Fink DJ, Beaty MW & Mata M (1991). Differential distribution of (Na, K)-ATPase alpha isoforms in the central nervous system. *Cell Mol Neurobiol* **11,** 253–262.

Hodgkin AL & Keynes RD (1956). Experiments on the injection of substances into squid giant axons by means of a microsyringe. *J Physiol* **131,** 592–616.1.

Hogan Q & Poroli M (1999). Hyperpolarization-activated Current (Ih) Contributes to Excitability of Primary Sensory Neurons in Rats. **6,** 102–110.

Holm TH & Lykke-hartmann K (2016). Insights into the Pathology of the α3 Na+/K+-ATPase in Neurological Disorders; Lessons from Animal Models. **7,** 1–8.

Holt GR & Koch C (1997). Shunting inhibition does not have a divisive effect on firing rates. *Neural Comput* **9,** 1001–1013.

Hughes GM & Wiersma CAG (1960). The co-ordination of swimmeret movements in the crayfish, *Procambarus Clarkii (Girard)*. *J Exp Biol* **37,** 657.

Hull MJ, Soffe SR, Willshaw DJ & Roberts A (2016). Modelling feedback excitation, pacemaker properties and sensory switching of electrically coupled brainstem neurons controlling rhythmic activity. *PLoS Comput Biol*.

Humphreys JM & Whelan PJ (2012). Dopamine exerts activation dependent modulation of spinal locomotor circuits in the neonatal mouse. *J Neurophysiol*3370–3381.

Hunanyan AS, Fainberg NA, Linabarger M, Arehart E, Leonard AS, Adil SM, Helseth AR, Swearingen AK, Forbes SL, Rodriguiz RM, Rhodes T, Yao X, Kibbi N, Hochman DW, Wetsel WC, Hochgeschwender U & Mikati MA (2015). Knock-in mouse model of alternating hemiplegia of childhood: Behavioral and electrophysiologic characterization. *Epilepsia* **56,** 82–93.

Ikeda K, Satake S, Onaka T, Sugimoto H, Takeda N, Imoto K & Kawakami K (2013). Enhanced inhibitory neurotransmission in the cerebellar cortex of Atp1a3-deficient heterozygous mice. *J Physiol* **591,** 3433–3449.

Inabayashi M, Miyauchi S, Kamo N & Jin T (1995). Conductance change in phospholipid bilayer membrane by an electroneutral ionophore, monensin. *Biochemistry* **34,** 3455–3460.

James PF, Grupp IL, Grupp G, Woo AL, Roger Askew G, Croyle ML, Walsh RA & Lingrel JB (1999). Identification of a specific role for the Na,K-ATPase a2 isoform as a regulator of calcium in the heart. *Mol Cell* **3,** 555–563.

Jankowska E, Jukes MG, Lund S & Lundberg A (1967). The effect of DOPA on the spinal cord. 5. Reciprocal organization of pathways transmitting excitatory action to alpha motoneurones of flexors and extensors. *Acta Physiol Scand* **70,** 369–388.

Jankowska E, Jukes MGM, Lund S & Lundberg A (1965). Reciprocal Innervation

through Interneuronal Inhibition. *Nature* **206,** 198–199.

Jay M, De Faveri F & McDearmid JR (2015). Firing dynamics and modulatory actions of supraspinal dopaminergic neurons during zebrafish locomotor behavior. *Curr Biol* **25,** 435–444.

Jessell TM (2000). Neuronal specification in the spinal cord: inductive signals and transcriptional codes. *Nat Rev Genet* **1,** 20–29.

Jiang Z, Carlin KP & Brownstone RM (1999). An in vitro functionally mature mouse spinal cord preparation for the study of spinal motor networks. *Brain Res* **816,** 493–499.

Jin W, Klem AM, Lewis JH & Lu Z (1999). Mechanisms of inward-rectifier K+ channel inhibition by tertiapin-Q. *Biochemistry* **38,** 14294–14301.

Johnson BR & Harris-Warrick RM (1990). Aminergic modulation of graded synaptic transmission in the lobster stomatogastric ganglion. *J Neurosci* **10,** 2066–2076.

Johnson BR, Kloppenburg P & Harris-Warrick RM (2003). Dopamine modulation of calcium currents in pyloric neurons of the lobster stomatogastric ganglion. *J Neurophysiol* **90,** 631–643.

Johnson SW, Seutin V & North R (1992). Burst firing in dopamine neurons induced by N-methyl-D-aspartate: role of electrogenic sodium pump. *Science* **258,** 665–667.

Kaczmarek LK (2013). Slack, Slick and Sodium-Activated Potassium Channels. *ISRN Neurosci*1–14.

Kang Y, Notomi T, Saito M, Zhang W & Shigemoto R (2004). Bidirectional interactions between h-channels and Na+-K+ pumps in mesencephalic trigeminal neurons. *J Neurosci* **24,** 3694–3702.

Kaplan JH (2002). Biochemistry of Na,K-ATPase. *Annu Rev Biochem* **71,** 511–535.

Katz PS (2016). Evolution of central pattern generators and rhythmic behaviours. *Philos Trans R Soc Lond B Biol Sci* **371,** 20150057.

Katz PS & Harris-Warrick MR (1999). The evolution of neural circuits underlying species-specific behavior. *Curr Opin Neurobiol* **9,** 628–633.

Keeler BE, Lallemand P, Patel MM, de Castro Bras LE & Clemens S (2015). Opposing aging-related shift of excitatory dopamine D1 and inhibitory D3 receptor protein expression in striatum and spinal cord. *J Neurophysiol* **115,** 363–369.

Keifer J & Summers CH (2016). Putting the “Biology” Back into “Neurobiology”: The Strength of Diversity in Animal Model Systems for Neuroscience Research. *Front Syst Neurosci* **10,** 1–9.

Kemnitz CP (1997). Dopaminergic modulation of spinal neurons and synaptic potentials in the lamprey spinal cord. *J Neurophysiol* **77,** 289–298.

Kiehn O (2016). Decoding the organization of spinal circuits that control locomotion.

Nat Rev Neurosci **17,** 224–238.

Kiehn O, Kjaerulff O, Tresch MC & Harris-Warrick RM (2000). Contributions of intrinsic motor neuron properties to the production of rhythmic motor output in the mammalian spinal cord. *Brain Res Bull* **53,** 649–659.

Kiernan MC, Lin CS-Y & Burke D (2004). Differences in activity-dependent hyperpolarization in human sensory and motor axons. *J Physiol* **558,** 341–349.

Kim JH & von Gersdorff H (2012). Suppression of spikes during posttetanic hyperpolarization in auditory neurons: the role of temperature, Ih currents, and the Na+-K+-ATPase pump. *J Neurophysiol* **108,** 1924–1932.

Kim JH, Sizov I, Dobretsov M & von Gersdorff H (2007). Presynaptic Ca2+ buffers control the strength of a fast post-tetanic hyperpolarization mediated by the alpha3 Na(+)/K(+)-ATPase. *Nat Neurosci* **10,** 196–205.

Kirshenbaum GS, Clapcote SJ, Duffy S, Burgess R, Petersen J, Jarowek KJ, Yücel YH, Cortez MA, Iii OCS, Vilsen B, Peever H, Ralph MR & Roder JC (2012*a*). Mania-like behavior induced by genetic dysfunction of the neuron-specific Na+,K+-ATPase a3 sodium pump. *Proc Natl Acad Sci* **109,** 2174–2174.

Kirshenbaum GS, Clapcote SJ, Duffy S, Burgess R, Petersen J, Jarowek KJ, Yücel YH, Cortez MA, Iii OCS, Vilsen B, Peever H, Ralph MR & Roder JC (2012*b*). Correction for Kirshenbaum et al., Mania-like behavior induced by genetic dysfunction of the neuron-specific Na+,K+-ATPase a3 sodium pump. *Proc Natl Acad Sci* **109,** 2174–2174.

Kirshenbaum GS, Clapcote SJ, Petersen J, Vilsen B, Ralph MR & Roder JC (2012). Genetic suppression of agrin reduces mania-like behavior in Na+, K+-ATPase a3 mutant mice. *Genes, Brain Behav* **11,** 436–443.

Kirshenbaum GS, Dawson N, Mullins JGL, Johnston TH, Drinkhill MJ, Edwards IJ, Fox SH, Pratt JA, Brotchie JM, Roder JC & Clapcote SJ (2013). Alternating Hemiplegia of Childhood-Related Neural and Behavioural Phenotypes in Na+,K+-ATPase α3 Missense Mutant Mice. *PLoS One*; DOI: 10.1371/journal.pone.0060141.

Kirshenbaum GS, Saltzman K, Rose B, Petersen J, Vilsen B & Roder JC (2011). Decreased neuronal Na+,K+-ATPase activity in atp1a3 heterozygous mice increases susceptibility to depression-like endophenotypes by chronic variable stress. *Genes, Brain Behav* **10,** 542–550.

Kjaerulff O & Kiehn O (1996). Distribution of networks generating and coordinating locomotor activity in the neonatal rat spinal cord in vitro: a lesion study. *J Neurosci* **16,** 5777–5794.

Kobayashi JI, Ohta M & Terada Y (1997). Evidence for the involvement of Na+-K+ pump and K+ conductance in the post-tetanic hyperpolarization of the tetrodotoxin-resistant C-fibers in the isolated bullfrog sciatic nerve. *Neurosci Lett* **236,** 171–174.

Koh DS, Jonas P, Bräu ME & Vogel W (1992). A TEA-insensitive flickering potassium

channel active around the resting potential in myelinated nerve. *J Membr Biol* **130,** 149–162.

Krey RA, Goodreau AM, Arnold TB & Del Negro CA (2010). Outward Currents Contributing to Inspiratory Burst Termination in preBötzinger Complex Neurons of Neonatal Mice Studied in Vitro. *Front Neural Circuits* **4,** 124.

Krishnan GP, Filatov G, Shilnikov A & Bazhenov M (2015). Electrogenic properties of the Na^+/K^+ ATPase controls transitions between normal and pathological brain states. *J Neurophysiol*jn.00460.2014.

Kueh D, Barnett WH, Cymbalyuk GS & Calabrese RL (2016). Na^+/K^+ pump interacts with the *h* -current to control bursting activity in central pattern generator neurons of leeches. *Elife* **5,** 1–36.

Lambert a. M, Bonkowsky JL & Masino MA (2012). The conserved dopaminergic diencephalospinal tract mediates vertebrate locomotor development in zebrafish larvae. *J Neurosci* **32,** 13488–13500.

Lambert TD, Li WC, Soffe SR & Roberts A (2004). Brainstem control of activity and responsiveness in resting frog tadpoles: Tonic inhibition. *J Comp Physiol A Neuroethol Sensory, Neural, Behav Physiol* **190,** 331–342.

Lanuza GM, Gosgnach S, Pierani A, Jessell TM & Goulding M (2004). Genetic identification of spinal interneurons that coordinate left-right locomotor activity necessary for walking movements. *Neuron* **42,** 375–386.

Lee FHF & Wong AHC (2010). Dopamine Receptor genetics in Neuropsychiatric Disorders. In *The Dopamine Receptors, Second Edition*, 2nd edn., ed. Neve KA, p. Ch. 19, 585-632. Humana Press Inc., Totowa, NJ.

Li W-C, Higashijima S, Parry DM, Roberts A & Soffe SR (2004*a*). Primitive roles for inhibitory interneurons in developing frog spinal cord. *J Neurosci* **24,** 5840–5848.

Li W-C & Moult PR (2012). The control of locomotor frequency by excitation and inhibition. *J Neurosci* **32,** 6220–6230.

Li W-C, Roberts A & Soffe SR (2009). Locomotor rhythm maintenance: electrical coupling among premotor excitatory interneurons in the brainstem and spinal cord of young Xenopus tadpoles. *J Physiol* **587,** 1677–1693.

Li W-C, Roberts A & Soffe SR (2010). Specific brainstem neurons switch each other into pacemaker mode to drive movement by activating NMDA receptors. *J Neurosci* **30,** 16609–16620.

Li W-C, Soffe SR & Roberts A (2002). Spinal inhibitory neurons that modulate cutaneous sensory pathways during locomotion in a simple vertebrate. *J Neurosci* **22,** 10924–10934.

Li W-C, Soffe SR & Roberts A (2004*b*). Glutamate and acetylcholine corelease at developing synapses. *Proc Natl Acad Sci U S A* **101,** 15488–15493.

Li W-C, Soffe SR, Wolf E & Roberts A (2006). Persistent responses to brief stimuli:

feedback excitation among brainstem neurons. *J Neurosci* **26,** 4026–4035.

Li YX, Bertram R & Rinzel J (1996). Modeling N-methyl-D-aspartate-induced bursting in dopamine neurons. *Neuroscience* **71,** 397–410.

Liang M & Knox FG (1999). Nitric oxide reduces the molecular activity of Na+,K+-ATPase in opossum kidney cells. *Kidney Int* **56,** 627–634.

Lichtshtein D, Dunlop K, Kaback HR & Blume a J (1979). Mechanism of monensin-induced hyperpolarization of neuroblastoma-glioma hybrid NG108-15. *Proc Natl Acad Sci U S A* **76,** 2580–2584.

Lichtstein D & Rosen H (2001). Endogenous digitalis-like Na+, K+-ATPase inhibitors, and brain function. *Neurochem Res* **26,** 971–978.

Lin YJ, Greif GJ & Freedman JE (1993). Multiple sulfonylurea-sensitive potassium channels: a novel subtype modulated by dopamine. *Mol Pharmacol* **44,** 907–910.

Lincoln TM & Komalavilias P (2000). Cyclic GMP-Mediated Signaling Mechanisms in Smooth Muscle. *Nitric Oxide Biol Pathobiol*401–425.

Liu Q, Manis PB & Davis RL (2014). Ih and HCN channels in murine spiral ganglion neurons: Tonotopic variation, local heterogeneity, and kinetic model. *JARO - J Assoc Res Otolaryngol* **15,** 585–599.

Liu W, Selever J, Lu M-F & Martin JF (2003). Genetic dissection of Pitx2 in craniofacial development uncovers new functions in branchial arch morphogenesis, late aspects of tooth morphogenesis and cell migration. *Development* **130,** 6375–6385.

Maccaferri G & McBain CJ (1996). The hyperpolarization-activated current (Ih) and its contribution to pacemaker activity in rat CA1 hippocampal stratum oriens-alveus interneurones. *J Physiol* **497 (Pt 1,** 119–130.

Madisen L, Zwingman TA, Sunkin SM, Oh SW, Zariwala HA, Gu H, Ng LL, Palmiter RD, Hawrylycz MJ, Jones AR, Lein ES & Zeng H (2010). A robust and high-throughput Cre reporting and characterization system for the whole mouse brain. *Nat Neurosci* **13,** 133–140.

Marder E, Bucher D, Schulz DJ & Taylor AL (2005). Invertebrate central pattern generation moves along. *Curr Biol* **15,** 685–699.

Mark MD & Herlitze S (2000). G-protein mediated gating of inward-rectifier K+ channels. *Eur J Biochem* **267,** 5830–5836.

Matsumoto M, Hidaka K, Tada S, Tasaki Y & Yamaguchi T (1996). Low levels of mRNA for dopamine D4 receptor in human cerebral cortex and striatum. *J Neurochem* **66,** 915–919.

McCormick DA & Pape HC (1990). Properties of a hyperpolarization-activated cation current and its role in rhythmic oscillation in thalamic relay neurones. *J Physiol* **431,** 291–318.

McDearmid JR, Scrymgeour-Wedderburn JF & Sillar KT (1997). Aminergic modulation of glycine release in a spinal network controlling swimming in *Xenopus laevis*. *J Physiol* **503,** 111–117.

McKee M, Scavone C & Nathanson J (1994). Nitric oxide, cGMP, and hormone regulation of active sodium transport. *Proc Natl Acad Sci U S A* **91,** 12056–12060.

McLean DL & Fetcho JR (2004*a*). Relationship of tyrosine hydroxylase and serotonin immunoreactivity to sensorimotor circuitry in larval zebrafish. *J Comp Neurol* **480,** 57–71.

McLean DL & Fetcho JR (2004*b*). Ontogeny and innervation patterns of dopaminergic, noradrenergic, and serotonergic neurons in larval zebrafish. *J Comp Neurol* **480,** 38–56.

McLean DL & Sillar KT (2000). The distribution of NADPH-diaphorase-labelled interneurons and the role of nitric oxide in the swimming system of Xenopus laevis larvae. *J Exp Biol* **203,** 705–713.

McLean DL & Sillar KT (2002). Nitric oxide selectively tunes inhibitory synapses to modulate vertebrate locomotion. *J Neurosci* **22,** 4175–4184.

McLean DL & Sillar KT (2004). Metamodulation of a spinal locomotor network by nitric oxide. *J Neurosci* **24,** 9561–9571.

McPherson DR & Kemnitz CP (1994). Modulation of lamprey fictive swimming and motoneuron physiology by dopamine, and its immunocytochemical localization in the spinal cord. *Neurosci Lett* **166,** 23–26.

Meehan CF, Grondahl L, Nielsen JB & Hultborn H (2012). Fictive locomotion in the adult decerebrate and spinal mouse in vivo. *J Physiol* **590,** 289–300.

Meeusen R, Watson P, Hasegawa H, Roelands B & Piacentini MF (2006). Central fatigue: The serotonin hypothesis and beyond. *Sport Med* **36,** 881–909.

Meiri H, Erulkar SD, Lerman T & Rahamimoff R (1981). The action of the sodium ionophore, monensin, on transmitter release at the frog neuromuscular junction. *Brain Res* **204,** 204–208.

Miles GB, Dai Y & Brownstone RM (2005). Mechanisms underlying the early phase of spike frequency adaptation in mouse spinal motoneurones. *J Physiol* **566,** 519–532.

Miles GB & Sillar KT (2011). Neuromodulation of Vertebrate Locomotor Control Networks. *Physiology* **26,** 393–411.

Moosmang S, Stieber J, Zong X, Biel M, Hofmann F & Ludwig A (2001). Cellular expression and functional characterization of four hyperpolarization-activated pacemaker channels in cardiac and neuronal tissues. *Eur J Biochem* **268,** 1646–1652.

Moran-Rivard L, Kagawa T, Saueressig H, Gross MK, Burrill J & Goulding M (2001). Evx1 is a postmitotic determinant of V0 interneuron identity in the spinal cord.

Neuron **29,** 385–399.

Morita K, David G, Barrett JN & Barrett EF (1993). Posttetanic hyperpolarization produced by electrogenic Na(+)-K+ pump in lizard axons impaled near their motor terminals. *J Neurophysiol* **70,** 1874–1884.

Morth JP, Pedersen BP, Buch-Pedersen MJ, Andersen JP, Vilsen B, Palmgren MG & Nissen P (2011). A structural overview of the plasma membrane Na+,K+-ATPase and H+-ATPase ion pumps. *Nat Rev Mol Cell Biol* **12,** 60–70.

Moseley AE, Williams MT, Schaefer TL, Bohanan CS, Neumann JC, Behbehani MM, Vorhees C V & Lingrel JB (2007). Deficiency in Na,K-ATPase a isoform genes alters spatial learning, motor Activity, and anxiety in mice. **27,** 616–626.

Moult PR, Cottrell GA & Li WC (2013). Fast silencing reveals a lost role for reciprocal inhibition in locomotion. *Neuron* **77,** 129–140.

Mulloney B & Smarandache C (2010). Fifty years of CPGs: Two neuroethological papers that shaped the course of neuroscience. *Front Behav Neurosci* **4,** 1–8.

Nakajima S & Takahashi K (1966). Post-tetanic hyperpolarization and electrogenic Na pump in stretch receptor neurone of crayfish. *J Physiol* **187,** 105–127.

Nakamura Y, Ohya Y, Abe I & Fujishima M (1999). Sodium-potassium pump current in smooth muscle cells from mesenteric resistance arteries of the guinea-pig. *J Physiol* **519,** 203–212.

del Negro CA, Hsiao C-F & Chandler SH (1999). Outward Currents Influencing Bursting Dynamics in Guinea Pig Trigeminal Motoneurons. *J Neurophysiol* **81,** 1478–1485.

Del Negro CA, Kam K, Hayes JA & Feldman JL (2009). Asymmetric control of inspiratory and expiratory phases by excitability in the respiratory network of neonatal mice in vitro. *J Physiol* **587,** 1217–1231.

Neve K (n.d.). The Dopamine Receptors. In *Dopamine and Glutamate in Psychiatric Disorders*, ed. Schmidt W & Reith M. Humana Press Inc., Totowa, NJ.

Nieuwkoop PD & Faber J (1956). *Normal Tables of Xenopus laevis (Daudin)*. North Holland Publishing Company, Amsterdam, North Holland.

Nikolić L, Kartelija G & Nedeljković M (2008). Effect of static magnetic fields on bioelectric properties of the Br and N1 neurons of snail Helix pomatia. *Comp Biochem Physiol - A Mol Integr Physiol* **151,** 657–663.

Nikolić L, Todorović N, Zakrzewska J, Stanić M, Rauš S, Kalauzi A & Janać B (2012). Involvement of Na +/K +pump in fine modulation of bursting activity of the snail Br neuron by 10 mT static magnetic field. *J Comp Physiol A Neuroethol Sensory, Neural, Behav Physiol* **198,** 525–540.

Noma A & Irisawa H (1976). A time- and voltage-dependent potassium current in the rabbit sinoatrial node cell. *Pflügers Arch Eur J Physiol* **366,** 251–258.

O'Connell L. & Hofmann H. (2012). Evolution of a vertebrate social decision-making network. *Science (80-)* **336,** 1154–1157.

Okamura H, Yasuhara JC, Fambrough DM & Takeyasu K (2003). P-type ATPases in Caenorhabditis and Drosophila: Implications for evolution of the P-type ATPase subunit families with special reference to the Na,K-ATPase and H,K-ATPase subgroup. *J Membr Biol* **191,** 13–24.

Olszynko-gryn J (2013). When pregnancy tests were toads. *Wellcome Hist*.

Pape H-C (1996). Queer current and pacemaker: The hyperpolarization-activated cation current in neurons. *Annu Rev Physiol* **58,** 299–327.

Parker D, Hill R & Grillner S (1996). Electrogenic pump and a Ca(2+)- dependent K+ conductance contribute to a posttetanic hyperpolarization in lamprey sensory neurons. *J Neurophysiol* **76,** 540–553.

Pavlovic D, Hall AR, Kennington EJ, Aughton K, Boguslavskyi A, Fuller W, Despa S, Bers DM & Shattock MJ (2013). Nitric oxide regulates cardiac intracellular Na+ and Ca2+ by modulating Na/K ATPase via PKCε and phospholemman-dependent mechanism. *J Mol Cell Cardiol* **61,** 164–171.

Peck JH, Gaier E, Stevens E, Repicky S & Harris-Warrick RM (2006). Amine modulation of Ih in a small neural network. *J Neurophysiol* **96,** 2931–2940.

Peña-Rangel MT, Mercado-C R & Hernández-Rodríguez J (1999). Regulation of glial Na+/K+-ATPase by serotonin: Identification of participating receptors. *Neurochem Res* **24,** 643–649.

Peng JHF, Zeng Y & Parker Jr. JC (1992). Highly ouabain-sensitive Alpha3 isoform of Na+,K+-ATPase in human brain. *J Neurochem* **58,** 1180–1183.

Pérez-Fernández J, Megías M & Pombal MA (2015). Expression of a Novel D4 Dopamine Receptor in the Lamprey Brain. Evolutionary Considerations about Dopamine Receptors. *Front Neuroanat* **9,** 165.

Perez-Fernandez J, Stephenson-Jones M, Suryanarayana SM, Robertson B & Grillner S (2014). Evolutionarily conserved organization of the dopaminergic system in lamprey: SNc/VTA afferent and efferent connectivity and D2 receptor expression. *J Comp Neurol* **522,** 3775–3794.

Perrins R, Walford A & Roberts A (2002). Sensory activation and role of inhibitory reticulospinal neurons that stop swimming in hatchling frog tadpoles. *J Neurosci* **22,** 4229–4240.

Pierani A, Moran-Rivard L, Sunshine MJ, Littman DR, Goulding M & Jessell TM (2001). Control of interneuron fate in the developing spinal cord by the progenitor homeodomain protein Dbx1. *Neuron* **29,** 367–384.

Pillai G, Brown NA, McAllister G, Milligan G & Seabrook GR (1998). Human D2 and D4 dopamine receptors couple through βγ G-protein subunits to inwardly rectifying K+ channels (GIRK1) in a Xenopus oocyte expression system: Selective antagonism by L-741,626 and L-745,870 respectively. *Neuropharmacology* **37,**

983–987.

Pirtle TJ & Satterlie RA (2007). The role of postinhibitory rebound in the locomotor central-pattern generator of *Clione limacina*. *Integr Comp Biol* **47,** 451–456.

Pirtle TJ, Willingham K & Satterlie RA (2010). A hyperpolarization-activated inward current alters swim frequency of the pteropod mollusk *Clione limacina*. *Comp Biochem Physiol - A Mol Integr Physiol* **157,** 319–327.

Puhl JG & Mesce KA (2008). Dopamine activates the motor pattern for crawling in the medicinal leech. *J Neurosci* **28,** 4192–4200.

Pulver SR & Griffith LC (2010). Spike integration and cellular memory in a rhythmic network from Na+/K+ pump current dynamics. *Nat Neurosci* **13,** 53–59.

Rang BYHP & Ritchie JM (1968). On the electrogenic sodium pump in mammalian non-myelinated nerve fibres and its activation by various external cations. **196,** 183–221.

Ranieri F & Di Lazzaro V (2012). The role of motor neuron drive in muscle fatigue. *Neuromuscul Disord* **22,** S157–S161.

Rauscent A, Le Ray D, Cabirol-Pol MJ, Sillar KT, Simmers J & Combes D (2006). Development and neuromodulation of spinal locomotor networks in the metamorphosing frog. *J Physiol Paris* **100,** 317–327.

Reimer MM, Norris A, Ohnmacht J, Patani R, Zhong Z, Dias TB, Kuscha V, Scott AL, Chen YC, Rozov S, Frazer SL, Wyatt C, Higashijima SI, Patton EE, Panula P, Chandran S, Becker T & Becker C (2013). Dopamine from the Brain Promotes Spinal Motor Neuron Generation during Development and Adult Regeneration. *Dev Cell* **25,** 478–491.

Reith CA (1996). *GABAergic modulation of locomotor rhythmicity during postembryonic development in Xenopus laevis (PhD thesis)* (thesis). University of St. Andrews, St. Andrews, Scotland, UK.

Reith CA (1998). A role for slow NMDA receptor-mediated, intrinsic neuronal oscillations in the control of fast fictive swimming in Xenopus laevis larvae. *Eur J Neurosci* **10,** 1329–1340.

Ritchie JM & Straub RW (1957). The hyperpolarization which follows activity in mammalian non-medullated fibres. *J Physiol* **136,** 80–97.

Roberts A, Li W-C & Soffe SR (2010). How neurons generate behavior in a hatchling amphibian tadpole: an outline. *Front Behav Neurosci* **4,** 16.

Roberts A, Li WC & Soffe SR (2012). A functional scaffold of CNS neurons for the vertebrates: The developing *Xenopus laevis* spinal cord. *Dev Neurobiol* **72,** 575–584.

Roberts A, Li WC, Soffe SR & Wolf E (2008). Origin of excitatory drive to a spinal locomotor network. *Brain Res Rev* **57,** 22–28.

Robertson RM (2004). Thermal stress and neural function: Adaptive mechanisms in insect model systems. *J Therm Biol* **29,** 351–358.

Robertson RM & Money TGA (2012). Temperature and neuronal circuit function: Compensation, tuning and tolerance. *Curr Opin Neurobiol* **22,** 724–734.

Robertson RM & Sillar KT (2009). The nitric oxide/cGMP pathway tunes the thermosensitivity of swimming motor patterns in Xenopus laevis tadpoles. *J Neurosci* **29,** 13945–13951.

Robinson RB & Siegelbaum SA (2003). Hyperpolarization-activated cation currents: from molecules to physiological function. *Annu Rev Physiol* **65,** 453–480.

Roeper J, Hainsworth AH & Ashcroft FM (1990). Tolbutamide reverses membrane hyperpolarisation induced by activation of D2 receptors and GABAB receptors in isolated substantia nigra neurones. *Pflügers Arch Eur J Physiol* **416,** 473–475.

Rozzo A, Ballerini L, Abbate G & Nistri A (2002). Experimental and modeling studies of novel bursts induced by blocking Na(+) pump and synaptic inhibition in the rat spinal cord. *J Neurophysiol* **88,** 676–691.

Rubin JE, Hayes JA, Mendenhall JL & Del Negro CA (2009). Calcium-activated nonspecific cation current and synaptic depression promote network-dependent burst oscillations. *Proc Natl Acad Sci U S A* **106,** 2939–2944.

Ruegsegger C, Maharjan N, Goswami A, de L'Etang AF, Weis J, Troost D, Heller M, Gut H & Saxena S (2015). Aberrant association of misfolded SOD1 with Na+/K+ATPase-α3 impairs its activity and contributes to motor neuron vulnerability in ALS. *Acta Neuropathol*.

Sadja R, Alagem N & Reuveny E (2003). Gating of GIRK channels: Details of an intricate, membrane-delimited signaling complex. *Neuron* **39,** 9–12.

Sautois B, Soffe SR, Li WC & Roberts A (2007). Role of type-specific neuron properties in a spinal cord motor network. *J Comput Neurosci* **23,** 59–77.

Schotland J, Shupliakov O, Wikström M, Brodin L, Srinivasan M, You ZB, Herrera-Marschitz M, Zhang W, Hökfelt T & Grillner S (1995). Control of lamprey locomotor neurons by colocalized monoamine transmitters. *Nature* **374,** 266–268.

Scuri R, Lombardo P, Cataldo E, Ristori C & Brunelli M (2007). Inhibition of Na+/K+ ATPase potentiates synaptic transmission in tactile sensory neurons of the leech. *Eur J Neurosci* **25,** 159–167.

Scuri R, Mozzachiodi R & Brunelli M (2002). Activity-dependent increase of the AHP amplitude in T sensory neurons of the leech. *J Neurophysiol* **88,** 2490–2500.

Senatorov V V, Stys PK & Hu B (2000). Regulation of Na+,K+-ATPase by persistent sodium accumulation in adult rat thalamic neurones. *J Physiol* **525 Pt 2,** 343–353.

Sharples S, Humphreys JM, Jensen AM, Dhoopar S, Delaloye N, Clemens S & Whelan PJ (2015). Dopaminergic modulation of locomotor network activity in the neonatal mouse spinal cord. *J Neurophysiol* **113,** 2500–2510.

Sharples S, Koblinger K, Humphreys JM & Whelan PJ (2014). Dopamine: a parallel pathway for the modulation of spinal locomotor networks. *Front Neural Circuits* **8,** 55.

Shen KZ & Johnson SW (1998). Sodium pump evokes high density pump currents in rat midbrain dopamine neurons. *J Physiol* **512,** 449–457.

Sherrington CS (1906). Observations on the scratch-reflex in the spinal dog. *J Physiol* **34,** 1–50.

Sherrington CS (1910). Flexion-reflex of the limb, crossed extension-reflex, and reflex stepping and standing. *J Physiol* **40,** 28–121.

Sillar KT, Combes D, Ramanathan S, Molinari M & Simmers J (2008). Neuromodulation and developmental plasticity in the locomotor system of anuran amphibians during metamorphosis. *Brain Res Rev* **57,** 94–102.

Sillar KT & Roberts a (1988). A neuronal mechanism for sensory gating during locomotion in a vertebrate. *Nature* **331,** 262–265.

Sillar KT & Robertson RM (2009). Thermal activation of escape swimming in post-hatching *Xenopus laevis* frog larvae. *J Exp Biol* **212,** 2356–2364.

Sillar KT, Wedderburn JF & Simmers A (1991). The development of swimming rhythmicity in post-embryonic *Xenopus laevis*. *Proc Biol Sci* **246,** 147–153.

Smith M & Perrier J-F (2006). Intrinsic properties shape the firing pattern of ventral horn interneurons from the spinal cord of the adult turtle. *J Neurophysiol* **96,** 2670–2677.

Sokolove PG & Cooke IM (1971). Inhibition of impulse activity in a sensory neuron by an electrogenic pump. *J Gen Physiol* **57,** 125–163.

Song J, Ampatzis K, Björnfors ER & El Manira A (2016). Motor neurons control locomotor circuit function retrogradely via gap junctions. *Nature*1–5.

Strausfeld NJ & Hirth F (2013). Deep homology of arthropod central complex and vertebrate basal ganglia. *Sci (New York, NY)* **340,** 157–161.

Stuart DG & Hultborn H (2008). Thomas Graham Brown (1882-1965), Anders Lundberg (1920-), and the neural control of stepping. *Brain Res Rev* **59,** 74–95.

Sugimoto H, Ikeda K & Kawakami K (2014). Heterozygous mice deficient in Atp1a3 exhibit motor deficits by chronic restraint stress. *Behav Brain Res* **272,** 100–110.

Svensson E, Woolley J, Wikström M & Grillner S (2003). Endogenous dopaminergic modulation of the lamprey spinal locomotor network. *Brain Res* **970,** 1–8.

Swanson JM, Kinsbourne M, Nigg J, Lanphear B, Stefanatos GA, Volkow N, Taylor E, Casey BJ, Castellanos FX & Wadhwa PD (2007). Etiologic subtypes of attention-deficit/hyperactivity disorder: Brain imaging, molecular genetic and environmental factors and the dopamine hypothesis. *Neuropsychol Rev* **17,** 39–59.

Takahashi T (1990). Inward rectification in neonatal rat spinal motoneurones. *J Physiol* **423,** 47–62.

Takeyasu K, Lemas V & Fambrough DM (1990). Stability of Na(+)-K(+)-ATPase alpha-subunit isoforms in evolution. *Am J Physiol* **259,** 619–630.

Talpalar AE, Bouvier J, Borgius L, Fortin G, Pierani A & Kiehn O (2013). Dual-mode operation of neuronal networks involved in left-right alternation. *Nature* **500,** 85–88.

Talpalar AE, Endo T, Low P, Borgius L, Hagglund M, Dougherty KJ, Ryge J, Hnasko TS & Kiehn O (2011). Identification of minimal neuronal networks involved in flexor-extensor alternation in the mammalian spinal cord. *Neuron* **71,** 1071–1084.

Talpalar AE & Kiehn O (2010). Glutamatergic mechanisms for speed control and network operation in the rodent locomotor CPG. *Front Neural Circuits* **4,** 1–14.

Tanaka S (2002). Development of inward rectification and control of membrane excitability in mesencephalic V neurons. *J Neurophysiol* **89,** 1288–1298.

Tang LS, Goeritz ML, Caplan JS, Taylor AL, Fisek M & Marder E (2010). Precise temperature compensation of phase in a rhythmic motor pattern. *PLoS Biol* **8,** 21–22.

Tay TL, Ronneberger O, Ryu S, Nitschke R & Driever W (2011). Comprehensive catecholaminergic projectome analysis reveals single-neuron integration of zebrafish ascending and descending dopaminergic systems. *Nat Commun* **2,** 171.

Therien A & Blostein R (2000). Mechanisms of sodium pump regulation. *Am J Physiol Cell Physiol* **279,** C541–C566.

Thirumalai V & Cline HT (2008). Endogenous dopamine suppresses initiation of swimming in prefeeding zebrafish larvae. *J Neurophysiol* **100,** 1635–1648.

Thoby-Brisson M, Telgkamp P & Ramirez JM (2000). The role of the hyperpolarization-activated current in modulating rhythmic activity in the isolated respiratory network of mice. *J Neurosci* **20,** 2994–3005.

Tobin A-E & Calabrese RL (2005). Myomodulin increases Ih and inhibits the NA/K pump to modulate bursting in leech heart interneurons. *J Neurophysiol* **94,** 3938–3950.

Trotier D & Døving KB (1996). Direct influence of the sodium pump on the membrane potential of vomeronasal chemoreceptor neurones in frog. *J Physiol* **490 (Pt 3,** 611–621.

Tryba AK & Ramirez J-M (2003). Response of the respiratory network of mice to hyperthermia. *J Neurophysiol* **89,** 2975–2983.

Tsuzawa K, Yazawa I, Shakuo T, Ikeda K, Kawakami K & Onimaru H (2015). Effects of ouabain on respiratory rhythm generation in brainstem-spinal cord preparation from newborn rats and in decerebrate and arterially perfused in situ preparation

from juvenile rats. *Neuroscience* **286,** 404–411.

Vallecorsa GM, Amatrudo JM & Angstadt JD (2007). Dopamine induces rhythmic activity and enhances postinhibitory rebound in a leech motor neuron involved in swimming and crawling behaviors. *Impulse (Sydney)*1–14.

Velázquez-Ulloa NA, Spitzer NC & Dulcis D (2011). Contexts for dopamine specification by calcium spike activity in the CNS. *J Neurosci* **31,** 78–88.

Vidal-Gadea A, Topper S, Young L, Crisp A, Kressin L, Elbel E, Maples T, Brauner M, Erbguth K, Axelrod A, Gottschalk A, Siegel D & Pierce-Shimomura JT (2011). *Caenorhabditis elegans* selects distinct crawling and swimming gaits via dopamine and serotonin. *Proc Natl Acad Sci* **108,** 17504–17509.

Wang D, Grillner S & Wallén P (2011). 5-HT and dopamine modulates CaV1.3 calcium channels involved in postinhibitory rebound in the spinal network for locomotion in lamprey. *J Neurophysiol* **105,** 1212–1224.

Wang GX & Poo M-M (2005). Requirement of TRPC channels in netrin-1-induced chemotropic turning of nerve growth cones. *Nature* **434,** 898–904.

Wang Y-C & Huang R-C (2006). Effects of sodium pump activity on spontaneous firing in neurons of the rat suprachiasmatic nucleus. *J Neurophysiol* **96,** 109–118.

Wang Y-C, Yang J-J & Huang R-C (2012). Intracellular Na+ and metabolic modulation of Na/K pump and excitability in the rat suprachiasmatic nucleus neurons. *J Neurophysiol* **108,** 2024–2032.

Wedemeyer C, Goutman JD, Avale ME, Franchini LF, Rubinstein M & Calvo DJ (2007). Functional activation by central monoamines of human dopamine D4 receptor polymorphic variants coupled to GIRK channels in Xenopus oocytes. *Eur J Pharmacol* **562,** 165–173.

Whelan P, Bonnot a & O'Donovan MJ (2000). Properties of rhythmic activity generated by the isolated spinal cord of the neonatal mouse. *J Neurophysiol* **84,** 2821–2833.

Wikstrom MA, Grillner S & El Manira A (1999). Inhibition of N- and L-type Ca2+ currents by dopamine in lamprey spinal motoneurons. *Neuroreport* **10,** 3179–3183.

William M, Vien J, Hamilton E, Garcia A, Bundgaard H, Clarke RJ & Rasmussen HH (2005). The nitric oxide donor sodium nitroprusside stimulates the Na+-K+ pump in isolated rabbit cardiac myocytes. *J Physiol* **565,** 815–825.

Wilson DM (1961). The central nervous control of flight in a locust. *J Exp Biol* **38,** 471–490.

Wilson DM & Wyman RJ (1965). Motor output patterns during random and rhythmic stimulation of locust thoracic ganglia. *Biophys J* **5,** 121–143.

Wu Z-Q, Chen J, Chi Z-Q & Liu J-G (2007). Involvement of dopamine system in regulation of Na+,K+-ATPase in the striatum upon activation of opioid receptors

by morphine. *Mol Pharmacol* **71,** 519–530.

Xie Z & Askari A (2002). Na+/K+-ATPase as a signal transducer. *Eur J Biochem* **269,** 2434–2439.

Yamada M, Inanobe A & Kurachi Y (1998). G protein regulation of potassium ion channels. *Pharmacol Rev* **50,** 723–760.

Zagoraiou L, Akay T, Martin JF, Brownstone RM, Jessell TM & Miles GB (2009). A Cluster of Cholinergic Premotor Interneurons Modulates Mouse Locomotor Activity. *Neuron* **64,** 645–662.

Zhang H-Y, Issberner J & Sillar KT (2011). Development of a spinal locomotor rheostat. *Proc Natl Acad Sci U S A* **108,** 11674–11679.

Zhang H-Y, Li W-C, Heitler WJ & Sillar KT (2009). Electrical coupling synchronises spinal motoneuron activity during swimming in hatchling Xenopus tadpoles. *J Physiol* **587,** 4455–4466.

Zhang H-Y, Picton L, Li W-C & Sillar KT (2015). Mechanisms underlying the activity-dependent regulation of locomotor network performance by the Na+ pump. *Sci Rep* **5,** 16188.

Zhang HY & Sillar KT (2012). Short-term memory of motor network performance via activity-dependent potentiation of Na +/K + pump function. *Curr Biol* **22,** 526–531.

Zhang J, Lanuza GM, Britz O, Wang Z, Siembab VC, Zhang Y, Velasquez T, Alvarez FJ, Frank E & Goulding M (2014). V1 and V2b interneurons secure the alternating flexor-extensor motor activity mice require for limbed locomotion. *Neuron* **82,** 138–150.

Zhang L-N, Li J-X, Hao L, Sun Y-J, Xie Y-H, Wu S-M, Liu L, Chen X-L & Gao Z-B (2013). Crosstalk between dopamine receptors and the Na+/K+-ATPase (Review). *Mol Med Rep* **8,** 1291–1299.

Zhang Y, Narayan S, Geiman E, Lanuza GM, Velasquez T, Shanks B, Akay T, Dyck J, Pearson K, Gosgnach S, Fan CM & Goulding M (2008). V3 spinal neurons establish a robust and balanced locomotor rhythm during walking. *Neuron* **60,** 84–96.

Zhang Y, Oliva R, Gisselmann G, Hatt H, Guckenheimer J & Harris-Warrick RM (2003). Overexpression of a hyperpolarization-activated cation current (Ih) channel gene modifies the firing activity of identified motor neurons in a small neural network. *J Neurosci* **23,** 9059–9067.

Zhong G, Droho S, Crone SA, Dietz S, Kwan AC, Webb WW, Sharma K & Harris-Warrick RM (2010). Electrophysiological characterization of V2a interneurons and their locomotor-related activity in the neonatal mouse spinal cord. *J Neurosci* **30,** 170–182.

Zhu H, Clemens S, Sawchuk M & Hochman S (2007). Expression and distribution of all dopamine receptor subtypes (D1-D5) in the mouse lumbar spinal cord: A real-

time polymerase chain reaction and non-autoradiographic in situ hybridization study. *Neuroscience* **149,** 885–897.